Genetic and Microbiological Tools to Unravel the Mechanism of Action of Novel Anti-Tuberculosis New Chemical Entities

by

Christopher Edward Burke

A thesis submitted to the University of Birmingham for the degree of

DOCTOR OF PHILOSOPHY

School of Biosciences

College of Life and Environmental Sciences

University of Birmingham

October 2020

UNIVERSITY OF
BIRMINGHAM

University of Birmingham Research Archive

e-theses repository

This unpublished thesis/dissertation is copyright of the author and/or third parties. The intellectual property rights of the author or third parties in respect of this work are as defined by The Copyright Designs and Patents Act 1988 or as modified by any successor legislation.

Any use made of information contained in this thesis/dissertation must be in accordance with that legislation and must be properly acknowledged. Further distribution or reproduction in any format is prohibited without the permission of the copyright holder.

Abstract

Mycobacterium tuberculosis, the causative agent of tuberculosis, is the leading cause of mortality from a single infectious agent. The treatment of this disease is a long and difficult process requiring full patient compliance, otherwise risking a recurrent infection and/or antibiotic resistance. The treatment time of drug susceptible tuberculosis is six months and uses drugs that are tolerable for the patient. Rifampicin resistant tuberculosis and multi-drug resistant tuberculosis treatments rely on drugs that are either poorly tolerated by the patient or have an unknown mechanism of action. Identifying new drugs that could shorten the treatment time of tuberculosis or have reduced side effects is imperative. This thesis focuses on drug discovery with an emphasis on using a target specific high-throughput phenotypic screening to identify potential hits and leads. The resulting hits are then re-examined, using microbiological, genetic, and biochemical techniques to confirm the target protein/complex of the hits. The first project uses a media supplementation assay to identify hits that inhibit amnio acid biosynthesis. These pathways are well-validated using known inhibitors of branched chain amino acid biosynthesis. The second project focuses on a large phenotypic screen designed to identify inhibitors of the protein synthesis pipeline. Finally, the third project uses numerous biochemical assays to assess the interactions of hits selected from an overexpression screen of the Antigen 85 protein, *fbpA*. The hits were then evaluated using a combination of biochemical assays, microbiological techniques, and whole genome sequencing to confirm the targets of the hit compounds. While the success rate of identifying hits from compound libraries is low in these projects, these methods have all been validated and would be suitable for a more industrialised method of high-throughput screening of compound libraries.

Declaration

The work presented in this thesis has been carried out under the supervision of Prof Gurdyal S. Besra and Dr Luke J. Alderwick in the School of Biosciences at the University of Birmingham, UK, B15 2TT during the period October 2017 to October 2020. The work in this thesis is original except where acknowledged by reference. This work has resulted in two publications, one with Dr Katherine A. Abrahams as co-author and one with Dr Monika Jankute as co-author. These publications may have similarities to Chapters 1, 2 and 3. These similar sections included in my thesis are my original work with no significant contribution to the text by Dr Katherine A. Abrahams, Dr Monika Jankute, Prof Gurdyal S. Besra and Dr. Luke J. Alderwick. No part of the work is being, or has been submitted for a degree, diploma or any other qualification at any other University.

Professor Gurdyal S. Besra

Dr Luke Alderwick

Dr Katherine Abrahams

Dr Monika Jankute

UNIVERSITY OF
BIRMINGHAM

University of Birmingham Research Archive

e-theses repository

This unpublished thesis/dissertation is copyright of the author and/or third parties. The intellectual property rights of the author or third parties in respect of this work are as defined by The Copyright Designs and Patents Act 1988 or as modified by any successor legislation.

Any use made of information contained in this thesis/dissertation must be in accordance with that legislation and must be properly acknowledged. Further distribution or reproduction in any format is prohibited without the permission of the copyright holder.

Acknowledgements

I would like to thank my supervisor, Professor Gurdyal Besra F.R.S, for his expertise, guidance, and quality memes throughout my PhD. I would also like to thank Dr Apoorva Bhatt, Dr Luke Alderwick, and Dr Patrick Moynihan for their support and knowledge.

I would like to thank everyone in the TB Labs, past and present, for their support and welcoming attitude. In particular, I would like to thank Dr Katherine Abrahams for her training, support, knowledge, equipment, supplies, kindness, motivation, and anything else I have needed over the years. I would like to thank Dr Monika Jankute and Dr Rebeca Balio for training me in CAT3 and then ensuring my survival.

I would like to thank my friends and fellow PhD students, Anja Đokić, Alice Moorey, Alice Lanne, Stephen Bethell, Hayleah Pickford, Bala Madduri, Helen Clayton, and Charlotte Cooper for their support and their adequate monster slaying skills…

Finally, I would like to thank my family for their confidence in me and the support they have provided throughout my PhD.

Contents

Abstract……i

Declaration……..ii

University of Birmingham Research Archive……..iii

Acknowledgements……iv

Contents……....v

Figure List……..xii

Table List……...xvi

Abbreviation List……xviii

Published Work……...xxii

1 General Introduction.....1

1.1 *Mycobacteria* and related genus 2
1.2 Tuberculosis - a Historic Disease 3
1.3 Tuberculosis Epidemiology 5
1.4 Clinical Presentation of Tuberculosis 8
1.5 Pathogenesis..... 10
1.6 Diagnosis of Tuberculosis 11
1.7 Treatment of Tuberculosis 14
1.7.1 Streptomycin and Aminoglycosides 16
1.7.2 Isoniazid 17
1.7.3 Pyrazinamide 19
1.7.4 Ethambutol 20
1.7.5 Rifampicin and Rifamycins 22
1.7.6 Fluoroquinolones 23
1.7.7 Polypeptides 25
1.7.8 *Para*-aminosalicylic Acid..... 26
1.7.9 Thioamides and Triclosan 27
1.7.10 D-Cycloserine and Terizidone 28
1.7.11 β-Lactams 29
1.7.12 Other Tuberculosis Treatments 31

1.7.13 New Generation Multi-Drug Resistance Treatments 32
1.8 The Mycobacterial Cell Wall 33
1.8.1 Peptidoglycan 34
1.8.2 Arabinogalactan 36
1.8.3 Mycolic Acids 38
1.8.4 Phosphatidyl-*myo*-Inositol and Elaborations 40
1.9 Model Organisms 41
1.10 Project Aims 42

2 Development and Validation of High-Throughput Phenotypic Screening Methods to Identify Inhibitors of *M. tuberculosis* Amino Acid Biosynthesis.....45

2.1 Introduction 45
2.2 Materials and Methods 50
2.2.1 Liquid Minimum Inhibitory Concentrations (MIC) of Validation Compounds 50
2.2.2 Dose Response of Amino Acid Supplementation for Validation Compounds 50
2.2.3 Amino Acid Drop-Out Validation 51
2.2.4 Restriction Free Cloning of Wild Type Acetolactate Synthase Genes 51
2.2.5 Spontaneous Resistant Mutant Generation for Metsulfuron-Methyl (MSM) and Sulfometuron-Methyl (SMM) 54
2.2.6 Restriction Cloning of *ilvB1* and *ilvN* Mutant Genes 54
2.2.7 Overexpression of Acetolactate Synthase (ALS) Genes in *M. bovis* BCG 55
2.2.8 Overexpression of Mutated Acetolactate Synthase (ALS) Genes in *M. bovis* BCG and *M. smegmatis* 56
2.2.9 TB Box Amino Acid Drug Rescue Screen 57
2.2.10 TB Box Amino Acid Dose Response Screen 58
2.2.11 TB Box Amino Acid Dropout Screen 58
2.2.12 TB Box Amino Acid Compounds Liquid Minimum Inhibitory Concentrations (MICs) 59
2.2.13 TB Box Amino Acid Compounds Solid Minimum Inhibitory Concentrations (MICs) 59
2.2.14 TB Box Amino Acid Compounds Drug Resistant Mutant Generation 60
2.3 Results 61

2.3.1 Minimum Inhibitory Concentrations (MICs) of Validation Compounds. 61
2.3.2 Rescue from Validation Compounds using Amino Acid Supplementation. 62
2.3.3 Single Amino Acid Supplement GSK TB Box Screens..... 64
2.3.4 All Amino Acids Supplemented GSK TB Box Screen 66
2.3.5 Dose Response Testing of All Amino Acid Screen Hits..... 67
2.3.6 Drop-Out Screen with Validation Hits 71
2.3.7 Drop-Out Screen with TB Box Compound Hits 72
2.3.8 Restriction Free Cloning of Acetolactate Synthase (ALS) Catalytic and Regulatory Subunits 75
2.3.9 Overexpression of Acetolactate Synthase (ALS) Genes 78
2.3.10 Liquid Minimum Inhibitory Concentrations (MICs) of Hit Compounds. 81
2.3.11 Drug Resistant Mutant Generation 82
2.3.12 Overexpression of Drug Resistant Mutant *ilvB1* and *ilvN* in *M. smegmatis* mc^2155 83
2.4 Discussion 85

3 High-Throughput Screening, Microbiological Techniques, and Biochemical Assays for Identifying Novel Inhibitors of the Protein Synthesis Pipeline.....91

3.1 Introduction 91
3.2 Materials and Methods..... 98
3.2.1 Preliminary mCherry Reporter Screen Using *M. tuberculosis* Protein Synthesis Inhibitors 98
3.2.2 High Throughput Single Shot Screen of the GlaxoSmithKlein TB Box.. 98
3.2.3 High Throughput Dose Response Screen of the GlaxoSmithKlein TB Box 99
3.2.4 Protein Synthesis Hits Liquid Minimum Inhibitory Concentrations (MICs) 99
3.2.5 Protein Synthesis Hits Solid Minimum Inhibitory Concentration (MIC) 100
3.2.6 Protein Synthesis Hits Drug Resistant Mutant (DRM) Generation..... 100
3.2.7 Hit 45 and 46 Drug Resistant Mutant (DRM) Cross Resistance Tests .. 101
3.2.8 Producing Artificial *rpoABCZ* Operon by Gibson Cloning 101
3.2.9 Overexpression of *rpoABCZ* Operon in *M. smegmatis* mc^2155 and *M. bovis* BCG 102
3.2.10 Restriction Cloning for RNA Polymerase Purification 103
3.2.11 Purification of RNA Polymerase Holo Enzyme..... 105

3.2.12 SigA Expression Trial 105
3.2.13 Purification of *M. smegmatis* mc^{2}155 Ribosomes 106
3.2.14 RNA Amplification and Purification 107
3.2.15 Ribosome Inhibition Assay 108
3.2.16 RNA Polymerase Assay 108
3.3 Results 110
3.3.1 Proprietary Screen 110
3.3.2 Single Shot High-Throughput Screen of GSK TB Box Set 114
3.3.3 Dose-response Screen of Hit Compounds 117
3.3.4 Liquid Minimum Inhibitory Concentrations (MICs) of Hit Compounds in *M. bovis* BCG and *M. smegmatis* mc^{2}155 120
3.3.5 Solid Minimum Inhibitory Concentrations (MICs) of Hits in *M. bovis* BCG, *M. tuberculosis* H37Rv and *M. tuberculosis* H37Rv *ΔleuDΔpanCD* 125
3.3.6 Spontaneous Drug Resistant Mutant (DRM) Generation and Mutant Re-testing 129
3.3.7 Whole Genome Sequencing (WGS) of *M. tuberculosis* H37Rv Hit 45 and 46 Drug Resistant Mutants (DRMs) 131
3.3.8 Mapping Resistance Mutations onto RNA Polymerase structure 132
3.3.9 Overexpression of Artificial *rpoABCZ* Operon in *M. smegmatis* mc^{2}155 133
3.3.10 RNA Polymerase Purification 136
3.3.11 *M. smegmatis* Purified Ribosome mCherry Assay 140
3.3.12 Broken Beacon *E. coli* RNA Polymerase Holo-Enzyme Assay 142
3.4 Discussion 144
4 The Use of Biochemical Assays and Microbiological Techniques to Assess Potential Inhibitors of *M. tuberculosis* Antigen 85 151
4.1 Introduction 151
4.2 Materials and Methods 157
4.2.1 Antigen 85A and C2 Purification 157
4.2.2 Production of 4-Nitrophenyl-6-Octanoyl-β-D-Glucopyranoside 157
4.2.3 4-Nitrophenyl Standard Curve 159
4.2.4 β-Glucosidase Activity on 4-Nitrophenyl-6-Octanoyl-β-D-Glucopyranoside 159
4.2.5 β-Glucosidase Activity on 4-Nitrophenyl-6-Octanoyl-β-D-Glucopyranoside including Antigen 85C2 159

4.2.6 Resorufin Standard Curve 160
4.2.7 The Effect of Resorufin Butyrate on the Rate of Antigen 85C2 160
4.2.8 The Effect of Trehalose on the Rate of Antigen 85 C2 160
4.2.9 Resorufin Butyrate Assay for Inhibitors of Antigen 85A and C2 161
4.2.10 Radiometric Assay for Activity Assessment of Antigen 85 A and C2 .. 161
4.2.11 Radiometric Assay for Inhibitors of Antigen 85A 162
4.2.12 Arabinogalactan-Peptidoglycan Purification..... 163
4.2.13 C-12 Nitro-Benzoxadiazol Fluorometric Assay 163
4.2.14 Minimum Inhibitory Concentrations (MICs) of Antigen 85 Compounds.... 164
4.2.15 Overexpression of *fbpA* 164
4.2.16 Radioactive Cell Wall Labelling 165
4.2.17 Polar and Non-Polar Lipid Extraction 165
4.2.18 Fatty Acid Methyl Ester (FAMEs) and Mycolic Acid Methyl Ester (MAMEs) Extraction..... 167
4.2.19 Solid Minimum Inhibitory Concentration (MIC) of Antigen 85 Compound C4 168
4.2.20 Compound C4 Drug Resistant Mutant Generation 168
4.3 Results..... 169
4.3.1 Antigen 85A and C2 Protein Purification..... 169
4.3.2 Radiometric Enzyme Activity Assessment 171
4.3.3 Optimisation of β-Glucosiadse Antigen 85 Assay 172
4.3.4 Resorufin Butyrate Assay Optimisation..... 174
4.3.5 Resorufin Butyrate Assay for Antigen 85 Hits..... 177
4.3.6 Radiometric Assay for Antigen 85 A Inhibitors..... 179
4.3.7 Trehalose-C-12-Nitro-Benzoxadiazol Assay for Antigen 85A Hits 181
4.3.8 *FbpA* Overexpression 183
4.3.9 Liquid Minimum Inhibitory Concentrations (MICs) for *M. bovis* BCG 184
4.3.10 Polar and Non-Polar Lipid Profiling of *M. bovis* BCG Treated with Hits... 186
4.3.11 Fatty Acid Methyl Esters (MAMEs) and Mycolic Acid Methyl Esters (MAMEs) Profiling of *M. bovis* BCG Treated with Hits..... 194
4.3.12 Polar and Non-Polar Lipid Profiling of *M. bovis* BCG Containing *fbpA* Overexpression Plasmid 195
4.3.13 Fatty Acid Methyl Esters (FAMEs) and Mycolic Acid Methyl Esters (MAMEs) Profiling of *M. bovis* BCG Containing *fbpA* Overexpression Plasmid 197

4.3.14 Solid Minimum Inhibitory Concentration (MIC) of Compound C4 and Drug Resistant Mutant Generation 197
4.4 Discussion 199
5 Conclusion 206

6 General Materials and Methods 209

6.1 Chemicals and Reagents 209
6.2 Culture Media 209
6.2.1 Luria-Bertani broth 209
6.2.2 Luria-Bertani Agar 209
6.2.3 Middlebrook 7H9 Media 209
6.2.4 Middlebrook 7H11 Agar 210
6.2.5 2xYT Media 210
6.2.6 Terrific Broth 210
6.2.7 Brain Heart Infusion Broth 210
6.2.8 ZYM-5052 Autoinduction Media 210
6.2.9 1000x Trace Metal Solution 211
6.2.10 Tryptic Soy Broth 211
6.3 Bacterial Culture and Transformation 212
6.3.1 Culture of Bacterial Strains 212
6.3.2 Cell Number Estimation 212
6.3.3 Chemically Competent *E. coli* 213
6.3.4 Electrocompetent Mycobacteria 213
6.3.5 Transformation of Competent *E. coli* 213
6.3.6 Electroporation of Electrocompetent Mycobacteria 214
6.4 Molecular Biology Methods 214
6.4.1 Mycobacterial Genomic Extraction 214
6.4.2 Polymerase Chain Reaction 215
6.4.3 Agarose Gel Electrophoresis 216
6.4.4 DNA Extraction from Agarose Gel 216
6.4.5 PCR Clean Up 217
6.4.6 Restriction Digest of PCR Products and Plasmids 218
6.4.7 DNA Ligation Reaction 219
6.4.8 Extraction of Plasmid DNA from *E. coli* 219
6.5 Protein Biochemistry 220

6.5.1 Protein Expression and Purification 220
6.5.2 Buffer Exchange/Salt Removal using Dialysis 221
6.5.3 Hi-Trap Q HP Anion Exchange..... 221
6.5.4 Sodium Dodecyl Sulfate-Polyacrylamide Gel Electrophoresis..... 221
6.5.5 Western Blot..... 222
6.6 Microplate Techniques 222
6.6.1 Resazurin Survival Assays 222
6.6.2 Z' Calculation..... 223
6.6.3 Percentage Normalisation..... 223
6.7 Other Methods 224
6.7.1 Thin Layer Chromatography (TLC)..... 224
7 Appendix 225
8 References.....230

Figure List

Figure 1. Estimated tuberculosis (TB) incidence rates in 2018.

Figure 2. Estimated TB mortality in HIV negative individuals in 2018.

Figure 3. Percentage of previously treated cases with rifampicin resistant/multi-drug resistant tuberculosis (RR/MDR-TB).

Figure 4. Structure of streptomycin and kanamycin A.

Figure 5. Structure of isoniazid.

Figure 6. Formation of the isoniazid and nicotinamide adenine dinucleotide hydrogen (NADH) adduct.

Figure 7. Structure of nicotinamide and pyrazinamide.

Figure 8. Conversion of pyrazinamide to pyrazinoic acid by PncA.

Figure 9. Structure of ethambutol.

Figure 10. Structure of rifampicin and associated rifamycins.

Figure 11. Structures of fluoroquinolones.

Figure 12. Structures of polypeptide antibiotics.

Figure 13. Structure of *para*-aminosalicylic acid.

Figure 14. Structure of thioamides and triclosan.

Figure 15. Structures of D-cycloserine and terizidone.

Figure 16. Structure of β-lactams, meropenem and imipenem, with cilastatin additive.

Figure 17. Structures of clofazimine, lincomycin, and clarithromycin.

Figure 18. Structures of bedaquline, pretomanid, and linezolid.

Figure 19. KEGG pathway of *Mycobacterium tuberculosis* amino acid biosynthesis pathways.

Figure 20. Synthesis of branched chain amino acids (BCAA) and inhibitors.

Figure 21. Minimum inhibitory concentration (MIC) graphs for validation hits.

Figure 22. Rescue from validation hits using amino acid supplementation.

Figure 23. Single amino acid supplementation screen results.

Figure 24. All amino acids supplementation screen results.

Figure 25. Rescue from hits using amino acid supplementation.

Figure 26. Drop-out screen with validation hits.

Figure 27. Amino acid drop-out of hits.

Figure 28. Mega primer PCR.

Figure 29. Colony PCR of first gene insertion.

Figure 30. Colony PCR of second gene insertion.

Figure 31. Survival of *Mycobacterium bovis* BCG overexpressing acetolactate synthase (ALS) treated with metsulfuron-methyl (MSM).

Figure 32. Survival of *M. bovis* BCG overexpressing acetolactate synthase (ALS) treated with sulfometuron-methyl (SMM).

Figure 33. Minimum Inhibitory Concentration (MIC) graphs for hits.

Figure 34. The effect of overexpressing mutant acetolactate synthase (ALS) genes on the minimum inhibitory concentration (MIC) of metsulfuron- methyl (MSM) (A) and sulfometuron-methyl (SMM) (B).

Figure 35. Broken beacon RNA polymerase assay.

Figure 36. Proprietary protein synthesis pipeline inhibitor screen results.

Figure 37. Single shot 1 μM high-throughput screen.

Figure 38. Single shot 10 μM high-throughput screen.

Figure 39. Dose-response of 18 hit compounds.

Figure 40. Liquid Minimum Inhibitory Concentration (MICs) for hit compounds and control compounds in *M. bovis* BCG.

Figure 41. Liquid Minimum Inhibitory Concentration (MICs) for hit compounds and control compounds in *Mycobacterium smegmatis* mc^2155.

Figure 42. Solid Minimum Inhibitory Concentration (MICs) of hits 45 and 46 in *M. bovis* BCG.

Figure 43. Solid Minimum Inhibitory Concentration (MICs) for hits 9, 10, 11, 13, 17, and 18 in *M. tuberculosis* H37Rv.

Figure 44. Hit compound re-test of 45 and 46 mutants and cross-resistance with rifampicin.

Figure 45. Mutant retesting for hit compounds 10 and 17.

Figure 46. *M. tuberculosis* RNA polymerase and RpoB inhibitors.

Figure 47. Overexpression of *rpoABCZ* Operon in *M. smegmatis* mc^2155.

Figure 48. RNA polymerase expression trial.

Figure 49. His-tag purification of RNA polymerase holo-enzyme.

Figure 50. SigA expression trial.

Figure 51. *M. smegmatis* ribosomal inhibition assay.

Figure 52. *E. coli* RNA polymerase holo-enzyme broken beacon inhibition assay**.**

Figure 53. Antigen 85 radioactive assay.

Figure 54. Antigen 85 β-glucosidase assay.

Figure 55. Antigen 85 resorufin butyrate assay.

Figure 56. Antigen 85 trehalose-C-12-nitro-benzoxadiazol (NBD) assay.

Figure 57. Protein gels of Antigen 85A purification.

Figure 58. Protein gels of Antigen 85C2 purification.

Figure 59. Thin layer chromatography (TLC) and scintillation counts of purified Antigen 85A and C2 activity.

Figure 60. Standard curve of 4-nitrophenyl.

Figure 61. Rate of reaction comparison with and without Antigen 85C2.

Figure 62. Resorufin standard curve.

Figure 63. Rates of reaction with different substrate concentrations.

Figure 64. Michaelis-Menten curves for resorufin butyrate and trehalose.

Figure 65. Resorufin butyrate assay with hits.

Figure 66. Thin layer chromatography (TLC) and scintillation counts of Antigen 85A activity with hits.

Figure 67. Trehalose-C-12-nitro-benzoxadiazol (NBD) assay results.

Figure 68. Antigen 85A (*FbpA*) overexpression in *M. bovis* BCG.

Figure 69. Minimum inhibitory concentration (MIC) for Antigen85A hits.

Figure 70. Thin-layer chromatography (TLC) of non-polar lipids run and system A.

Figure 71. Thin-layer chromatography (TLC) of non-polar lipids run and system B.

Figure 72. Thin-layer chromatography (TLC) of non-polar lipids run and system C.

Figure 73. Thin-layer chromatography (TLC) of non-polar lipids run and system D.

Figure 74. Thin-layer chromatography (TLC) of polar lipids run and system D.

Figure 75. Thin-layer chromatography (TLC) of polar lipids run and system E.

Figure 76. Thin-layer chromatography (TLC) of FAMEs and MAMEs.

Figure 77. Thin-layer chromatography (TLC) of polar and non-polar lipid analysis and systems A to E.

Figure 78. Thin-layer chromatography (TLC) of FAMEs and MAMEs.

Figure 79. Solid Minimum Inhibitory Concentration (MIC) of hit C4 in *M. tuberculosis* H37Rv.

Figure 80. *M. tuberculosis* H37Rv *ΔleuDΔpanCD* drug resistant mutants to compound C4.

Table List

Table 1. First line treatments for drug susceptible TB.

Table 2. Drug-groupings for drug-resistant TB treatment.

Table 3. Primers used for restriction free cloning of acetolactate synthase (ALS) genes.

Table 4. Primers for *ilvB1* cloning into pMV261a.

Table 5. Wild type plasmids electroporated into *M. bovis* BCG.

Table 6. Wild type and mutant plasmids electroporated into *M. bovis* BCG and *M. smegmatis* mc^2155.

Table 7. Minimum Inhibitory Concentration (MIC) values for validated hits and mycobacterial species tested.

Table 8. Percentage difference data and compound plate designations for hits.

Table 9. Minimum Inhibitory Concentration (MICs) for hits.

Table 10. Whole genome sequencing (WGS) data of *M. bovis* BCG mutants to metsulfuron-methyl (MSM) and sulfometuron-methyl (SMM).

Table 11. Primers for *rpoABCZ* operon Gibson cloning.

Table 12. Primers and restriction enzymes for cloning RNA polymerase.

Table 13. Selection antibiotic for plasmids.

Table 14. Conditions in expression trial.

Table 15. TAMRA and BHQ2 oligonucleotides.

Table 16. Liquid minimum inhibitory concentrations (MICs) established for *M. bovis* BCG and *M. smegmatis* mc^2155.

Table 17. Solid minimum inhibitory concentrations (MICs) established for *M. bovis* BCG, *M. tuberculosis* H37Rv and *M. tuberculosis* H37Rv *ΔleuDΔpanCD.*

Table 18. Whole genome sequencing (WGS) data of hit 45 and 46 resistant mutants.

Table 19. Thin-layer chromatography (TLC) solvent systems for polar and non-polar lipid analysis.

Table 20. 1000x trace metal solution mixture.

Table 21. Thermocycling conditions for routine PCR.

Table 22. Cut sites of NEB restriction enzymes.

Table 23. Letter designation and structures of hit compounds from Section 3.3.1.

Table 24. Number designation and structures of hit compounds from Section 3.3.3.

Abbreviation List

ADC	Albumin, Dextrose, Catalase
ALS	Acetolactate Synthase
aPBP	Class A Penicillin Binding Proteins
BCAA	Branched Chain Amino Acid
BCG	Bacillus Calmette-Guérin
BHI	Brain Heart Infusion
BHQ2	Black Hole Quencher 2
CFP10	Culture Filtrate Protein 10
Da	Dalton
DMSO	Dimethyl Sulfoxide
DNA	Deoxyribonucleic Acid
DOTS	Directly Observed Treatment Short-Course
DPA	Decaprenyl Phosphoryl-d-Arabinose
DRM	Drug Resistant Mutants
DTT	Dithiothreitol
EF-Tu	Elongation Factor Thermo Unstable
ELISA	Enzyme-Linked Immunosorbent Assay
ELISS	Enzyme-Linked Immunosorbent Spot
ESAT6	Early Secreted Antigenic Target 6
FAMEs	Fatty Acid Methyl Esters
g	Gram
GSK	GlaxoSmithKlien
HIV	Human Immunodeficiency Virus

IGRA	Interferon Gamma Release Assay
INH	Isoniazid
IPTG	IsoPropyl β-d-1-ThioGalactopyranoside
kDa	Kilo Dalton
L	Litre
LAM	Lipoarabinomannan
LB	Luria-Bertani
LF-LAM	Lateral Flow Lipoarabinomannan
LM	Lipomannan
M	Molar
mDAP	*Meso*-Diaminopimelate
MDR-TB	Multi-Drug Resistant Tuberculosis
mg	Milli Gram
MIC	Minimum Inhibitory Concnetration
mL	Milli Litre
mM	Milli Molar
mMol	Milli Moles
Mol	Moles
MPI	Mannosyl Phosphate Inositol
mRNA	Messenger Ribonucleic Acid
MSM	Metsulfuron-Methyl
MAMEs	Mycolic Acid Methyl Esters
NADH	Nicotinamide Adenine Dinucleotide
NBD	Nitro-Benzoxadiazol
NEB	New England Biolabs

ng	Nano Gram
nL	Nano Litre
nm	Nano Meter
nM	Nano Molar
nMol	Nano Moles
NTM	Non-Tubeculosis Mycobacteria
OADC	Oleic Acid, Albumin, Dextrose, Catalase
OD600	Optical Density at 600 nm
PAS	*Para*-Aminosalicylic Acid
PBP	Penicillin Binding Protein
PCR	Polymerase Chain Reaction
pH	Power of Hydrogen
PI	Phosphatidyl-*myo*-Inositol
PIM	Phosphatidyl-*myo*-Inositol Mannoside
PKS13	Polyketide Synthase 13
pM	Pico Molar
pMol	Pico Moles
PPM	Polyprenyl-Phosphate-Mannopyranose
PZA	Pyrazinamide
RIF	Rifampicin Resistant Tuberculosis
RNA	Ribonucleic Acid
RRF	Ribosome Recycling Factor
rRNA	Ribosomal Ribonucleic Acid
RR-TB	Rifampicin Resistant Tuberculosis
RUT	Rho Utilization

SD	Shine-Dalgarno
SDS	Sodium Dodecyl Sulfate
SDS-PAGE	Sodium Dodecyl Sulfate-Polyacrylamide Gel Electrophoresis
SMM	Sulfometuron-Methyl
TB	Tuberculosis
TBS	Tris Buffered Saline
TBST	Tris Buffered Saline with 0.05 % Tween 20
TDM	Trehalose Di-Mycolate
TDR-TB	Totally Drug Resistant Tuberculosis
TLC	Thin Layer Chromatography
TMM	Trehalose Mono-Mycolate
TMS	Trimethylsilyl
tRNA	Transfer Ribonucleic Acid
TSB	Tryptic Soy Broth
v/v	Volume per Volume
w/v	Weight per Volume
WHO	World Health Organisation
XDR-TB	Extensivly Drug Resistant Tuberculosis
ZN	Ziehl-Neelsen
µg	Micro Gram
µL	Micro Litre
µm	Micro Meter
µM	Micro Molar
µMol	Micro Moles

Published work associated with this thesis

Burke, C., Abrahams, K., Richardson, E., Loman, N., Alemparte, C., Lelievre, J., and Besra, G. S. Development of a whole-cell high-throughput phenotypic screen to identify inhibitors of mycobacterial amino acid biosynthesis. *FASEB BioAdvances* **1**, 246–254 (2019).

Burke, C., Jankute, M., Moynihan, P., Gonzalez del Rio, R., Li, X., Esquivias, J., Lelievre, J., Cox, J., Sacchettini, J., Besra, G. S. Development of a novel secondary phenotypic screen to identify hits within the mycobacterial protein synthesis pipeline. *FASEB Bioadvances*, 1-13 (2020).

Chapter 1

General Introduction

1 General Introduction

1.1 *Mycobacteria* and related genus

Mycobacterium tuberculosis is an incredibly successful pathogen that is responsible for causing human tuberculosis (TB). Taxonomically, *M. tuberculosis* falls into the *Actinobacteria* phylum, a large collection of Gram-positive bacteria with high-GC DNA content located in both aqueous and terrestrial environments, with a high prevalence in soil environments[1]. *Mycobacteria* are located within the order of *Actinomycetales* first outlined in 1916 as bacteria that display filamentous, branching growth in a mould like fashion[2]. The sub-order *Corynebacterineae* contains the *Mycobacteriaceae* family of which *Mycobacterium* is the only genus[3]. As well as containing the genus *Mycobacteria*, the phylum *Actinobacteria* and the order *Actinomycetales* also contains other notable bacterial genus, such as *Streptomyces* and *Corynebacterium*[1]. *Streptomyces* species are of high importance due to their prolific production of antibiotics[4] and *Corynebacterium* species are used in the production of amino acids, are frequently used as a model organism for TB research, and cause opportunistic infections[5].

There are currently 192 *Mycobacteria* species identified and validated as published in the List of Prokaryotic names with Standing in Nomenclature when accessed on the 11/05/2020[6–8]. These species are split into two categories, fast-growing species and slow-growing species[9]. Slow-growing species are defined as taking seven days or longer to grow on solid agar medium, while fast-growing species take less than seven days[10]. The fast-growing species are currently split into six groupings. These include *Mycobacterium fortuitum*, *Mycobacterium smegmatis*, the *Mycobacterium chelonae*/*Mycobacterium abscessus* complex, *Mycobacterium mucogenicum*, *Mycobacterium mageritense*/*Mycobacterium wolinskyi*, and the pigmented fast-growing species[11]. Mycobacteria species are also split into two different groups based upon the type of

disease caused. They are split into the tuberculosis causing *Mycobacterium tuberculosis* complex[12] and the non-tuberculosis mycobacteria (NTM)[13]. NTMs have a sub-category of organisms referred to as the *Mycobacterium avium* complex[14]. The separation of these groups is important due to differences in treatment regimen[12]. The *Mycobacterium tuberculosis* complex includes *M. tuberculosis*, *Mycobacterium bovis*, *Mycobacterium africanum*, *Mycobacterium microti*, *Mycobacterium canetti*, *Mycobacterium caprae*, *Mycobacterium pinnipedii*, *Mycobacterium orygis* and *Mycobacterium mungi*[15–21].

Mycobacteria are acid-fast, Gram-positive and rod-shaped bacilli[22]. They are described as acid-fast because staining methods to visualise the bacterium must use a high concentration of acid for decolourisation[23]. This is due to the unique lipid rich composition of the outer cell wall. Composed of long chain fatty acids up to 90 carbon atoms in length, they are covalently attached to the arabinogalactan-peptidoglycan framework of the cell wall and this enhanced cell wall structure constitutes a major hydrophobicity barrier to not only cell stains, but also antibiotics[24].

1.2 Tuberculosis - a Historic Disease

TB is an ancient scourge of great apes from before the dawn of human civilisation. Approximately 3 million years ago, hominids in eastern Africa were likely infected by a progenitor of *M. tuberculosis*[25]. Indeed, evidence suggests that the *Mycobacterium* genus may date back as far as the Jurassic period before the break-up of the Pangaean supercontinent[26]. Fossilised skull fragments indicate that TB infected *Homo erectus* approximately 500,000 years ago[27] and modern *M. tuberculosis* may have emerged around 20,000-15,000 years ago due to a genetic bottleneck[28,29]. Lipid biomarkers indicate that there were TB infected individuals in the eastern Mediterranean 9,000 years ago[30] and there is DNA evidence for the presence of TB in Egypt in 3,000 BC[31].

In ancient Greece, TB was known as phthisis. Hippocrates described phthisis in detail in *Of the Epidemics, Book 1* and noted that most people died[32]. Isocrates later suggested that phthisis was an infectious disease, in contrast to Hippocrates, whom suggested the disease was inherited and Aristotle suggested the infectious nature of scrofula[33]. In the middle ages scrofula became known as King's Evil, this was due to the belief that the disease could be cured with a Royal touch. It was not until much later that phthisis and scrofula were connected in 1679 by Sylvius de la Boë, a physician in Amsterdam, in his book *Opera Medica*[34]. In addition, Sylvius de la Boë detailed that TB caused lung lesions that often progressed to cavitation[34]. Benjamin Marten suggested in 1720, in a book entitled, *A New Theory of Consumptions, More Especially of a Phthisis or Consumption of the Lungs*, that TB might be caused by animalcules living inside the lesions[35]. In 1779, the spinal form of TB was described by Percival Pott, leading to the naming of this variant as Pott's disease[36]. Bizarrely, in the 19th century TB became a somewhat romanticised and fashionable disease with the poet, Lord Byron stating 'I should like, I think, to die of a consumption'[37].

In 1882, the landmark discovery that *M. tuberculosis* is the infectious agent responsible for TB was outlined by Robert Koch in a lecture named *Die Aetiologie der Tuberculose*[22], ultimately proving Benjamin Marten correct. By using methylene blue, Koch could visualise rod shaped bacilli in isolates from TB infected animals. Koch proved that this bacillus was the cause of TB by culturing the bacterium on dried bovine blood serum slopes and then using the scaly colonies that grew to infect guinea pigs. These guinea pigs quickly became infected with TB and thus *M. tuberculosis* was discovered.

In the 18th century Edward Jenner heard a claim from a dairy-maid stating, 'I shall never have smallpox for I have had cow pox'. This would eventually lead to his world changing discovery of a vaccine for smallpox and the diseases subsequent eradication[38]. In the 20th

century, Albert Calmette and Camille Guérin were attempting to culture *M. tuberculosis* but faced issues with cell clumping. They treated the cells with ox bile to reduce the clumping, but also noted that this reduced virulence and prompted an idea for a TB vaccine[39,40]. This led to them procuring a strain of *Mycobacterium bovis* and sub-culturing the bacteria approximately 230 times on their bile, glycerine, and potato media. After 11 years of culturing they tested the bacteria by injecting animals, which did not develop progressive TB[40]. The vaccine was latter named Bacille Calmette-Guérin, the BCG vaccine. The BCG vaccine has been the subject of much scrutiny since its introduction and has debateable efficiency in preventing TB[41]. No clear benefit to vaccination has ever been proven and additionally the BCG vaccine can interfere with the tuberculin skin test in up to 80% of cases leading to false positive individuals[42].

The 20th century also saw the discovery of the first antibiotic for treating TB, streptomycin in 1944[43]. Shortly after *para*-aminosalicylic acid was discovered in 1946[44,45]. In 1952 isoniazid and pyrazinamide were discovered[46,47]. Ethambutol was discovered in 1961[48] and rifampicin was designed in 1965[49,50]. The 20th century culminated with the publishing of the whole genome sequence of *M. tuberculosis* H37Rv by Cole *et al*, bringing TB research into the modern era[51].

1.3 Tuberculosis Epidemiology

In 1993, TB was declared a global health emergency by the World Health Organisation (WHO), but TB is still the biggest cause of death from a single infectious agent today. In 2018, between 9 million and 11.1 million people acquired TB[52]. These numbers have remained stable over the past few years[53,54]. There were approximately 1.45 million deaths from TB in HIV-positive and negative-individuals combined[52]. TB disproportionately affects South-East Asia, Africa and the Western Pacific, with these regions accounting for 86 % of the worlds TB cases[52]. As illustrated in Figure 1, the map

shows rates of newly diagnosed TB in 2018. Eight countries accounted for 67 % of global cases. These countries are: India (27 %), China (9 %), Indonesia (8 %), the Philippines (6 %), Pakistan (6 %), Nigeria (4 %), Bangladesh (4 %) and South Africa (3 %)[52]. The highest mortality rates for TB are found in the southern half of the African continent, as shown in Figure 2. The current treatment success rate for TB without any confounding factors is 85 %.

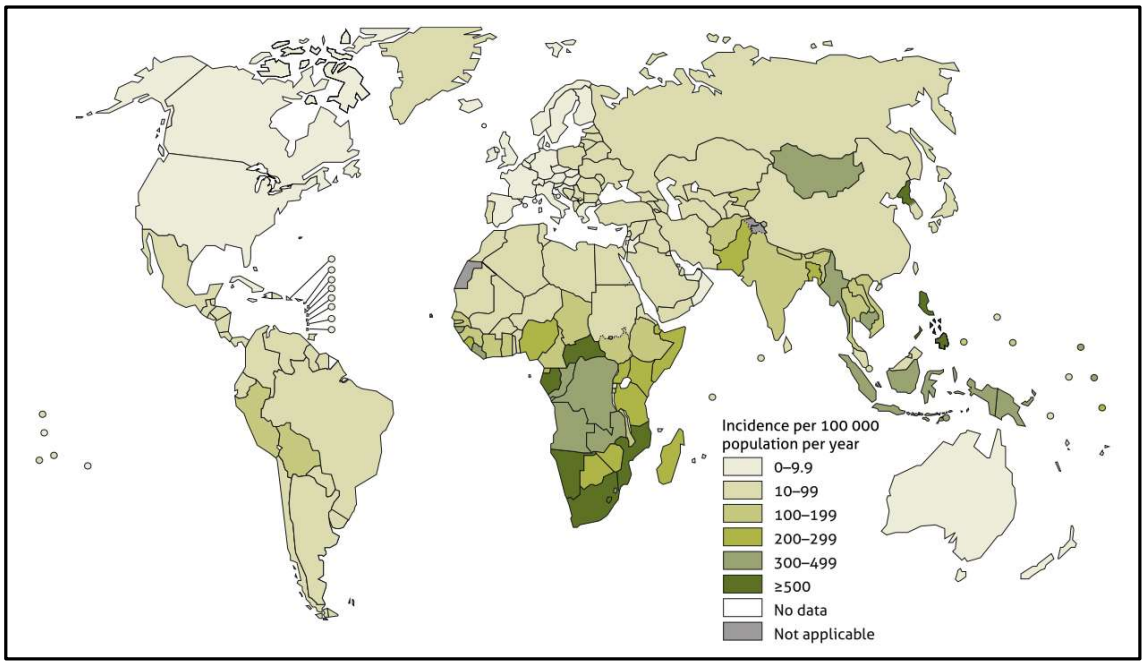


Figure 1. Estimated TB incidence rates in 2018[52].

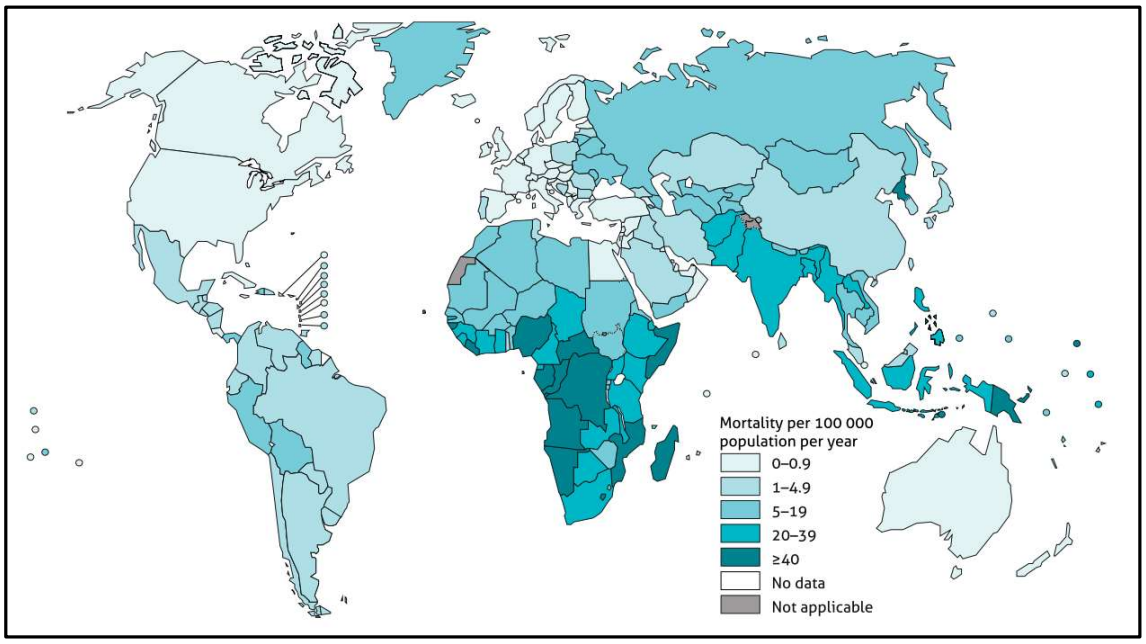


Figure 2. Estimated TB mortality in HIV negative individuals in 2018[52].

Name a more iconic duo, *M. tuberculosis* and Human Immunodeficiency Virus (HIV), co-infection account for 8.6 % of global TB cases[52]. In some areas of Southern Africa, TB and HIV co-infections can account for up to 50 % of cases. Individuals infected with HIV are 19 times more likely to develop an active TB infection over HIV negative individuals[52]. One third of deaths attributed to HIV/AIDS, are through co-infection with TB, accounting for 250,000 deaths. The treatment success rate for TB and HIV co-infection is 75 %.

In 2018, 3.4 % of new TB cases were rifampicin resistant TB (RR-TB) or multi-drug resistant TB (MDR-TB). MDR-TB is defined as TB cases resistant to rifampicin and isoniazid. There were an estimated 484,000 new cases of RR/MDR-TB. The WHO estimates that up to 78 % of RR-TB cases could be MDR-TB. In some countries of the former Soviet Union, 50 % or more of previously treated cases were classified as RR/MDR-TB as shown in Figure 3. In 2018 cases of extensively drug resistant TB (XDR-TB) had been confirmed by 131 countries. XDR-TB is an infection that is resistant to

rifampicin, isoniazid, one fluoroquinolone antibiotic, and one of either amikacin, capreomycin or kanamycin. Approximately 6.2 % of MDR-TB cases could be XDR-TB. RR/MDR-TB only has a treatment success rate of 56 % and XDR-TB has an even lower success rate of 39 %. The increasing prevalence of these highly resistant forms of TB infection underline the need for discovery and development of new drugs for novel targets. Worryingly, reports have been increasing of totally drug resistant TB (TDR-TB). Several cases from Italy[55], Iran[56], India[57,58], and South Africa[59] have reported TB infections resistant to all drugs available. The WHO does not currently recognise TDR-TB, and classifies these cases as XDR-TB[60].

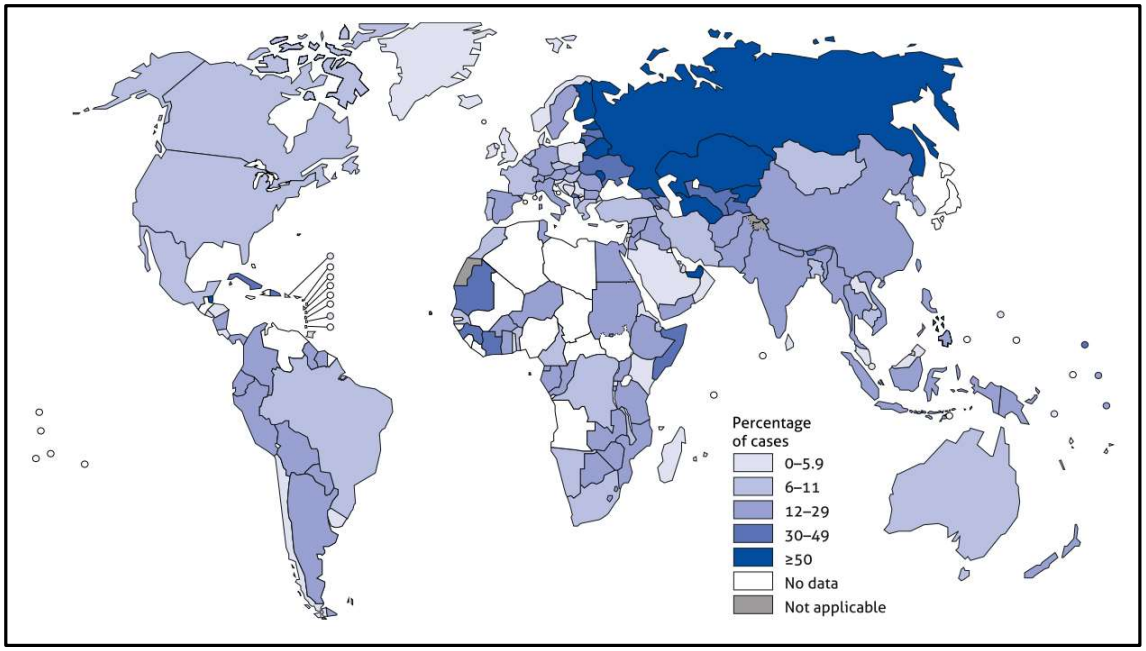


Figure 3. Percentage of previously treated cases with rifampicin resistant/multi-drug resistant tuberculosis (RR/MDR-TB)[52].

1.4 Clinical Presentation of Tuberculosis

TB is a chronic infection most commonly presenting as a pulmonary infection, however active disease cases are surprisingly low with only 10 % of infected individuals developing TB with the rest developing a latent infection[61]. In a latent infection a person

displays no outward signs of infection. The only way to know if someone is latently infected is by testing an individual's immune response. Pulmonary TB presents with symptoms traditionally associated with pulmonary disease[62]. The most common symptoms are coughing (72.8 %), fatigue (59.7 %) and fever (52.3 %)[63]. There are also a range of less common symptoms, such as weight loss, sweats, anorexia, chest pain, diarrhoea and haemoptysis[63].

Mycobacterial cervical lymphadenitis, also known as scrofula and King's evil, is a mycobacterial infection of the neck lymph nodes and the most common presentation of extra-pulmonary TB[64]. Symptoms common to TB are present in scrofula, such as fatigue, fever, weight loss and night sweats[64,65]. Symptoms unique to scrofula are large firm painless masses[64] or ulcerations[65] in the neck from infected lymph nodes. The excision of the lymph nodes is not recommended[64]. The second most common form of extra-pulmonary TB is pleural TB, an infection in the pleural lining of the lungs[64]. In addition to standard TB symptoms, individuals will suffer from pleuritic chest pain and a non-productive cough[66]. Chest X-ray shows unilateral pleural effusion and thickening of the pleura[64]. Miliary TB is characterised by disseminated lesions of small diameter present throughout the body, usually concentrated in organs, such as either the liver, pancreas or spleen[67] and in rarer cases can cause meningitis[68]. Many symptoms are congruous with that of other TB infections with the additional symptoms of failing organ systems with a high burden of lesions[67]. Cutaneous[69] and ocular[70] lesions are not uncommon and can be valuable for diagnosis. Skeletal and joint TB, most famously Pott's disease, is a form of vertebral TB, is characterised by a slow onset of symptoms mostly resulting in symptoms of osteomyelitis and arthritis accompanied by traditional TB symptoms[64]. The slow onset of Pott's disease results in a high degree of neurological symptoms, such as either bone deformities, granulation tissue or abscesses which compress the spinal cord[71]. Nearly all

cases of Pott's disease display spinal curvature which can persist after successful treatment[71].

1.5 Pathogenesis

TB is transmitted by aerosolisation of droplets containing the *M. tuberculosis* bacillus and the inhalation of the droplets by another individual. The aerosolisation can occur from coughing, sneezing and even talking. TB infection often occurs across two stages known as primary TB and secondary (post-primary) TB[72]. Primary TB is the first exposure to *M. tuberculosis* and usually occurs in the lungs[73]. Due to the low number of bacilli required to initiate a primary infection it can often be removed by the innate immune system alone without inducing a response from the adaptive immune system[74]. In the event that the infection is not cleared, but controlled, the infection becomes latent. Latency is when the immune response is sufficient to control but not eradicate the infection. In this state, the bacteria and the infection persist, there is a constant state of immune control with no symptoms or transmissibility[75].

In a pulmonary infection, a caseating locus of infection, a granuloma termed a Ghon's focus, is often formed in the upper lung lobes near the lobe interface. Alveolar macrophages and dendritic cells engulf and carry the bacteria into the parenchyma of the lung and to nearby lymph nodes disseminating the infection[76]. In an innate immune system driven process, macrophages are recruited and a granuloma is formed around the locus of infection. As the granuloma grows the centre begins to caseate[77]. The primary locus of infection and the infected lymph nodes are referred to as Ghon's Complex[73]. While the Ghon's complex is most commonly found in the lungs, a primary TB infection can occur almost anywhere including; the mucosa of the oral cavity[78], tongue[79] and tonsils[80], skin[81] and soft tissue[82], brain[83], breast[84], gastrointestinal tract[85] and liver[86], and bones[87].

A failure to control the infection leads to a more serious progressive primary infection. If the primary infection is controlled by the immune system, then the infection becomes a latent infection. An infection is described as latent when the individual is infected with a stable number of *M. tuberculosis* bacilli but displays no outward signs or symptoms in addition to being non-infectious[88]. Most *M. tuberculosis* infections result in latent infection[61]. Latency is being viewed, increasingly, as a delicate interplay between various levels of microbial activity and different immune responses[75]. The longer an infection spends in the latent phase the lower the chances of the infection reactivating and causing a secondary TB disease state. Secondary TB is a reactivation or reinfection when the immune system has been primed to recognise *M. tuberculosis* in the past[72]. Secondary TB results in the characteristic formation of cavities in the lungs when necrotic tissue is expelled *via* coughing. The cavities result in the release of large amounts of active bacillus from the individual and are responsible for most of the disease spread.

1.6 Diagnosis of Tuberculosis

Until recently the diagnosis of TB has been difficult and time consuming. This is due to the slow growth of *M. tuberculosis*. If a suspected case could not be identified using microscopy or the tuberculin test, then the only option was the culture of *M. tuberculosis* on Lowenstein-Jensen media[89] from sputum samples. The appearance of colonies on the media was used as diagnostic proof of infection but colonies can take weeks to grow. Drug sensitivity testing still relies heavily on bacterial culture to detect phenotypic changes to growth. Liquid culture allows faster determination of resistance than solid media. While some genotypic methods have been developed for identifying resistance to first line antibiotics, resistance to second line antibiotics must still be detected with phenotypic culture techniques. The gold standard for drug sensitivity testing for resistance to second line antibiotics is liquid bacterial culture[90].

The analysis of sputum samples using staining and microscopy greatly reduces the time for diagnosis. The stain of choice for diagnostic TB microscopy is the Ziehl-Neelsen (ZN) stain. Cheap and readily available in most healthcare laboratories the ZN stain colours the *M. tuberculosis* bacillus a bright red/pink colour which is highly visible in the sputum sample. In samples with a low level of bacilli, ZN staining may not be conclusive and false negatives are possible[90]. Around 5000 bacilli per mL are required in sputum as the sensitivity for this diagnosis is low. Additionally, distinguishing between different mycobacterial species is not possible. The WHO currently suggests that examination of two adequate sputum samples is able to identify 95-98 % of TB positive patients[90].

The tuberculin skin test is used to assess an individual's immune response to *M. tuberculosis.* The tuberculin skin test works on the basis of a delayed hypersensitivity reaction where T-cells primed in a previous exposure recognise the purified protein derivative (PPD) injected[91]. Upon recognition of the tuberculin, T-cells release signalling lymphokines to initiate an immune response. The immune response causes a localised induration to appear at the site of the injection between 24-72 hours[92]. The diameter of the induration is measured and when combined with information about the patient can be used to determine if a person has been exposed to a mycobacterial species[92]. There are a plethora of downsides to the tuberculin skin test, mostly based around the many factors that can influence the results. Even a correctly interpreted test does not necessarily indicate the individual is currently infected with *M. tuberculosis.* Prior exposure to NTMs and immunisation with the BCG vaccine can lead to false positive results. A new TB infection or a very old infection can read as a false negative[92].

Chest X-rays have been a standard tool for TB diagnostics for many years. The ability of X-rays to pick up abnormalities in the lungs makes this technique very sensitive for TB. However, many of the presentations of TB may also appear similar to other diseases of

the lung and combined with the qualitative nature of X-ray data, makes X-rays vulnerable to misinterpretation and false diagnosis. The WHO insists that X-rays not be used alone for diagnosis and be combined with bacterial identification techniques[93].

PCR based methods are seeing increasing use for TB diagnosis. The speed and sensitivity of PCR techniques is much greater than any other testing method. Line-probe[94] and GeneXpert MTB/RIF assays[95] can be used for detection of *M. tuberculosis* and can also identify the most common resistance conferring mutations for rifampicin and isoniazid. The short comings of these systems are that resistance to second line antibiotics is much more varied, as such these methods are not appropriate for second line drug sensitivity testing[90].

Interferon gamma release assays (IGRA) are an *in vitro* blood test that uses proteins, such as Early Secreted Antigenic Target 6 (ESAT6) and Culture Filtrate Protein 10 (CFP10), to stimulate T cells in blood samples. These proteins are specific to bacilli in the *M. tuberculosis* complex, excluding *M. bovis* BCG[96]. The interferon gamma released by T cells is measured *via* either an enzyme-linked immunosorbent assay (ELISA) using QuantiFERON Gold tests or an enzyme-linked immunosorbent spot (ELISS) in T-SPOT.TB tests[97]. The lack of ESAT6 and CFP10 expressed by *M. bovis* BCG means that IGRA tests are able to identify individuals with latent TB infection that have been previously immunised with BCG[96]. The specificity of the IGRA test has been reported to be >93 % and the sensitivity >70 %. Of the two commercial tests available, QuantiFERON Gold has higher specificity, and T-SPOT.TB has higher sensitivity[98]. IGRA tests are currently used for diagnosis of latent TB infection in high-income countries with a low TB and HIV burden, they are not currently recommended by the WHO for middle/low-income countries with a high TB and HIV burden[99].

Lateral flow lipoarabinomannan (LF-LAM) testing methods for patients co-infected with TB and HIV are currently being developed. One of the newest developments is an improved method for the detection of LAM in the urine of patients. This method uses a pair of antibodies highly specific for LAM, one bound to the test strip, the other conjugated to a small gold bead. The primary gold bead labelled antibody is added to the urine sample and then washed over the test strip with the second antibody. This immobilises the LAM and gold bead labelled antibody to the test strip. The gold bead then undergoes silver amplification to increase the size and visibility of the bead[100]. The WHO currently recommends that lateral flow LAM only be used for seriously ill HIV positive patients with a CD4 cell count of <100 cells/μL[101]. This policy has not yet been updated with recommendations based upon this new method.

1.7 Treatment of Tuberculosis

The standard treatment regime for new cases of drug sensitive TB, called Directly Observed Treatment Short-Course (DOTS), is a long process requiring four drugs, ethambutol, isoniazid, pyrazinamide and rifampicin over a period of six months. The initial intensive phase of treatment uses all four drugs for a period of two months with the remaining four months utilising only isoniazid and rifampicin[102]. For relapsed patients, that have a confirmed drug sensitive infection, the treatment is altered to use all five first line drugs[102].

Table 1. First line treatments for drug susceptible TB. H, Isoniazid. R, Rifampicin. Z, Pyrazinamide. E, Ethambutol. S, Streptomycin.

Infection Type	Drug Sensitivity	Phase 1	Phase 2	Phase 3
New Infection	Sensitive	HRZE (2 Months)	HR (4 Months)	N/A
Recurrent Infection	Sensitive	HRZES (1 Month)	HRZE (1 Month)	HRE (1 Month)

The treatment plan for drug resistant TB functions differently with drugs split into hierarchical groups of effectiveness and patient safety. Four principals are followed for designing a patient's custom treatment regime. Firstly, at least four drugs must be used in combination for treatment and the infection must be tested for sensitivity. Secondly, the drugs used cannot have any form of cross-resistance. For example, two rifamycin class drugs could not be used together. Thirdly drugs, which are not safe for the patient, cannot be used. Finally, drugs must be used from lower groupings preferentially.

Table 2. Drug-groupings for drug-resistant TB treatment. Adapted from information present in WHO 2019 documentation[103].

Group	Drugs
Group A: Include all three drugs if possible.	Levofloxacin/Moxifloxacin
	Bedaquiline
	Linezolid
Group B:	Clofazimine
	Cycloserine/Terizidone
Group C: Only to be used when a treatment regime cannot be completed with group A or B drugs.	Ethambutol
	Delamanid
	Pyrazinamide
	Imipenem and Cilastatin/Meropenem
	Amikacin/Streptomycin
	Ethionamide/Prothionamide
	Para-Aminosalicylic Acid

1.7.1 Streptomycin and Aminoglycosides

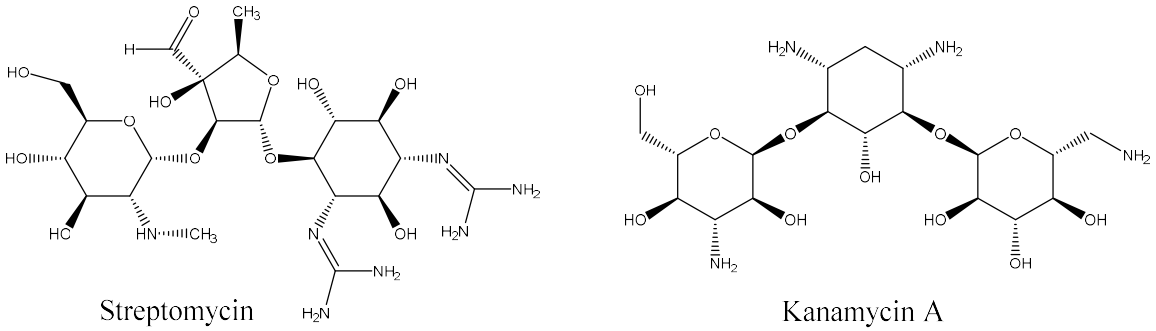


Figure 4. Structure of streptomycin and kanamycin A.

Streptomycin, an aminoglycoside antibiotic, was discovered in 1944 when it was isolated from *Actinomyces griseus*[43]. Streptomycin was found to be active against TB soon after its discovery, however, in the same study extremely high levels of resistance were reported in some clinical isolates, with some being up to 8000-times more resistant than *M. tuberculosis* H37Rv[104].

Aminoglycosides inhibit protein synthesis by binding to the ribosome and impairing the proofreading function of the ribosome resulting in truncated or defective protein production[105,106]. Streptomycin binds between the 50s and 30s subunits of the 70s ribosome to the 30s ribosome subunit[107]. This does not interfere with the binding of formyl-methionyl-tRNA or prevent translation initiation or mRNA binding, but does interfere with the ribosomal proof reading allowing the incorporation of non-cognate amino acids[108,109]. X-ray crystallography data of streptomycin bound to the 30s ribosome shows a distortion of the 16s rRNA. Lateral displacement of nucleotides A1492 and A1493 reduces the GTPase activity for elongation factor thermo-unstable (EF-Tu) with cognate tRNA and increases the GTPase activity for EF-Tu with non-cognate tRNA[110]. This results in similar levels of GTPase activity for cognate and non-cognate tRNA meaning that the ability to discriminate the addition of non-cognate tRNA is lost.

Resistance to streptomycin can occur in the 16s rRNA found in the 30s subunit, encoded by the *rrs* gene or in protein S12 found in the 30s subunit, encoded by *rpsL*[111]. Additionally, mutations in *gidB*, a rRNA methyltransferase, can confer low levels of resistance[111]. The mutations may cause a change in methylation at position G518 in the 530 stem loop of the 16s rRNA which interferes with streptomycin binding[112]. Also mutations in Rv1258c, an efflux pump, can increase levels of resistance[111] as it has been shown that this pump can export streptomycin[113].

1.7.2 Isoniazid

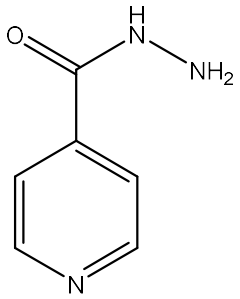


Figure 5. Structure of isoniazid.

In 1951 pharmaceutical company Roche tested several chemical scaffolds containing pyridine rings for the treatment of TB. A couple of the compounds, most notably isonicotinaldehyde thiosemicarbazone, showed anti-TB activity[114]. This led to the development of isonicotinic acid hydrazide or isoniazid (INH) in 1952[46]. In clinical trials INH was shown to rapidly improve the health of patients, with a reduction in coughing, weight gain, and improved lung health. During the clinical trial there were no deaths caused by progression of the disease and all patients saw an improvement in condition[115].

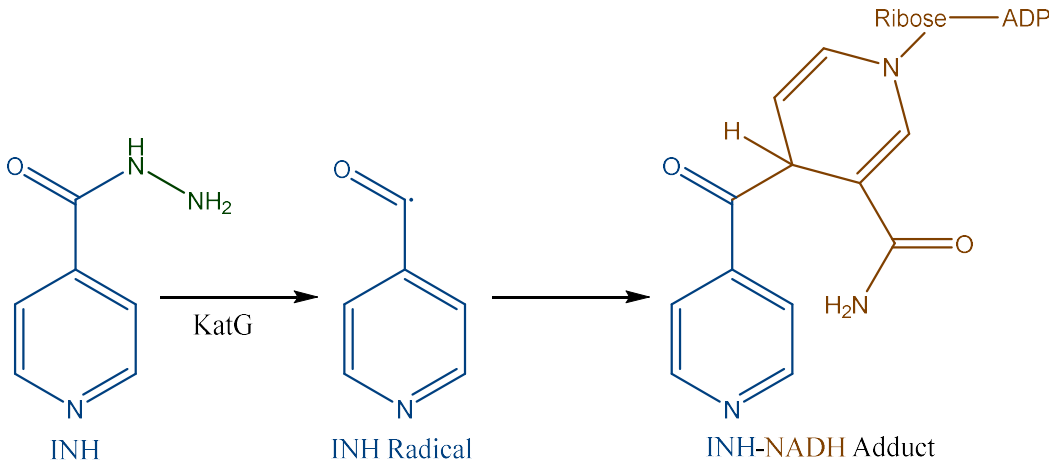


Figure 6. Formation of the isoniazid and NADH adduct.

Isoniazid is a pro-drug that is metabolised into its active form by a *M. tuberculosis* catalase-peroxidase, KatG[116]. The metabolism of isoniazid by KatG creates a reactive species that forms an adduct with nicotinamide adenine dinucleotide (NADH). The INH-NADH molecule is a potent inhibitor of InhA[117], an essential enoyl acyl carrier protein involved with the biosynthesis of mycolic acids[118]. The INH-NADH adduct has increased affinity for the binding pocket of InhA when compared to NADH alone. This is due to the nitrogen atom in the pyridine ring hydrogen bonding with a local water residue and hydrophobic interactions between the ring and several surrounding amino acid residues[119]. This results in the active site being blocked by the INH-NADH adduct.

Isoniazid resistance occurs commonly by reducing or halting the enzymatic activity of KatG. A reduction in the activity of KatG will reduce the amount of INH-NADH produced therein preserving the activity of InhA[120]. Modification of the INH-NADH binding pocket in InhA can also confer resistance. A Ser94Ala mutation, a mutation in the binding pocket of InhA, will cause resistance to isoniazid by decreasing the affinity for NADH therefore allowing the INH-NADH adduct to release from the binding pocket[119].

1.7.3 Pyrazinamide

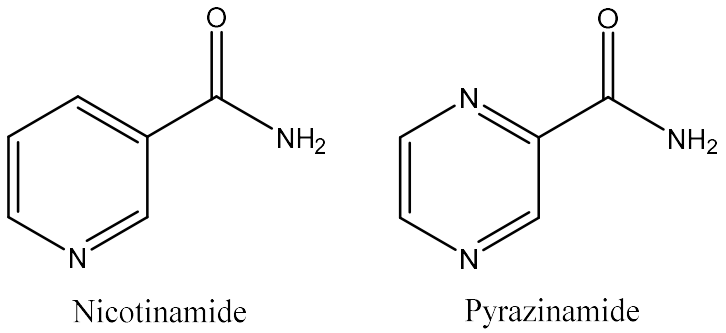


Figure 7. Structure of nicotinamide and pyrazinamide.

In 1945, Vitamin B3 also known as nicotinamide was found to have anti-mycobacterial properties[121]. Pyrazinamide (PZA), an analogue of nicotinamide, was first tested against tuberculosis infected mice in 1952[47].

Pyrazinamide only works against non-dividing bacteria and it is thought that the acidic conditions of approximately pH 5.5 inside the tuberculoma/granuloma are where the drug works most effectively[122]. Like isoniazid, pyrazinamide is a pro-drug converted to its active form, pyrazinoic acid, by PncA, a pyrazinamidase[123]. The pyrazinoic acid diffuses out of the bacillus and, into an acidic environment, becomes protonated and diffuses back into the bacillus and increases the acidity inside the cell[124,125]. The decrease in internal pH is thought to inhibit enzymes inside the bacillus in a non-specific manner leading to cellular death[126].

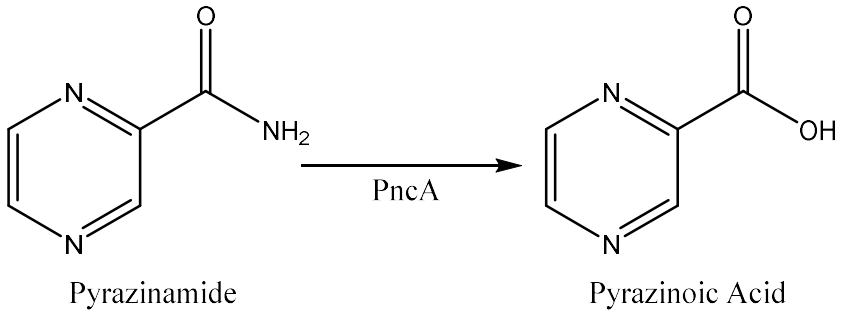


Figure 8. Conversion of pyrazinamide to pyrazinoic acid by PncA.

An alternate mechanism of cell death by pyrazinoic acid has been suggested, that being the inhibition of the S1 protein of the ribosome, RpsA, and *trans*-translation[127,128]. *Trans*-translation is essential for breaking down non-stop and no-go ribosome complexes and releasing the ribosomes from the unfinished protein and the mRNA[129]. However, this mechanism of killing has recently been discounted[130]. Not all mycobacteria are susceptible to pyrazinamide. For pyrazinamide to be effective the drug needs to be actively transported into the cell using dedicated nicotinamide transporters and activated intracellularly by a pyrazinamidase[131]. The most common form of resistance to pyrazinamide is the reduction of amidase activity[132] usually by the mutation of PncA[133]. There is a very high variation in mutations of PncA with the majority resulting in a loss of amidase activity[133,134].

1.7.4 **Ethambutol**

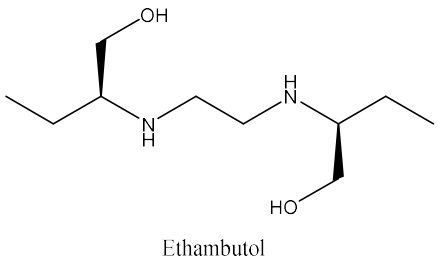


Figure 9. Structure of ethambutol.

Ethambutol was discovered to be active against mycobacteria in 1961[48]. Ethambutol is a bacteriostatic agent that interferes with cell wall mycolation by preventing arabinan polymerisation[135] by targeting the enzymes of the *M. tuberculosis* EmbCAB operon[136]. The EmbCAB operon encodes three arabinosyltransferases responsible for the polymerisation of arabinose found within arabinogalactan and lipoarabinomannan[135,137]. The EmbCAB operon has been found to be essential in *M. tuberculosis*[138–140]. Inhibiting EmbC results in a truncated lipoarabinomannan by preventing α(1→5) arabinofuranose polymerisation[141,142], and inhibiting EmbA and EmbB prevents the attachment of mycolic acids to the arabinogalactan by inhibiting the terminal branching α(1→3) arabinofuranosyltransferase[143,144].

Although resistance to ethambutol can arise in any of the genes in the EmbCAB operon, they usually occur in EmbB in a highly conserved region. The most common mutation occurs at position Met306. The methionine residue is swapped for one of the branched-chain amino acids, leucine, valine or isoleucine[145]. Nearly three quarters of ethambutol resistance mutations occur in EmbB, with over 50% of those being a Met306Val/Leu/Ile substitution[146].

1.7.5 Rifampicin and Rifamycins

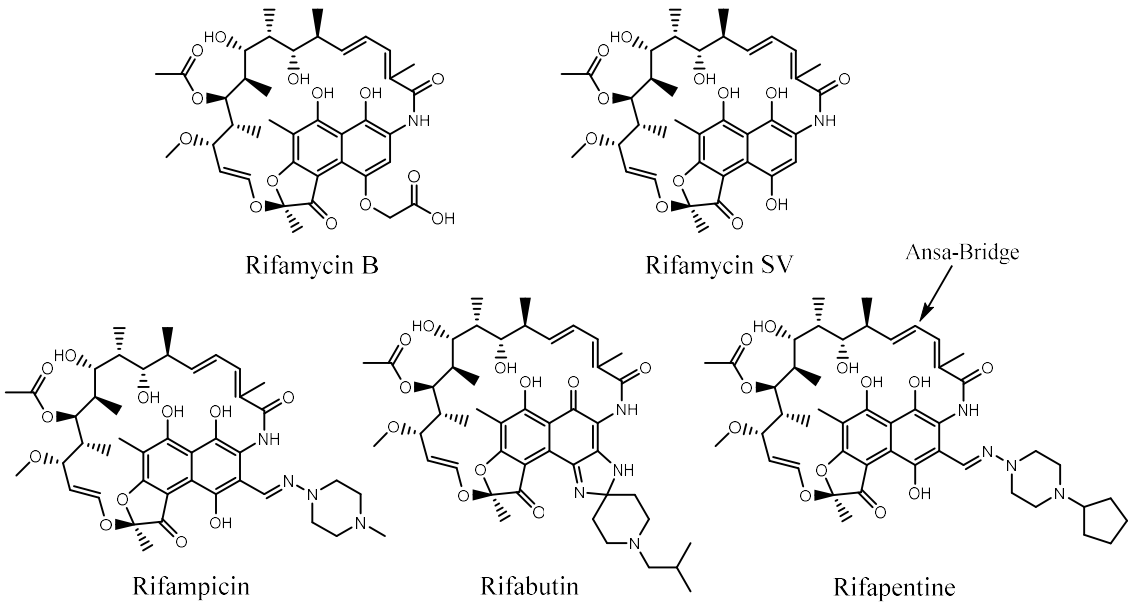


Figure 10. Structure of rifampicin and associated rifamycins.

The rifamycin class of antibiotics was discovered in 1957 in cultures of *Amycolatopsis mediterranei*, previously known as *Streptomyces mediterranei*[147–149]. The first discovered was rifamycin B, which has no antibacterial properties. It was discovered that rifamycin B degrades into rifamycin O and then to rifamycin S, which displays potent antibacterial properties[149–151]. Several derivatives of rifamycin B were discovered, such as rifamycin SV[151] and an orally active derivative, rifampicin (RIF), which was designed in 1965[49,50].

Rifampicin inhibits *M. tuberculosis* RNA polymerase[152,153] preventing the transcription of DNA into RNA by binding to the β subunit of RNA polymerase[154]. Rifampicin blocks the production of RNA product sterically at the 5' end preventing elongation past 2-3 bases due to blocking exit of the RNA strand from the enzyme[155,156].

Mutations in the *M. tuberculosis* RNA polymerase β subunit gene *rpoB* confers resistance to rifampicin. The majority of resistance mutations occur in the cluster I region of the *rpoB* gene, a region of 22 codons stretching from codon 436 to 458. Mutations at codons

438, 451 or 456 cause the strongest resistance phenotype[157]. The most common, clinically relevant, mutations in RpoB are Ser456Leu (47%), His451Tyr (12%) and Asp441Val (9%)[154]. Ser456Leu causes a change in confirmation in the RpoB binding pocket that increases the space between RIF and the edge of the pocket. This increases solvent access and reduces the van der Waals holding RIF into the binding pocket[158]. His451Tyr causes a protrusion into the binding pocket which results in steric blocking of the RIF ansa-bridge preventing binding[158]. Asp441Val changes the overall charge of an area of the binding pocket to have a more positive charge. The change in charge repels RIF from binding with RpoB[158].

1.7.6 Fluoroquinolones

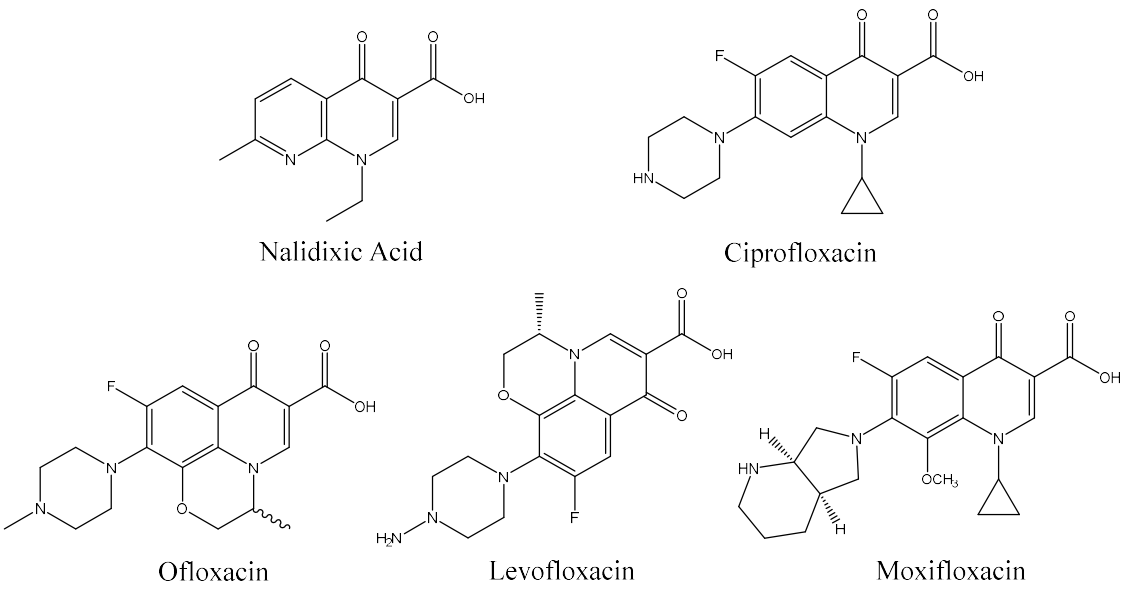


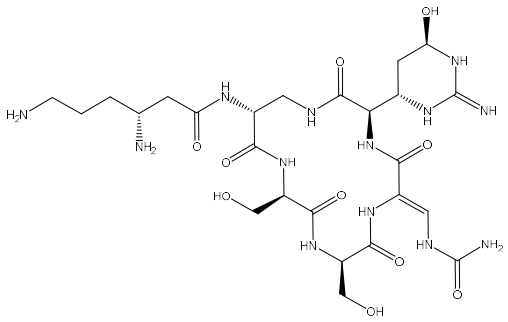
Figure 11. Structures of fluoroquinolones.

Nalidixic acid, a naphthyridine derivative, was found to display antibacterial activity against several bacteria in 1962[159]. At first it was thought that Nalidixic Acid inhibited DNA synthesis [160], however this was disproven[161].

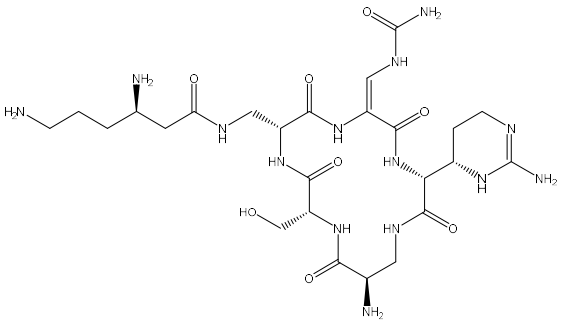
Fluoroquinolones inhibit type IIA topoisomerases, namely, topoisomerase II (DNA Gyrase) and topoisomerase IV. DNA gyrase and topoisomerase IV are heterotetramers consisting of two sets of two subunits. DNA Gyrase generates negative supercoils in DNA and topoisomerase IV relaxes positive supercoils in DNA. This is achieved by creating a double stranded break in the held DNA and allowing the other held strand to move through the gap before ligating the broken strand together again[162]. Type IIA topoisomerases make a double stranded DNA cut with a 4 base pair overhang, two fluoroquinolones interact with the complex, one positioned between the cut ends of each DNA strand[163]. This interaction stabilises the complex and does not allow the release of either strand of DNA, the passage of the uncut strand between the cut strand or the ligation of the cut DNA.

M. tuberculosis has a copy of DNA gyrase, formed from GyrA and GyrB, but does not have a copy of topoisomerase IV. *M. tuberculosis* DNA Gyrase has an intrinsic insensitivity to fluoroquinolones, particularly older generation drugs, such as ciprofloxacin when compared to newer generation drugs, such as moxifloxacin[164]. This resistance is due to Ala90 in GyrA, in other bacterial orthologs this is instead Ser90. Unlike Ser90, Ala90 does not contribute to fluoroquinolone binding which relies on Mg^{2+} and a water bridge[164]. The common resistance mutation, Ala90Val[165], leads to steric blocking of the magnesium ion and water bridge preventing binding of fluoroquinolones[164].

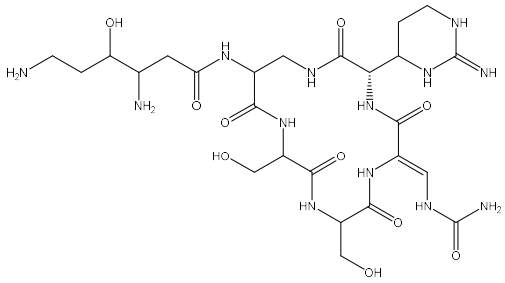
1.7.7 Polypeptides



Viomycin



Capreomycin



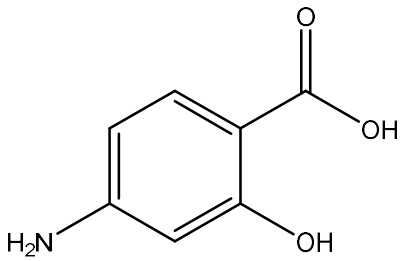
Enviomycin

Figure 12. Structures of polypeptide antibiotics.

Viomycin, capreomycin and enviomycin are a group of structurally related polypeptide antibiotics that inhibit protein synthesis in *M. tuberculosis*. Viomycin has been shown to inhibit the elongation of the peptide chain from the ribosome[166]. Viomycin binds in the A site of the ribosome after EF-Tu has inserted a tRNA or after EF-G has bound to translocate the tRNA to the P site[167]. Viomycin binding at either of these steps prevents the translocation of the tRNA until the viomycin has dissociated. This slows down the creation of the peptide chain by repeatedly stalling the ribosome complex. Crucially this does not prevent GTP expenditure by EF-G, increasing the energy cost of protein synthesis[167]. While the precise mode of action of capreomycin, and enviomycin are not

known, capreomycin inhibits interaction between ribosomal proteins L10 and L12 preventing protein synthesis[168].

1.7.8 *Para*-aminosalicylic Acid



Para-Aminosalicylic Acid

Figure 13. Structure of *para*-aminosalicylic acid.

Para-aminosalicylic Acid (PAS) was the second antibiotic discovered for treating tuberculosis[44,45]. PAS was phased out of general use a long time ago but is now seeing a resurgence in the clinic due to increasing levels of drug resistant TB[169]. PAS targets the folate biosynthetic pathway and prevents biosynthesis of tetrahydrofolate[170]. Dihydropteroate synthase converts PAS to hydroxyl dihydropteroate. The hydroxyl dihydropteroate is then used as a substrate by dihydrofolate synthase to produce hydroxyl dihydrofolate[170]. Hydroxyl dihydrofolate is bound by dihydrofolate reductase due to the similarity to the natural substrate dihydrofolate. The bound hydroxyl dihydrofolate prevents the activity of dihydrofolate reductase[170]. The folate biosynthetic pathway is important for the biosynthesis of many products, including the amino acid methionine[171].

1.7.9 Thioamides and Triclosan

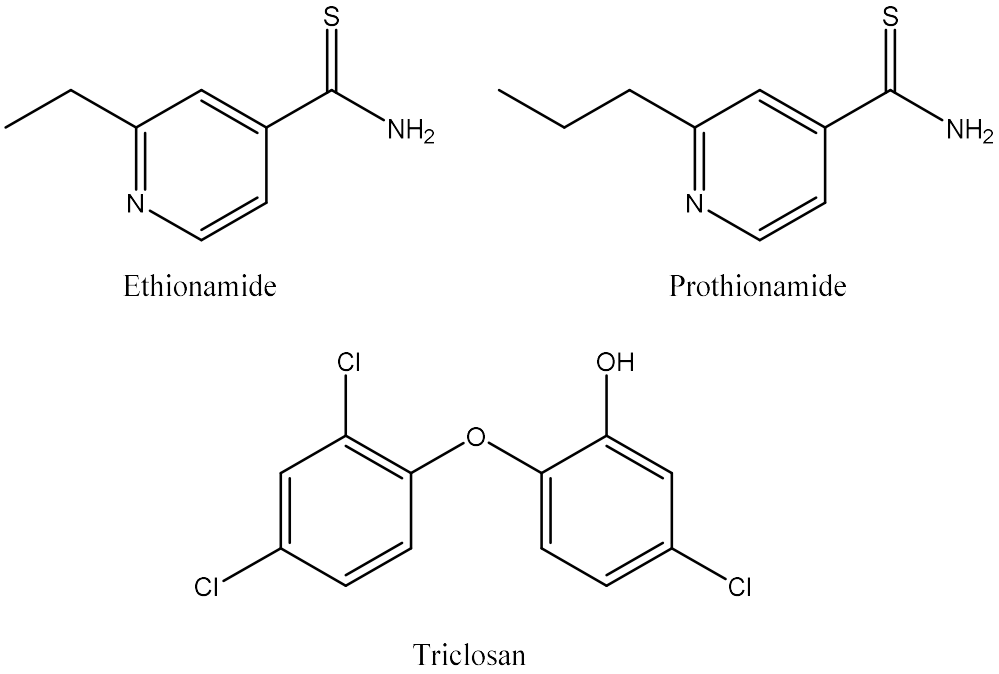


Figure 14. Structure of thioamides and triclosan.

Ethionamide and prothionamide are related compounds with a similar mechanism of action to isoniazid. Ethionamide and prothionamide are both activated by EthA a monooxygenase and form an adduct with NAD[172]. This thioamide-NAD adduct can then, like the isoniazid-NADH adduct, inhibit InhA preventing mycolic acid biosynthesis[172,173]. Due to the similar mechanism of action it is common for isoniazid and thioamide resistance to occur together[172].

Triclosan, an unrelated compound to the thioamides, inhibits fatty acid synthesis is a different way. When InhA binds with NAD, triclosan can interact and form a stable complex[174]. The formation of this complex prevents any further activity of InhA and results in a similar mechanism of lethality to isoniazid and thioamides, but with a different mode of action.

1.7.10 D-Cycloserine and Terizidone

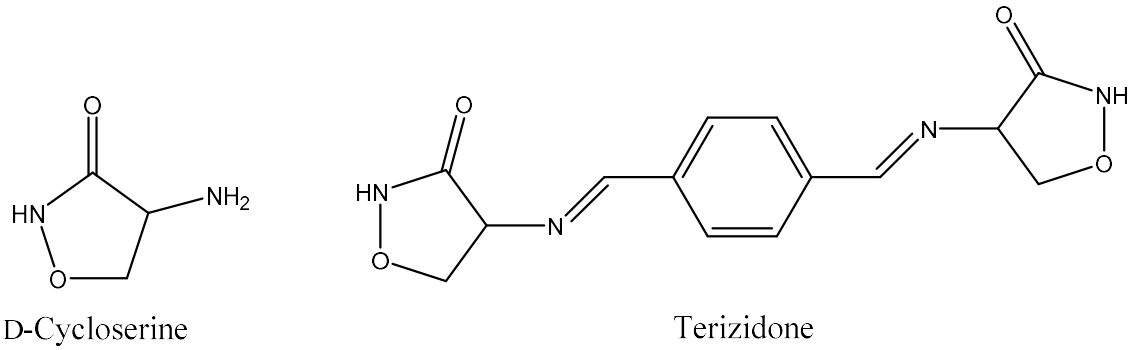


Figure 15. Structures of D-cycloserine and terizidone.

Treatment with D-cycloserine, a D-alanine analogue, leads to a cessation of peptidoglycan biosynthesis in mycobacteria[175]. D-Cycloserine interferes with the activity of two enzymes, alanine racemase[176] and D-alanine-D-alanine ligase[177]. The construction of peptidoglycan requires a five amino acid peptide stem branching from the glycan backbone[24]. The final two amino acids in the peptide stem are both D-alanine, an amino acid that is not found naturally and must be converted from L-alanine by alanine racemase[175]. The two D-alanine units are linked together by D-alanine-D-alanine ligase before attachment to the peptide stem[178]. The terminal D-alanine units are essential for cross-linking of peptidoglycan strands and the correct formation of the cell wall.

As a D-alanine analogue, D-cycloserine competes with the natural substrates of alanine racemase and D-alanine-D-alanine ligase and prevents activity. While both enzymes can be inhibited, the inhibition of D-alanine-D-alanine ligase is the primary lethal target of D-cycloserine[179]. The inhibition of peptidoglycan synthesis has a knock on effect on the cellular metabolism too, causing an increase in peptidoglycan precursors and cellular catabolism[179]. Terizidone is a molecule that contains two D-cycloserine units connected to terephthalaldehyde *via* a condensation reaction. The mechanism by which D-

cycloserine is released from terizidone is not understood and when measured, the release of D-cycloserine from terizidone was ten times lower than expected[180].

1.7.11 β-Lactams

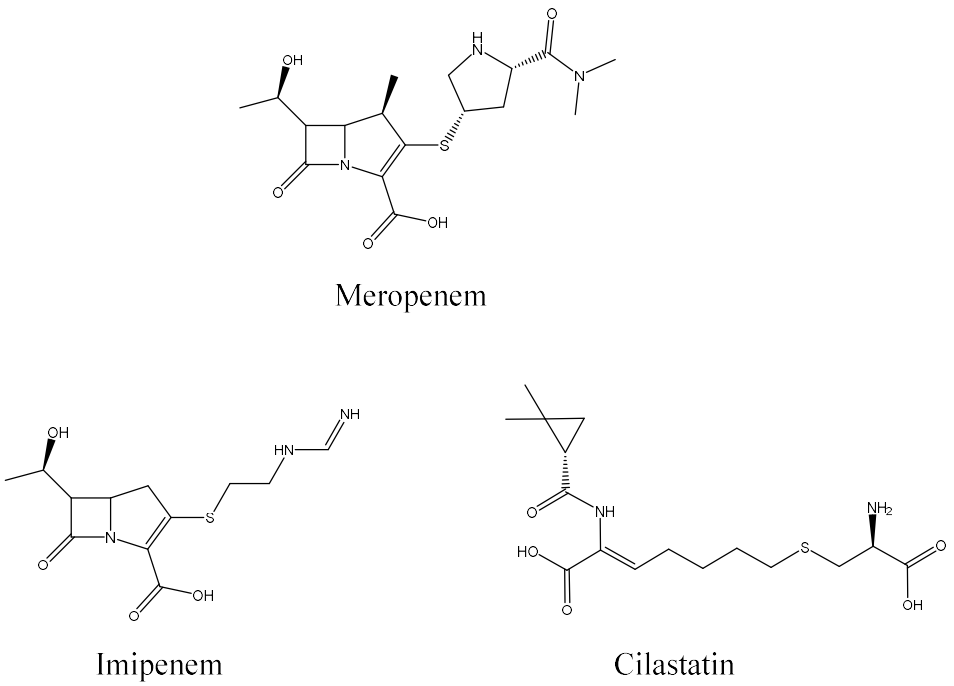


Figure 16. Structure of β-lactams, meropenem and imipenem, with cilastatin additive.

β-lactam antibiotics, more commonly known as penicillins, are named as such because they all contain a β-lactam ring structure. β-lactams are analogues of the D-alanine-D-alanine terminal structure of the peptidoglycan peptide stem structure[181]. Normally the peptide stems of peptidoglycan are cross linked by D,D-transpeptidase activity of the penicillin binding proteins (PBP)[182]. To make the crosslinks PBPs recognise the terminal D-alanine-D-alanine motif and because β-lactams mimic this structure, they are also recognised. Once a β-lactam is in a PBP active site the β-lactam ring opens and covalently attaches to the active site and irreversibly damages the enzyme[181].

β-lactams are not commonly used to treat TB. The reasons for this are two fold, firstly most β-lactams only target D,D-transpeptidase activity. *M. tuberculosis* also possess L,D-transpeptidase activity reducing the overall effectiveness of β-lactamases[181]. Secondly, *M. tuberculosis* also possess high activity β-lactamases that can open the β-lactam ring and deactivate the antibiotic safely[183]. Despite the natural protection from β-lactam antibiotics there are a few combinations are recommended by the WHO for drug resistant infections[103]. Meropenem[184] and imipenem[185] are both highly resistant to β-lactamase inactivation, however imipenem must be co-administered with cilastatin to prevent degradation by renal dehydropeptidase 1[186].

1.7.12 Other Tuberculosis Treatments

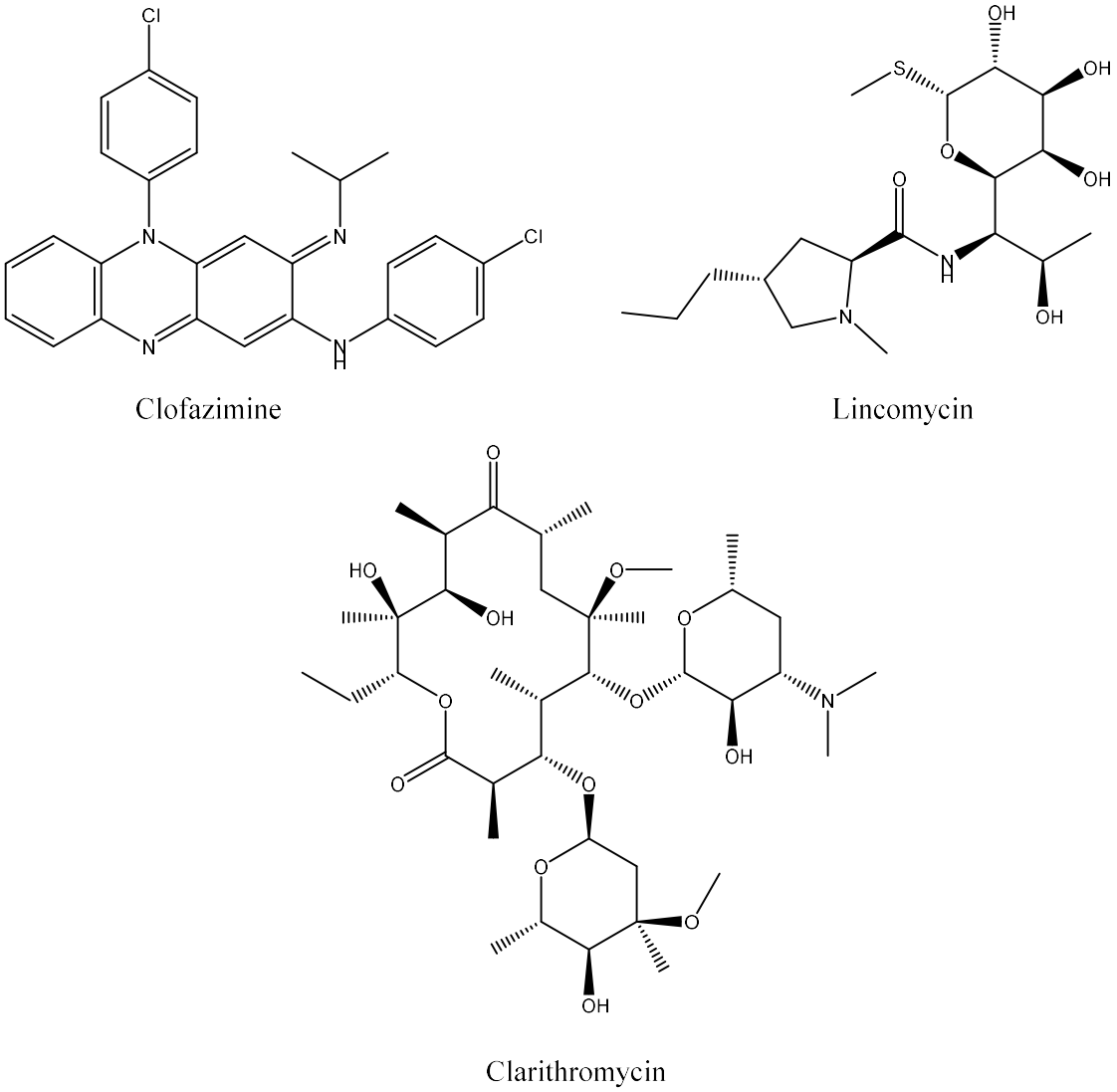


Figure 17. Structures of clofazimine, lincomycin, and clarithromycin.

These treatments for TB do not fall into a particular category and/or are not recommended for general use by the WHO. Clofazimine is a drug that has been used for treating leprosy, another mycobacterial infection that has been repurposed for treating TB. While the mode of action is not clear, recent evidence suggests that clofazimine is a pro-drug that competes with menaquinone-4 in the electron transfer chain[187].

Clarithromycin is a macrolide antibiotic, characterised by a large lactone ring. Macrolide antibiotics bind to the 50S subunit of the ribosome and inhibit protein synthesis[188]. When bound, macrolide antibiotics prevent the peptidyl transferase activity of the ribosome by blocking exit of the peptide chain from the ribosome[189]. Similar to macrolides, lincosamides, like lincomycin, inhibit the ribosome with the same mechanism[190].

1.7.13 New Generation Multi-Drug Resistance Treatments

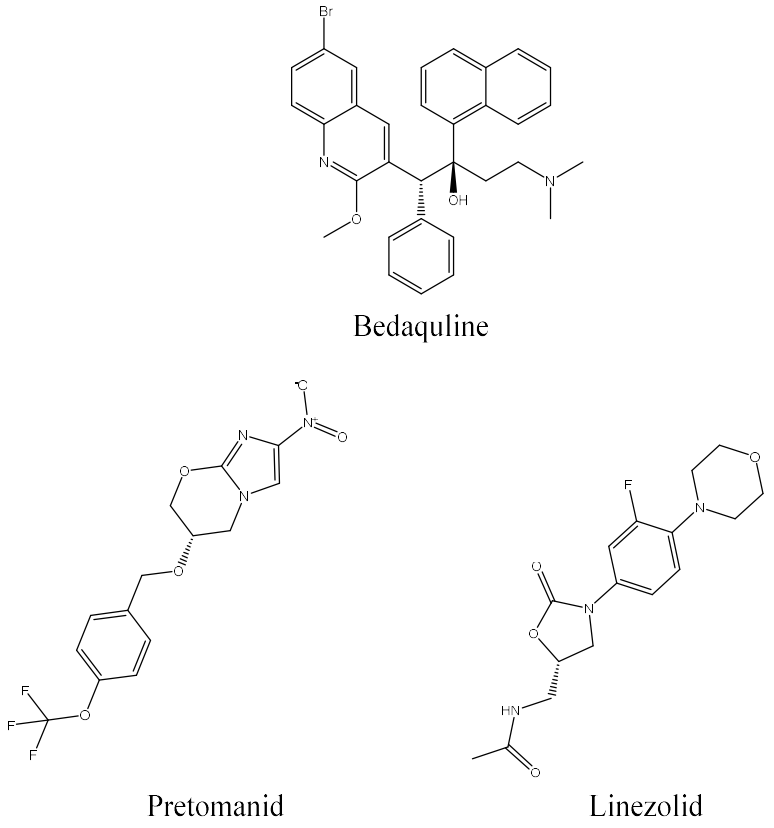


Figure 18. Structures of bedaquline, pretomanid, and linezolid.

Until recently the treatment of MDR-TB took between 18 and 24 months. This prolonged treatment combined with the use of up to seven drugs at once and their poor tolerability results in a very difficult process for the patient and could contribute to poor compliance[191]. A new combination of drugs for treating MDR-TB is close to approval

that should reduce treatment time and increase treatment success. Bedaquline, pretaminid, and linezolid, are the core of this new treatment regime.

Bedaquiline, a dairylquinalone antibiotic, is a new class of inhibitor that targets ATP synthase and is bactericidal even when mycobacteria are in a dormant state[192]. Dairylquinalones bind to ATP synthase and prevent proton transfer and the rotational conformational change required for ATP generation[193]. Resistance to bedaquiline can occur by point mutations changing the binding site to reduce affinity, or by efflux pumps, typically of the MmpL family of pumps[194]. Pretomanid, formerly known as PA-824, is a bicyclic nitroimidazole pro-drug activated by deazaflavin dependent nitroreductase. Transcriptional profiling indicates that pretomanid has a dual mode of action, targeting fatty acid synthesis and causing respiratory poisoning[195]. Another nitroimidazole of interest for TB treatment is delaminid. Delaminid is also a pro-drug, but primarily inhibits mycolic acid synthesis[196]. Linezolid is a protein synthesis inhibitor that inhibits protein synthesis by binding to rRNA in the 30s and 50s subunits and inhibits formation of the initiation complex[197]. This results in the rate of transcription slowing. Due to the unique binding site, linezolid had little to no cross resistance with other protein synthesis inhibitors[198].

1.8 The Mycobacterial Cell Wall

The mycobacterial cell wall is a complex structure of polysaccharides, polypeptides, and long chain fatty acids. Some of these structural motifs are common in other Gram positive and Gram negative bacteria, some are unique to mycobacteria[24]. The structure of the mycobacterial cell wall is the greatest strength of *M. tuberculosis*, imparting high cellular impermeability to antibiotics, but also its greatest weakness, as it offers a plethora of additional drug targets unique to mycobacteria.

From a macroscopic view, the cell wall consists of three distinct covalently linked layers. The chassis of the cell wall is formed of peptidoglycan, common to nearly all bacteria, with a few modifications from the standard template[24]. Attached to the peptidoglycan is the first of two major deviations from standard cell wall structure, the arabinogalactan layer. Arabinogalactan is a polysaccharide consisting of a galactofuranose backbone with branch like elaborations of polymerised arabinofuranose chains[199]. The last portion of the cell wall, and the layer that contributes most to the resistance to permeation, is the mycolic acid layer, covalently linked to the arabinogalactan termini[24]. Inter-dispersed with the covalently linked mycolic acids are free lipids in the form of trehalose mono-mycolate (TMM) and trehalose di-mycolate (TDM)[24]. Together these form a nearly impermeable, waxy, lipid layer. In addition to those above, the surface of *M. tuberculosis* also displays other unique lipid bound macromolecules in the cytoplasmic membrane, such as lipomannan (LM) and LAM, as a way of modulating the host immune system[200–202].

1.8.1 Peptidoglycan

Peptidoglycan is a crucial element of the bacterial cell wall providing mechanical strength and shape to bacteria, as well as resisting internal cellular turgor to prevent lysis[203]. Preventing correct synthesis and maintenance of peptidoglycan or allowing enzymatic digestion will cause the peptidoglycan sacculus to split and cell lysis[203]. Peptidoglycan also serves as a framework for external cell structures to be built upon. In mycobacteria, peptidoglycan is an attachment point for the unique macromolecules of the mycobacterial outer membrane complex[24]. The polysaccharide portion of peptidoglycan consists of alternating β(1→4)-linked N-acetylglucosamine and N-acetylmuramic acid residues that form long glycan backbone chains, and attached to the glycan chains are short penta-peptide stems[24]. In mycobacterial species the glycan backbone is modified by converting

some N-acetylmuramic acid residues to N-glycolylmuramic acid residues[204]. The penta-peptide stem consists of L-alanine, D-isoglutamate, *meso*-diaminopimelate (mDAP), D-alanine, and D-alanine attached to the N-acetyl or N-glycolylmuramic acid[24]. Crosslinking between the peptide stems attaches the individual peptidoglycan strands together in a rigid mesh like structure. The links between the peptide stems are formed directly in the A1γ format, unlike some other types of peptidoglycan which have short peptide linkage units between the peptide stems[24,205]. Unlike other bacteria with A1γ subtype peptidoglycan which form 3-4 linkages between mDAP and D-alanine, mycobacteria primarily form 3-3 linkages between the mDAP residues with only a few 3-4 linkages[206,207]. Immature mycobacterial peptidoglycan also displays mono- and tri- methylation of the carboxylic acid groups of the D-isoglutamine, mDAP, and terminal D-alanine[208]. These same groups can also be mono-, di-, and tri-amidated[208].

GlmU, an enzyme with dual acetyltransferase and uridyltransferase activity, starts peptidoglycan biosynthesis by acetylating glucosamine-1-phosphate into N-acetylglucosamine-1-phosphate using acetyl-Coenzyme A[209]. GlmU then activates the product with a free UMP into UDP-N-acetylglucosamine[209]. MurA converts some of the produced UDP-N-acetylglucosamine by attaching an enoyl-pyruval from phosphoenoyl-pyruval to produce enoyl-pyruval-N-acetylglucosamine[210]. This product is subsequently reduced by MurB to produce UDP-N-acetylmuramic acid[211], the majority of which is hydroxylated by NamH to UDP-N-glycolylmuramic acid[204,212]. The UDP- N-glycolylmuramic acid and remaining UDP-N-acetylmuramic acid are then modified by MurC, D, and E in succession to add the first three residues of the penta-peptide, L-alanine, D-isoglutamate, and mDAP[213,214]. D-alanine:D-alanine ligase connects two D-alanine residues together[178] and they are attached as a pair by MurF to complete the penta-peptide[214]. The UDP-N-glycolylmuramic acid and UDP-N-acetylmuramic acid with

attached penta-peptide are ready for lipidation by MurX and are now known as Park's nucleotide[215]. MurX attaches a Park's nucleotide to a decaprenyl phosphate to produce Lipid I and situates the molecule into the inner membrane[213,215]. Attachment of UDP-N-acetylglucosamine to Lipid I in a β(1→4) linkage by MurG produces the basic peptidoglycan building block Lipid II[216]. Lipid II is flipped to the outer membrane by a flippase. MurJ or FtsW are thought to be candidates for this process, but this is unconfirmed[217–222]. In contrast to this, there is recent evidence of FtsW as a glycosyltransferase[223–225]. In support of MurJ, the protein has a cytoplasmic gate, a cytoplasmic entrance and a periplasm exit, and segments which resemble transport regions[226,227]. The periplasmic class A penicillin binding proteins (aPBP), PonA1, A2, and A3 polymerise Lipid II into the long peptidoglycan chains with glycosyltransferase activity[228,229]. The aPBPs also crosslink the peptide stems with a 3-4 linkage by cleaving one terminal D-alanine residue with transpeptidase activity. D, D-carboxypeptidases and L,D-transpeptidases work in tandem to remove a terminal D-alanine residue[182] and create the 3-3 crosslink[230], respectively, finishing the peptidoglycan structure.

1.8.2 Arabinogalactan

Covalently linked to the peptidoglycan, arabinogalactan is a polysaccharide that forms branch like protrusions from the cell surface[199,231]. The arabinoglactan is linked at the base of the structure *via* a linker unit[232]. The linker comprises of a phosphate group, N-acetylglucosamine, and L-rhamnose[233]. The stem of the structure is comprised of approximately 30 β-D-galactofuranose residues with link through alternating β(1→5) and β(1→6) linkages[232]. On the galactan chain at positions 8, 10, and 12, there are α(1→5) linked arabinofuranose branch points[143, 232]. These branch points are elaborated with arabinofuranose residues connected with α(1→5)-links[234, 236]. These arabinose chains

also contain further branches through α(1→3) arabinofuranose branch points[232]. Each arabinose chain culminates in a forked structure consisting of an arabinose α(1→3) and α(1→5) branch, each extended with a single β(1→2) arabinofuranose residue[232]. These fork branches provide the attachment points for mycolic acids, of which about two-thirds are mycolated[235]. The arabinofuranose unit upon which these two forks originate is also modified with an α(1→2)-D-galactosamine residue when that fork is mycolated[236–239] or a succinyl residue when not mycolated[240].

WecA initiates arabinogalactan biosynthesis by producing C_{50}-P-P-N-acetylglucosamine, a precursor to the linker unit, by combining N-acetylglucosamine-1-phosphate with C_{50}-P[241]. L-rhamnose is added by WbbL[242] using UDP- L-rhamnose produced by RmlD[243] to complete the linker unit. GlfT1 adds two galactofuranose residues[244,245], the first with a β(1→4) link and the second with a β(1→5)-link[246]. The main chain is constructed by GlfT2 which polymerises approximately 28 galactofuranose units with alternating β(1→6) and β(1→5) linkages[247,248]. The lipid attached linker unit and polymerised galactofuranose chain is flipped to the outer membrane by an unknown flippase, potentially Rv3781 or Rv3783[249]. Once on the outer membrane, arabinose polymerisation can begin using decaprenyl phosphoryl-D-arabinose (DPA) as a an arabinofuranose donor. DPA is produced from ribose-5-phosphate by several enzymes. The primary carbon is pyrophosphorylated by PrsA using ATP to produce phosphor-α−D-ribosyl-1-pyrophosphate[250]. The terminal phosphate from the pyrophosphate is removed and UbiA adds decaprenyl phosphate[143,251,252]. The phosphate at position C5 is removed by Rv3807c[253] and the resulting decaprenyl-1-phosphoribose is epimerized by DprE1 and DprE2 for the final product DPA[254]. AftA primes the galactofuranose chain at a single β(1→5) linked residue at positions 8, 10, and 12 of the galactan chain[143,255]. An unknown glycosyltransferase polymerises long chains of α(1→5) linked arabinofuranose

residues[143]. Additional branching is introduced by AftC and elongation by AftD[256,257]. To terminate the synthesis of arabinogalactan, AftB adds β(1→2) arabinofuranose caps to the two available arabinofuranose residues immediately after an α(1→3) branch point[258]. Additional, modifications to the structure are the addition of D-galactosamine by Rv3779[238,239,259,260] or succinyl by an unknown enzyme. Lcp1, a phosphotransferase, transfers and ligates the competed arabinogalactan to peptidoglycan[233].

1.8.3 Mycolic Acids

The waxy outer portion of the cell wall consists of mycolic acids. Mycolic acids are long chain fatty acids that consist of two chains, a longer mero-mycolate chain ranging from 42 to 62 carbons in length, and a shorter saturated α-chain of 24 to 26 carbons in length[24]. Some of the mycolic acids are covalently attached to the terminal end structures of arabinogalactan while others are attached to trehalose in the form of TMM or TDM. The TMM and TDM are inter-dispersed with the arabinogalactan attached mycolic acid layer to form an additional pseudo-lipid bi-layer, which contributes to the impermeability and drug resistance of mycobacteria[261]. The generic term mycolic acid referrers to three similar variations of lipid with different structural modifications[24,262,263]. α-mycolates contain *cis*-configuration cyclopropane rings. Methoxy-mycolates contain *cis* or *trans* cyclopropane rings and a methoxy group. Similar to methoxy-mycolates, keto-mycolates contain the same ring structures and a keto-group. Most mycobacteria have approximately two of these functional groups per mycolate, however some strains, such as *M. tuberculosis* H37Ra have up to three groups[262].

Mycolic acids are produced by the combination of two fatty acid synthases (FAS)-I and FAS II. FAS-I produces shorter lipids up to 26 carbon units in length. For mycolic acid synthesis, FAS-I elongates a C_{14}-CoA primer chain. Firstly, FabD transacylates the acyl

carrier protein, AcpM, with a malonyl group to form malonyl-AcpM[264]. This malonyl-AcpM is the basic extension unit used by FAS-II to produce mycolic acids. FabH condenses a C_{14}-CoA chain with malonyl-AcpM to produce C_{16}-AcpM[265]. C_{16}-AcpM is now able to utilise the FAS-II system starting with a keto-reduction reaction catalysed by MabA[266]. The resulting hydroxyl group is dehydrated by HadAB/BC to produce a double bond[267]. The double bond then undergoes an enoyl-reduction reaction catalysed by InhA which is the end of one cycle of extension[117]. For subsequent cycles, KasA/KasB replaces the action of FabH to condense the extended lipid with another malonyl-AcpM[268,269]. Each cycle extends the chain length by two carbon atoms and this continues until the mero-mycolate chain length reaches between 42-62 carbons in length. After completing the FAS-II pathway the mero-mycolate undergoes additional modification for the cyclopropane rings, methoxy and keto-groups that differentiate the different types of mycolic acids[270–273]. FabD32 ligates AMP to the mero-mycolate chain to prime it[274] for addition to a C_{26} α-alkyl-CoA produced by FAS-I by polyketide synthase 13 (PKS13)[275,276]. Finally, the mycolate is matured by a reduction reaction catalysed by Rv2509[277]. For the final construction of the cell wall, the completed mycolic acids need to be transported outside of the cell by a currently unknown method. It is currently thought that mycolic acids are attached to trehalose to make TMM, which is then transported outside of the cell by the *mmpL* class of efflux pumps, MmpL3[278]. One suggested method has the mycolate transferred from PKS13 to a D-mannopyranosyl-1-phospho-heptaprenol by mycolyl-transferase I, by a currently unknown enzyme[279]. A mycolyl-transferase II swaps the mycolate to trehalose-6-phosphate with the phosphate group being removed before transport[279]. Once outside the cell the three mycolyl-transferase isoforms of Antigen 85 take varying, but overlapping, roles in attaching the mycolic acids to the arabinogalactan, and producing TMM and TDM[280].

1.8.4 Phosphatidyl-*myo*-Inositol and Elaborations

Phosphatidyl-*myo*-inositol (PI) and the derivatives produced from it are an important component of the inner and outer membrane of mycobacteria[281,282]. PI and phosphatidyl-*myo*-inositol mannosides (PIMs) constitute 56 % of the phospholipids in the mycobacterial cell wall and 37 % in the cytoplasmic membrane. PI consists of a diacylglycerol attached to a *myo*-inositol sugar ring *via* a phosphate linkage[283]. PI is elaborated with two mannopyranose sugars and up to two acyl chains to form mannosyl phosphate inositol (PIM_2)[284,285]. The addition of two more mannopyranose creates the basic PIM units of Ac_1PIM_4 or Ac_2PIM_4[284,285]. From these PIMs units more elaborated PIMs can be synthesised along with the much larger LM and LAM[286].

The biosynthesis of PI is initiated by phosphatidyl-*myo*-inositol phosphate synthase, PgsA1. PgsA1 catalyses the addition of diacylglycerol to the primary carbon of D-*myo*-inositol-3-phosphate by cleaving the CDP from CDP-diacylglycerol[283]. This produces phosphatidyl-*myo*-inositol-3-phosphate and the additional 3-phophate group is removed by an unknown phosphatase to produce PI. PimA attaches a mannopyranose from GDP-Mannose to carbon two of the inositol to produce PIM_1[287,288]. PimB attaches a second mannopyranose from GDP-Mannose to carbon four of the inositol to produce PIM_2[289]. The position two mannopyranose residue is acylated by Rv2611c at the sixth position[290] and the inositol ring is acylated at the third position by an unknown transacylase. These are now referred to as MPI or Ac_1PIM_2/Ac_2PIM_2 depending on the number of acyl chains attached. PimC and PimD add the third and fourth mannopyranose residues, also using GDP-Mannose as a sugar donor[291]. These are attached to the position four mannopyranose connected to the inositol to produce Ac_1PIM_4/Ac_2PIM_4. For further mannosylation to occur Ac_1PIM_4/Ac_2PIM_4 must be attached and flipped across the membrane and a lipid linked sugar donor utilised. Ppm1 takes mannopyranose from GDP-

mannose and attaches it to a C_{50}/C_{35} polyprenyl-phosphate to afford polyprenyl-phosphate-mannopyranose (PPM)[292,293]. The mechanism of flipping for Ac_1PIM_4/Ac_2PIM_4 and PPM has not been determined.

Once the early PIMs are situated in the outer membrane, synthesis of higher tier PIMs, LM and LAM can commence. PimE and an unidentified glycosyltransferase catalyse the addition of two α(1→2) terminal mannopyranose residues to Ac_1PIM_4/Ac_2PIM_4 to produce mature Ac_1PIM_6/Ac_2PIM_6 using PPM[294]. These elaborations are exclusive to the higher PIMs and are not found in LM and LAM. For synthesis of LM and LAM, Ac_1PIM_4/Ac_2PIM_4 is elaborated by MptA and MptB with α(1→6) mannopyranose residues from PPM[295,296]. MptC introduces branching in the form of α(1→2) side chains[297,298]. If elaboration is not continued, then this forms LM. LAM has further additions in the form of arabinose structures attached to the mannose backbone. An unknown arabinofuranosyl transferase primes the mannan spine with arabinofuranose residues from DPA in a similar manner to arabinogalactan. EmbC polymerises 12-16 arabinofuranose residues with an α(1→5) linkage to the priming arabinofuranose[141,142]. The arabinogalactan branching enzymes AftC and AftD perform the same function on the LAM and introduce internal α(1→3) branches followed by α(1→5) elongation[257,299]. After polymerisation is complete AftB, as for arabinogalactan, caps the arabinose chains with a β(1→2) linkage to complete LAM[258]. The capping can be modified with two additional α(1→2) mannopyranose residues by CapA[300] and MptC[297] to produce ManLAM. Finally, the mannose cap can be terminated with attachment of an α(1→4) 5-deoxy-5-methyl-thio-xylofuranose by an unknown enzyme[301,302].

1.9 Model Organisms

The biosafety level of *M. tuberculosis* can be prohibitive to laboratory study, unless there is a functional Containment Safety Level 3 (CSL-3) laboratory available, and trained

staff. To circumvent this the model organism *M. bovis* BCG can be used as a surrogate. Ordinarily, *M. bovis* is also a biosafety level 3 organism due to its inclusion in the *M. tuberculosis* complex and ability to cause human tuberculosis. However, the attenuated *M. bovis* BCG strain can be used at Containment Level 2. *M. bovis* BCG has a similar rate of growth and has 99.95 % genetic homology to *M. tuberculosis* making it suitable as a model organism[303].

The slow growth rate of *M. tuberculosis* and *M. bovis* BCG can hold back research. *Mycobacterium smegmatis* is a non-pathogenic rapidly growing mycobacterial species with a doubling of approximately 4 hours. *M. smegmatis* has the common features of mycobacterial species, such as the cell wall, but due to differences in pathogenicity screening for drugs with *M. smegmatis* only turns up 50 % of hits when compared to *M. tuberculosis*[304]. *M. smegmatis* has value as a model organism where rapid results are needed, but *M. tuberculosis* and *M. bovis* BCG are superior for drug screening.

1.10 Project Aims

With rising levels of antibiotic resistance, the need for new antibiotics is greater than ever. High-throughput screening of large compound libraries offers the highest chances of success for discovering new hits and leads. Due to the nature of high-throughput screening, there are a very diverse range of inhibitors that can be found that need to be re-investigated, however the time and effort for mode of action studies is substantial and may often result in identifying sub-optimal targets. Designing high-throughput screens to identify hits and leads of a specific known drug target allows for rapid target identification. The main aim of these projects was to identify novel inhibitors of *M. tuberculosis*. This was split into three smaller aims:

1. **Validate new screening methods to preferentially identify inhibitors of known drug targets.**

This aim was centred around validating new screens using a phenotypic readout with either, *M. bovis* BCG or *M. tuberculosis,*by using known inhibitors of the target protein to validate the screening method.

2. **Use the screening method in a high-throughput screen to identify hits from compound libraries.**

This aim was to use the validated screening method in a high-throughput format to identify new hits for a known protein/complex target.

3. **Use biochemical assays and genetic techniques to identify the targets of the new hits.**

This aim was to take inhibitors identified by screening and properly identify their target protein/complex by conducting biochemical assays, whole genome sequencing of spontaneous drug resistant mutants, and over expression studies of the target in question.

Chapter 2

Development and Validation of High-Throughput Phenotypic Screening Methods to Identify Inhibitors of *M. tuberculosis* Amino Acid Biosynthesis

2 Development and Validation of High-Throughput Phenotypic Screening Methods to Identify Inhibitors of *M. tuberculosis* Amino Acid Biosynthesis

2.1 Introduction

M. tuberculosis possesses the genes for an extensive system of enzymes for the biosynthesis of all 20 standard amino acids[51]. This network is likely required by *M. tuberculosis* for survival, as a common defence mechanism of host cells suffering from intracellular infection is nutrient limitation, including amino acids[305]. Tryptophan degradation is also a common response to many intracellular pathogens[306–308], however *M. tuberculosis* is resistant to this strategy due to the ability to enzymatically synthesise tryptophan[309]. The essentiality of these biosynthetic pathways to the virulence of *M. tuberculosis* is further highlighted by numerous studies on amino acid auxotrophs. Auxotrophic strains are often generated for testing as vaccine candidates and commonly display stress and starvation vulnerability and attenuation in mice models of infection. Auxotrophs for branched-chain amino acids (BCAA)[310–313], lysine[314], arginine[315], methionine[316], cystine[317], proline and tryptophan[318] in mycobacterial species display attenuation in mice models of infection. Disruption of isoleucine biosynthesis decreases *M. tuberculosis* survival under stress[319]. Attempts to construct *M. tuberculosis* strains that were deficient in shikimate kinase and therefore shikimate, a precursor molecule for aromatic amino acid biosynthesis, led to non-viable cells, suggesting the importance of the aromatic amino acids; phenylalanine, tyrosine and tryptophan[320]. Histidine biosynthesis auxotrophs are unable to survive for extended periods of histidine starvation[321].

Due to the essentiality of amino acids in protein synthesis, the depletion of amino acids inside *M. tuberculosis* results in cell death. While the biosynthesis of all amino acids is

crucial for cell survival, some represent better targets than others. Analysis of the KEGG pathway[322–324] for the biosynthesis of amino acids in *M. tuberculosis* H37Rv as shown in Figure 19 makes it clear that there are various bottlenecks in the pathways that could be exploited. For example, the shikimate pathway supplies the precursor molecule, chorismate, for the biosynthesis of all the aromatic amino acids[320,325–328]. IlvB1 is an acetolactate synthase (ALS) that is used to produce all three BCAA[329] and HisA is a common enzyme used for both histidine and tryptophan synthesis[330]. Preventing the biosynthesis of multiple essential products is very desirable from a drug treatment perspective. Conversely, as shown in Figure 19, some amino acids have multiple hypothetical pathways for biosynthesis, such as cysteine, proline, and lysine making them undesirable targets. Recently inhibitors of amino acid biosynthesis, particularly that of tryptophan and serine, have been the subject of interest. Several inhibitors of tryptophan synthase have been outlined in the literature[331,332]. These inhibitors target the TrpA/B complex to prevent the final step of tryptophan biosynthesis, the removal of indole from indole-3-glycerol phosphate and the subsequent attachment to L-serine[331]. SerB2, also known as phosphoserine phosphatase is the final step in L-serine biosynthesis and is responsible for dephosphorylating L-3-phosphoserine to produce L-serine[333]. Several inhibitors of SerB2 have been identified from high-throughput screening[334,335].

This chapter uses two compounds, Metsulfuron-Methyl (MSM) and Sulfometuron-Methyl (SMM), to validate the new screening method developed in this study. MSM and SMM, traditionally used as herbicides, are BCAA biosynthesis inhibitors that inhibit ALS in mycobacteria and other organisms[312,336]. ALS can process two different substrates that produce distinct products as shown in Figure 20. Decarboxylation of pyruvate and condensation with another molecule of pyruvate produces acetolactate for further modification into valine or leucine[337,338]. Substitution of the second pyruvate with a 2-

ketobutyrate produces acetohydroxybutyrate for isoleucine synthesis[337,338]. There are five *M. tuberculosis* genes associated with ALS. There are four large catalytic subunits (ilvB1, ilvB2, ilvG, and ilvX) and one small regulatory subunit (ilvN)[51]. In *E. coli* ALS operates as a heterotetramer of two large catalytic subunits and two small regulatory subunits in a complex[339]. The use of MSM and SMM as validation compounds serves two purposes. Firstly, ALS is a currently unexploited drug target that has been suggested as an area of interest for drug development due to essentiality and the lack of an ortholog in humans[312,329,340,341]. Secondly, ALS represents one of the ideal drug targets outlined above that is responsible for the biosynthesis multiple amino acids. The use of MSM and SMM for validation ensures that the methods developed are suitable for identifying hits.

In this study, we will develop new high-throughput screening methods to identify hits of amino acid biosynthesis from large compound libraries. The aim of these screening methods is to incorporate preliminary target identification into the screening in an attempt to mitigate the time sink of spontaneous drug resistant mutant isolation. Additionally, this study will use more conventional methods to learn more about the validation compounds, MSM and SMM, and their relationship with the ALS of *M. tuberculosis*. The validation of the screening methods has shown that they are suitable for the identification of amino acid biosynthesis hits from large compound libraries. The dropout methodology has also been shown to be able to identify which amino acid biosynthetic pathways are targeted by an inhibitor, in this case MSM and SMM. While the trial screen did not isolate any inhibitors of amino acid biosynthesis, the validation of these methods has shown their effectiveness in a screening capacity. Data from whole genome sequencing (WGS) and mutant gene overexpression indicates that the target of MSM and SMM in *M. tuberculosis* is IlvB1 and that inhibition of this enzyme prevents biosynthesis of all BCAA.

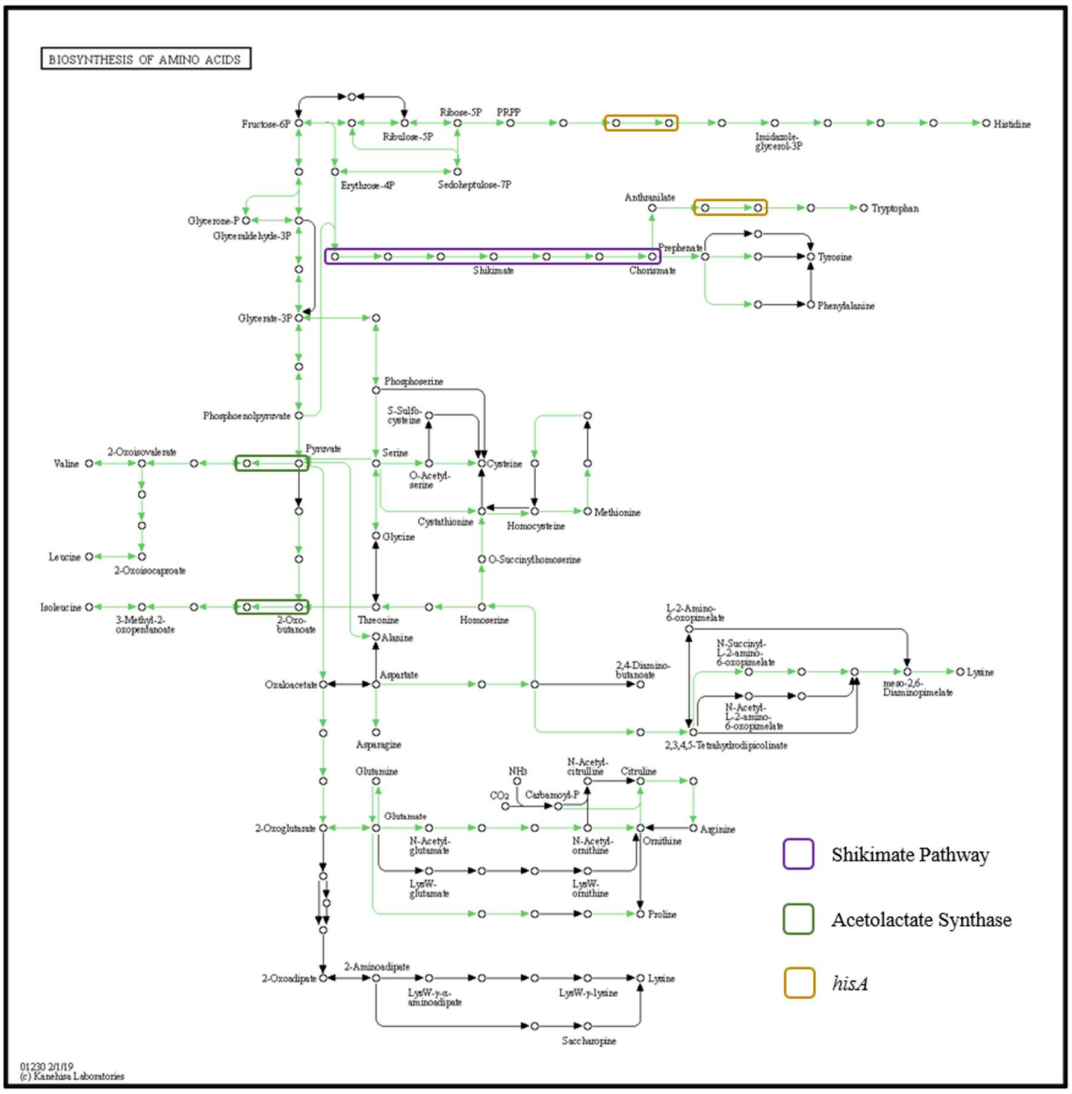


Figure 19. KEGG pathway of *M. tuberculosis* amino acid biosynthesis pathways. Coloured boxes indicate potential bottlenecks in amino acid biosynthesis. Green arrows are annotated with genes on KEGG website. Black arrows have no annotation. Used with permission from Kanehisa Laboratories.

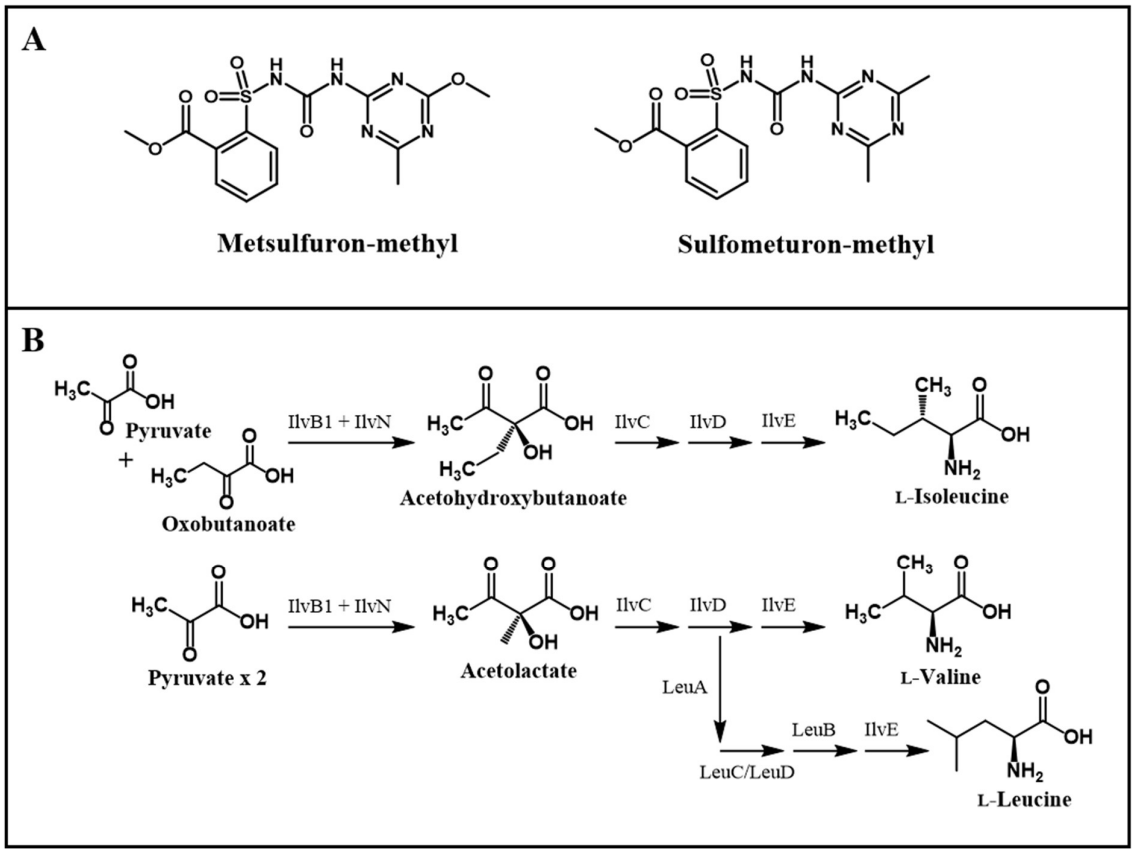


Figure 20. Synthesis of branched chain amino acids (BCAA) and inhibitors. A. Inhibitors of IlvB1 acetolactate synthase subunit. **B.** *M. tuberculosis* biosynthetic pathway of BCAA. Adapted from Figures in Burke, C. *et al.* 2019[329]. The catalytic subunit and regulatory subunit complex formed from *ilvB1* and *ilvN* respectively synthesize the BCAA precursors acetohydroxybutanoate and acetolactate. These products undergo further enzymatic modification to produce the BCAAs.

2.2 Materials and Methods

2.2.1 Liquid Minimum Inhibitory Concentrations (MIC) of Validation Compounds

The validation compounds MSM, SMM and pyrimethanil were dissolved in DMSO. Several dilutions of the compounds were made in compound plates (Greiner, 96 well, PP, V-bottom. Ref - 651201), at 100x final concentration. The final concentrations for this experiment are displayed in **Figure 21**. In separate microplates (Greiner, 96 well, PS, F-bottom, black, sterile. Ref - 655086) for each compound, 1 µL of the 100x dilutions was added in triplicate to each plate as well as triplicate wells of 1 µL DMSO and 100 µM rifampicin. Each well was made up to 100 µL with mid-log (OD_{600} 0.4-0.8) *M. smegmatis* mc^2155 or *M. bovis* BCG that had been normalised to a cell density of $1x10^6$ cells per mL. This gave $1x10^5$ cells per well. The plates were sealed with parafilm and tin foil and incubated at 37 °C and 5 % CO_2. *M. smegmatis* microplates were incubated overnight and *M. bovis* microplates were incubated for 7 days after which a resazurin survival assay was carried out (**Method 6.6.1**).

2.2.2 Dose Response of Amino Acid Supplementation for Validation Compounds

Dilutions of MSM and SMM were made at 100x concentration in DMSO and 1 µL was added to the wells of 3 microplates (Greiner, 96 well, PS, F-bottom, black, sterile. Ref - 655086), for each compound. Stock mixtures of all twenty amino acids and of the three BCAAs were made up at a concentration of 2 mM in dH_2O and filter sterilized. The stocks were diluted to make 2x the required experiment concentration with sterile dH_2O. 50 µL of the 2x concentration amino acids or BCAA were added to each well of the microplates. A mid-log (OD_{600} 0.4-0.8) *M. bovis* BCG culture was diluted to $2x10^6$ cells per mL in 2x

7H9 media and 50 µL was added to each well. This resulted in a 1 mM concentration of all 20 amino acids or BCAA with $1x10^5$ cells per well in 1x concentration 7H9 media. The microplates were incubated at 37 °C and 5 % CO_2 for 7 days after which a resazurin survival assay was carried out (**Method 6.6.1**).

2.2.3 Amino Acid Drop-Out Validation

Twenty mixtures of 19 amino acids (each mixture lacked a different amino acid) were made to a 2 mM concentration. Microplates (Greiner, 96 well, PS, F-bottom, black, sterile. Ref - 655086) were set up with 1 µL of 5 mM stock MSM or SMM per well. Nineteen amino acid mixtures (50 µL) were added to the wells. A mid-log (OD_{600} 0.4-0.8) *M. bovis* BCG culture was diluted to $2x10^6$ cells per mL in 2x Middlebrook 7H9 media and 50 µL was added to each well. This resulted in a 1 mM concentration of the desired amino acids with $1x10^5$ cells per well in 1x concentration 7H9 media. The microplates were incubated at 37 °C and 5 % CO_2 for 7 days after which a resazurin survival assay was carried out (**Method 6.6.1**).

2.2.4 Restriction Free Cloning of Wild Type Acetolactate Synthase Genes

Restriction free cloning was used to clone the wild type ALS catalytic subunits, *ilvB1, ilvB2, ilvG* and *ilvX* and the regulatory subunit *ilvN* into pVV16. Plasmids were made for each subunit individually as well as plasmids with one of the catalytic subunits and the regulator. Forward and reverse primers, 50 base pairs long, were designed with a 25 base pair overlap with the start and end of the gene and the flanking portions of plasmid sequence. The forward and reverse primers also included NdeI or HindIII restriction sites, respectively. For cloning *ilvB2*, *ilvG*, and *ilvX* with *ilvN*, 2 sets of primers were required. The *ilvN* + 100 bp, *ilvB2* Duo, *ilvG* Duo, and *ilvX* Duo primers were used for these

plasmids. The *ilvN* + 100 bp primer sequence started 100 base pairs upstream of the start codon to include the promotor. The *ilvB2* Duo, *ilvG* Duo, and *ilvX* Duo reverse primers included the start of the *ilvN* + 100 bp sequence instead of plasmid DNA sequence. For *ilvB1* and *ilvN* together the forward *ilvB1* and reverse *ilvN* primers were used and amplified as one PCR product. The first PCR step was used as outlined in **Method 6.4.2** and used to amplify the genes of interest using the primers in Table 3. The PCR products were purified by gel extraction (**Methods 6.4.3** and **6.4.4**). The second PCR step used the same PCR mix but instead of primers, 10 ng of fresh pVV16 plasmid DNA and 4 µL of purified PCR product were added. Where two genes were being cloned this step was the *ilvN* + 100 bp product. The step was repeated using the catalytic subunit gene PCR product for plasmids with two genes. Once the PCR steps were completed for each plasmid the mixture were treated with 1 µL of *DpnI* for 2 hours at 37 °C for 2 hours to digest methylated template plasmid and the reaction was cleaned as in **Method 6.4.5**. Finished plasmids were transformed into *E. coli* Top10 (**Method 6.3.5**) and selected for with 50 µg/ml kanamycin. The plasmids were extracted (**Method 6.4.8**) and were then sequenced by Eurofins Genomics.

Table 3. Primers used for restriction free cloning of acetolactate synthase (ALS) genes.

Gene Name(s)	Forward Primer 5'- 3' Plasmid/Gene PCR Product (NdeI Cutsite)	Reverse Primer 5'- 3' Plasmid/Gene PCR Product (HindIII Cutsite)
ilvB1	gatccggaggaatcacttc**catatg**/gtgagcgcaccaaccaagccacact	agtggtggtggtggtggtg**aagctt**/ggcgtggccttcggtgatgtcgtcg
ilvB2	gatccggaggaatcacttc**catatg**/gtgaccgtcggggatcatctcgtcg	agtggtggtggtggtggtg**aagctt**/tcgacccagtccaatgtcgggtttg
ilvG	gatccggaggaatcacttc**catatg**/atgagcaccgacaccgccccggccca	agtggtggtggtggtggtg**aagctt**/agccaggttggatcggcgtggataa
ilvX	gatccggaggaatcacttc**catatg**/gtgaacggtgctcaggccctgatca	agtggtggtggtggtggtg**aagctt**/ccccacaagcgatggcaccactaca
ilvN	gatccggaggaatcacttc**catatg**/atgagcccgaagacgcacacgttgt	agtggtggtggtggtggtg**aagctt**/cttggcggtgccgatgccgcgcgga
ilvB1 + *ilvN*	gatccggaggaatcacttc**catatg**/gtgagcgcaccaaccaagccacact	agtggtggtggtggtggtg**aagctt**/cttggcggtgccgatgccgcgcgga
ilvN + 100 bp	gatccggaggaatcacttc**catatg**/aagtgtggccgatggtggccgcggg	agtggtggtggtggtggtg**aagctt**/cttggcggtgccgatgccgcgcgga
ilvB2 Duo	gatccggaggaatcacttc**catatg**/gtgaccgtcggggatcatctcgtcg	cccgcggccaccatcggccacactt/tcgacccagtccaatgtcgggtttg
ilvG Duo	gatccggaggaatcacttc**catatg**/atgagcaccgacaccgccccggccca	cccgcggccaccatcggccacactt/agccaggttggatcggcgtggataa
ilvX Duo	gatccggaggaatcacttc**catatg**/gtgaacggtgctcaggccctgatca	cccgcggccaccatcggccacactt/ccccacaagcgatggcaccactaca

2.2.5 Spontaneous Resistant Mutant Generation for Metsulfuron-Methyl (MSM) and Sulfometuron-Methyl (SMM)

M. bovis BCG Drug Resistant Mutants (DRM) were isolated on 20 mL 7H11 agar plates supplemented with 10, 20, 30, 40, and 50 μM MSM or SMM. $1x10^8$ mid-log *M. bovis* BCG cells were plated on the plates and incubated at 37 °C and 5 % CO_2 until colonies appeared (approximately 1-2 months). The colonies were inoculated into 7H9 media and their MICs determined using resazurin (**Method 6.6.1**) to confirm resistance to MSM or SMM. The genomic DNA of the resistant mutants was extracted (**Method 6.4.1**) and sent for whole genome sequencing (WGS) to MicrobesNG (University of Birmingham).

2.2.6 Restriction Cloning of *ilvB1* and *ilvN* Mutant Genes

The mutant and wild type copies of *ilvB1* and *ilvN* were cloned into plasmids for overexpression using restriction enzymes. Mutant and wild type genes of *ilvB1* were cloned into pMV261a using the primers displayed in Table 4. The *ilvN* and full *ilvB1* plus *ilvN* operon were cloned into pVV16 using the primers from the restriction free cloning shown in Table 3. These primers contained NdeI or HindIII restriction digest sites for redundancy. The genes were amplified using PCR (**Method 6.4.2**) using the primers above. For PCR of the mutant genes, where the template DNA was substituted with the extracted genome of drug resistant mutants. The PCR products were purified (**Method 6.4.5**) and the PCR products and plasmids were digested with the appropriate NEB restriction enzymes (**Method 6.4.6**). The digested DNA products were purified using gel extraction (**Methods 6.4.3** and **6.4.4**) and then ligated (**Method 6.4.7**). Finished plasmids were transformed into *E. coli* Top10 (**Method 6.3.5**). Plasmid pVV16 was selected using

50 μg/mL kanamycin and pMV261a was selected using 50 μg/mL apramycin. The plasmids were extracted (**Method 6.4.8**) and were then sequenced by Eurofins Genomics.

Table 4. Primers for *ilvB1* cloning into pMV261a.

Gene Name	Direction	Primer 5'- 3' (Cutsite HindIII)
ilvB1	Foward	catgcatg**aagctt**atagcgcaccaaccaag
ilvB1	Reverse	catgcatg**aagctt**tcaggcgtggccttc

2.2.7 Overexpression of Acetolactate Synthase (ALS) Genes in *M. bovis* BCG

ALS pVV16 plasmids in Table 5 were electroporated (**Method 6.3.6**) into *M. bovis* BCG and selected using 25 μg/mL kanamycin 7H11 agar plates. Colonies were picked and inoculated into 7H9 media supplemented with 25 μg/mL kanamycin and grown until mid-log (OD_{600} 0.4-0.8). At this point *M. bovis* BCG containing pVV16-*ilvG* and pVV16-*ilvG+ilvN* failed to grow sufficiently and were excluded. MSM and SMM dilutions were made at 100x desired concentration in DMSO and 1 μL was pipetted into microplate (Greiner, 96 well, PS, F-bottom, black, sterile. Ref - 655086) wells in triplicate. Rifampicin was included at 1 μM as a negative control and 1 μL of DMSO only was included as a positive control. Cells were adjusted to $1x10^6$ cells/mL using 7H9 media and 100 μL was added to each well. The microplates were incubated for 7 days at 37 °C and 5% CO_2. The microplates were read using the resazurin survival assay (**Method 6.6.1**).

Table 5. Wild type plasmids electroporated into *M. bovis* BCG.

Parent Plasmid	Plasmid Name	Gene Inserts	Resistance Antibiotic
pVV16		No insert	25 µg/mL Kanamycin
pVV16	pVV16_*ilvB1*	*ilvB1*	25 µg/mL Kanamycin
pVV16	pVV16_*ilvB1+ilvN*	*ilvB1* + *ilvN*	25 µg/mL Kanamycin
pVV16	pVV16_ *ilvB2*	*ilvB2*	25 µg/mL Kanamycin
pVV16	pVV16_ *ilvB2+ilvN*	*ilvB2* + *ilvN*	25 µg/mL Kanamycin
pVV16	pVV16_ *ilvG*	*ilvG*	25 µg/mL Kanamycin
pVV16	pVV16_ *ilvG+ilvN*	*ilvG* + *ilvN*	25 µg/mL Kanamycin
pVV16	pVV16_ *ilvX*	*ilvX*	25 µg/mL Kanamycin
pVV16	pVV16_ *ilvX+ilvN*	*ilvX* + *ilvN*	25 µg/mL Kanamycin
pVV16	pVV16_ *ilvN*	*ilvN*	25 µg/mL Kanamycin

2.2.8 Overexpression of Mutated Acetolactate Synthase (ALS) Genes in *M. bovis* BCG and *M. smegmatis*

Wild type and mutated ALS genes in plasmids pVV16 and pMV261a in Table 6 were electroporated (**Method 6.3.6**) into *M. bovis* BCG and *M. smegmatis* mc^2155 and selected using 25 µg/mL kanamycin or apramycin 7H11 agar plates. Colonies were picked and inoculated into 7H9 media supplemented with 25 µg/mL kanamycin or apramycin and grown until mid-log (OD_{600} 0.4-0.8). MSM and SMM dilutions were made at 100x desired concentration in DMSO and 1 µL was pipetted into microplate (Greiner, 96 well, PS, F-bottom, black, sterile. Ref - 655086) wells in triplicate. Rifampicin was included at 1 µM for *M. bovis* BCG and isoniazid at 10 µg/mL for *M. smegmatis* mc^2155 as negative controls. DMSO (1 µL) only was included as a positive control. Cells were adjusted to $1x10^6$ cells/mL using 7H9 media and 100 µL was added to each well. *M. bovis* BCG microplates were incubated for 7 days at 37 °C and 5% CO_2. *M. smegmatis* mc^2155

microplates were incubated for 24 hours. The microplates were read using the resazurin survival assay (**Method 6.6.1**).

Table 6. Wild type (WT) and mutated plasmids electroporated into *M. bovis* BCG and *M. smegmatis* mc^2155.

Parent Plasmid	Plasmid Name	Gene Inserts	Resistance Antibiotic
pMV261a		No inserts	25 µg/mL Apramycin
pMV261a	pMV261a_WT *ilvB1*	WT *ilvB1*	25 µg/mL Apramycin
pMV261a	pMV261a_MSM *ilvB1*	MSM *ilvB1*	25 µg/mL Apramycin
pMV261a	pMV261a_SMM *ilvB1*	SMM *ilvB1*	25 µg/mL Apramycin
pVV16		No inserts	25 µg/mL Kanamycin
pVV16	pVV16_WT *ilvN*	WT *ilvN*	25 µg/mL Kanamycin
pVV16	pVV16_MSM *ilvN*	MSM *ilvN*	25 µg/mL Kanamycin
pVV16	pVV16_SMM *ilvN*	SMM *ilvN*	25 µg/mL Kanamycin
pVV16	pVV16_WT *ilvB1+ilvN*	WT *ilvB1* + *ilvN*	25 µg/mL Kanamycin
pVV16	pVV16_MSM *ilvB1+ilvN*	MSM *ilvB1* + *ilvN*	25 µg/mL Kanamycin
pVV16	pVV16_SMM *ilvB1+ilvN*	SMM *ilvB1* + *ilvN*	25 µg/mL Kanamycin

2.2.9 TB Box Amino Acid Drug Rescue Screen

Approximately 1 µL of 200 compounds in DMSO were aliquoted from three 20 µM stock compound plates into 8 microplates (Greiner, 96 well, PS, F-bottom, black, sterile. Ref - 655086). Mid-log (OD_{600} 0.4-0.8) cells were adjusted to $1x10^6$ cells/mL in 7H9 and were supplemented with one of twelve different 10 mM amino acid solutions to 100 µM. Cells (100 µL) were added to each well and the plates incubated at 37 °C in 5 % CO_2 for 7 days. The microplates were read using the resazurin survival assay (**Method 6.6.1**). The amino acids supplemented were as follows: methionine, asparagine, alanine, arginine, aspartic

acid, cystine, glutamic acid, glutamine, glycine, proline, serine, and tyrosine. Additionally, this experiment was carried out using all twenty amino acids supplemented together at two different concentrations, 100 μM and 1 mM using a 2 mM stock. Supplementation at 1 mM was achieved by using the 2 mM stock of all twenty amino acids and 2x 7H9 media mixed in a 1/1 ratio. All the screens were conducted in singlet.

2.2.10 TB Box Amino Acid Dose Response Screen

Dilutions of the compounds pulled out in the drug rescue screen were made at 100x concentration in DMSO and 1 μL was added to each well of a microplate (Greiner, 96 well, PS, F-bottom, black, sterile. Ref - 655086). Isoniazid at 1mg/mL (1 μL) was added as a negative control. Stock mixtures of all twenty amino acids were made up at a concentration of 2 mM in dH_2O and filter sterilized. The stocks were diluted to make 2x the required experiment concentration with sterile dH_2O. The 2x concentration amino acids (50 μL) was added to each well of the microplate. A mid-log (OD_{600} 0.4-0.8) *M. bovis* BCG culture was diluted to $2x10^6$ cells per mL in 2x 7H9 media and 50 μL was added to each well. This resulted in a 1 mM concentration of all twenty amino acids with $1x10^5$ cells per well in 1x concentration 7H9 media. The microplate was incubated at 37 °C and 5 % CO_2 for 7 days after which a resazurin survival assay was carried out (**Method 6.6.1**). Due to compound restraints this experiment was conducted in singlet.

2.2.11 TB Box Amino Acid Dropout Screen

Twenty mixtures of 19 amino acids (each mixture lacked a different amino acid) were made to a 2 mM concentration. Microplates (Greiner, 96 well, PS, F-bottom, black, sterile. Ref - 655086) were set up with 1 μL of compound per well at 100x the desired concentration. Isoniazid (1 μL of 1 mg/mL) was included as a negative control. Nineteen

amino acid (50 µL) mixtures were added to the wells. A mid-log (OD_{600} 0.4-0.8) *M. bovis* BCG culture was diluted to $2x10^6$ cells per mL in 2x Middlebrook 7H9 media and 50 µL was added to each well. This resulted in a 1 mM concentration of the desired amino acids with $1x10^5$ cells per well in 1x concentration 7H9 media. The microplates were incubated at 37 °C and 5 % CO_2 for 7 days after which a resazurin survival assay was carried out (**Method 6.6.1**). Due to compound restraints this experiment was conducted in singlet.

2.2.12 TB Box Amino Acid Compounds Liquid Minimum Inhibitory Concentrations (MICs)

The TB Box compounds were dissolved in DMSO at 2 mM. Several dilutions of the compounds were made in compound plates (Greiner, 96 well, PP, V-bottom. Ref - 651201), at 100x concentration. In separate microplates (Greiner, 96 well, PS, F-bottom, black, sterile. Ref - 655086) for each compound, 1 µL of the 100x dilutions was added in triplicate to each plate as well as triplicate wells of 1 µL DMSO and 100 µM rifampicin. Each well was made up to 100 µL with mid-log (OD600 0.4-0.8) *M. bovis* BCG that had been normalised to a cell density of $1x10^6$ cells per mL. This gave $1x10^5$ cells per well. The plates were sealed with parafilm and tin foil and incubated at 37 °C and 5 % CO2 for 7 days after which a resazurin survival assay was carried out (**Method 6.6.1**).

2.2.13 TB Box Amino Acid Compounds Solid Minimum Inhibitory Concentrations (MICs)

Small 10 mL 7H11 agar plates were set up containing the TB Box compounds at concentrations of 10, 20, 30, and 40 µM. Mid-log (OD_{600} 0.4-0.8) *M. bovis* BCG was spotted onto the surface of the plates 4 times in 10 µL volumes. Each spot had a different number of cells; 1000, 100, 10, and 1 cells/10 µL. The plates were incubated at 37 °C at

5 % CO_2 until growth was seen on the no drug control plate. The solid MIC was approximated as the first plate with no growth on any of the spots.

2.2.14 TB Box Amino Acid Compounds Drug Resistant Mutant Generation

9 cm diameter 20 mL 7H11 agar plates were set up containing the TB Box compounds at the desired concentration with a maximum DMSO concentration of 1 %. Concentrations varied depending on the compound MICs but were typically 5x, 10x, and 20x the solid or liquid MIC. Mid-log (OD_{600} 0.4-0.8) *M. bovis* BCG or *M. tuberculosis* H37Rv cultures were adjusted to $1x10^9$ cells/mL and 100 µL of cells were spread out on the agar plate for $1x10^8$ cells on each plate. The agar plates were incubated at 37 °C with 5 % CO_2 until colonies appeared (approximately 1-2 months).

2.3 Results

2.3.1 Minimum Inhibitory Concentrations (MICs) of Validation Compounds

We aimed to design, validate and use a high-throughput phenotypic screening method to identify amino acid biosynthesis inhibitors from large chemical libraries due to the success of a previous screen identifying a tryptophan biosynthesis inhibitor. Three known amino acid biosynthesis inhibitors were selected as validation compounds and examined for activity against mycobacterial species. The inhibitors chosen were two inhibitors of BCAA synthesis, MSM and SMM, and an inhibitor of methionine biosynthesis, pyrimethanil. The data in Table 7 shows the MIC values for each compound and Figure 21 shows the graphs used to determine those values. Pyrimethanil was immediately discontinued due to a very high MIC when first tested.

Table 7. Minimum inhibitory concentration (MIC) values for validation compounds and mycobacterial species tested.

Compound	Organism	MIC
Metsulfuron-methyl (MSM)	*M. bovis* BCG	15 μM
Metsulfuron-methyl (MSM)	*M. smegmatis* mc^2155	12 μM
Sulfometuron-methyl (SMM)	*M. bovis* BCG	10 μM
Sulfometuron-methyl (SMM)	*M. smegmatis* mc^2155	5 μM
Pyrimethanil	*M. bovis* BCG	~ 500 μM

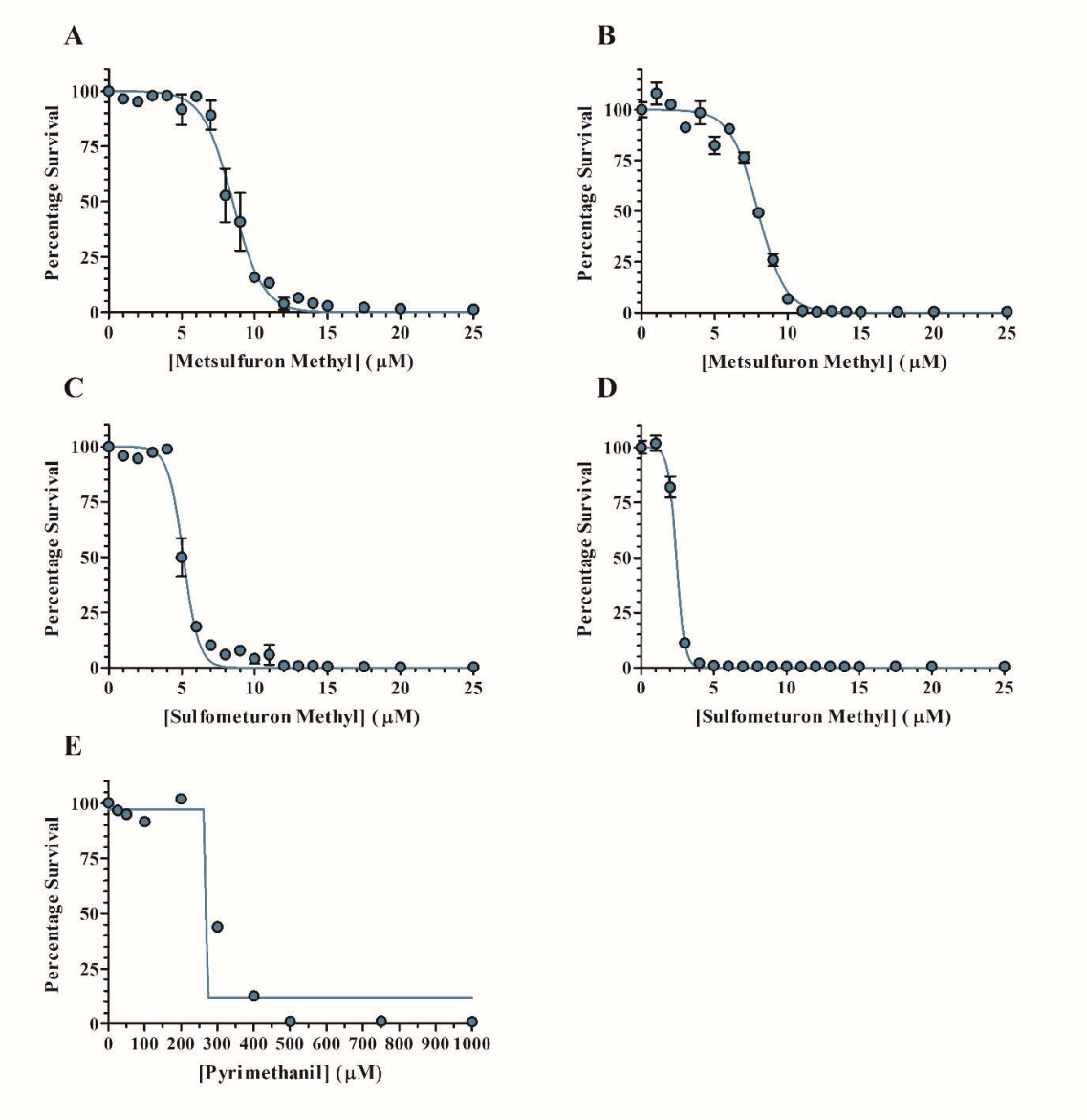


Figure 21. Minimum inhibitory concentration (MIC) graphs for validation hits. A and **B** *M. bovis BCG* and *M. smegmatis* mc^2155 MIC graphs for metsulfuron-methyl (MSM) respectively, in triplicate. **C** and **D** *M. bovis BCG* and *M. smegmatis* mc^2155 MIC graphs for sulfometuron-methyl (SMM) respectively, in triplicate. **E** *M. bovis* BCG MIC graph for pyrimethanil, in singlet. Data shown as the mean and standard deviation.

2.3.2 Rescue from Validation Compounds using Amino Acid Supplementation

M. bovis BCG was subjected to various concentrations of MSM and SMM with increasing concentrations of amino acid supplementation. When supplemented with all twenty

amino acids, as shown in Figure 22, A and B, *M. bovis* BCG was rescued from MSM and SMM based inhibition. Given enough supplemented amino acids the cells could be rescued from 2-3 times the MIC of the validation compounds without a phenotypically detectable change from the normal control cells. When supplemented with only the BCAA as in Figure 22, C and D, leucine, valine, and isoleucine, this effect was even more pronounced with less BCAA required for rescue. The phenotypically detectable rescue from the amino acid synthesis inhibitors indicated that this may be a good strategy for a larger HTS.

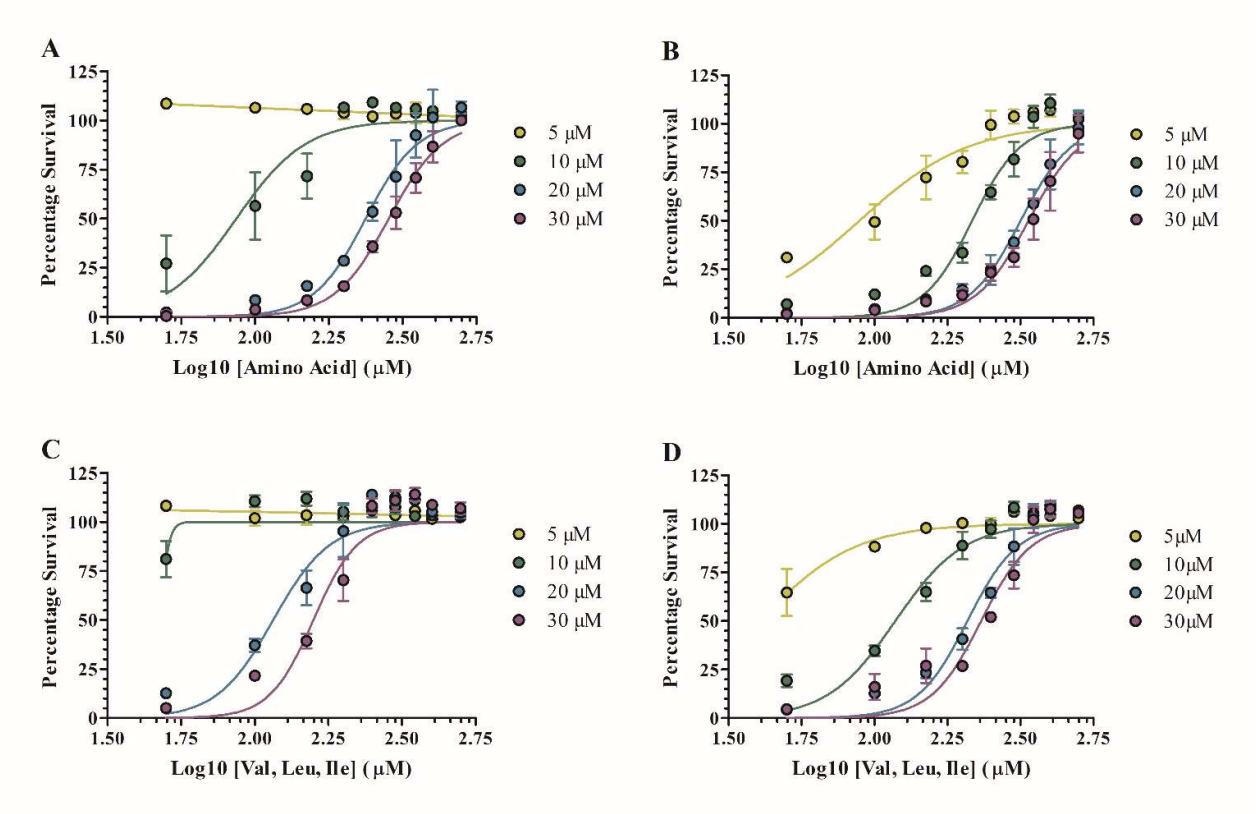


Figure 22. Rescue from validation hits using amino acid supplementation. Data shown as the mean and standard deviation of triple replicate. **A** and **B** *M. bovis* BCG treated with multiple metsulfuron-methyl (MSM) and sulfometuron-methyl (SMM) concentrations, respectively and supplemented with increasing concentrations of all twenty standard amino acids. **C** and **D** *M. bovis* BCG treated with multiple metsulfuron-methyl (MSM) and sulfometuron-methyl (SMM) concentrations, respectively and supplemented with increasing concentrations of BCAA.

2.3.3 Single Amino Acid Supplement GSK TB Box Screens

M. Bovis BCG was screened for the ability to survive when twelve different amino acids were individually supplemented into the growth media at 100 μM while treated with two hundred and eight compounds from the GSK TB box. The other eight amino acids had been screened previously by Dr Katherine Abrahams (University of Birmingham). Cells were subjected to each compound twice, once with amino acid supplementation and once without. The percentage survival was calculated for each well. The percentage survival without amino acid supplementation was subtracted from percentage survival with amino acid to give a difference in survival. These were plotted on graphs, shown in Figure 23, and any difference of 25 % or greater was considered a hit.

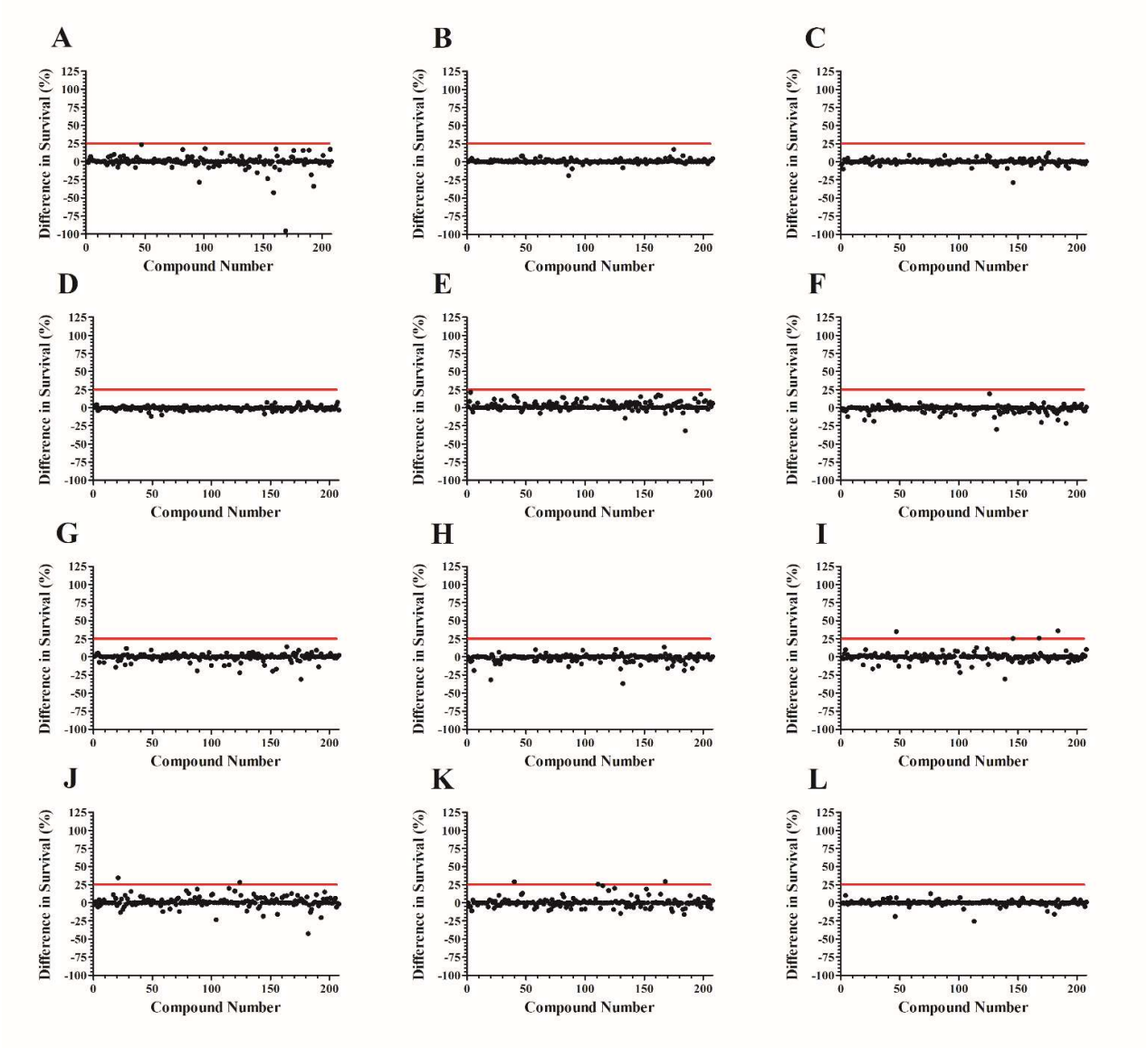


Figure 23. Single amino acid supplementation screen results. Difference in percentage survival between *M. bovis* BCG with and without 100 µM amino acid supplementation when treated with 20 µM compound. Data points are single replicate. **A –** Alanine. **B –** Arginine. **C –** Asparagine. **D –** Aspartic Acid. **E –** Cystine. **F –** Glutamine. **G –** Glutamic Acid. **H –** Glycine. **I –** Methionine. **J –** Proline. **K –** Serine. **L –** Tyrosine.

2.3.4 All Amino Acids Supplemented GSK TB Box Screen

The same two hundred and eight compounds were screened again with simultaneous supplementation of all twenty amino acids at 1 mM. The percentage survival was calculated for each well. The percentage survival without amino acid supplementation was subtracted from percentage survival with amino acid to give a difference in survival. These were plotted on graphs, shown in Figure 24, and any difference of 20 % or greater was considered a hit. All twenty amino acids combined with increased concentration of supplementation resulted in a much more robust screen. A total of eighteen hits were found and are displayed in Table 8 which was equal to an 8.6 % hit rate for the screen. One of the hits found was an inhibitor discovered in previous amino acid screening with tryptophan biosynthesis by Abrahams *et al*[331].

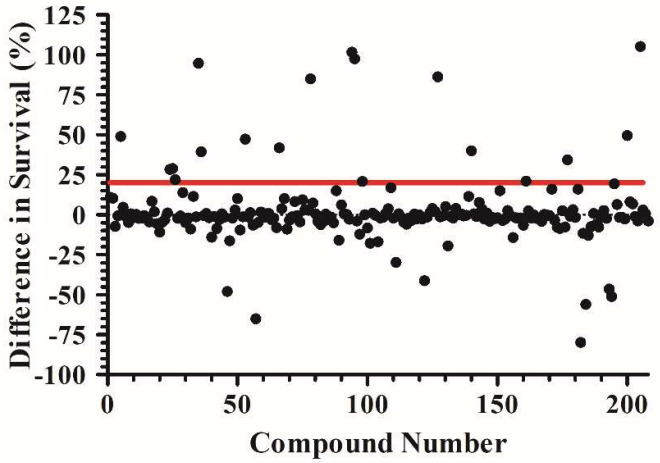


Figure 24. All amino acids supplementation screen results. Difference in percentage survival between *M. bovis* BCG with and without 1 mM amino acid supplementation when treated with 20 μM compound. Data points are single replicate.

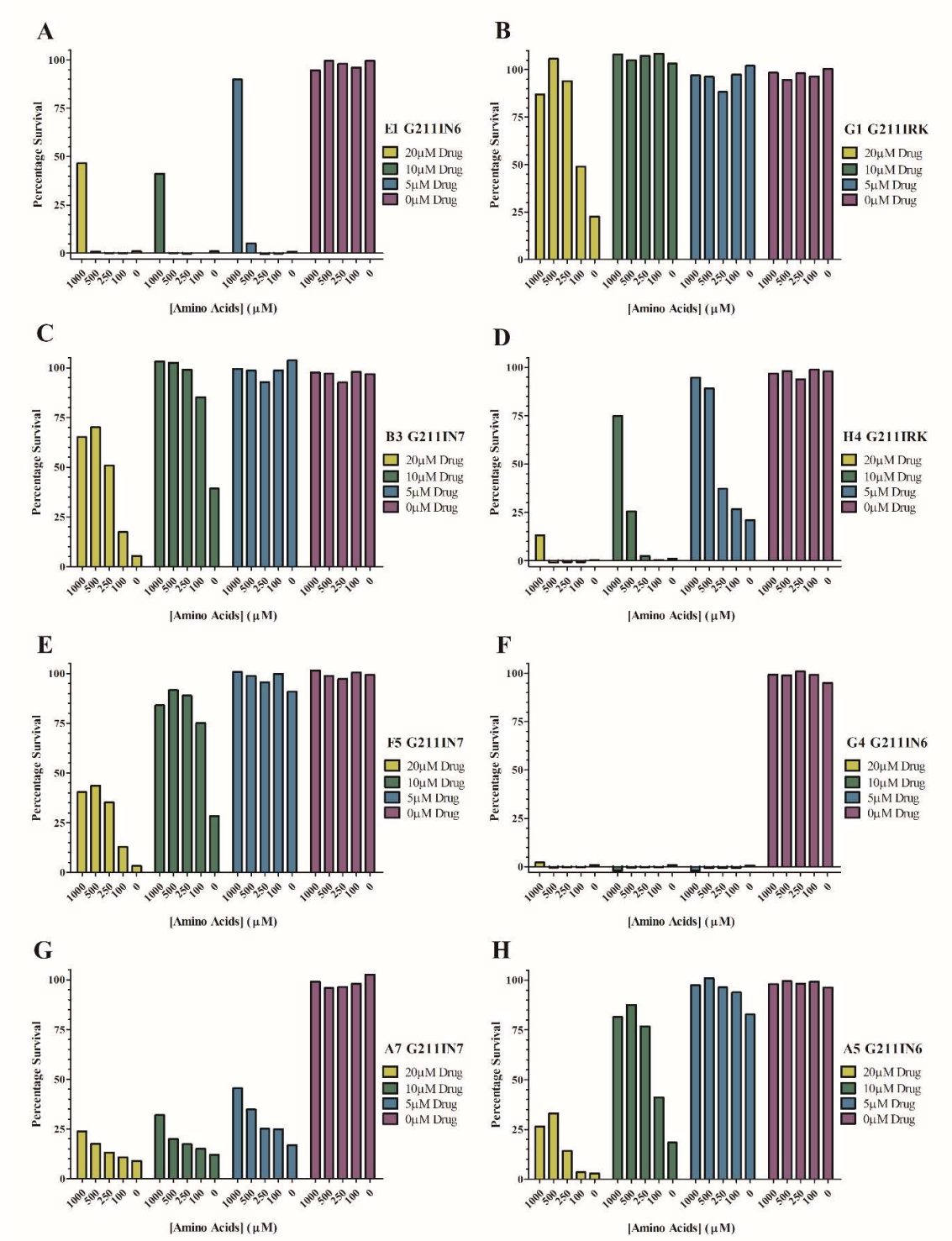
Table 8. Percentage difference data and compound plate designations for hits.

Compound Plate Designation	Percentage Difference
E1 G211IN6	105.17 %
H5 G211IN7 - TrpA/B inhibitor[331]	101.66 %
G1 G211IRK	97.54 %
B3 G211IN7	94.71 %
H4 G211IRK	86.25 %
F5 G211IN7	85.02 %
G4 G211IN6	49.48 %
A7 G211IN7	48.90 %
A5 G211IN6	47.31 %
G8 G211IN7	41.93 %
G1 G211IN6	39.99 %
D10 G211IN7	39.48 %
B7 G211IRK	34.27 %
G6 G211IN6	28.92 %
E6 G211IRK	28.28 %
G2 G211IN6	22.03 %
E5 G211IRK	21.02 %
E4 G211IN7	20.78 %

2.3.5 Dose Response Testing of All Amino Acid Screen Hits

Dose response testing was conducted on fifteen of the hits from the all amino acid supplementation screen that had adequate remaining supply. This comprised of testing the survival of *M. bovis* BCG when treated with four different concentrations of compound with five different concentrations of amino acid supplementation. This was performed in singlet due to limitations with the amount of compound provided by GSK. The percentage survival was calculated and plotted on graphs shown in Figure 25. E1

G211IN6 (**A**), G1 G211IRK (**B**), B3 G211IN7 (**C**), H4 G211IRK (**D**), F5 G211IN7 (**E**), A7 G211IN7 (**G**), A5 G211IN6 (**H**), and G8 G211IN7 (**I**) displayed a dose response that indicated that higher concentration of amino acid supplemented resulted in increased cell survival across multiple compound concentrations.


A
E1 G211IN6
B
G1 G211IRK
C
B3 G211IN7
D
H4 G211IRK
E
F5 G211IN7
F
G4 G211IN6
G
A7 G211IN7
H
A5 G211IN6
Percentage Survival
[Amino Acids] (μM)
20μM Drug
10μM Drug
5μM Drug
0μM Drug

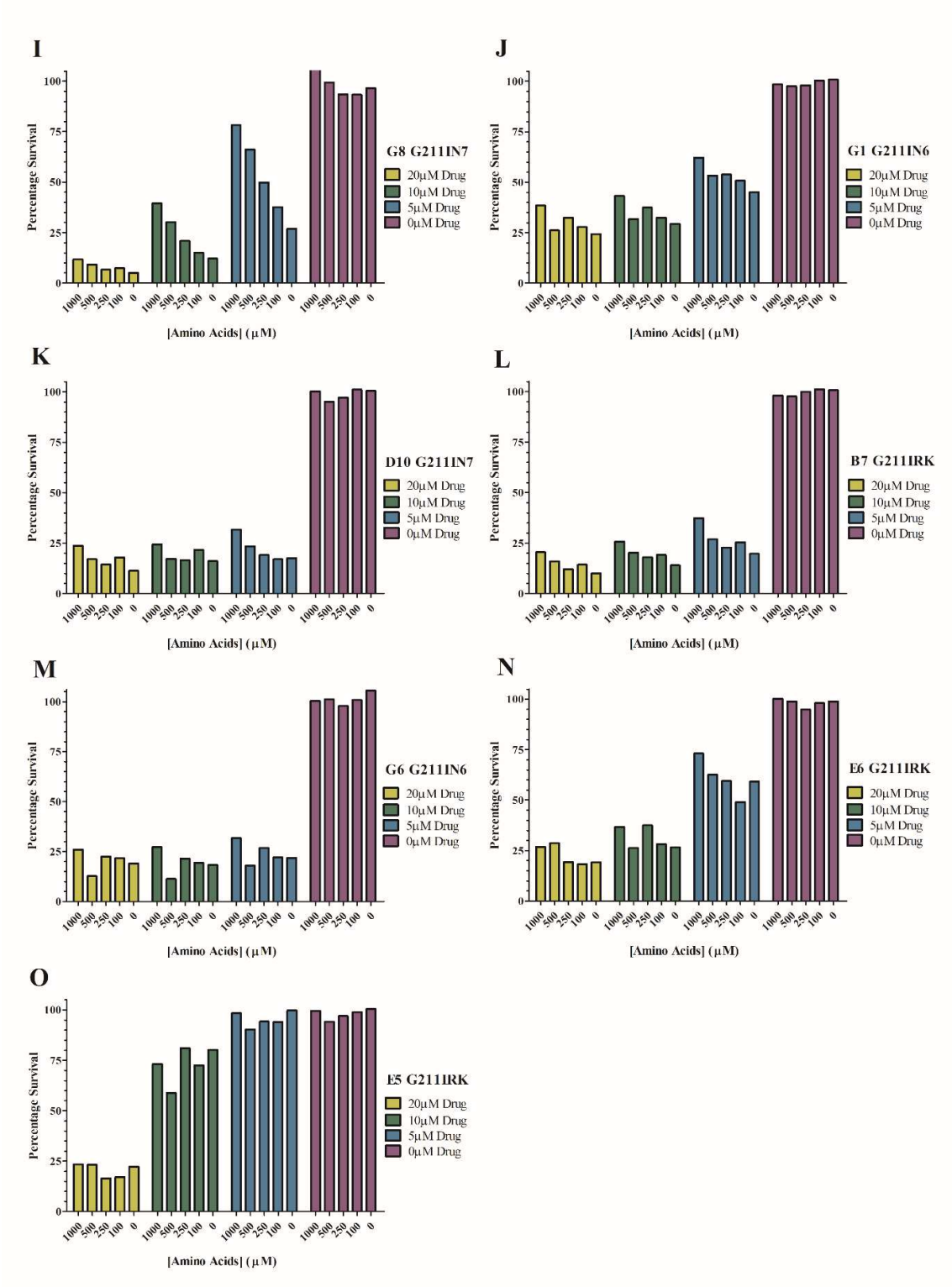


Figure 25. Rescue from hit compounds using amino acid supplementation. *M. bovis* BCG treated with four different concentrations of compound and supplemented with five different concentrations of all twenty amino acids. Single replicate.

2.3.6 Drop-Out Screen with Validation Hits

The drop-out screen was designed to determine whether it was possible to establish which specific amino acids were causing the rescue effect. Due to the entanglement of the amino acid biosynthesis pathways we decided that dropping individual amino acids from the mixture of twenty and looking for a reduction in survival was the best strategy. Figure 26 shows the survival of *M. bovis* BCG in different mixtures of nineteen amino acids when treated with 50 μM of MSM or SMM. MSM and SMM target BCAA biosynthesis and therefore, when valine, leucine, or isoleucine was removed from the media there was a drastic reduction in cell viability. This indicates that this method may work well to narrow down which amino acid biosynthetic pathways are targeted by unknown compounds.

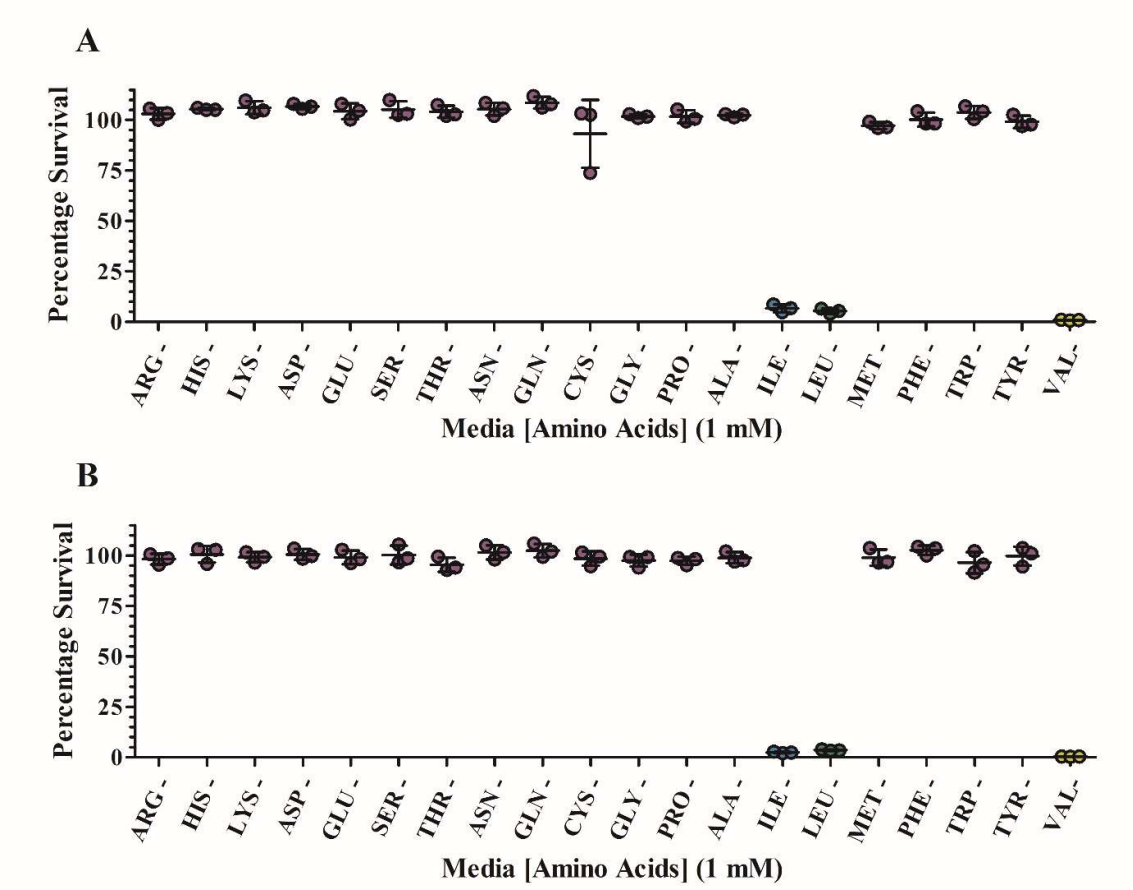
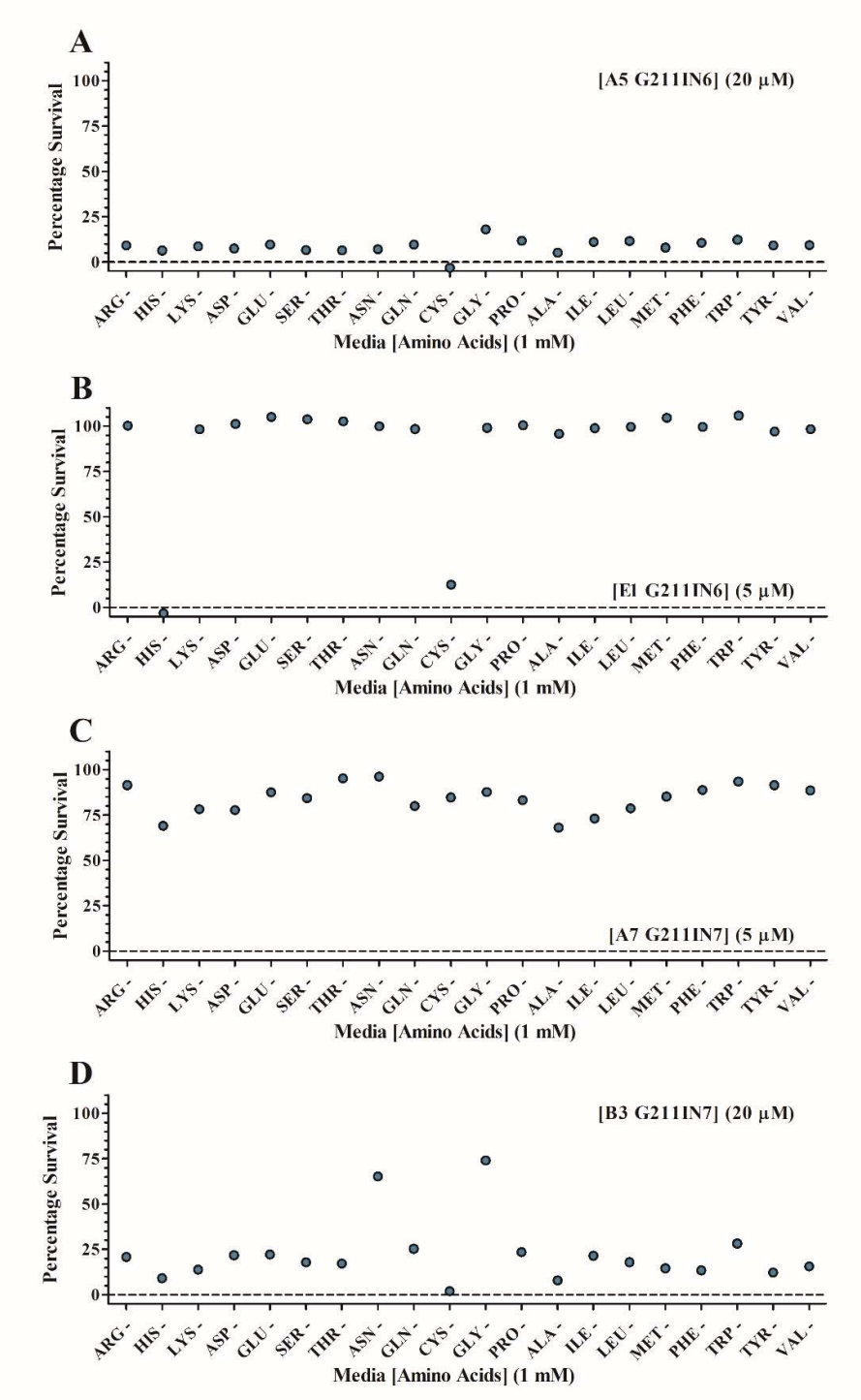


Figure 26. Drop-out screen with validation hits. A MSM supplemented at 50 µM. **B** SMM supplemented at 50 µM. Each data set is labelled by which amino acid was removed from the mixture. Data shown as the mean and standard deviation of triple replicate.

2.3.7 Drop-Out Screen with TB Box Compound Hits

The eight compounds with a favourable response to amino acid supplementation from the dose-response testing were examined for amino acid specificity with the drop-out screen. *M. bovis* BCG was treated with compound based upon the dose response and the concentrations that showed the best range of recovery. Many of the compounds tested showed no clear result with the background noise being much greater than when the same experiment was conducted with the validation compounds. E1 G211IN6 (**B**) and H4 G211IRK (**H**) both showed a heavy reduction in survival when lacking histidine in the media and to a lesser extent a survival reduction when lacking cysteine. G1 G211IRK (**G**)

also showed a reduction without cysteine and with alanine. It must be noted that when lacking cysteine many of the compounds show a slight reduction in survival and when lacking glycine show a slight increase in growth.



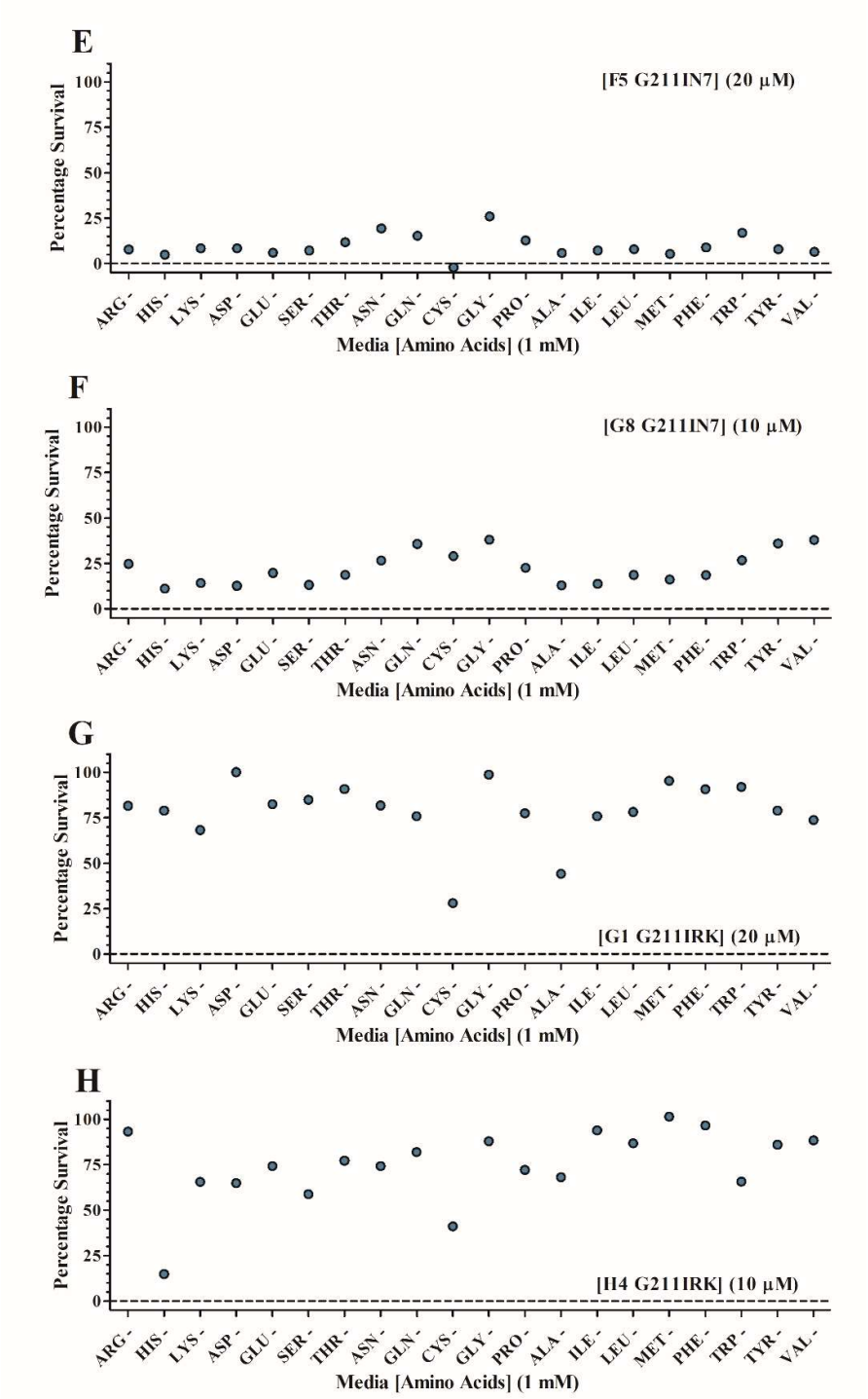


Figure 27. Amino acid drop-out of hits. Cells were treated with compound at the concentration labelled on each graph. Data sets are labelled by which amino acid was removed from the mixture. Single replicate.

2.3.8 Restriction Free Cloning of Acetolactate Synthase (ALS) Catalytic and Regulatory Subunits

The catalytic (*ilvB1*, *ilvB2*, *ilvG*, and *ilvX*) subunits and regulatory (*ilvN*) subunit of ALS were cloned individually and together as pairs into pVV16 using restriction free cloning. The first PCR generated the gene fragments that are used as mega primers for the second PCR stage, as shown in Figure 28. The second PCR used the mega primers to clone the whole plasmid, which results in the incorporation of the gene fragment inside the mega primer. For the paired cloning pVV16 containing *ilvN* with 100 base pairs upstream was used in a third PCR using the catalytic subunit mega primer. These cloned plasmids were then transformed into *E. coli* TOP10 and colony PCR was used to confirm the presence of the gene in the plasmid and shown in Figures 29 and 30. Completed plasmids were sequenced by Eurofins Genomics to check there were no mutations incorporated during the cloning.

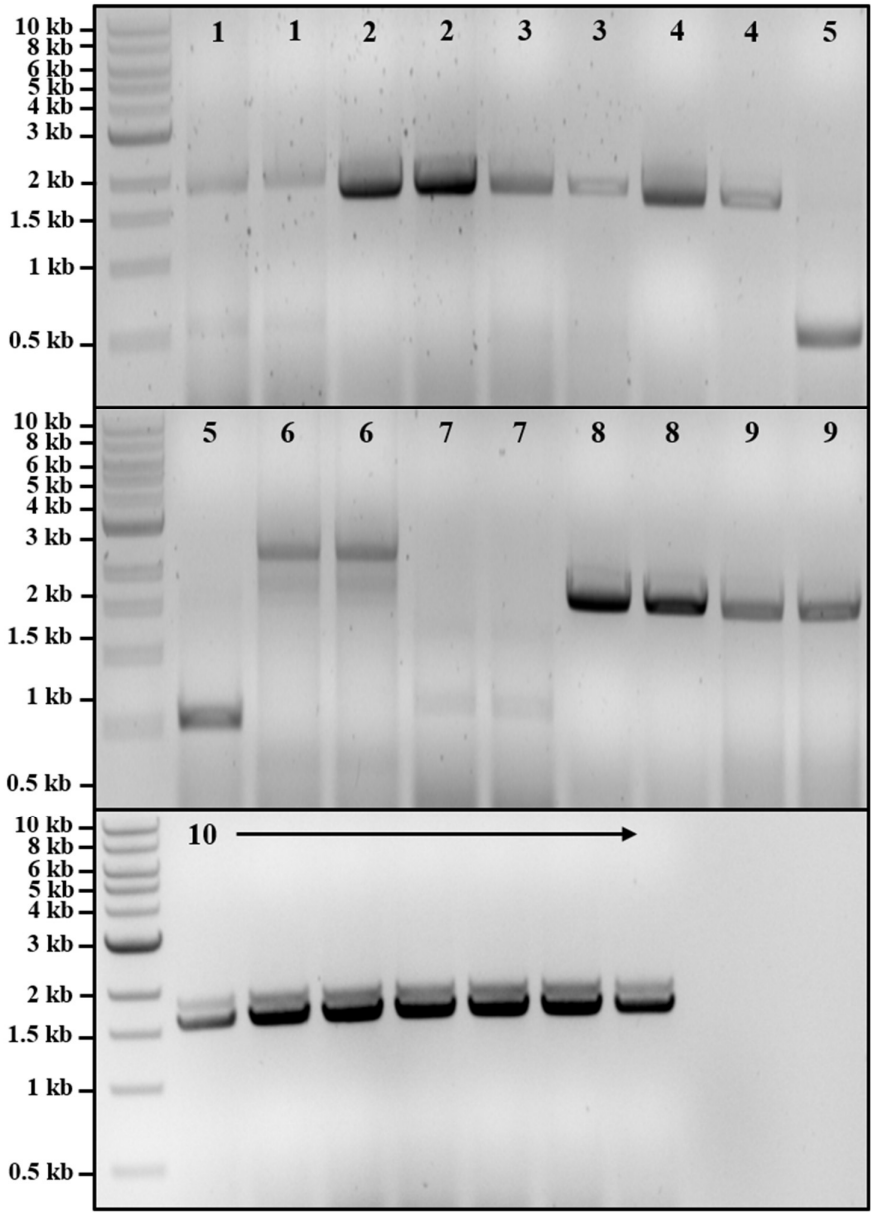


Figure 28. Mega primer PCR. 1 – *ilvB1* 1857 bp, 2 – *ilvB2* 1659 bp, 3 – *ilvG* 1644 bp, 4 – *ilvX* 1548 bp, 5 – *ilvN* 507 bp, 6 – *ilvB1* + *ilvN* 2364 bp, 7 – *ilvN* + 100 bp 607 bp, 8 – *ilvB2* duo 1659 bp, 9 – *ilvG* duo 1644 bp, 10 – *ilvX* duo 1548 bp (lower band).

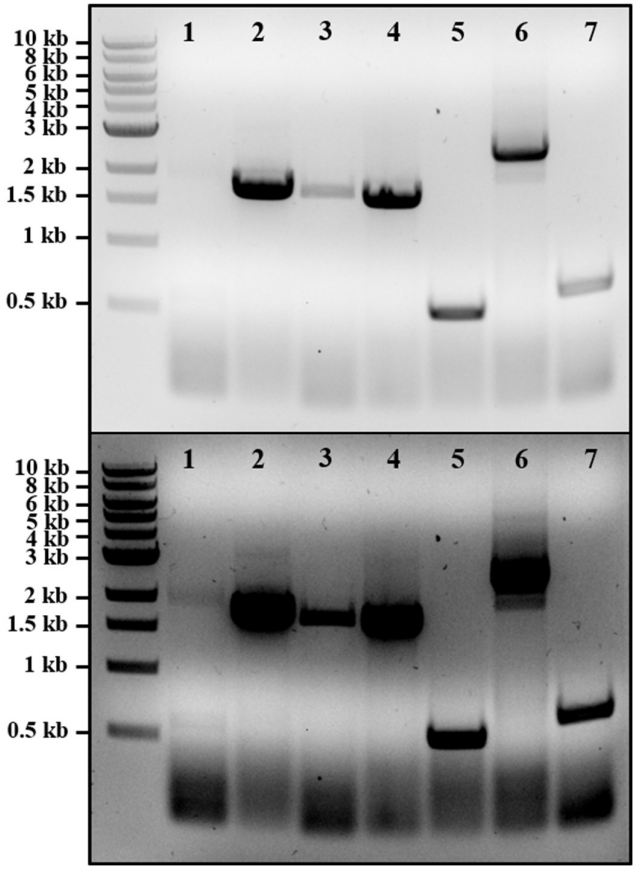


Figure 29. Colony PCR of first gene insertion into plasmid pVV16. 1 – *ilvB1* 1857 bp, 2 – *ilvB2* 1659 bp, 3 – *ilvG* 1644 bp, 4 – *ilvX* 1548 bp, 5 – *ilvN* 507 bp, 6 – *ilvB1* + *ilvN* 2364 bp, 7 – *ilvN* + 100 bp 607 bp. Lower gel image is the same as above with greater exposure to see *ilvB1* fragment.

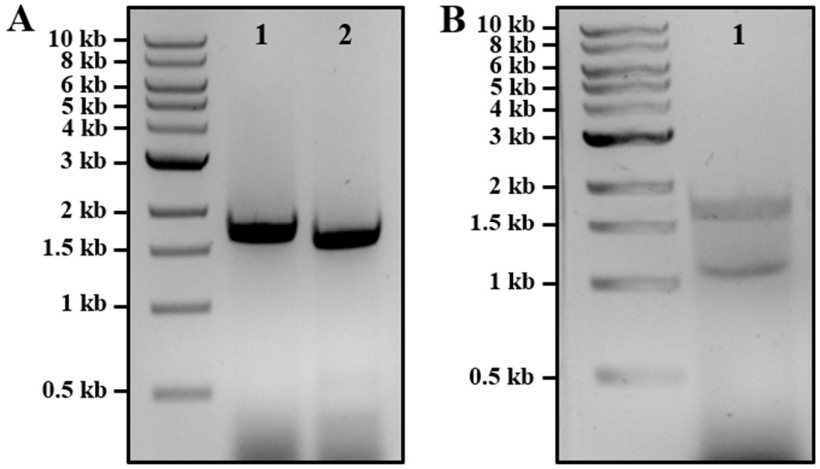


Figure 30. Colony PCR of second gene insertion into plasmid pVV16 containing the *ilvN* + 100 bp fragment. A 1 – *ilvB2* duo 1659 bp, 2 – *ilvG* duo 1644 bp. **B** 1 – *ilvX* duo 1548 bp.

2.3.9 Overexpression of Acetolactate Synthase (ALS) Genes

The ALS genes were cloned into pVV16 and overexpressed in *M. bovis* BCG and treated with MSM and SMM to look for changes in the MIC. When *M. bovis* BCG was electroporated with a plasmid containing *ilvG* the bacteria failed to grow sufficiently, therefore was not tested. The data shown in Figure 31B shows a slight shift in curve for overexpression of *ilvB1* from empty plasmid, however the data points still indicate a similar MIC. The data shown in Figures 31 and 32 show that no significant shift in the MIC for MSM and SMM, when overexpressing ALS genes. This suggests that a mutation in one of the ALS genes is needed to see any change in the MIC.

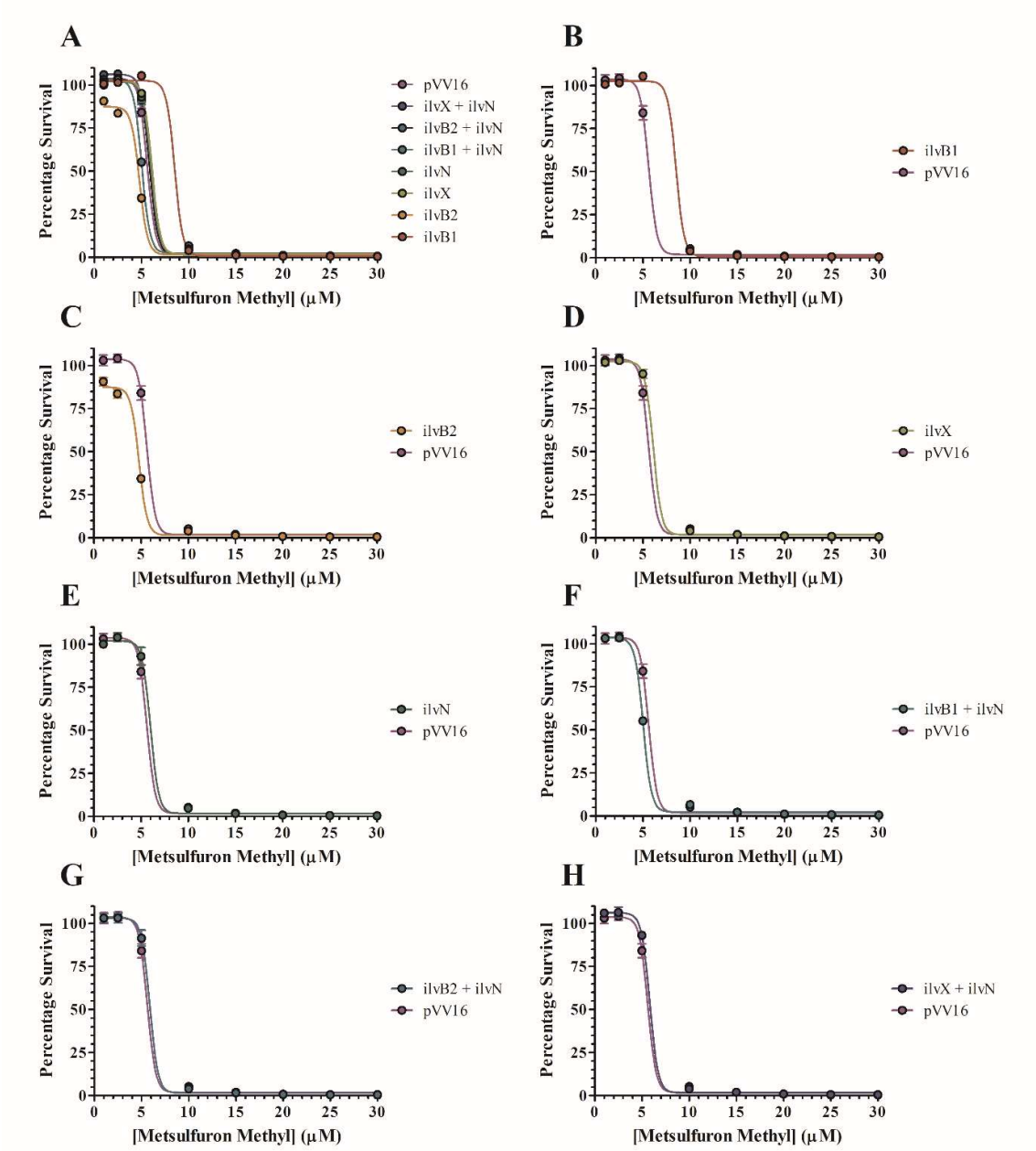


Figure 31. Survival of *M. bovis* BCG overexpressing acetolactate synthase (ALS) treated with metsulfuron-methyl (MSM). Data shown as the mean and standard deviation of triple replicate. **A** Overlaid curves. **B - H** Individual curves. **B** shows a slight shift in curve from the empty plasmid.

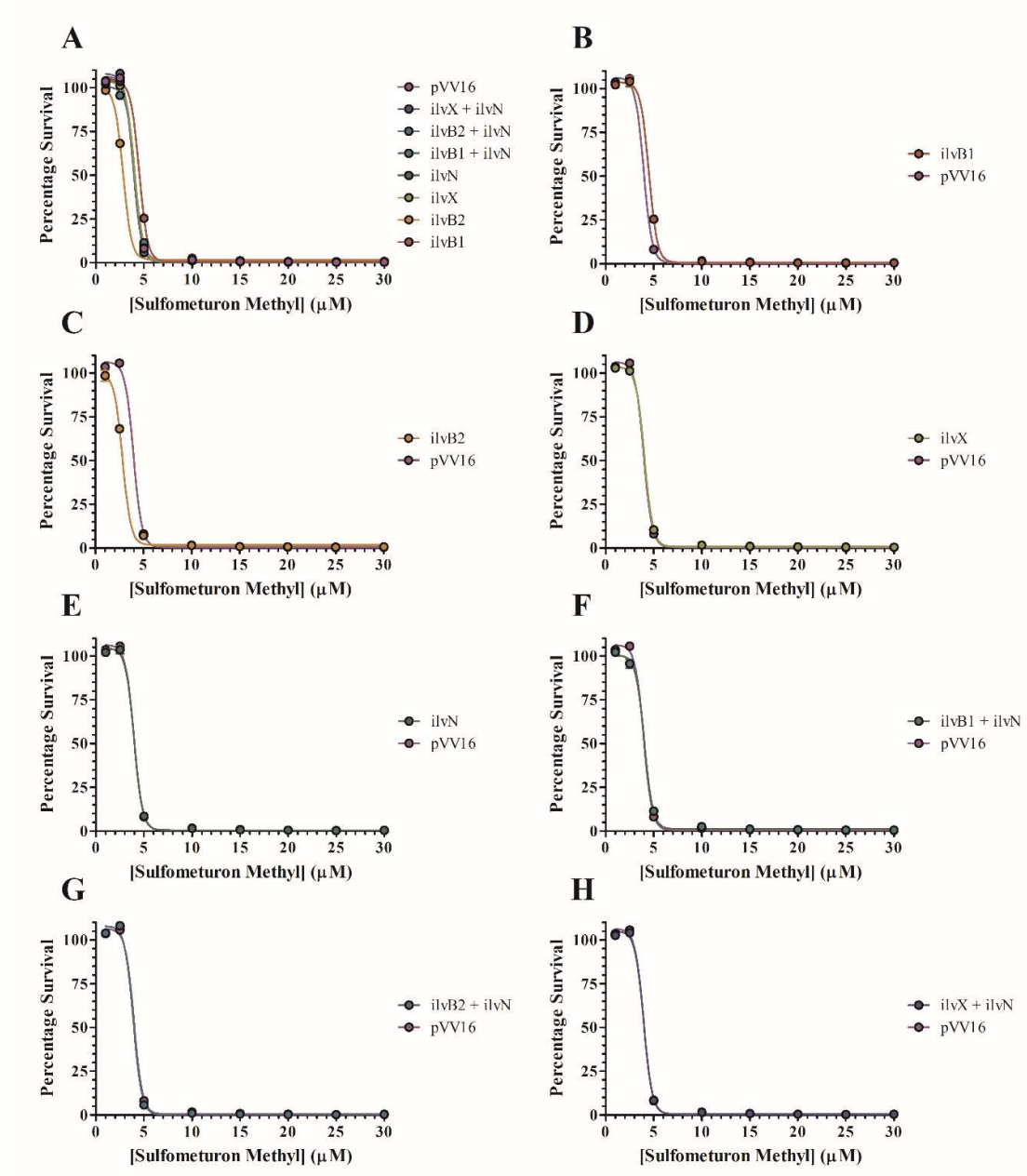


Figure 32. Survival of *M. bovis* BCG overexpressing acetolactate synthase (ALS) treated with sulfometuron-methyl (SMM). Data shown as the mean and standard deviation of triple replicate. **A,** Overlaid curves. **B - H,** Individual curves.

2.3.10 Liquid Minimum Inhibitory Concentrations (MICs) of Hit Compounds

To progress further with the hit compounds the liquid MICs were established. The graphs are shown in Figure 33 and MICs are in Table 9. An MIC for G1 G211IRK (**F**) could not be established despite being repeated. A7 G211IN7 was not able to be progressed due to a compound shortage.

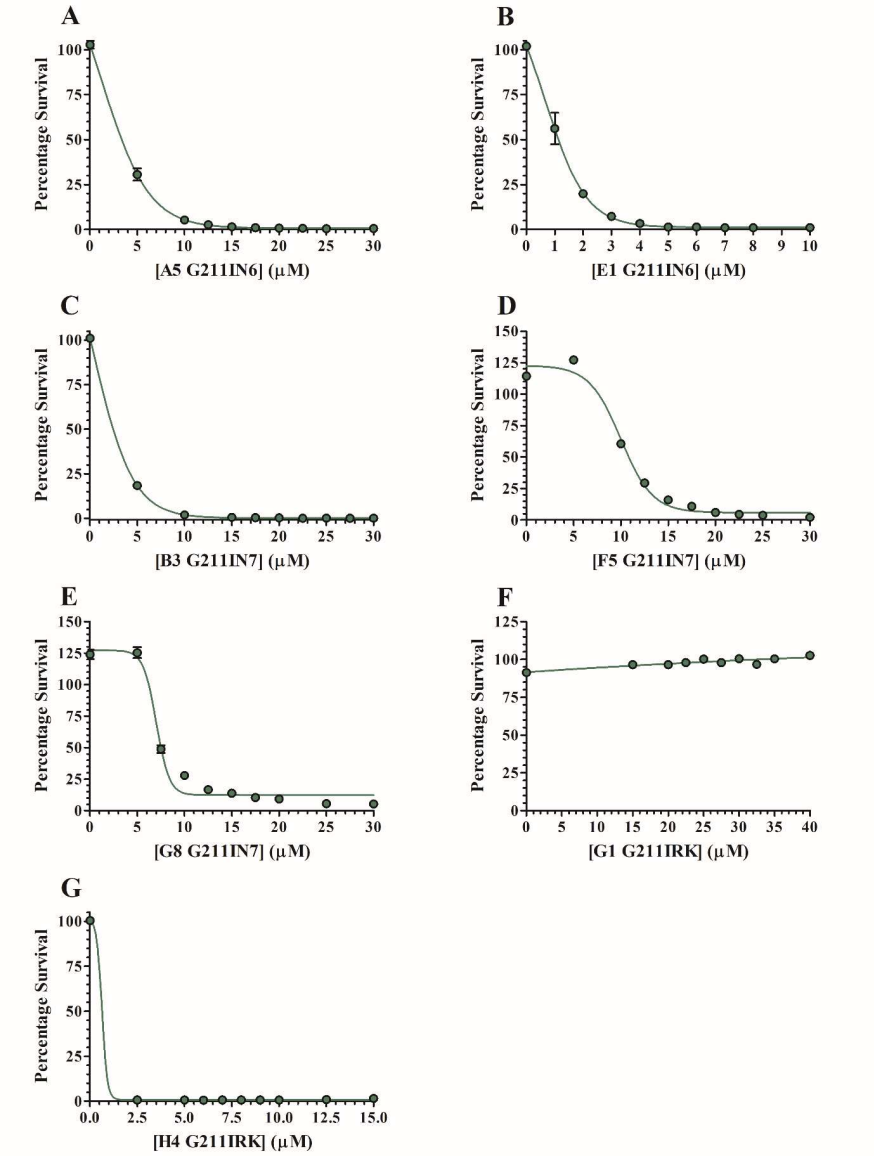


Figure 33. Minimum inhibitory concentration (MIC) graphs for hits. Data shown as the mean and standard deviation of triple replicate.

Table 9. Minimum inhibitory concentrations (MICs) for hits.

Compound	MIC
A5 G211IN6	15 μM
E1 G211IN6	5 μM
B3 G211IN7	15 μM
F5 G211IN7	25 μM
G8 G211IN7	30 μM
G1 G211IRK	>40 μM
H4 G211IRK	<2.5 μM

2.3.11 Drug Resistant Mutant Generation

Spontaneous drug resistant mutants can be isolated from a bacterial culture by plating the cells on media containing high levels of drug. Only the bacteria that can grow in the prescence of the drug will form colonies and allows these mutants to be selected from a large bacterial culture. Isolation of drug resistant mutants to four of the hit compounds and both validation compounds was attempted. Unfortunately, mutant isolation for the hit compounds was unsuccessful with two compounds giving lawns of *M. tuberculosis* H37Rv and the other two showing no growth. This was caused by having to use liquid MIC values which do not always match solid MICs meaning the concentrations of compounds used were too high or too low. Due to a lack of compound the other hits could not be attempted, and the unsuccessful attempts could not be repeated. The validation compounds both produced several colonies of mutant *M. bovis* BCG. Whole genome sequencing revealed that single nucleotide polymorphisms occurred in both *ilvB1* and *ilvN* in each mutant. While there were several different mutations in *ilvB1*, all the *ilvN* mutations were the same with a substitution of threonine for isoleucine at position 50. The different mutations are outlined in Table 10.

Table 10. Whole genome sequencing (WGS) data of *M. bovis* BCG mutants to metsulfuron-methyl (MSM) and sulfometuron-methyl (SMM).

Compound	Mutant	Gene	Base Change	Amino Acid Substitution
MSM	1	*ilvB1*	tGg/tTg	Trp516Leu
		ilvN	aCc/aTc	Thr50Ile
MSM	2	*ilvB1*	gaC/gaA	Asp317Glu
		ilvN	aCc/aTc	Thr50Ile
MSM	3	*ilvB1*	Ccg/Tcg	Pro66Ser
		ilvN	aCc/aTc	Thr50Ile
SMM	1	*ilvB1*	tGg/tTg	Trp516Leu
		ilvN	aCc/aTc	Thr50Ile
SMM	2	*ilvB1*	Ccg/Tcg	Pro66Ser
		ilvN	aCc/aTc	Thr50Ile
SMM	3	*ilvB1*	gTc/gCc	Val137Ala
		ilvN	aCc/aTc	Thr50Ile

2.3.12 Overexpression of Drug Resistant Mutant *ilvB1* and *ilvN* in *M. smegmatis* mc^{2}155

Following the WGS of the MSM and SMM resistant mutants the *ilvB1* and *ilvN* were cloned into pMV261a and pVV16, respectively from mutants with different mutations. To prove the involvement of these mutations an overexpression experiment of *M. smegmatis* mc^{2}155 was conducted to look for a MIC shift of MSM and SMM. The results of the overexpression experiment are shown in Figure 34. The overexpression of wild type *ilvB1* showed slight improvement over the plasmid only control. Both mutant copies of *ilvB1* showed a much greater increase in survivability even at the highest concentrations tested. The overexpression of wild type *ilvN* and mutant *ilvN* showed no

increase in survivability over the plasmid control. Overexpression of both wild type genes together showed a modest increase in survivability, whereas the overexpression of both mutant genes resulted in a level of survival similar to the mutant *ilvB1* overexpressed alone. These results indicate that the most important mutation for resistance to MSM and SMM are in the catalytic protion of the enzyme, IlvB1. The mutations in the regulatory domain, IlvN, may play a role in the stability or regulation of the mutant enzyme complex.

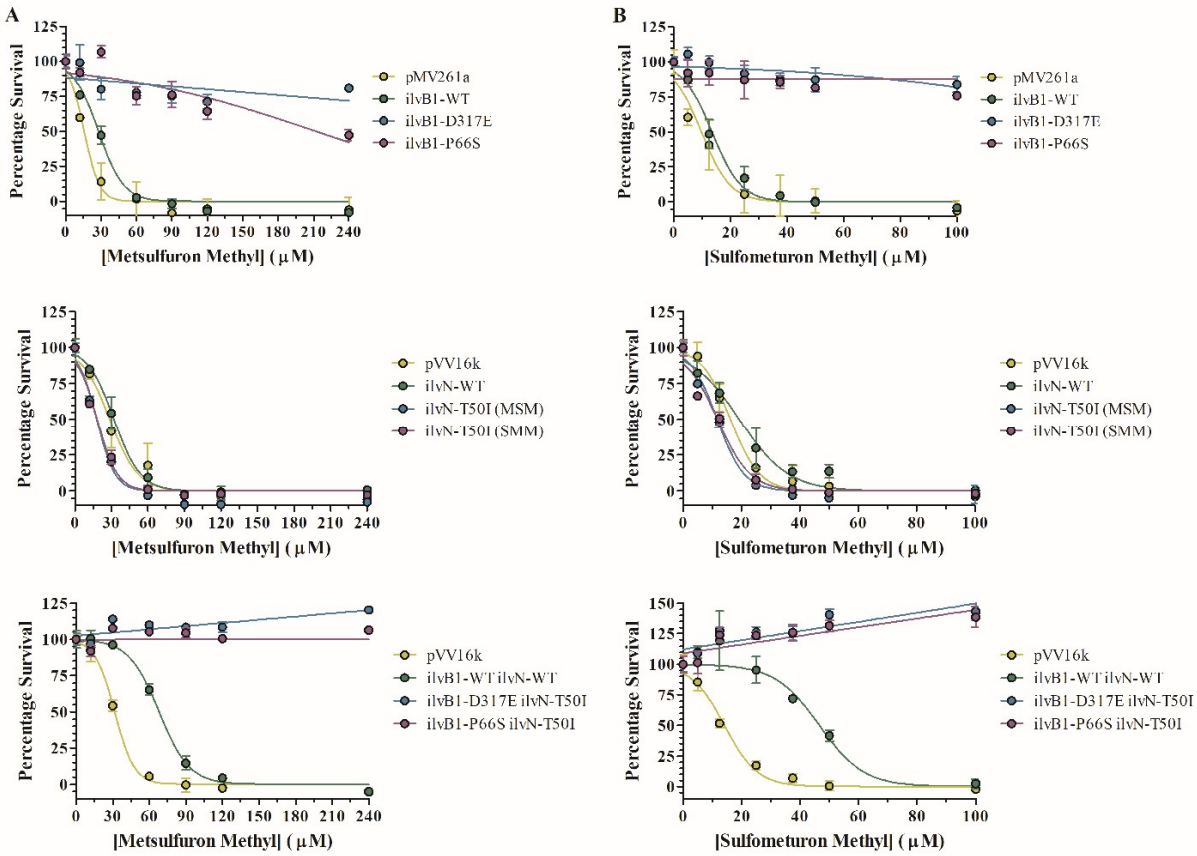


Figure 34. The effect of overexpressing mutant acetolactate synthase (ALS) genes on the minimum inhibitory concentration (MIC) of metsulfuron-methyl (MSM) (A) and sulfometuron-methyl (SMM) (B). Data shown as the mean and standard deviation of triple replicate.

2.4 Discussion

The aim of this project was to design, validate, and utilise a phenotypic screening method for identifying inhibitors of amino acid biosynthesis from large compound libraries. The rationale behind this is to preferentially search for inhibitors of known effective drug targets and to reduce reliance on resistant mutant generation by incorporating target identification into screening.

To identify amino acid synthesis inhibitors *M. bovis* BCG was treated with compounds and supplemented with an amino acid to look for a 'rescue' phenotype. A rescue phenotype was defined as cells that were saved from a compound by supplementation of an amino acid. In practice this was assessed by comparing the survival of *M. bovis* BCG treated with an inhibitor and supplemented with an amino acid to cells without amino acid supplementation. Single amino acid supplementation has been previously shown by Abrahams *et al* (2017) to be effective at identifying tryptophan synthesis inhibitors[331]. Initially this project followed a similar method for screening two hundred and eight compounds from the GSK TB Box set. After screening the compounds with twelve amino acids separately (Figure 23) it became apparent that this method was not effective for all amino acid biosynthesis inhibitors. Many amino acids have shared biosynthetic pathways meaning that the biosynthesis of multiple amino acids could be compromised by a single inhibitor. Single amino acid supplementation will only rescue cells from depletion of that amino acid. This means that biosynthetic inhibitors of two or more amino acids would display as false negatives with this screening method.

The method was adapted using supplementation of all twenty amino acids at once to identify biosynthetic inhibitors of multiple amino acids. This change was validated using BCAA synthesis inhibitors MSM and SMM in a dose response fashion. These inhibitors prevent the biosynthesis of valine, leucine, and isoleucine by inhibiting the activity of

acetolactate synthase. This makes them ideal for testing methods for finding biosynthetic inhibitors of multiple amino acids. As shown in Figure 22 the level of cell survival was dependant on the amount of amino acid and inhibitor the cells were treated with. A phenotypically measurable relationship between cell survival, amino acid supplementation, and inhibitor treatment was ideal for the purpose of this project. The screen was repeated with supplementation of all twenety amino acids giving more convincing results (Figure 24). A total of eighteen hits were found, which were defined as compounds, which displayed a 20 % or greater rescue phenotype. This value was chosen to reduce false positives as much as possible. The list of hit compounds included the TrpA/B inhibitor found by Abrahams *et al*[331]. This indicates that this method was appropriate for finding biosynthetic inhibitors of single amino acids as well as multiple amino acids. Most of the hit compounds were retested with a dose response checkerboard to confirm the relationship between cell survival, hit compound, and amino acid supplementation. Of the compounds retested, eight showed results that were consistent with the dose response displayed by the validation compounds (Figure 25).

A second phase of drop-out screening was designed to narrow down which amino acids were essential for rescue from a hit compound. The survival of *M. bovis* BCG treated with hit compound was measured as in the first phase of screening. The amino acid supplementation was adjusted. Only nineteen of the twenty amino acids were supplemented at once. This resulted in twenty different combinations of nineteen amino acids. This screening method was again validated with MSM and SMM (Figure 26) and found that individually dropping out any of valine, leucine, or isoleucine resulted in a complete loss of cell survival. This is consistent with MSM and SMM inhibiting acetolactate synthase and preventing BCAA biosynthesis, therefore making the supplementation of all those amino acids essential for cell survival. The drop-out

screening was also applied to the hit compounds. Compounds E1 G211IN6 and H4 G211IRK both showed a loss of survival when histidine and cystine were lost from the media. G1 G211IRK showed a loss of survival when cystine and alanine were lost from the media. The cystine hits may have been false positives. Across all the compounds tested, 75 % showed a low survival or the lowest survival when cystine was removed compared to the other conditions. It was thought that this may be due to the thiol group of the cystine participating in redox. This was not investigated further in this project. In addition, the heavy survival reductions without cystine mentioned above have no biosynthetic pathway in common with the other amino acids that were dropping out, histidine or alanine. This is unlikely unless the compound can inhibit enzymes in two different pathways. In general, when compared to the drop-out of the validation compounds the background noise was much higher and this may indicate that the compounds are acting in a way that is nonspecific to amino acid biosynthesis.

In mycobacteria there are several different proteins categorised as catalytic acetolactate synthase subunits: IlvB1, IlvB2, IlvG, and IlvX, and a single regulatory subunit, IlvN, that form a complex together. To see which of these enzymes was inhibited by MSM and SMM the wild type genes were cloned for overexpression in *M. bovis* BCG. The genes were successfully cloned separately and in pairs of catalytic subunit and regulator (Figures 28-30). Overexpression of the genes caused no detectable increase in resistance to MSM and SMM when compared to an empty plasmid strain (Figures 31 and 32). Cells transformed with plasmids containing *ilvG* failed to thrive and were not tested.

Drug resistant mutants were generated for MSM and SMM, and several attempts were made to generate mutants to the hit compounds. Whole genome sequencing (WGS) of several mutant colonies for MSM and SMM revealed that both compounds targeted a single catalytic subunit, IlvB1. Furthermore, many of the mutations were the same for

each compound. In addition, every mutant had a complimentary mutation present in IlvN, which were all the same. While attempted, no mutants could be raised against the hit compounds and stocks of the compounds in question ran out and could not be replenished. The lack of resistant mutants could, in part, be explained by the usage of liquid MICs rather than solid MICs. Variation between liquid and solid MICs is not uncommon and as such the compound concentrations used for mutant generation could have been too high or too low to permit effective mutant selection.

Two mutant copies of *ilvB1* and *ilvN* were cloned from the drug resistant mutants to retry overexpression. The genes were cloned and overexpressed in *M. smegmatis* mc^2155 and compared to empty plasmid and wild type *ilvB1* and *ilvN*. Overexpression of the mutant copies of IlvB1 led to a large increase in resistance to MSM and SMM compared to the wild type and empty plasmid. In contrast, overexpression of the mutant IlvN showed no increased resistance to MSM and SMM. Overexpression of the mutant IlvB1 and IlvN together showed the same resistance profile as mutant IlvB1. Overexpression of wild type IlvB1 and IlvN did show a modest increase in resistance to MSM and SMM in contrast to what was found in the original overexpression in *M. bovis* BCG.

The validation of these screening methods with MSM and SMM has shown that they are capable of filtering out and partially identifying the targets of amino acid biosynthesis hits. The initial screening of MSM and SMM showed a potent dose response in line with what would be expected of amino acid biosynthesis inhibitors. The drop-out screen was able to identify which amino acids were critical to cellular survival when treated with MSM and SMM. These results were also supported by the whole genome sequencing (WGS) of drug resistant mutants and overexpression experiments. In practice screening for unknown inhibitors of amino acid biosynthesis from a compound library was not as easy. While the primary screen was good at filtering a large number of compounds to a

small number of hits, the drop out screen was not as reliable. High levels of background noise and potential false positives meant that the results were not as useful. The lack of resistant mutants for genome sequencing meant that the project could not progress as planned. These screening methods are probably more suited for a specific subset of amino acid, which have relatively isolated biosynthetic pathways. Amino acids, such as tryptophan, tyrosine, phenylalanine, valine, leucine, isoleucine and histidine are good candidates for this type of screening. Indeed, valine, leucine, and isoleucine biosynthesis inhibitors were used for the validation of these methods and a tryptophan biosynthesis inhibitor was discovered using similar methods[331]. In an ideal situation where compound was not limited this project would have benefited from the drop-out screen being repeated in triplicate. In addition, more compound would have meant that solid MICs could have been measured allowing for more effective attempts at drug resistant mutant generation. While a secondary objective of this project aimed to reduce reliance on drug resistant mutants, that reliance could not be eliminated completely.

Chapter 3

High-Throughput Screening, Microbiological Techniques, and Biochemical Assays for Identifying Novel Inhibitors of the Protein Synthesis Pipeline

3 High-Throughput Screening, Microbiological Techniques, and Biochemical Assays for Identifying Novel Inhibitors of the Protein Synthesis Pipeline

3.1 Introduction

The protein synthesis pipeline is the system that produces protein *via* DNA transcription to RNA, then translation of the RNA into protein. This is an essential process for all biological life and there are a number of conserved enzymes to perform this sequence of events. The primary enzyme components to the pipeline are RNA polymerase and its associated regulators, tRNA synthases and the ribosome. RNA polymerase is a large enzyme complex responsible for translating DNA into RNA. RNA polymerase is made up of five subunits, two α subunits (RpoA), a β subunit (RpoB), a β' subunit (RpoC), and a ω subunit (RpoZ)[342,343]. There are multiple types of RNA produced, including messenger RNA (mRNA), transfer RNA (tRNA) and ribosomal RNA (rRNA), all of which are essential for protein synthesis. The ribosome then translates the mRNA into protein by matching codons from the mRNA with the codons on tRNA and using the associated amino acid in the protein chain.

Transcription begins with the attachment of RNAP to a sigma factor to form RNAP-Holo, which then binds to the promotor region of a gene. The formation of RNAP-Holo is stabilised by two essential transcription factors, CarD[344,345] and RbpA[346]. CarD stabilises RNAP-Holo by inserting a tryptophan residue into the upstream edge of the transcription bubble[345] which prevents the bubble collapsing[347–349]. RbpA acts by anchoring the promotor DNA to RNAP-Holo[346]. The unstructured N-terminal tail of RbpA fits into the active site grove and has an unknown interaction with the -5 position base of the template strand[350]. CarD and RbpA work together synergistically to stabilise the usually short-lived *M. tuberculosis* RNAP-Holo complex[347]. *M. tuberculosis* has thirteen sigma factors of the sigma 70 variety[51,351] of which SigA is the group 1, primary 'housekeeping' factor

of the bacterium. Promotor regions contain two areas of six high probability bases, known as the -10 and -35 consensus regions[352], which serve as a recognition site for the sigma factor in the RNAP-Holo complex. Once RNAP-Holo has bound to the DNA it enters an open confirmation and separates the DNA into single strands from the -12 base to the +2 base[343]. After synthesis of a short DNA-RNA hybrid strand of approximately 8-9 base pairs long RNAP-Holo begins 'scrunching', where RNAP-Holo continues to synthesise RNA without moving along the DNA, because it is still attached to the promoter, by pulling DNA inside the complex and scrunching the DNA up[353]. Scrunching allows the RNAP-Holo to continue transcription and provides the tension in the complex to allow promoter escape[354].

Once detachment from the promoter is achieved the sigma factor detaches and the RNAP enters the elongation phase. During the elongation phase one base pair of the double stranded DNA downstream is decoupled at a time in front of the active site[355]. This only allows for the addition of one nucleotide substrate at a time. Additionally, one base pair from the DNA-RNA hybrid, furthest from the active site, decouples and one base pair of coding strand DNA and non-coding strand DNA anneal upstream of the enzyme[355].

Termination of transcription happens downstream of the translation stop codon and can occur with or without aid from a DNA-RNA Helicase, Rho. Rho independent transcription termination occurs when a C/G rich hairpin structure forms in the extruded RNA that causes a pause in RNA transcription. This pause in transcription needs to be coupled with the DNA-RNA hybrid being formed mostly of uridines. The strong C/G rich hairpin allows a stall in progress long enough for the weaker DNA-RNA hybrid bond to dissociate and the RNA to leave[356]. Rho dependant transcription termination requires the Rho helicase to thread the new RNA through a central pore. Rho then uses ATP hydrolysis to traverse along the RNA in the 5' to 3' direction to catch up to the RNAP

and remove the RNA from the RNAP[357]. In order for Rho to catch RNAP there is a pause in movement of RNAP caused by a RNA hairpin structure[358]. The binding of Rho to the RNA is dependent on the accessibility of Rho utilisation (RUT) sites, loop structures in the RNA can often obscure RUT sites allowing a degree of control over premature termination [359].

The mRNA produced by RNA polymerase is then used by the ribosome to produce protein. The bacterial ribosome is a large RNA and protein structure formed of two subunits, the small reading 30S subunit and the large catalytic 50S subunit. These subunits, together form the bacterial 70S ribosome. The 30S subunit consists of the 16S RNA strand and twenty one proteins, and the 50S subunit consists of the 23S and 5S RNA strands and thirty six proteins[360]. Most of these elements are highly conserved but mycobacterial ribosomes have a few deviations[361]. The 70S ribosome has three sites of activity located in the cleft between the 30S and 50S subunits called A, P, and E. The A (Aminoacyl or Acceptor) site receives tRNA complimentary to the mRNA[362]. The P (Peptidyl) site forms a peptide bond between the amino acid in the P site and the new amino acid in the A site. The E (Exit) site is the release site for the tRNA after the amino acid has been added to the growing peptide chain.

The initiation of translation is driven by the formation of the pre-initiation complex. This is the binding of mRNA to the 30S subunit in combination with initiation factors 1[363], 2[364] and 3[365], and N-formylmethionine loaded tRNA. The binding is facilitated by a purine rich location in the mRNA upstream of the translation start site, known as the ribosome binding site or the Shine-Dalgarno (SD) sequence. The SD sequence associates with a complimentary anti-SD nucleotide sequence in the 30S subunit. The 30S subunit then relocates so that the start codon of the mRNA is in the P site, where the 50S subunit binds and initiates translation using N-formylmethionine loaded tRNA[366]. A second type of

initiation bacteria are capable of using called leaderless translation occurs with mRNA transcripts without a SD sequence. The mRNA needs to start with an AUG or GUG codon and the 5' end must be phosphorylated[367,368]. Pre-formed 70S ribosomes can translate from this mRNA with assistance from initiation factor 2[369].

Once the 70S complex is formed around the mRNA the elongation phase can begin with the assistance of three elongation factors, EF-Tu, EF-Ts, and EF-G. Elongation involves the movement of mRNA through the APE sites of the ribosome one codon at a time. As a new codon is ratcheted into the A site an amino acid loaded tRNA with the corresponding anti-codon is inseted into the A site by EF-Tu[370]. The peptide bond is formed between the amino acids in the A and P site. EF-G then pushes the tRNA along to the next site[371]. This results in the A site becoming available for a new tRNA and a tRNA sans amino acid being expelled from the E site. EF-Ts complexes with an unloaded EF-Tu and allows the release of the bound GDP, this allows EF-Tu to pick up a fresh GTP and tRNA[372].

Translation termination is controlled by the presence of a stop codon in the mRNA sequence and by three proteins known as release factors. Once a stop codon has moved into the A site tRNA will no longer be able to interact. Instead the stop codon is recognised by release factors RF1 and RF2. RF1 and RF2 cause the hydrolysis of the bond between the finished peptide chain and the tRNA in the P site[373]. The stop codons, UAA, UAG, and UGA[374], are recognised by specific release factors. RF1 recognises UAG, RF2 recognises UGA, and both recognise UAA[375,376]. RF3 starts the ribosome recycling process by catalysing the release of RF1 or RF2 from the ribosome[377–379]. Ribosome recycling factor (RRF) and EF-G are required to break down the 70S ribosome once translation is complete[380–383]. First the mRNA is displaced from the complex, then the last

tRNA molecule present in the P site[384]. Once these are removed the ribosome can dissociate freely.

For the ribosome to carry out translation efficiently it needs a steady supply of tRNA loaded with amino acids. The process of loading tRNA in *M. tuberculosis* is carried out by approximately twenety two tRNA synthases[51]. Synthesis of tRNA begins with transcription of the tRNA gene by RNA polymerase which usually terminates in a Rho independent manner[385]. The 5'and 3' ends of the tRNA often need post translational editing to form mature tRNA ready for loading. The 5' end is edited by ribonuclease P, a universally conserved protein across all domains of life[386,387]. The 3' end of tRNA requires a CCA tail to accept the attachment of an amino acid. Of the forty five annotated *M. tuberculosis* H37Rv tRNA genes in Mycobrowser[388], only ten have a CCA tail, meaning that many tRNA need additional processing at the 3' end[385]. Once the tRNA is matured it can be loaded with an amino acid by a tRNA synthase. The tRNA synthase uses ATP to transfer an amino acid to the 2nd or 3rd hydroxyl group of adenine in the terminal 3' CCA tail[389,390]. The loaded tRNA can then picked up by EF-Tu and used in translation.

The majority of the enzymes and co-factors involved in the protein synthesis pipeline are crucial to all bacteria including *M. tuberculosis.* Many antibiotics already target parts of the protein synthesis pipeline. The first drug used for the treatment of TB was streptomycin, a protein synthesis disruptor that interferes with the proofreading ability of the ribosome[105–110]. Rifampicin, a drug currently used as part of the frontline treatment of TB inhibits RNA polymerase by blocking the exit of the RNA chain from the polymerase[152–156]. A few inhibitors have been described that inhibit tRNA synthetase in mycobacteria although they are not currently used as treatments[391–394]. The abundance of targets in the protein synthesis pipeline and there near universal essentiality for

mycobacterial survival make large-scale screens dedicated to finding these inhibitors an attractive prospect. This project focused on the development and use of a new phenotypic screening method for protein synthesis pipeline inhibitors and biochemical assays to identify where in the pathway an inhibitor takes effect.

Assays to assess inhibitor effectiveness against RNA polymerase and ribosome targets were developed as part of this study. The RNA polymerase assay used the broken-beacon technique[395], shown in Figure 35, to detect RNA transcripts produced. In short, commercial *E. coli* polymerase was given the start portion of the *mmsA* gene to transcribe. A twenty four base pair DNA probe with a 5' TAMRA fluorophore was made to be complimentary to the *mmsA* gene. A shorter, 14 base pair DNA probe with an attached 3' black hole quencher 2 (BHQ2) was produced to be complimentary to the fluorescent probe. When the DNA probes are hybridised the 5' TAMRA and 3' BHQ2 line up and the fluorescence is quenched. When the hybridised probes encounter the *mmsA* transcript the longer fluorescent probe separates from the quencher probe and hybridises with the transcript. This allows the TAMRA to fluoresce, which can be detected by a plate reader. The fluorescence is proportional to the amount of RNA transcript produced by RNA polymerase. The ribosomal assay used a commercial Δ ribosome Purexpress kit and purified *M. smegmatis* ribosomes. The ribosomes were given an RNA template of mCherry to translate. This resulted in the production of fluorescent mCherry, which can be detected by a plate reader.

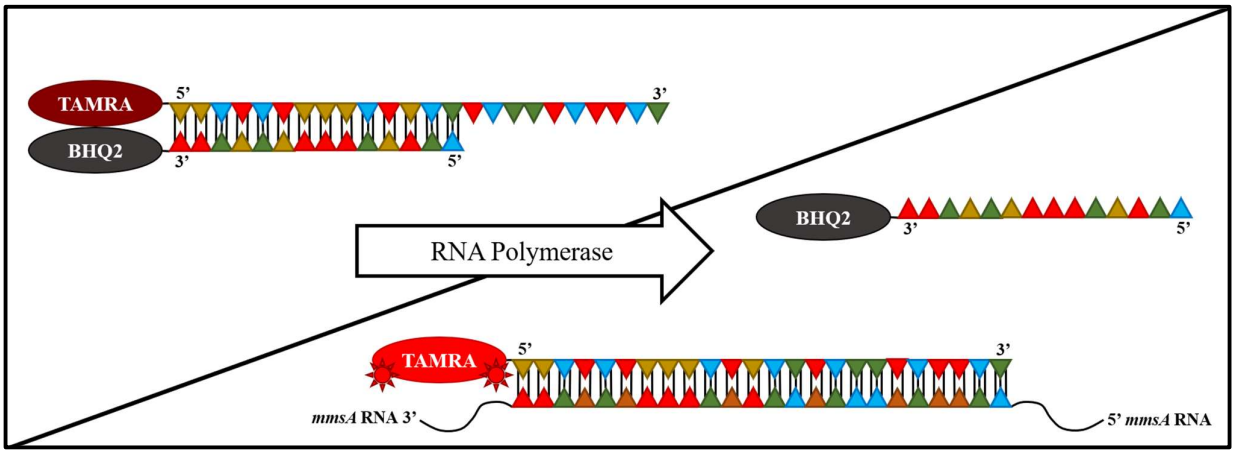


Figure 35. Broken beacon RNA polymerase assay. A 24 base pair DNA oligo with a 5' TAMRA flurophore modification complimentary to the *M. tuberculosis mmsA* gene is hybridised with a 14 base pair DNA with a 3' BHQ2 quencher modification. While the TAMRA and BHQ2 oligos are hybridised the BHQ2 quenches any fluorescence. When exposed to mRNA of *mmsA* gene produce by RNA polymerase from an *mmsA* double stranded template the TAMRA oligo preferentially hybridises with the longer mRNA strand. This releases the short BHQ2 quencher oligo and results in a detectable increase in fluorescence.

3.2 Materials and Methods

3.2.1 Preliminary mCherry Reporter Screen Using *M. tuberculosis* Protein Synthesis Inhibitors

A test screen was designed using hits identified as protein synthesis inhibitors by Professor James Sacchettini (Unversity of Texas A & M) using a cell free extract system. The hits were dissolved in DMSO and were pipetted into microplates (Greiner, 384 well, PS, F-clear bottom, black, sterile. Ref – 781097) using an Echo Acoustic dispenser (Labcyte) by GlaxoSmithKlein (GSK). *M. tuberculosis* H37Rv containing pTIC6a-*mCherry* was grown to mid-log (OD_{600} 0.4-0.8) supplemented with 25 μg/mL kanamycin. The cells were pelleted at 4,000 rpm and washed twice in 7H9 without kanamycin to remove trace kanamycin from the cultures. The cells were split into two groups and adjusted to OD_{600} 0.4 and one group was induced with 100 ng/mL of anhydrotetracycline and the other group was left uninduced. Each well was made up to 50 μL with cells and incubated at 37 °C with 5 % CO_2 for 48 hours. A PHERAstar FS BMG labTech plate reader at excitation 580 nm and emission 620 nm was used to read the mCherry fluorescence. The resazurin survival assay was then carried out (**Method 6.6.1**) but was modified for a volume of 50 μL. Plates were assessed individually by eye for colour change in the resazurin.

3.2.2 High Throughput Single Shot Screen of the GlaxoSmithKlein TB Box

M. tuberculosis H37Rv containing pTIC6a-*mCherry* were prepared as in **Section 3.2.1** and supplemented with 100 ng/mL of anhydrotetracycline. The screen was conducted in microplates (Greiner, 384 well, PS, F-clear bottom, black, sterile. Ref – 781097) and each hit had two different final concentrations, 10 μM and 1 μM. Hits were dissolved in 100 % DMSO and were dispensed into microplates at GSK by an Echo Acoustic dispenser

(Labcyte). Each well was made up to 50 µL with cells and incubated at 37 °C with 5 % CO_2 for 60 hours. A PHERAstar FS BMG labTech plate reader at excitation 580 nm and emission 620 nm was used to read the mCherry fluorescence. The resazurin survival assay was then carried out (**Method 6.6.1**) but was modified for a volume of 50 µL.

3.2.3 High Throughput Dose Response Screen of the GlaxoSmithKlein TB Box

M. tuberculosis H37Rv containing pTIC6a-*mCherry* were prepared as in **Section 3.2.1** and supplemented with 100 ng/mL of anhydrotetracycline. The screen was conducted in microplates (Greiner, 384 well, PS, F-clear bottom, black, sterile. Ref – 781097) and each compound had a range of final concentrations spanning from 50 µM to 0.846 nM. Hits were dissolved in 100 % DMSO and were dispensed into microplates at GSK by an Echo Acoustic dispenser (Labcyte). Each well was made up to 50 µL with cells and incubated at 37 °C with 5 % CO_2 for 60 hours. A PHERAstar FS BMG labTech plate reader at excitation 580 nm and emission 620 nm was used to read the mCherry fluorescence. The resazurin survival assay was then carried out (**Method 6.6.1**) but was modified for a volume of 50 µL.

3.2.4 Protein Synthesis Hits Liquid Minimum Inhibitory Concentrations (MICs)

Several dilutions of the protein synthesis hits were made in compound plates (Greiner, 96 well, PP, V-bottom. Ref - 651201) at 100x concentration. In separate microplates (Greiner, 96 well, PS, F-bottom, black, sterile. Ref - 655086) for each compound, 1 µL of the 100x dilutions was added in triplicate to each plate as well as triplicate wells of 1 µL DMSO and 100 µM rifampicin. Each well was made up to 100 µL with mid-log (OD_{600} 0.4-0.8) *M. bovis* BCG or *M. smegmatis* mc^2155 that had been normalised to a cell density of $1x10^6$ cells/mL. This gave $1x10^5$ cells per well. The plates were sealed with parafilm

and tin foil and incubated at 37 °C and 5 % CO2 for 1 day for *M. smegmatis* mc^2155 or 7 days for *M. bovis* BCG after which a resazurin survival assay was carried out (**Method 6.6.1**).

3.2.5 Protein Synthesis Hits Solid Minimum Inhibitory Concentration (MIC)

Dilutions of hits were made at 100x the desired concentration in DMSO. Each hit (10 µL) was pipetted into 1.5 mL microcentrifuge tubes. 7H11 agar (1 mL) was mixed with the hit in the microcentrifuge tubes and pipetted into a 48 well microplate (Corning Costar, 48 Well Cell Culture Cluster, 3548). The agar was allowed to set. A mid-log (OD_{600} 0.4-0.8) *M. tuberculosis* H37Rv *ΔleuDΔpanCD* strain culture was adjusted to $2x10^4$ cells/µL and 5 µL were spotted into the centre of each well. The plate was incubated at 37 °C with 5 % CO_2 for 3 weeks until the control spots had grown sufficiently. The MIC was determined as the well with the lowest concentration of the hit on which there was no growth. A few hits had their solid MIC determined in wild type *M. tuberculosis* H37Rv using the same method.

3.2.6 Protein Synthesis Hits Drug Resistant Mutant (DRM) Generation

Large 20 mL 7H11 agar plates for the growth of the *M. tuberculosis* H37Rv *ΔleuDΔpanCD* strain were set up containing compounds at the desired concentration with a maximum DMSO concentration of 1 %. Concentrations were typically 0x, 2.5x, 5x, and 10x the minimum inhibitory concentration (MIC). Plates were sent to Dr Alistair K. Brown (University of Newcastle) and plates inoculated. Mid-log (OD_{600} 0.4-0.8) *M. tuberculosis* H37Rv *ΔleuDΔpanCD* strain cultures were adjusted to $1x10^9$ cells/mL and 100 µL of cells were spread out on the agar plate for $1x10^8$ cells on each plate. The agar plates were incubated at 37 °C with 5 % CO_2 until colonies appeared (approximately 1-2

months). A few compounds had DRMs generated in wild type *M. tuberculosis* H37Rv using the same method.

3.2.7 Hit 45 and 46 Drug Resistant Mutant (DRM) Cross Resistance Tests

Hits 45 and 46 DRMs were tested using rifampicin for cross-resistance. Rifampicin was aliquoted into a plate (Greiner, 96 well, PP, V-bottom. Ref - 651201) at 100x, the desired concentration. Rifampicin (1 μL) at each concentration was added to the wells of the microplate (Greiner, 96 well, PS, F-clear bottom, black, sterile. Ref – 655090). Cultures of *M. tuberculosis* H37Rv and the DRM of *M. tuberculosis* H37Rv were grown to mid-log (OD_{600} 0.4-0.8) and had cell density adjusted to $1x10^6$ cells/mL. Cells (100 μL) were added to each well. The plates were sealed with parafilm and tin foil and incubated at 37 °C and 5 % CO_2 for 7 days after which a resazurin survival assay was carried out (**Method 6.6.1**).

3.2.8 Producing Artificial *rpoABCZ* Operon by Gibson Cloning

An artificial *rpoABCZ* operon was created by cloning each gene and inserting them into pMV261k. Primers approximately 30 base pairs long were designed by the NEBuilder website (nebuilder.neb.com) to have a forward and reverse sequence for cloning each gene fragment with complementary overhangs for the adjacent fragments. Primers are listed in Table 11. The fragments were replicated using a standard PCR (**Method 6.4.2**), run using agarose gel electrophoresis (**Method 6.4.3**) and purified from the agarose (**Method 6.4.4**). The fragments were assembled using a NEBuilder HiFi DNA Assembly Cloning Kit (NEB, E5520S). Fragments (0.5 pmol) were mixed in a 1:1 ratio, 10 μL of NEBuilder HiFi DNA assembly master mix was added and the reaction was made up to 20 μL with dH_2O. The reaction was incubated at 50 °C for 1 hour. The assembled plasmid

was transformed into 5-alpha competent *E. coli* (NEB) using the SOC outgrowth medium provided in the kit (**Method 6.3.5**). Cells were plated out onto LB agar plates with 50 µg/mL kanamycin and incubated at 37 °C overnight. Colonies were picked and tested using colony PCR (**Method 6.4.2**) and the plasmid extracted (**Method 6.4.8**). Plasmids were sequenced by Eurofins Genomics.

Table 11. Primers for *rpoABCZ* operon Gibson cloning.

Gene Fragment	Primer Direction	Sequence 5'- 3' (Overlap/Anneal)
pMV261k	Forward	gggcgagtga/atcgatgtcgacgtagttaactagc
pMV261k	Reverse	agatcagcat/gccacggatgccaccaca
rpoA	Forward	catccgtggc/atgctgatctcacagcgc
rpoA	Reverse	gaatctgcca/tcaaagctgttcggtttcg
rpoB	Forward	acagctttga/tggcagattcccgccagag
rpoB	Reverse	acgtcgagca/tcacgcaagatcctcgacac
rpoC	Forward	tcttgcgtga/tgctcgacgtcaacttcttc
rpoC	Reverse	gagatactca/tcagcggtagtcgctgtag
rpoZ	Forward	ctaccgctga/tgagtatctcgcagtccgac
rpoZ	Reverse	cgacatcgat/tcactcgccctcggtgtg

3.2.9 Overexpression of *rpoABCZ* Operon in *M. smegmatis* mc^{2}155 and *M. bovis* BCG

Electrocompetent *M. smegmatis* mc^{2}155 and *M. bovis* BCG were electroporated with pMV261k-*rpoABCZ* as *per* **Method 6.3.6** and selected using 25 µg/mL kanamycin. Colonies were picked and grown in 7H9 with 25 µg/mL kanamycin until mid-log (OD_{600} 0.4-0.8). Test hits, rifampicin and isoniazid were dissolved in DMSO and diluted into a compound plate (Greiner, 96 well, PP, V-bottom. Ref - 651201) at 100x the desired concentration and 1 µL of pipetted in triplicate into a microplate (Greiner, 96 well, PS, F-

bottom, black, sterile. Ref - 655086). The cells were adjusted to a density of $1x10^6$ cells/mL and 100 µL was added to each well. The plates were sealed with parafilm and tin foil and incubated at 37 °C and 5 % CO2 for 1 day for *M. smegmatis* mc^2155 or 7 days for *M. bovis BCG* after which a resazurin survival assay was carried out (**Method 6.6.1**).

3.2.10 Restriction Cloning for RNA Polymerase Purification

For protein purification *rpoA*, *rpoB*, *rpoC*, *rpoZ*, and *sigA* were cloned into various overexpression vectors. Several vectors were made, pACYC Duet-*rpoA+sigA*, pACYC Duet-*rpoA+rpoZ*, pCDF Duet-*rpoB+rpoC*, and pET28a-*sigA*. Inserts were amplified with PCR (**Method 6.4.2**) using the primers in Table 12. Inserts were purified from an agarose gel (**Methods 6.4.3** and **6.4.4**) and inserts and plasmids were digested (**Method 6.4.6**) using the restrictions enzymes for each primer in Table 12. Digested DNA was cleaned (**Method 6.4.5**) and ligated in a standard ligation (**Method 6.4.7**). Competent *E. coli* was transformed (**Method 6.3.5**) and grown overnight at 37 °C with selection antibiotic appropriate for each plasmid shown in Table 13. Plasmids were extracted using a Qiagen Miniprep kit (**Method 6.4.8**). For duet vectors the process was repeated over with the fresh purified plasmid for the second insert. Plasmids were checked with colony PCR (**Method 6.4.2**) and sequenced by Eurofins Genomics.

Table 12. Primers and restriction enzymes for cloning RNA polymerase.

Gene Name	Primer Direction	Restriction Enzyme	Primer Sequence 5'- 3' (Junk/Cutsite/Anneal)
rpoA+**10 His tag**	Forward	ncoI (NEB)	catgcatg/ccatgg/gc**catcaccatcaccatcaccatcaccat cac**ctgatctcacagc
rpoA	Reverse	hindIII (NEB)	catgcatg/aagctt/ctaaagctgttcgg
rpoB	Forward	ncoI (NEB)	gatcgatc/ccatgg/ggttggcagattcccgccagagc
rpoB	Reverse	bamHI (NEB)	gatcgatc/ggatcc/ttacgcaagatcctcgacacttgc
rpoC	Forward	ndeI (NEB)	gatcgatc/catatg/ctcgacgtcaacttcttcgatgaactccgc
rpoC	Reverse	ecoRV (NEB)	catgcatg/gatatc/ctagcggtagtcgctgtag
rpoZ	Forward	ndeI (NEB)	catgcatg/catatg/agtatctcgcagtccgac
rpoZ	Reverse	kpnI (NEB)	catgcatg/ggtacc/ctactcgccctcggtgtg
sigA pACYC	Forward	ndeI (NEB)	catgcatg/catatg/gcagcgaccaaagc
sigA pACYC	Reverse	kpnI (NEB)	catgcatg/ggtacc/tcagtccaggtagtcg
sigA pET28a	Forward	ndeI (NEB)	catgcatg/catatg/gcagcgaccaaagc
sigA pET28a	Reverse	notI (NEB)	catgcatg/gcggccgc/tcagtccaggtagtcgc

Table 13. Selection Antibiotic for plasmids.

Plasmid	Antibiotic
pACYC Duet	34 µg/mL Chloramphenicol
pCDF Duet	100 µg/mL Spectinomycin
pET28a	50 µg/mL Kanamycin

3.2.11 Purification of RNA Polymerase Holo Enzyme

Competent *E. coli* BL21 was transformed sequentially with pACYC Duet-*rpoA+sigA* and pCDF Duet-*rpoB+rpoC* and grown in 1 L 2X YT media cultures. Protein was extracted and purified using a His-Trap HP column (GE Healthcare) as in **Method 6.5.1**. The protein was dialysed (**Method 6.5.2**) and purified further by using anion exchange (**Method 6.5.3**). Protein gels (**Method 6.5.4**) and Western blots (**Method 6.5.5**) were used to assess the presence and purity of the protein.

3.2.12 SigA Expression Trial

E. coli BL21 and T7 Shuffle were transformed (**Method 6.3.5**) with pET28a-*sigA* and pET30a-*sigA* (donated by Joelle Brodeur, Univerité de Sherbrooke). The plasmids were selected for using 25 μg/mL kanamycin. 50 mL cultures were set up in different media listed in Table 14. The cultures were grown to mid-log (OD_{600} 0.4) and induced with 1 mM IPTG if necessary. Cultures were then incubated overnight at 16 °C. The cells were harvested, lysed, and the lysate clarified as in **Method 6.5.1**. The clarified lysate and pellet were examined on protein gels (**Method 6.5.4**) and Western blots (**Method 6.5.5**) for the presence of SigA.

Table 14. Conditions in expression trial.

Cell Line	Plasmid	Media	IPTG Induction
E. coli BL21	pET30a-*sigA*	Terrific Broth	Yes
E. coli BL21	pET30a-*sigA*	ZYM-5052 Autoinduction Media	No
E. coli BL21	pET28a-*sigA*	Terrific Broth	Yes
E. coli BL21	pET28a-*sigA*	ZYM-5052 Autoinduction Media	No
E. coli BL21	pET28a-*sigA*	2X YT Media	Yes
E. coli T7 Shuffle	pET30a-*sigA*	Terrific Broth	Yes
E. coli T7 Shuffle	pET28a-*sigA*	Terrific Broth	Yes

3.2.13 Purification of *M. smegmatis* mc^{2}155 Ribosomes

M. smegmatis mc^{2}155 was grown in 1 L LB broth cultures to mid-log (OD_{600} 0.4-0.6) at 37 °C with 180 rpm shaking. Cells were harvested by centrifugation at 6,000 RPM at 4 °C. Pelleted cells were resuspended in French Press buffer (20 mM Tris-HCL pH 7.5, 50 mM magnesium acetate, 100 mM ammonium chloride, 1 mM dithiothreitol, 0.5 mM EDTA) at a 1:2 (w/v) ratio. 10 units of RNase Free DNAse (ThermoScientific) was added and incubated at 4 °C for 20 minutes. Cells were lysed in a French press at 16,000 psi and the lysate was clarified by centrifugation at 25,000 rpm for 30 minutes. The lysate was layered 1:1 over a cushion of High-Salt Sucrose Cushion buffer (20 mM Tris-HCL pH 7.5, 50 mM magnesium acetate, 100 mM ammonium chloride, 1 mM dithiothreitol, 0.5

mM EDTA, 1.1 M RNAse free sucrose) in an ultracentrifuge tube (Beckman Coulter, 344058) and centrifuged at 100,000 g for 16 hours. The ribosomes were pelleted at the bottom of the tube with a brown layer deposited on top, which was discarded. The ribosomes were resuspended in French press buffer and the sucrose cushion and centrifugation was repeated twice more. The ribosomes were then dialysed (**Method 6.2.2**) into Tight Couples buffer (10 mM Tris-HCL pH 7.5, 6 mM magnesium acetate, 50 mM ammonium chloride, 1 mM dithiothreitol, 0.5 mM EDTA).

3.2.14 RNA Amplification and Purification

Template *mCherry* RNA was amplified from a pHIT88-*mCherry* plasmid produced by Dr Katherine Abrahams (University of Birmingham) using a HiScribe T7 High Yield RNA Synthesis Kit (NEB, E2040S). 100 mM each of ATP, GTP, CTP, and UTP (2 µL) were added into a mirocentrifuge tube. 10x Reaction Buffer (2 µL) was added along with 1 µg of pHIT88-*mCherry* DNA template. The reaction was made up to 18 µL with dH_2O and 2 µL of T7 RNA Polymerase was added. The reaction was mixed and incubated at 37 °C for 2 hours. The RNA was cleaned using a Monarch RNA Cleanup kit (NEB, T2030). The volume of the RNA sample was adjusted to 50 µL with nuclease free dH_2O and 100 µL of Binding Buffer added. 150 µL of ethanol was added and the sample was loaded into the column. The sample was centrifuged at 13,000 rpm for 1 minute and the flow through discarded. Wash Buffer (500 µL) was added and the sample was centrifuged as before. The flow through was discarded and the previous step repeated. After washing the column was transferred to a RNAse free microcentrifuge tube and the RNA was eluted off with 20 µL of nuclease free dH_2O and centrifuged as before. The RNA was stored at 4 °C until use.

3.2.15 Ribosome Inhibition Assay

The ribosome inhibition assay was conducted using a PURExpress Δ Ribosome Kit (NEB, E3313S), *mCherry* RNA template, and *M. smegmatis* mc^{2}155 ribosomes. In a PCR tube 5 µL Solution A, 1.5 µL Factor Mix, 200 ng RNA template, and 100 µM test compound in DMSO were made up to 18.5 µL with dH_2O. The mixtures were added to a microplate (Greiner, 384 well, PS, F-clear bottom, black, sterile. Ref – 781097). *M. smegmatis* mc^{2}155 ribosomes (6.5 µL) was added to each for a final concentration of 60 pmols. The top of the plate was covered with a plastic adhesive lid to prevent evaporation. The plate was read on a BMG plate reader at excitation and emission for 1000 cycles every 30 seconds.

3.2.16 RNA Polymerase Assay

BHQ2 and TAMRA oligos were hybridised in a 2:1 ratio, 8 µM:4 µM in a 500 µL aliquot. 40 µL of 100 µM BHQ2 oligo, 20 µL of 100 µM TAMRA oligo, 100 µL 5x SSPE buffer, 25 µL 20x Denhardt's reagent and 315 µL of dH_2O were added into a 1.5 mL microcentrifuge tube. The mixture was heated at 95 °C which reduced by 10 °C every 5 minutes. The oligos were checked for hybridisation and fluorophore quenching on a BMG plate reader. Reactions of 20 µL were set up with *E. coli* RNA Polymerase, Holoenzyme (NEB, M0551S). 4 µL of 5x RNA polymerase buffer, 1 µL *E.coli* RNA polymerase, 125 µM ATP, 125 µM CTP, 125 µM GTP, 125 µM UTP, 5 µL of hybridised TAMRA/BHQ2 oligos, 40 nM of *mmsA* DNA template were made up to 19 µL with RNase free dH_2O. 1 µL of 200 µM or 2 mM compound in 20 % DMSO was added for 10 µM or 100 µM compound in 1 % DMSO. The reactions were read on a BMG plate reader every 30 seconds for 1000 cycles.

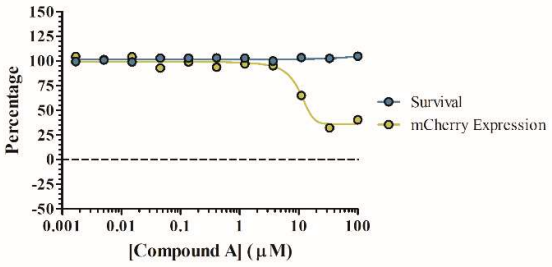
Table 15. TAMRA and BHQ2 Oligonucleotides.

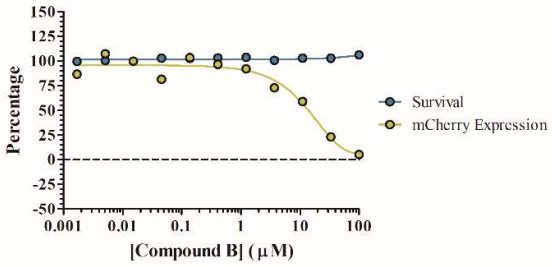
DNA Sequence 5' – 3'	Modifications
ttcacatttcatcgacggacaacg	5' – TAMRA
cgatgaaatgtgaa	3' – BHQ2

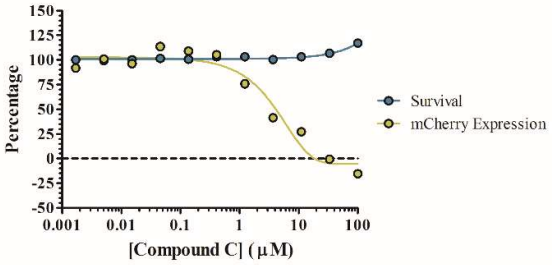
3.3 Results

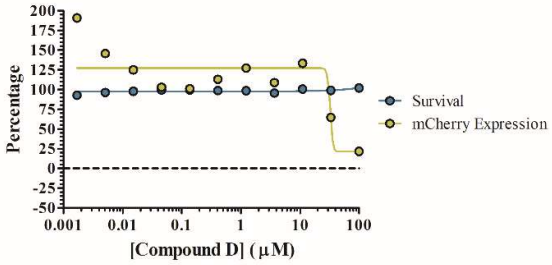
3.3.1 Proprietary Screen

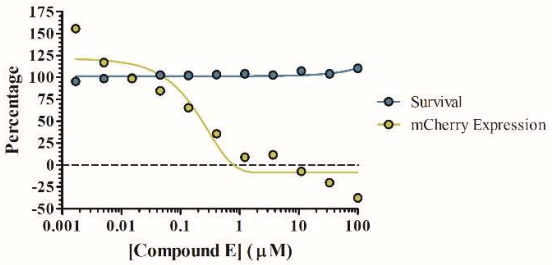
A screen using *M. tuberculosis* H37Rv containing pTIC6a-*mCherry* was designed to identify inhibitors of the protein synthesis pipeline from compound libraries phenotypically. The screen was tested with 38 hits, including blind controls, provided by Professor James Sacchettini (University of Texas A & M). The hits in question were identified as inhibitors of the mycobacterial ribosome by cell free assays. The data was analysed by calculating the percentage normalisation for mCherry expression and cell survival as outlined in **Method 6.6.3**. The screen identified 23 hits, shown in Figure 36, that were able to penetrate the cell wall and inhibit mCherry production in a dose dependant response including 2 blind controls, rifampicin, and linezolid. In addition, comparing the decrease in mCherry fluorescence to the resazurin fluorescence indicates that the reduction in mCherry fluorescence is not due to cellular death. This screen using known inhibitors of the ribosome shows that using inducible expression of mCherry could be a powerful tool for screening for protein synthesis pipeline hits.

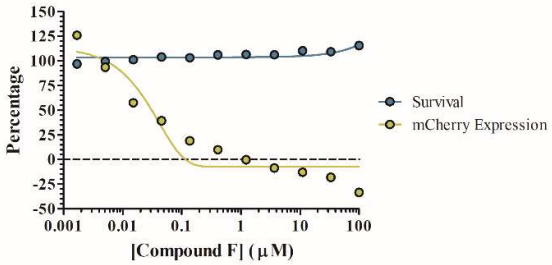

Percentage
[Compound A] (μM)
Survival
mCherry Expression

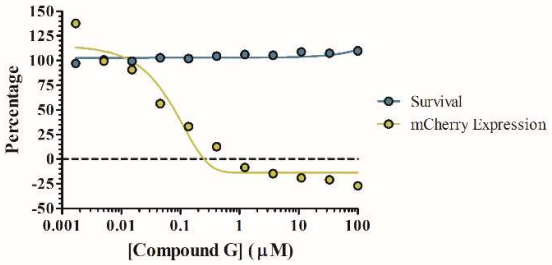

Percentage
[Compound B] (μM)
Survival
mCherry Expression

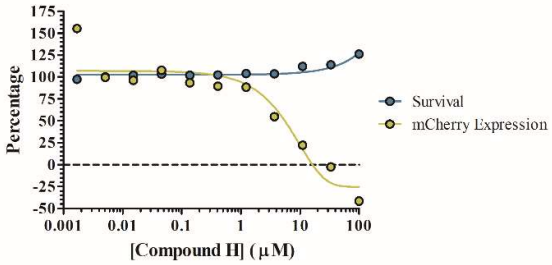

Percentage
[Compound C] (μM)
Survival
mCherry Expression

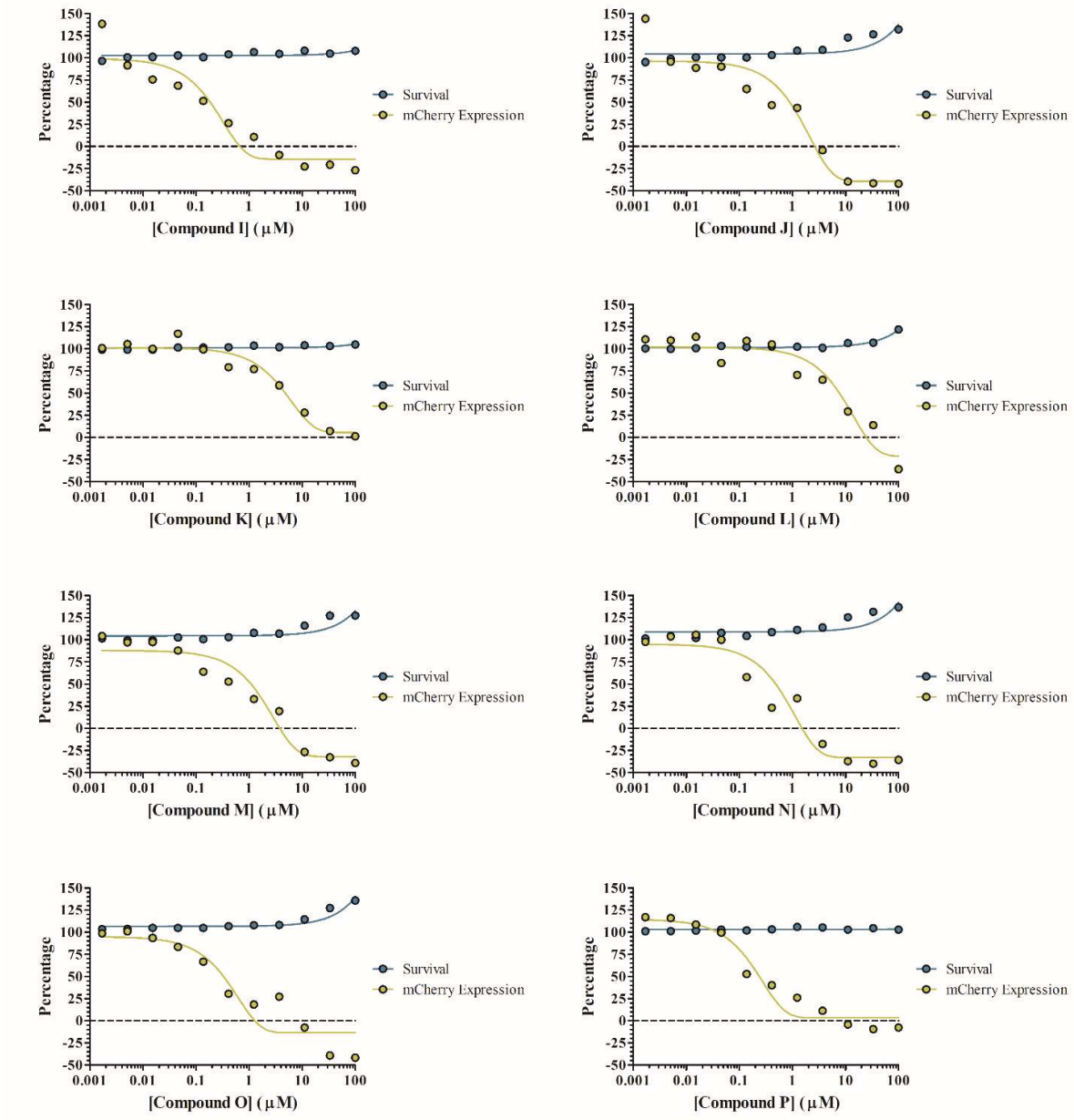

Percentage
[Compound D] (μM)
Survival
mCherry Expression


Percentage
[Compound E] (μM)
Survival
mCherry Expression


Percentage
[Compound F] (μM)
Survival
mCherry Expression


Percentage
[Compound G] (μM)
Survival
mCherry Expression


Percentage
[Compound H] (μM)
Survival
mCherry Expression


Percentage
Survival
mCherry Expression
[Compound I] (μM)
[Compound J] (μM)
[Compound K] (μM)
[Compound L] (μM)
[Compound M] (μM)
[Compound N] (μM)
[Compound O] (μM)
[Compound P] (μM)

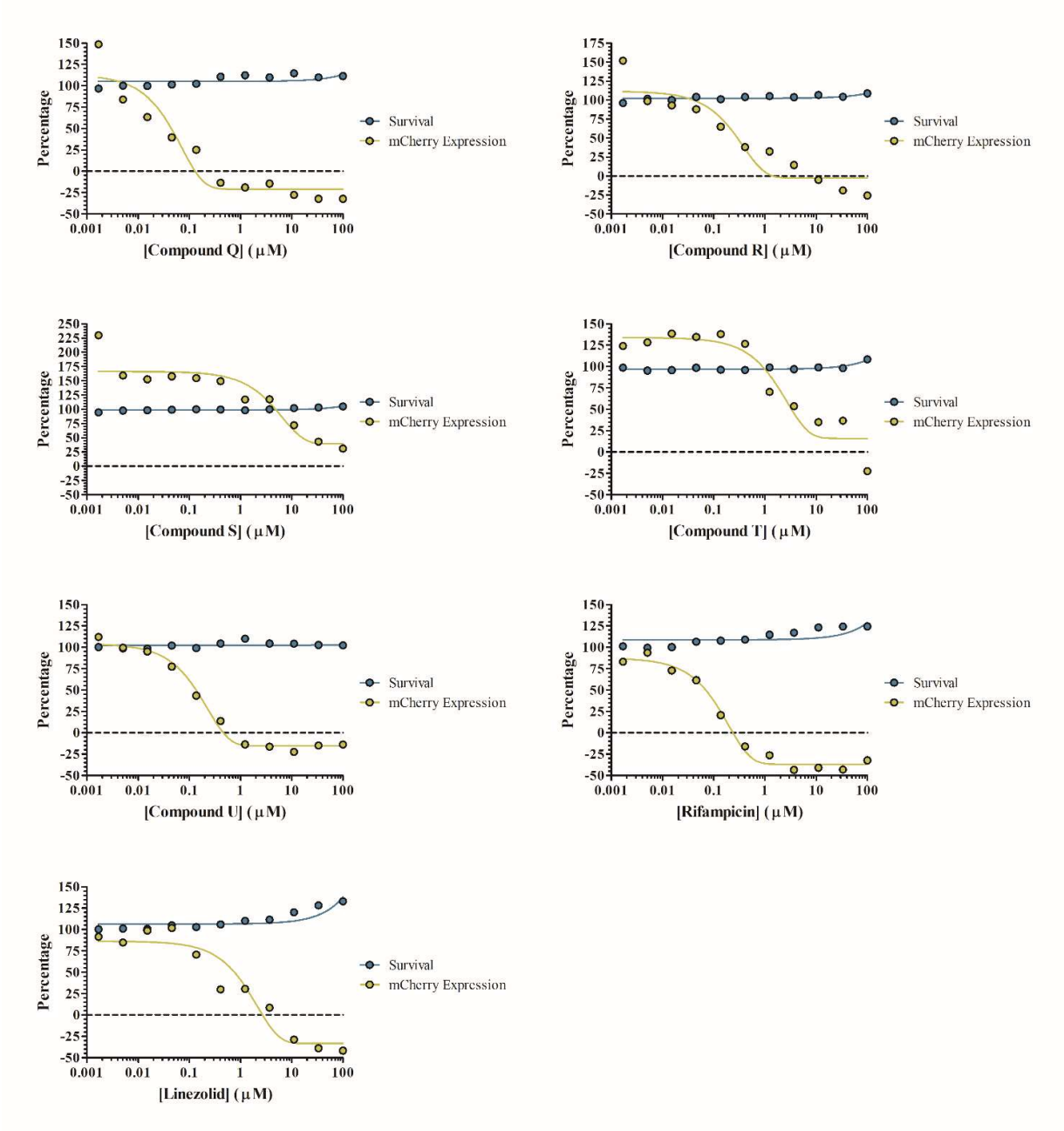


Figure 36. Proprietary protein synthesis pipeline inhibitor screen results. Each graph shows the percentage mCherry expression compared to the percentage survival of *M. tuberculosis* H37Rv. Single replicate.

3.3.2 Single Shot High-Throughput Screen of GSK TB Box Set

The single shot high-throughput screen was used to reduce the 2799 compounds of the GSK TB box set to a manageable number of hits. Two single well experiments were conducted for each compound with different final concentrations, 1 μM (Figure 37) and 10 μM (Figure 38). The data was analysed by calculating the percentage normalisation for mCherry expression and cell survival as outlined in **Method 6.6.3**. Hit compounds were identified by causing either a 50 % or greater reduction in percentage mCherry fluorescence at 10 μM or at both concentrations for a pseudo dose-response. In addition, the percentage cell survival needed to indicate that the reduction in mCherry fluorescence was not due to cell death. A total of 91 hits fit the criteria to be designated a true hit compound. This represented 3.25 % of the total compounds screened.

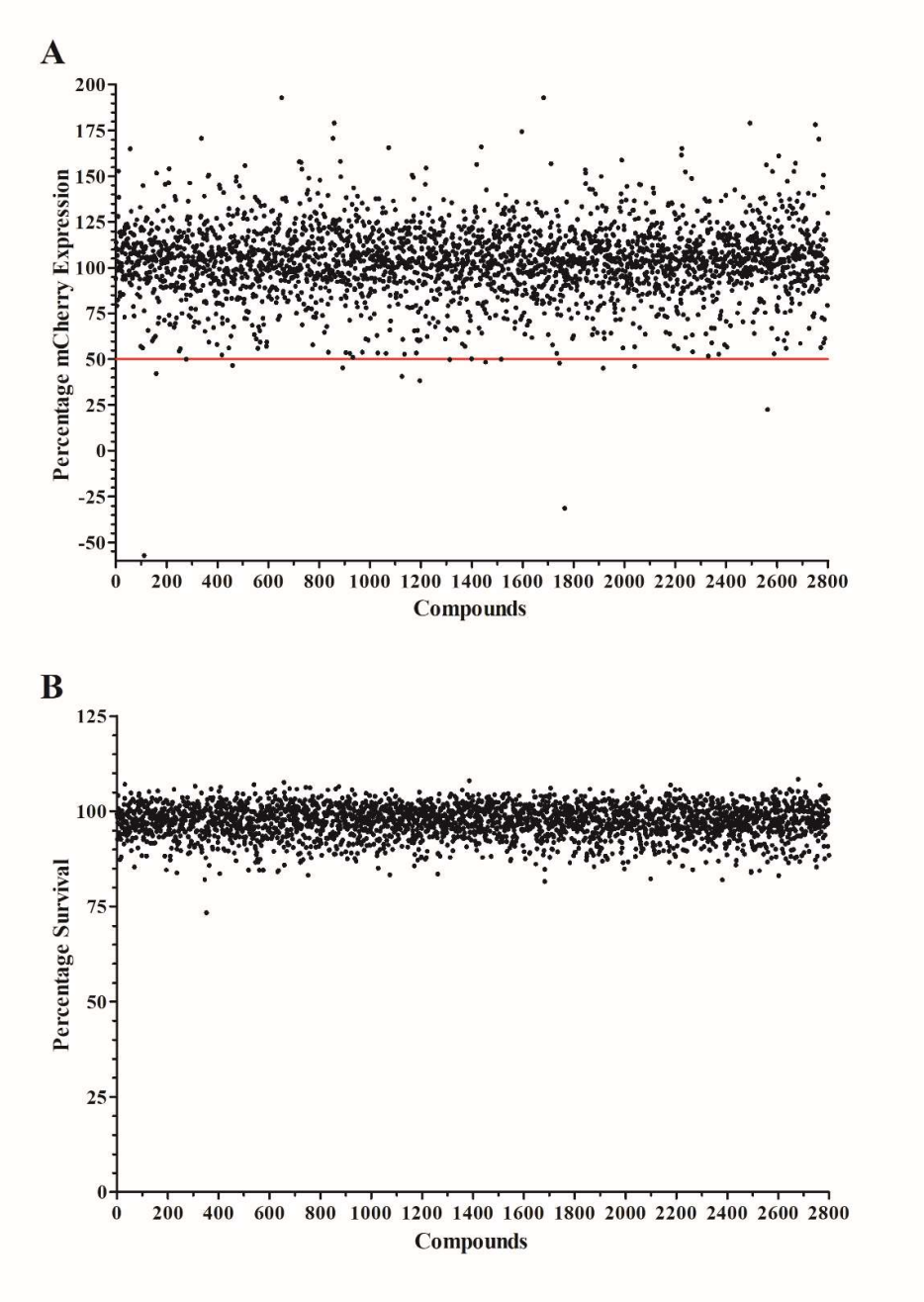


Figure 37. Single shot 1 μM high-throughput screen. Single replicate. **A -** Percentage mCherry expression of *M. tuberculosis* H37Rv, cut off value shown by red line. **B -** Resazurin percentage cell survival of *M. tuberculosis* H37Rv.

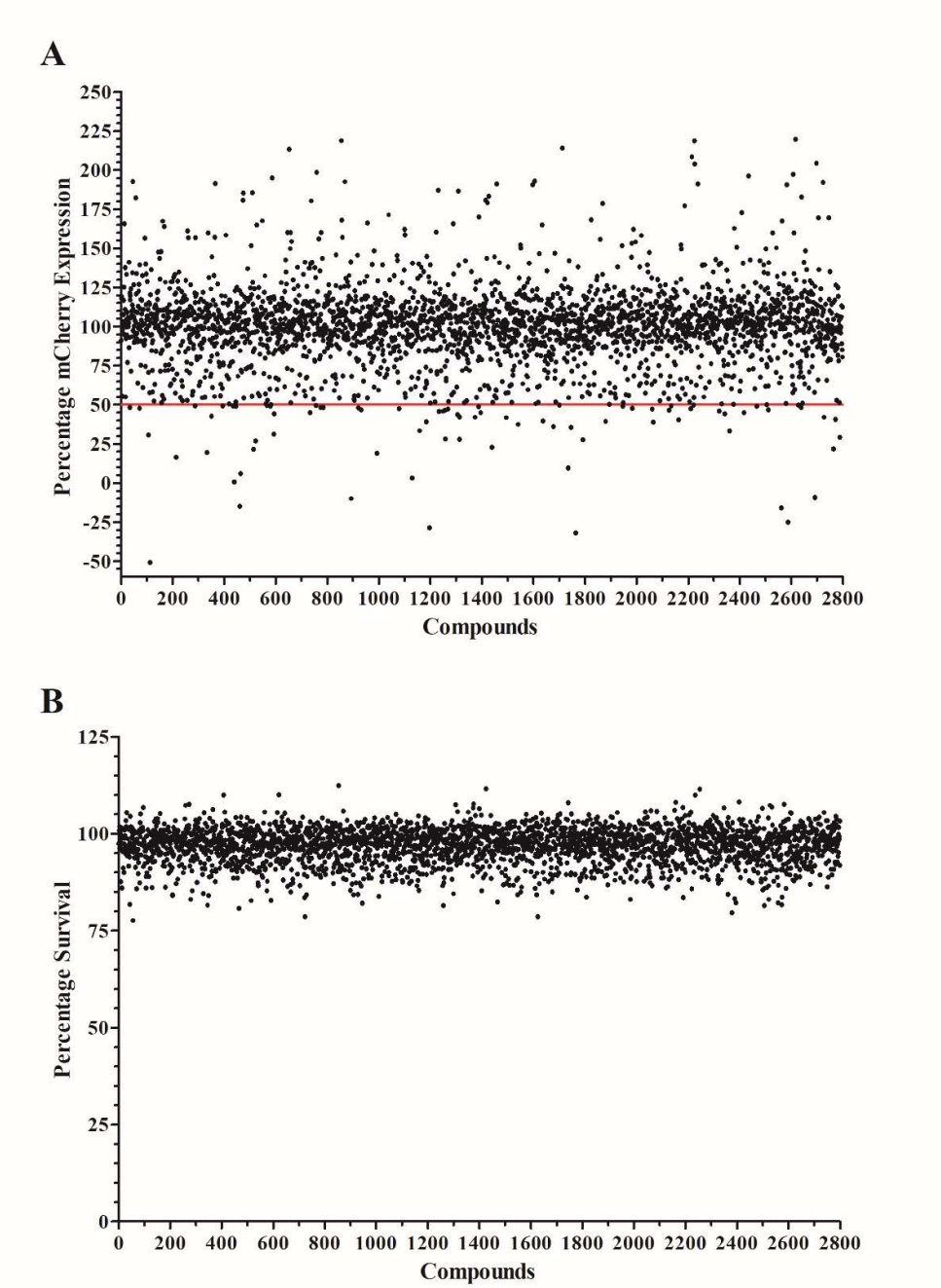
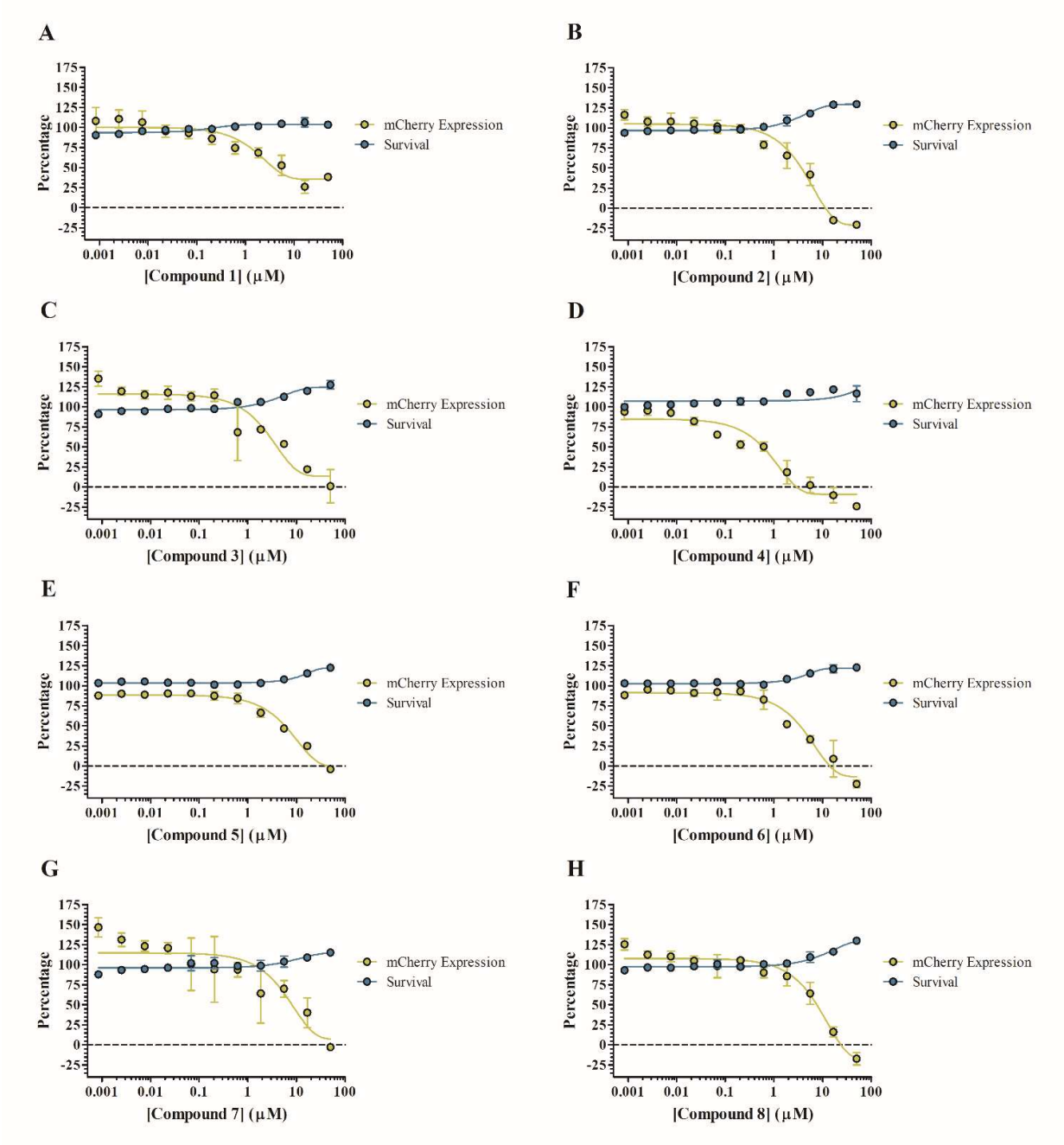
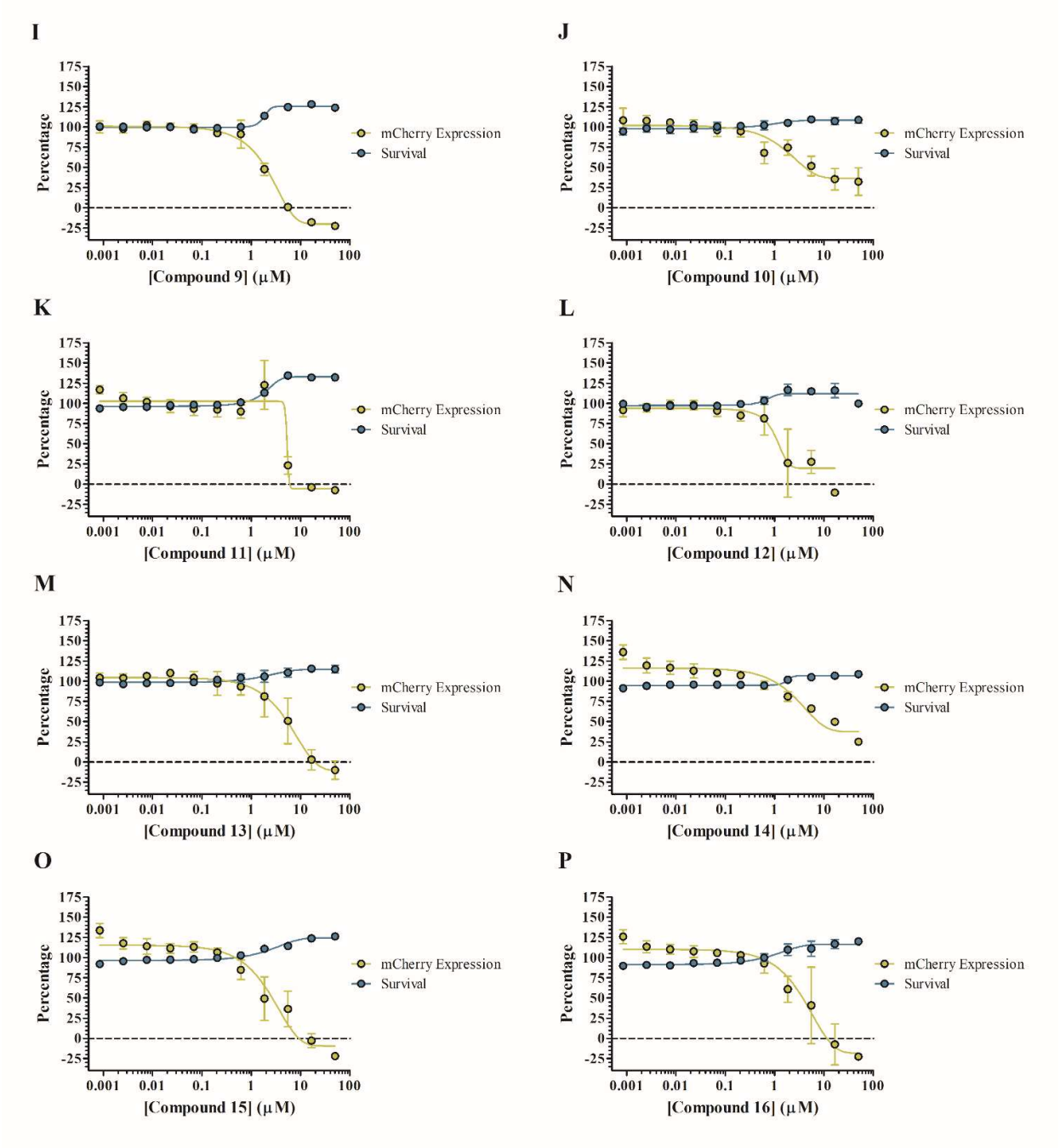


Figure 38. Single shot 10 μM high-throughput screen. Single replicate. **A -** Percentage mCherry expression of *M. tuberculosis* H37Rv, cut off value shown by red line. **B -** Resazurin percentage cell survival of *M. tuberculosis* H37Rv.

3.3.3 Dose-response Screen of Hit Compounds

The ninety one hit compounds were further tested with a dose response screen. A two part screening method allows the initial single shot screen to be more relaxed and the selection critera for hit compounds to be more permissive. The second, more rigerous, dose-response phase of screening can then filter out any false positive results found in the initial screen. The concentration range used in the dose-response, 50 μM to 0.846 nM, spanned higher and lower than the concnetrations in the original single shot screen to pick up a wide array of activity. The Z' of the plates was calculated (**Method 6.6.2**) and any plates with a Z' of less than 0.5 were excluded from the results. The Z' measures the seperation between the positive and negative controls. Poor seperation between the controls means the the data is poor quality. This exclusion critera meant that one plate had to be excluded, resulting in one data set being triplicate instead of quadruplicate. The data was analysed by calculating the percentage normalisation for mCherry expression and cell survival as outlined in **Method 6.6.3**. Of the ninety-one hits tested, eighteen showed a favourable dose-response patten. Once again, the percentage cell survival was plotted to show that the mCherry fluorescence reduction was not due to cell death. The data in Figure 39 shows the comparison between mCherry fluorescence and cell survival with rifampicin and linezolid included as controls. The eighteen hits amount to 0.64 % of the total compounds screened.


A
B
C
D
E
F
G
H
Percentage
175
150
125
100
75
50
25
0
-25
0.001
0.01
0.1
1
10
100
mCherry Expression
Survival
[Compound 1] (µM)
[Compound 2] (µM)
[Compound 3] (µM)
[Compound 4] (µM)
[Compound 5] (µM)
[Compound 6] (µM)
[Compound 7] (µM)
[Compound 8] (µM)


I
J
K
L
M
N
O
P
Percentage
175
150
125
100
75
50
25
0
-25
0.001
0.01
0.1
1
10
100
mCherry Expression
Survival
[Compound 9] (µM)
[Compound 10] (µM)
[Compound 11] (µM)
[Compound 12] (µM)
[Compound 13] (µM)
[Compound 14] (µM)
[Compound 15] (µM)
[Compound 16] (µM)

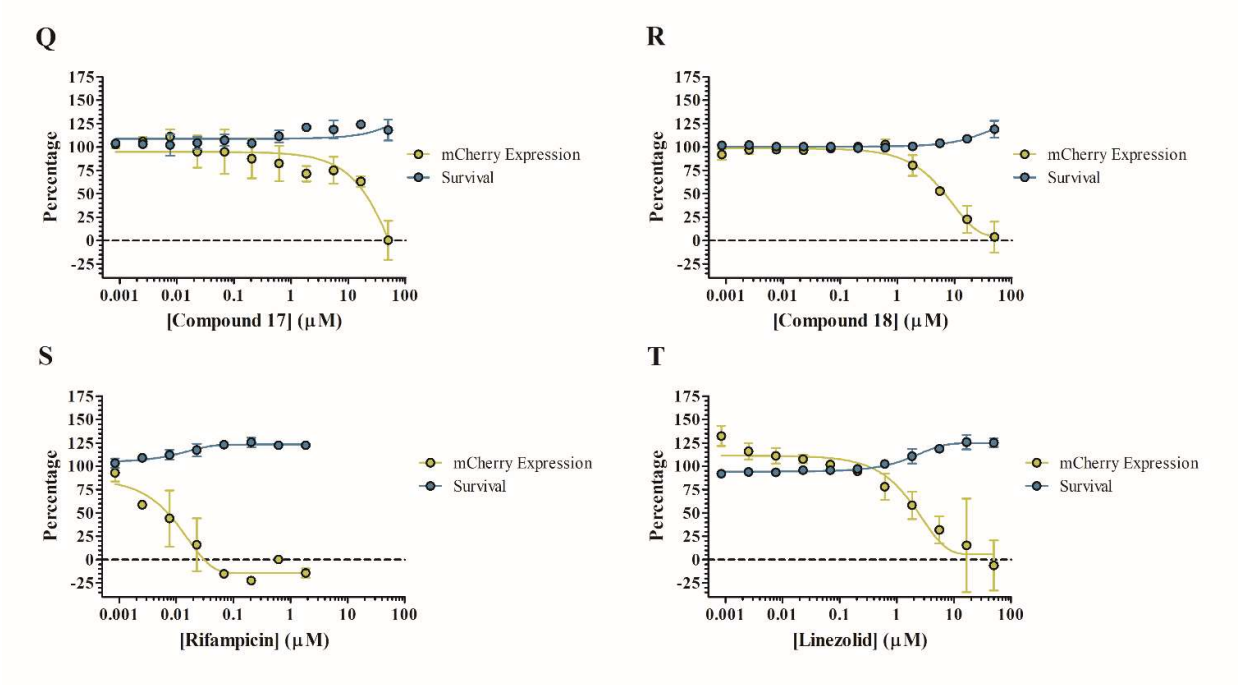


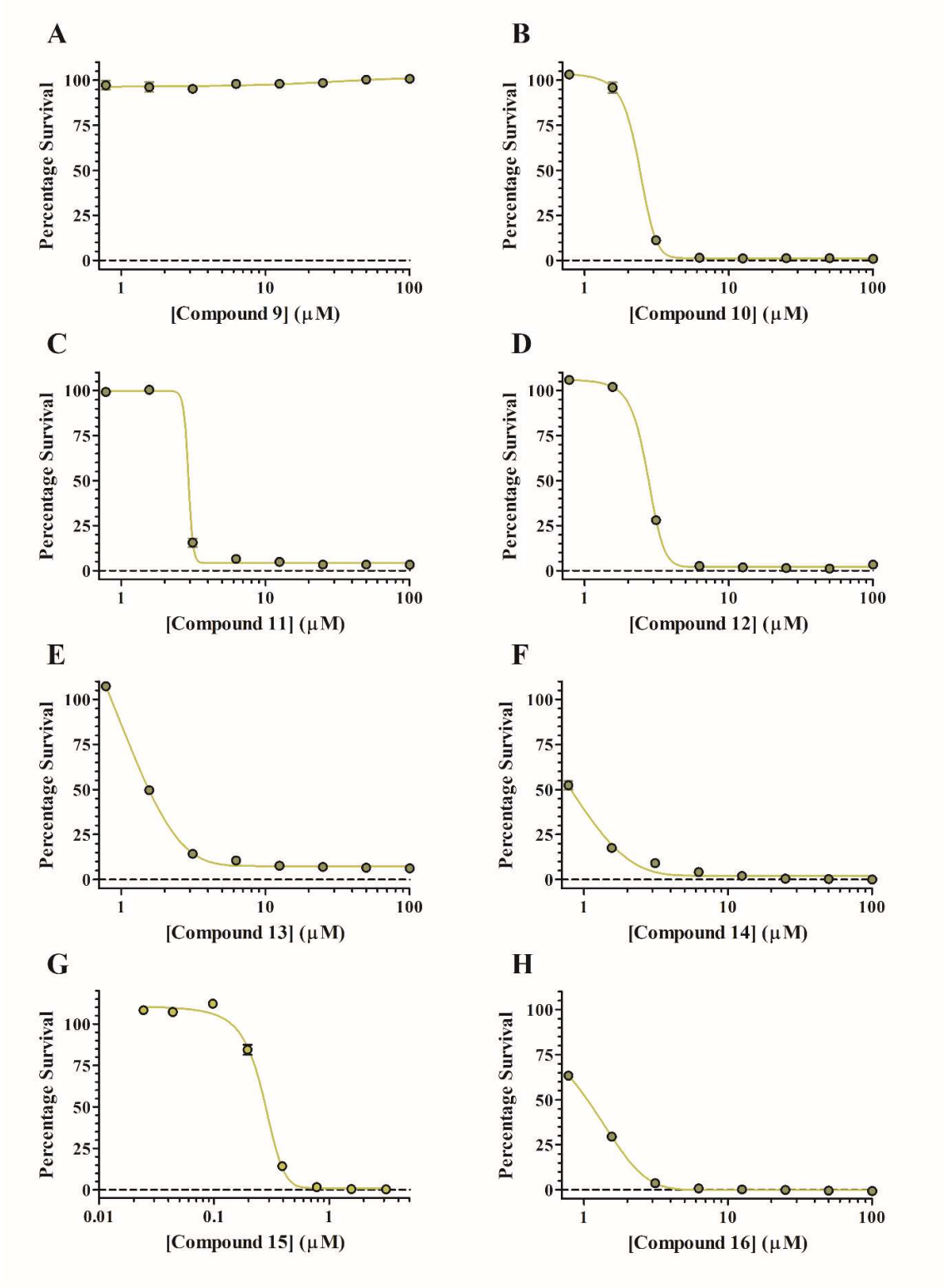
Figure 39. Dose-response of 18 hit compounds. Each graph shows the percentage mCherry expression compared to the percentage survival of *M. tuberculosis* H37Rv. Data shown as the mean and standard deviation of triple or quadruple replicate.

3.3.4 Liquid Minimum Inhibitory Concentrations (MICs) of Hit Compounds in *M. bovis* BCG and *M. smegmatis* mc^{2}155

Hits 9 to 18 from the dose response, were chosen to be progressed for full mode of action studies. This was based on information from GSK, which suggested that these compounds were more suitable for testing. In addition to those ten hits, compounds 45 and 46 were included due to WGS of DRMs suggesting that these compounds targeted RNA polymerase. All the hits had their MICs established in *M. bovis* BCG. Due to a lack of compound, 45 was excluded from MIC testing in *M. smegmatis* mc^{2}155. The data in Table 16 shows the MICs established for the hits and Figures 40 and 41 show the graphs for *M. bovis* and *M. smegmatis,* respectively.

Table 16. Liquid **minimum inhibitory concentrations (**MICs) established for *M. bovis* BCG and *M. smegmatis* mc^2155.

Hit	MIC in *M. bovis* BCG	MIC in *M. smegmatis* mc^2155
9	> 100 μM	> 100 μM
10	6.25 μM	12.5 μM
11	12.5 μM	> 100 μM
12	6.25 μM	> 100 μM
13	12.5 μM	> 100 μM
14	6.25 μM	100 μM
15	0.78 μM	12.5 μM
16	6.25 μM	< 1 μM
17	12.5 μM	6.25 μM
18	6.25 μM	> 100 μM
45	1.56 μM	N/A
46	100 μM	12.5 μM
Rifampicin	7.8 nM	5 μM
Isoniazid	0.9375 μM	N/A


A
Percentage Survival
100
75
50
25
0
1
10
100
[Compound 9] (μM)
B
Percentage Survival
100
75
50
25
0
1
10
100
[Compound 10] (μM)
C
Percentage Survival
100
75
50
25
0
1
10
100
[Compound 11] (μM)
D
Percentage Survival
100
75
50
25
0
1
10
100
[Compound 12] (μM)
E
Percentage Survival
100
75
50
25
0
1
10
100
[Compound 13] (μM)
F
Percentage Survival
100
75
50
25
0
1
10
100
[Compound 14] (μM)
G
Percentage Survival
100
75
50
25
0
0.01
0.1
1
[Compound 15] (μM)
H
Percentage Survival
100
75
50
25
0
1
10
100
[Compound 16] (μM)

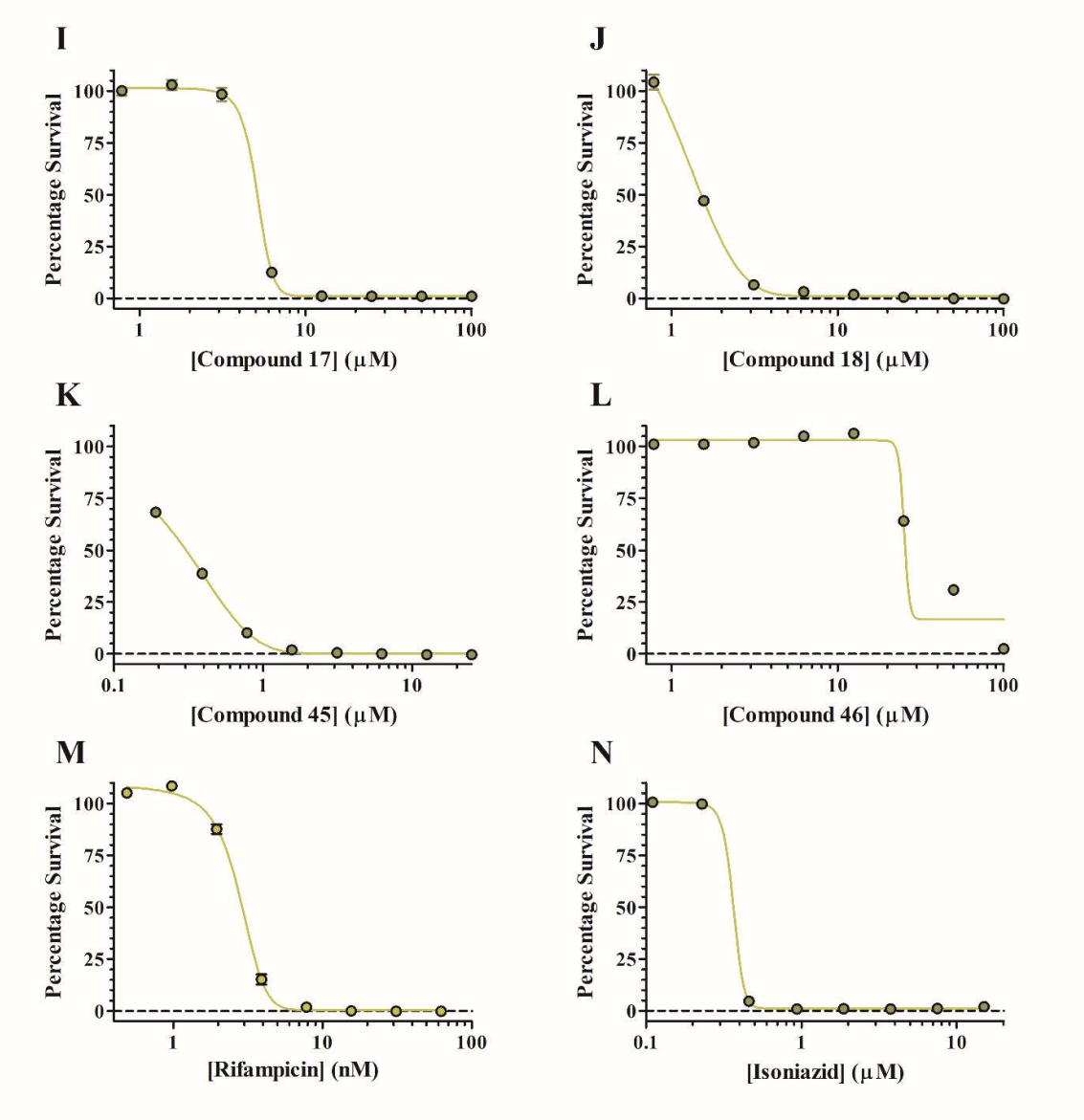
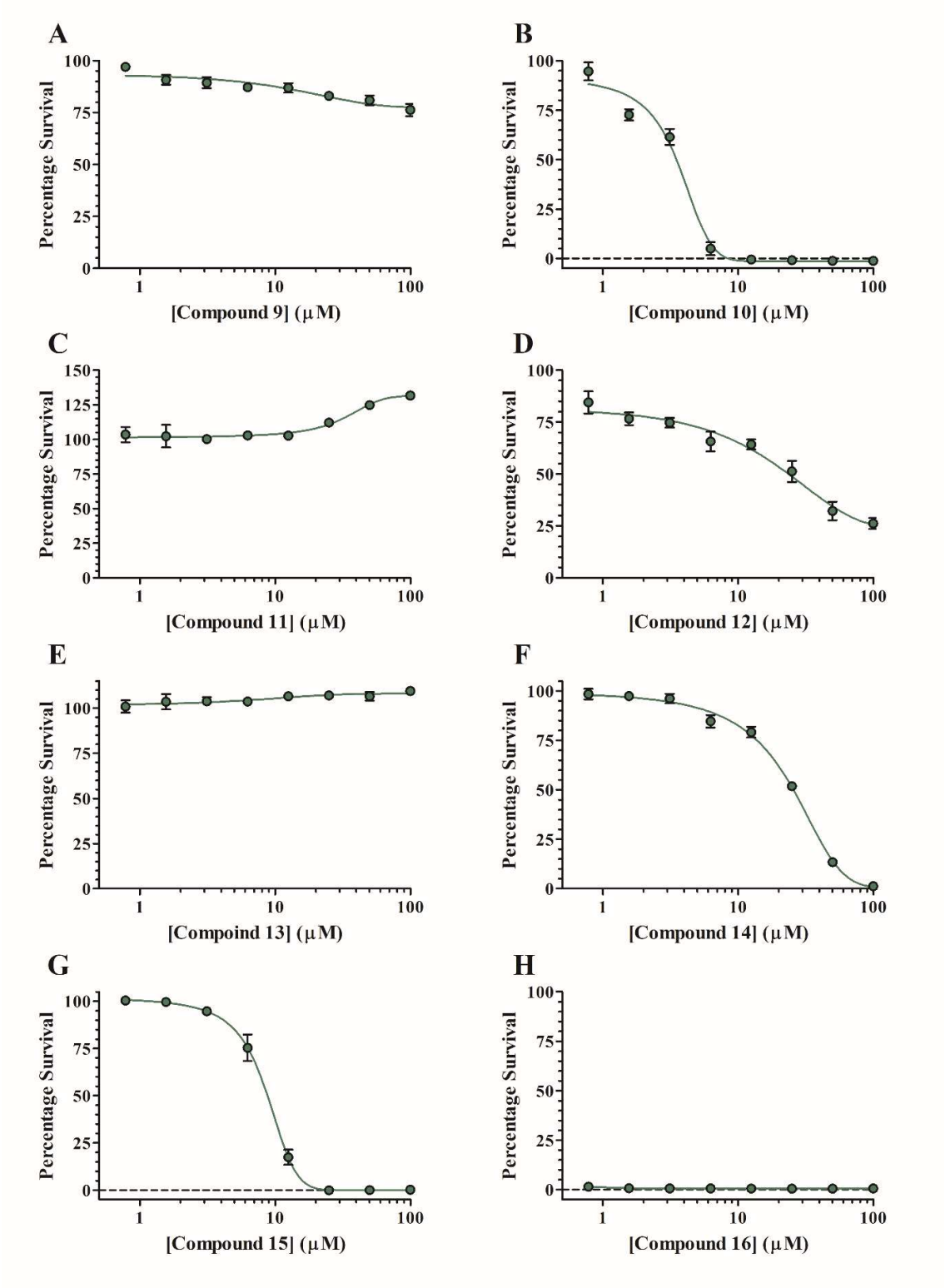


Figure 40. Liquid minimum inhibitory concentrations (MICs) for hit compounds and control compounds in *M. bovis* BCG. Data shown as the mean and standard deviation of triple replicate.


A
Percentage Survival
[Compound 9] (μM)
B
Percentage Survival
[Compound 10] (μM)
C
Percentage Survival
[Compound 11] (μM)
D
Percentage Survival
[Compound 12] (μM)
E
Percentage Survival
[Compoind 13] (μM)
F
Percentage Survival
[Compound 14] (μM)
G
Percentage Survival
[Compound 15] (μM)
H
Percentage Survival
[Compound 16] (μM)

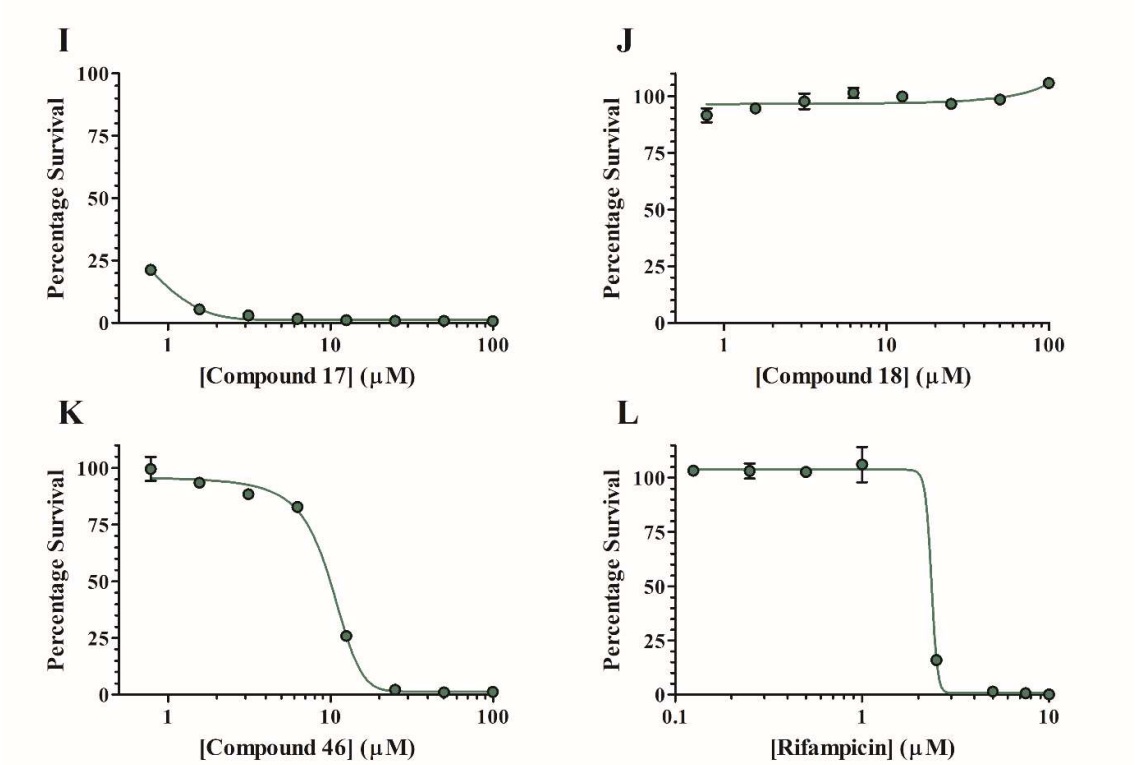


Figure 41. Liquid minimum inhibitory concentrations (MICs) for hit compounds and control compounds in *M. smegmatis* mc^{2}155. Data shown as the mean and standard deviation of triple replicate.

3.3.5 Solid Minimum Inhibitory Concentrations (MICs) of Hits in *M. bovis* BCG, *M. tuberculosis* H37Rv and *M. tuberculosis* H37Rv *ΔleuDΔpanCD*

Solid MICs were determined for the majority of hits where there was enough stock compound. The solid MICs for all hits tested are displayed in Table 17. Hits 45 and 46 (Figure 42) MICs were established before compounds 9 to 18 in *M. bovis* BCG. Liquid MICs established by GSK in *M. tuberculosis* H37Rv were used as a basis for the concentrations used in agar plates. Hits 9, 10, 11, 13, 17, and 18 had MICs established in *M. tuberculosis* H37Rv as shown in Figure 43. Hits 9, 11, 13, 14, 17 and 18 also had their MICs established in the *M. tuberculosis* H37Rv *ΔleuDΔpanCD*, an attenuated BSL2

strain, by Dr Alistair K. Brown (University of Newcastle). Hits 12, 15 and 16 lacked sufficient stocks to have solid MIC testing.

Table 17. Solid minimum inhibitory concentrations (MICs) established for *M. bovis* BCG, *M. tuberculosis* H37Rv, and *M. tuberculosis* H37Rv *ΔleuDΔpanCD.* MICs labelled N/A were not able to be conducted due to compound shortages.

Hit	MIC in *M. bovis* BCG	MIC in *M. tuberculosis* H37Rv	MIC in *M. tuberculosis* H37RV *ΔleuDΔpanCD*
9	N/A	> 50 μM	> 100 μM
10	N/A	10 μM	N/A
11	N/A	< 1 μM	0.6 μM
12	N/A	N/A	N/A
13	N/A	> 50 μM	> 100 μM
14	N/A	N/A	5 μM
15	N/A	N/A	N/A
16	N/A	N/A	N/A
17	N/A	5 μM	< 1 μM
18	N/A	> 50 μM	40 μM
45	1.95 μM	N/A	N/A
46	32.8 μM	N/A	N/A

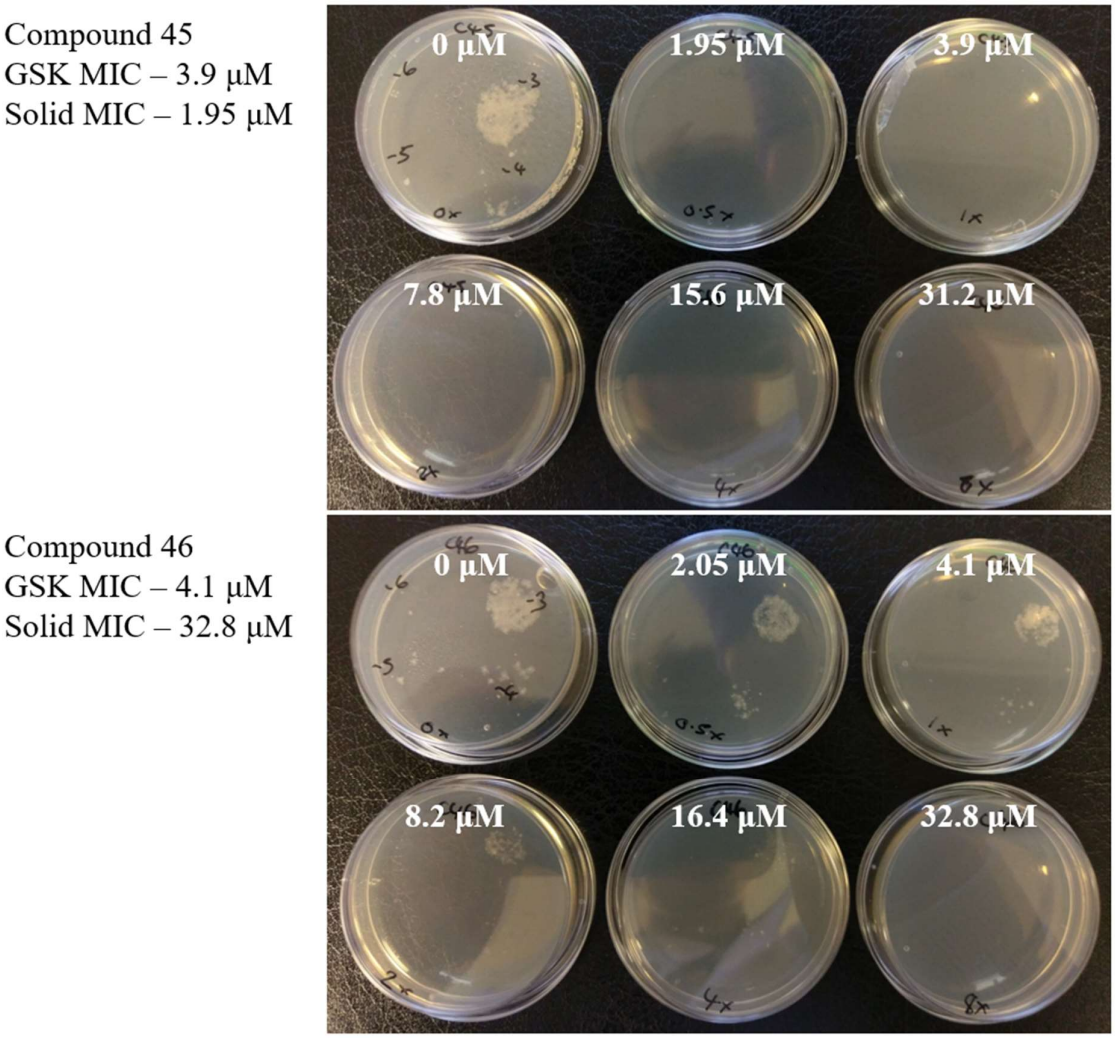
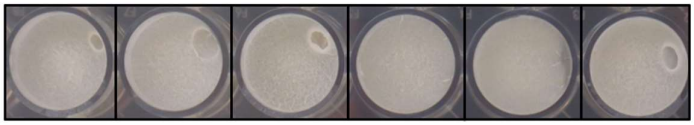


Figure 42. Solid minimum inhibitory concentrations (MICs) of hits/compounds 45 and 46 in *M. bovis* BCG. GSK MIC was established by GSK in *M. tuberculosis* H37Rv. Solid MIC determined as the first plate with no cell growth at any dilution.

Compound 9 Solid MIC = > 50 µM

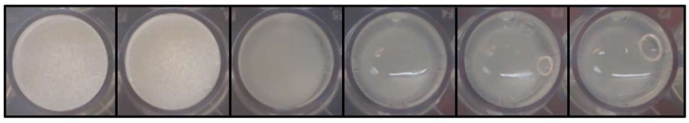


0 µM 1 µM 5 µM 10 µM 15 µM 20 µM

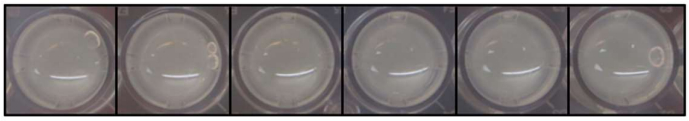


25 µM 30 µM 35 µM 40 µM 45 µM 50 µM

Compound 10 Solid MIC = 10 µM

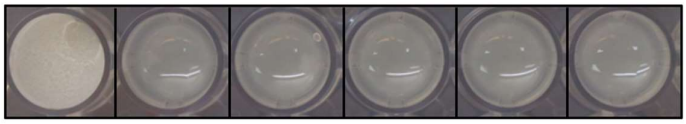


0 µM 1 µM 5 µM 10 µM 15 µM 20 µM

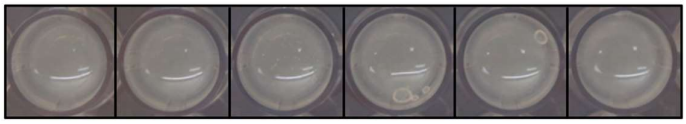


25 µM 30 µM 35 µM 40 µM 45 µM 50 µM

Compound 11 Solid MIC = < 1 µM

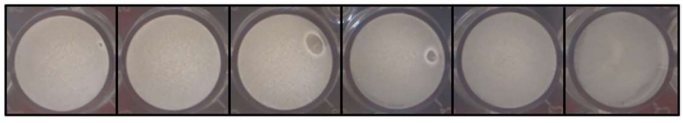


0 µM 1 µM 5 µM 10 µM 15 µM 20 µM

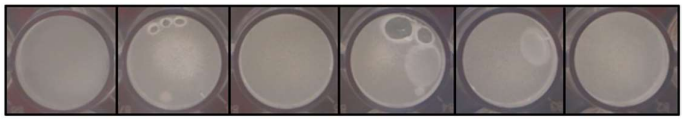


25 µM 30 µM 35 µM 40 µM 45 µM 50 µM

Compound 13 Solid MIC = > 50 µM



0 µM 1 µM 5 µM 10 µM 15 µM 20 µM



25 µM 30 µM 35 µM 40 µM 45 µM 50 µM

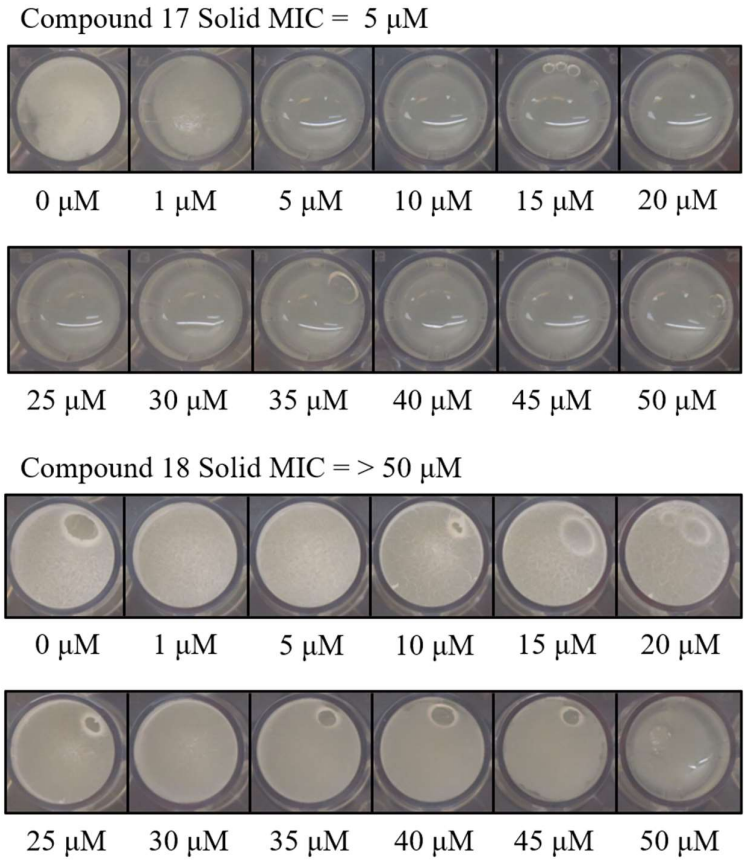


Figure 43. Solid minimum inhibitory concentrations (MICs) for hits/compounds 9, 10, 11, 13, 17, and 18 in *M. tuberculosis* H37Rv. Solid MIC determined as the first well with no cell growth.

3.3.6 Spontaneous Drug Resistant Mutant (DRM) Generation and Mutant Re-testing

DRM generation was attempted in either *M. tuberculosis* H37Rv or *M. tuberculosis* H37Rv *ΔleuDΔpanCD* for compounds with sufficient stock. *M. tuberculosis* H37Rv resistant mutants to hits 45 and 46 were isolated using agar plates. The plates contained 5x and 10x the MIC provided by GSK, 3.9 µM and 4.1 µM for 45 and 46, respectively. Each hit produced 6 mutant colonies. The mutants were then retested in liquid medium with up to 20x the MIC (Figure 44 A and B). All the mutants showed varying levels of increased survival over *M. tuberculosis* H37Rv. The genomes of the resistant mutants

were extracted and the whole genomes sequenced, which showed SNPs in the *rpoB* gene of RNA polymerase. The mutants were tested for cross-resistance to rifampicin to see whether these mutations in *rpoB* would affect the MIC (Figure 44 C and D). Hits 10 and 17 had mutants generated in *M. tuberculosis* H37Rv *ΔleuDΔpanCD* by Dr Alistair K. Brown (University of Newcastle). Hit 10 mutants were generated at 50 µM (5x MIC *M. tuberculosis* H37Rv) and hit 17 at 12.5 µM (2.5x MIC *M. tuberculosis* H37Rv). Both sets of mutants were re-tested with 2x the MIC for *M. tuberculosis* H37Rv. DRM generation was also attempted in *M. tuberculosis* H37Rv *ΔleuDΔpanCD* by Dr Alistair K. Brown (University of Newcastle) for hits 11, 14, and 18 but no colonies appeared.

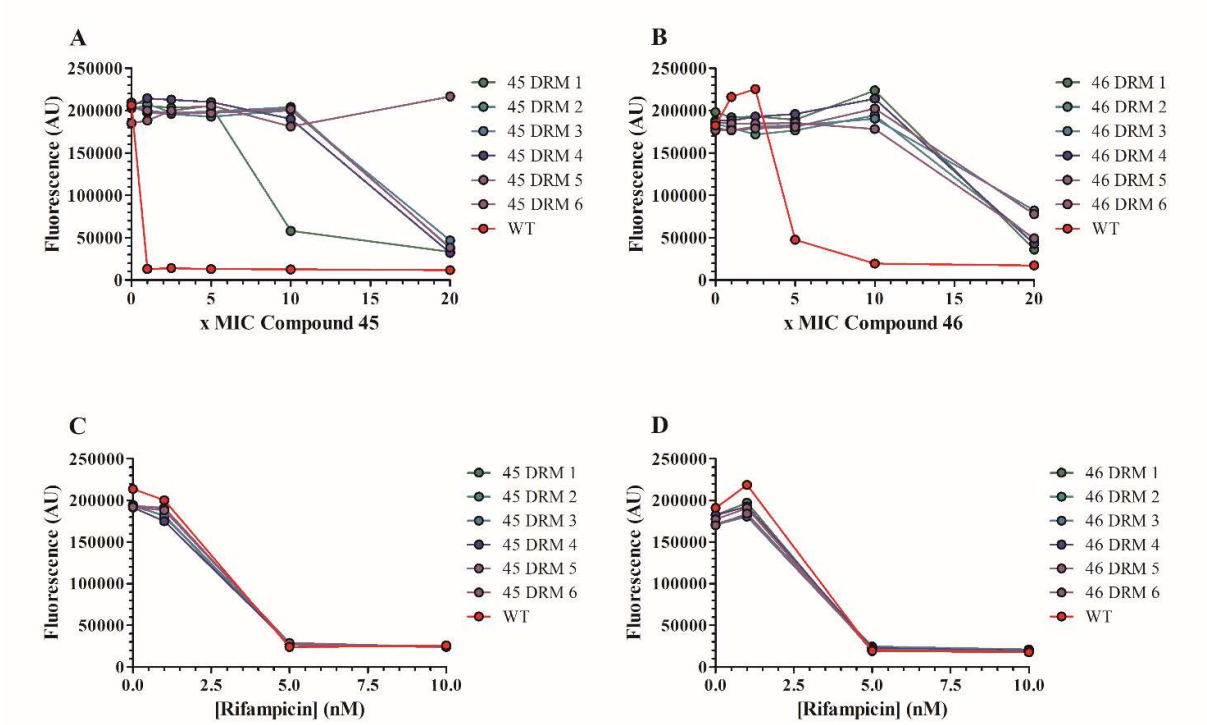
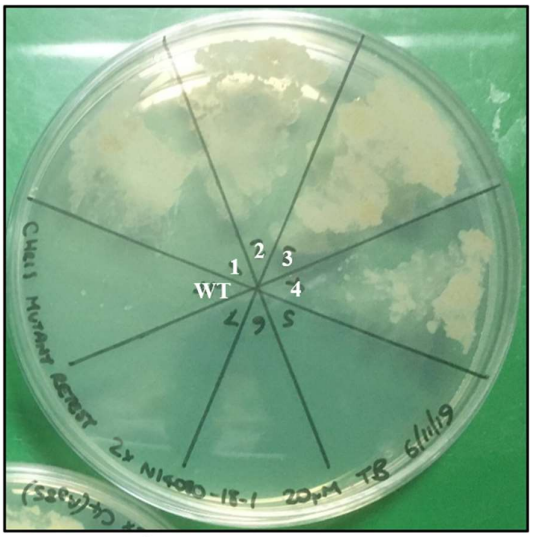
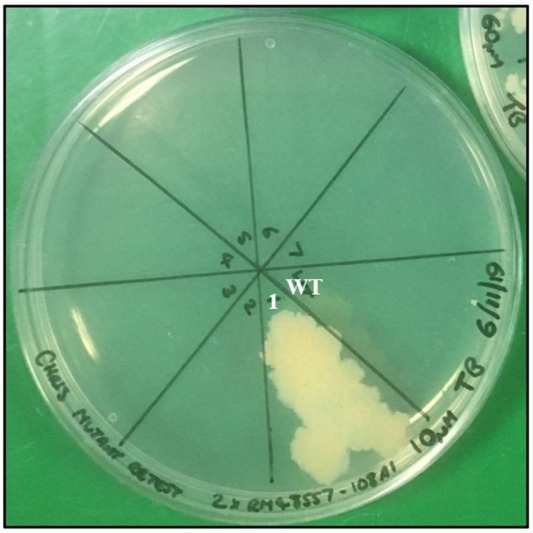


Figure 44. Hit compound retest of 45 and 46 mutants and cross-resistance with rifampicin. A. Hit 45 resistant mutants retest. **B.** Hit 46 mutants re-test. **C.** Hit 45 resistant mutants rifampicin cross-resistance. **D.** Hit 46 resistant mutants rifampicin cross-resistance. Data is single replicate only.



Compound 10 2x MIC Retest



Compound 17 2x MIC Retest

Figure 45. Mutant retesting for hit compounds 10 and 17. Four DRMs were isolated for hit/compound 10 and one DRM for hit/compound 17. All DRMs showed resistance to appropriate compound greater than the wild type.

3.3.7 Whole Genome Sequencing (WGS) of *M. tuberculosis* H37Rv Hit 45 and 46 Drug Resistant Mutants (DRMs)

The six DRMs for each of hit 45 and 46 were sequenced. SNPs in *rpoB* were present in ten of the twelve mutants with the other two mutants displaying no mutations of interest.

Out of these mutations 60 % were a Gly560Ser substitution and another was a Gly560Val substitution. The remaining 20 % of mutants contained an Asp574Asn mutation, with one of those being a complex mutation with Val575Gly. There were no mutations in other portions of the Rpo complex. Base changes and amino acid substitutions are shown fully in Table 18.

Table 18. Whole genome sequencing (WGS) data of hits 45 and 46 resistant mutants.

Hit	Mutant	Gene	Base Change	Amino Acid Substitution
45	1	*rpoB*	Gac/Aac	Asp574Asn
	2	*rpoB*	GacgTc/AacgGc	Asp574Asn / Val575Gly
	3	*rpoB*	Ggc/Agc	Gly560Ser
	4	*rpoB*	cGc/cCc	Arg557Pro
	6	*rpoB*	Ggc/Agc	Gly560Ser
46	1	*rpoB*	Ggc/Agc	Gly560Ser
	2	*rpoB*	Ggc/Agc	Gly560Ser
	3	*rpoB*	gGc/gTc	Gly560Val
	5	*rpoB*	Ggc/Agc	Gly560Ser
	6	*rpoB*	Ggc/Agc	Gly560Ser

3.3.8 Mapping Resistance Mutations onto RNA Polymerase structure

The structure of the *M. tuberculosis* RNA polymerase-holo enzyme has been previously solved[396], using this structure the locations of the most common clinically relevant rifampicin resistance mutations, Asp435Val, His445Tyr, and Ser450Leu[158] were mapped onto the structure, as well as all the resistance mutations for hits 45, 46 and the Arg556Ala resistance mutation for the structurally similar D-APP1 and D-IX336[396]. The images in Figure 46 show the hits 45 and 46 likely bind far from rifampicin and bind at the same location as D-APP1 and D-IX336.

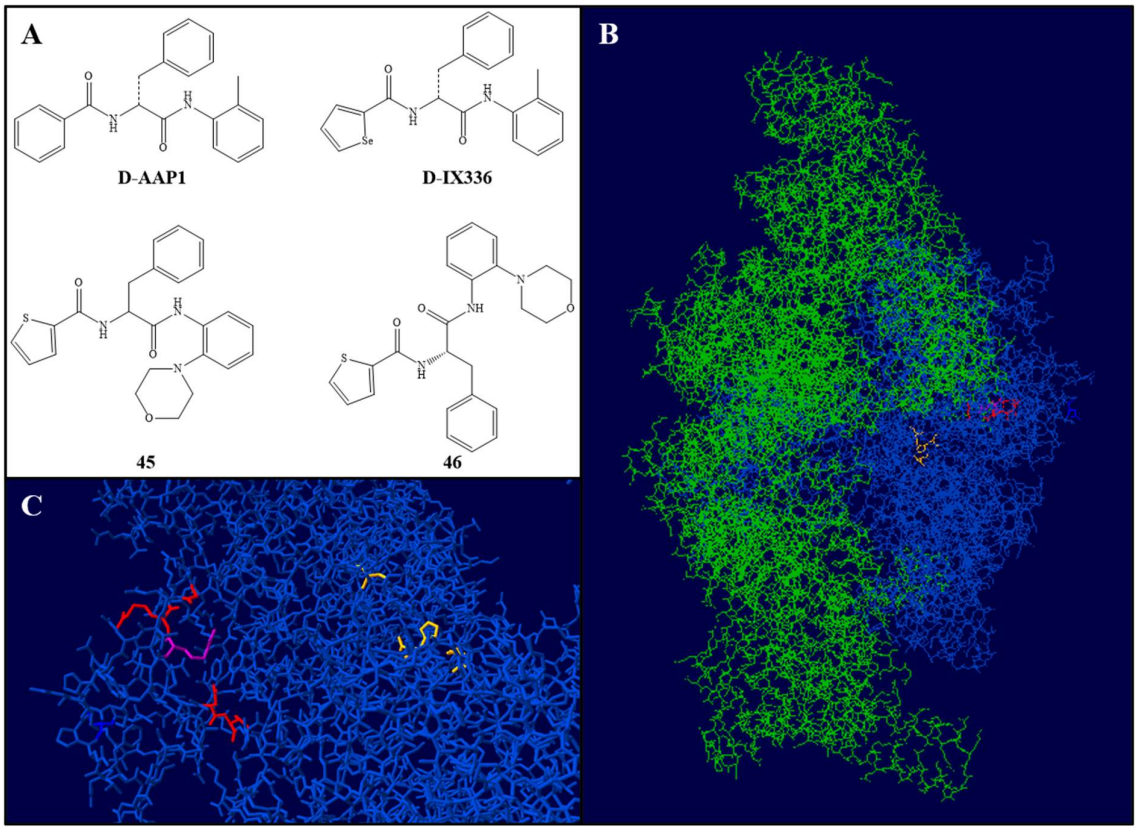


Figure 46. *M. tuberculosis* RNA polymerase and RpoB inhibitors. A. Hits 45 and 46 with analogues D-AAP1 and D-IX336. **B.** *M. tuberculosis* RNAP (RpoB Blue, Rest Green) with common rifampicin mutations (Yellow), 45 and 46 mutations (Red) and D-AAP1 mutation (Purple). **C.** Close up of *M. tuberculosis* RpoB (Blue) with common rifampicin mutations (Yellow), 45 and 46 mutations (Red) and D-AAP1 mutation (Purple). *M. tuberculosis* structure adapted from published PDB structure[396].

3.3.9 Overexpression of Artificial *rpoABCZ* Operon in *M. smegmatis* mc^{2}155

A screen overexpressing RNA polymerase was devised to use as a tool for identifying RNA polymerase inhibitors. This screen would work by observing an increase in the MIC of compounds when compared to the MIC of WT *M. smegmatis*. Gibson cloning was used to create a pMV261k plasmid containing the genes for *M. tuberculosis* RNA polymerase. *RpoA*, *rpoB*, *rpoC*, and *rpoZ* were inserted one after another into pMV261k including 20 base pairs upstream of *rpoB*, *rpoC*, and *rpoZ* to include the ribosome binding sites. The

plasmid was inserted into *M. smegmatis* mc^2155. The data in Figure 47 shows the percentage survival of *M. smegmatis* mc^2155 with pMV261k-*rpoABCZ* plasmid compared with empty pMV261k when treated with the hit compounds. Concentrations were based off the liquid MICs from **Section 4.3.4**. Not all compounds were tested due to shortage. While some of the curves display a slight increase in resistance to the hit compounds the shift is too small to be conclusive. Rifampicin also displays a similar shift, whereas isoniazid does not.

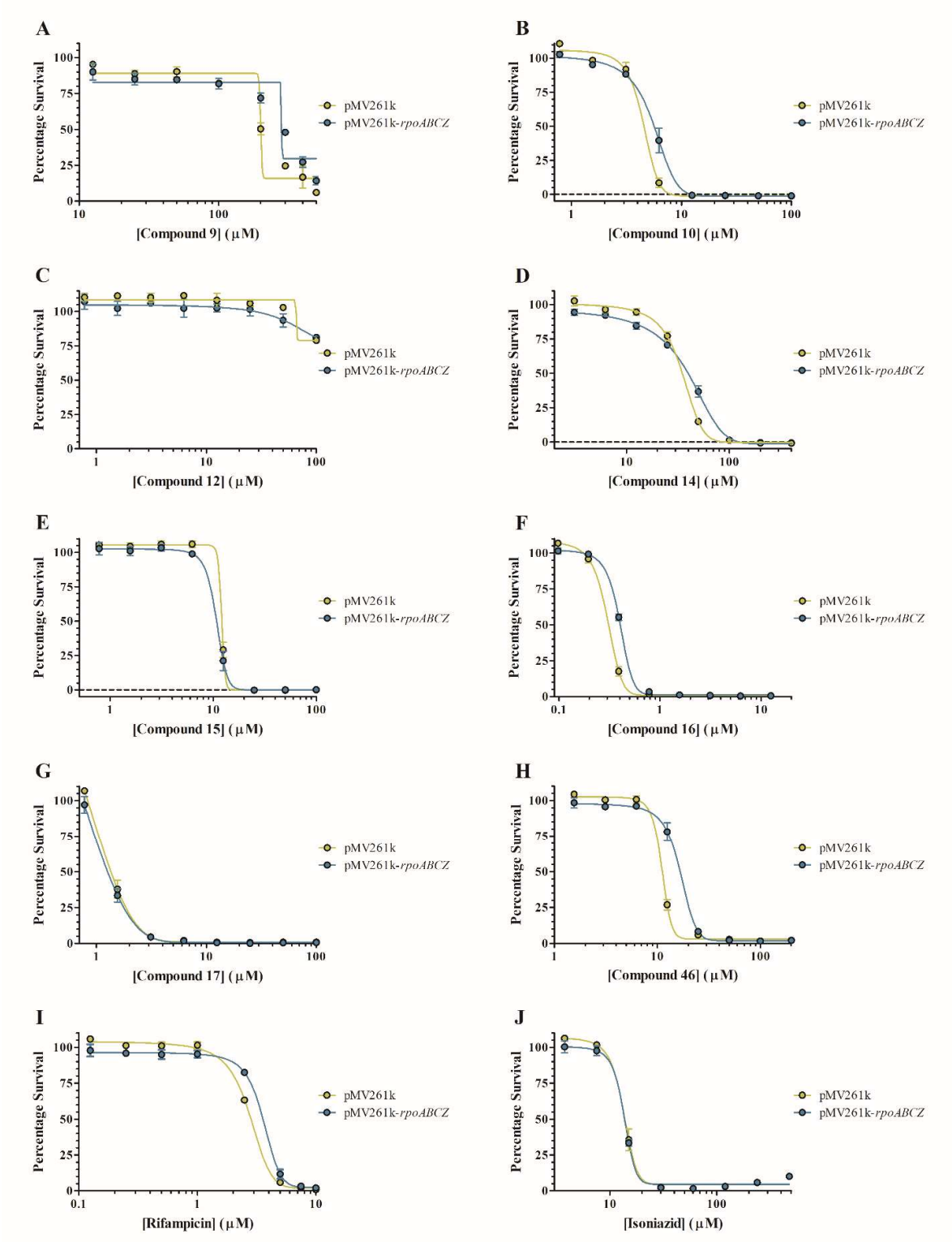


Figure 47. Overexpression of *rpoABCZ* Operon in *M. smegmatis* mc²155 to identify RNA polymerase inhibitors. Data shown as the mean and standard deviation of triple replicate.

3.3.10 RNA Polymerase Purification

Purification of *M. tuberculosis* RNA polymerase to use in biochemical assays was conducted using 2 duet plasmids, pACYC-*rpoA+sigA* and pCDF-*rpoB+rpoC*. A previous study had shown that the presence of RpoZ was not required for enzyme function and that co-expression of the core enzyme with SigA increased enzyme activity[397]. The plasmids were designed to be transformed into *E. coli* and for all four proteins to be purified as the RNA polymerase holo-enzyme by using a ten residue long histidine-tag on RpoA. The data in Figure 48 shows the soluble and insoluble fractions of the expression trial of the plasmids in *E. coli* BL21 individually as well as Western blot staining of the RpoA his-tag using Penta-His antibodies. Proteins roughly corresponding to the sizes of RpoA (37.7 kDa), RpoB (129.2 kDa), and RpoC (146.7 kDa) were visualised in both the soluble and insoluble fractions. SigA was only seen in the insoluble fraction and ran higher than its desired kDa of 57.7, however no equivalent band was visible in the empty plasmid sample, this is likely to be SigA. The Western blot showed a single defined band within heavy smearing at just under 46 kDa, which is approximate to the kDa of RpoA (37.7 kDa). While SigA was present in the insoluble fraction, it was hoped that when the plasmids were co-expressed together more soluble Rpo proteins would make the SigA more soluble with complex formation. The data in Figure 49 shows the large-scale His-tag purification of RNA polymerase holo-enzyme in *E. coli* BL21. As predicted the co-expression of the plasmids did result in more SigA in the soluble fraction. The 100 mM imidazole fraction was chosen for additional purification due to the highest amount of SigA being present in that fraction. While there was an increased amount of SigA in this purification a separate expression trial of SigA using different type of media and different induction methods was conducted (Figure 50). Unfortunately, the trial did not show any bands that appeared to relate to SigA. The RNA polymerase holo-enzyme was purified

several times and all purifications were assessed for activity using gel electrophoresis to identify the prescence of a new RNA band after incubation in a reaction. None of the gels showed any evidence of RNA production.

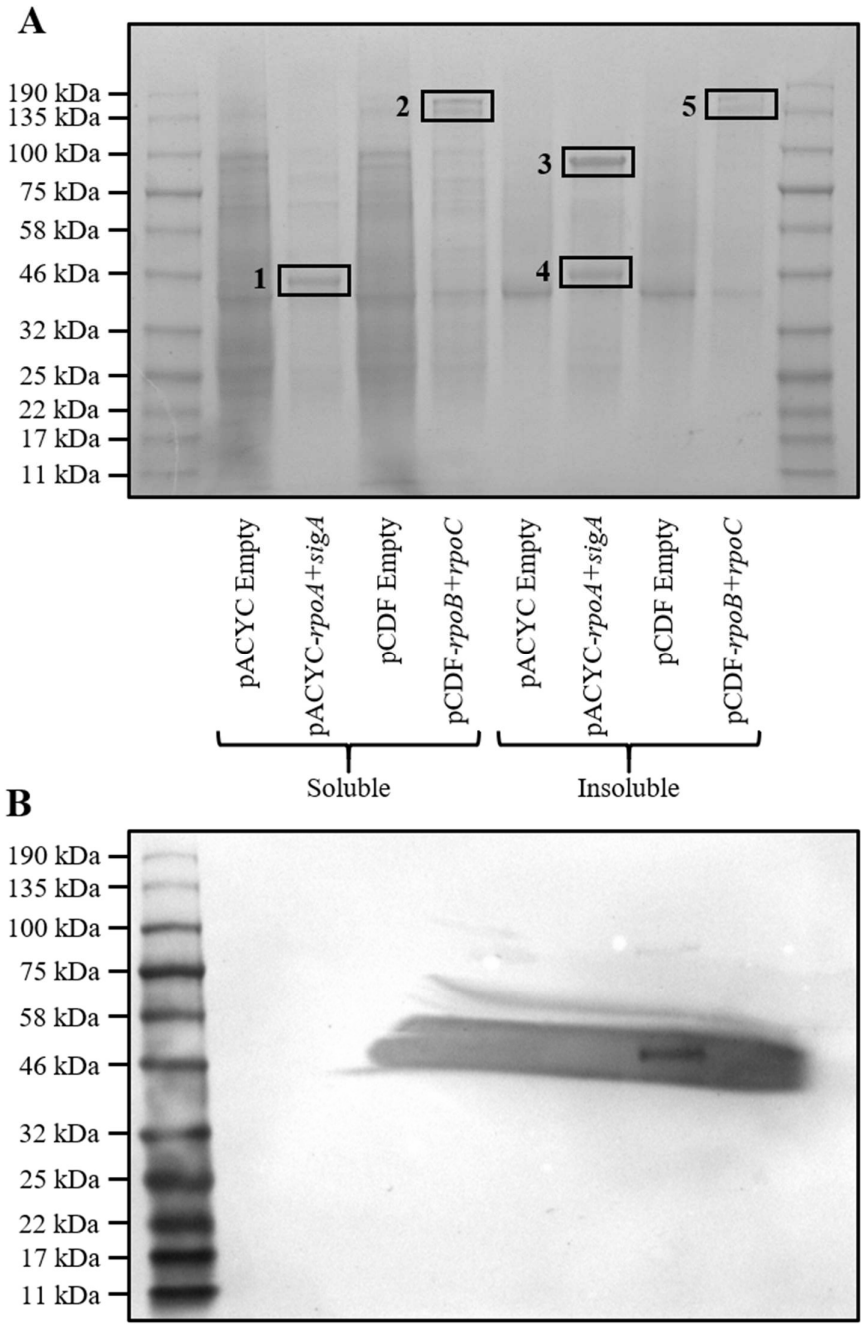


Figure 48. RNA polymerase expression trial. A. Protein gel of soluble and insoluble fractions. Box 1 – Soluble RpoA 37.7 kDa. Box 2 – Soluble RpoB 129.2 kDa and RpoC

146.7 kDa. Box 3 – Insoluble RpoA 37.7 kDa. Box 4 – Insoluble SigA 57.7 kDa. Box 5 – Insoluble RpoB 129.2kDa and RpoC 146.7 kDa. **B.** Western blot of expression trial.

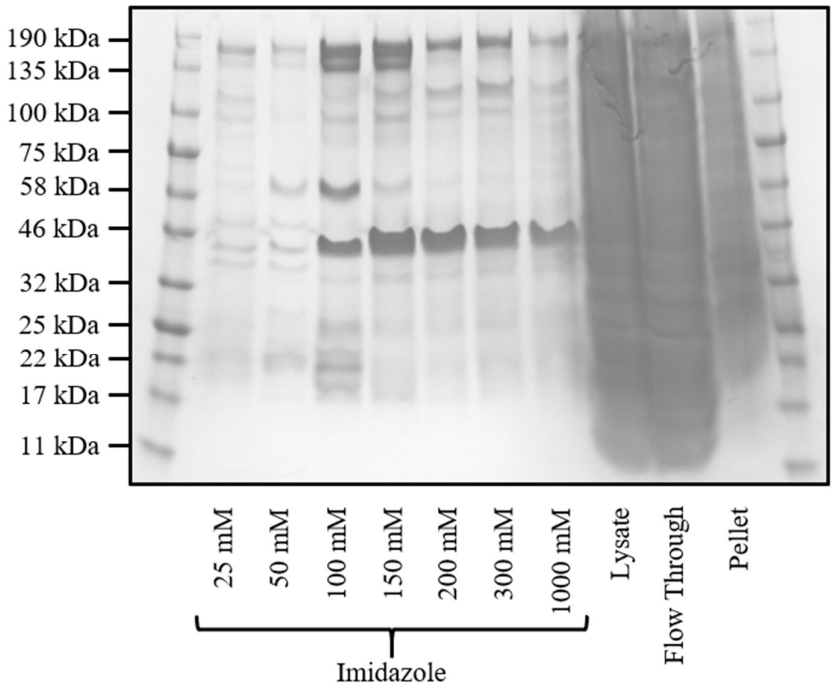
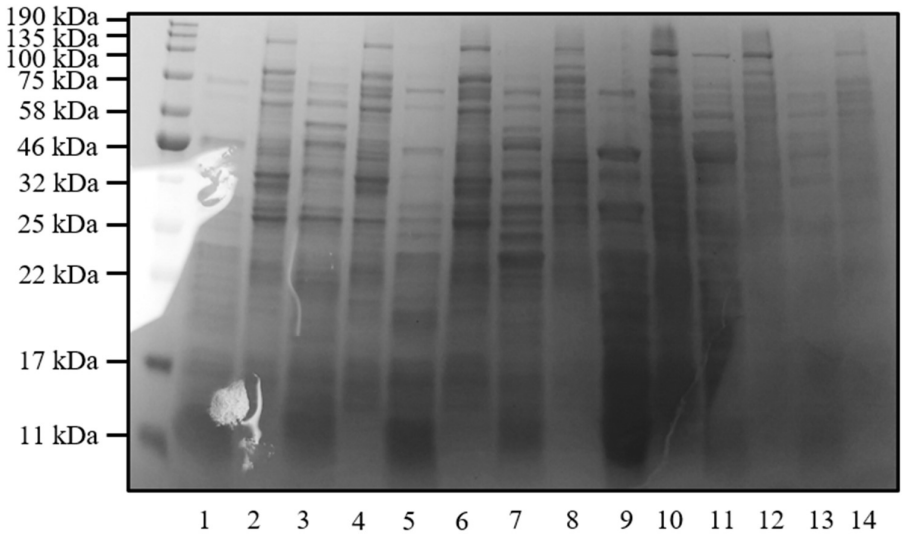


Figure 49. His-tag purification of RNA polymerase holo-enzyme. RpoC 146.7 kDa, RpoB 129.2kDa, SigA 57.7 kDa, and RpoA 37.7 kDa.



	Organism	Plasmid	Media	Fraction
1	*E. coli* BL21	pET30a-*sigA*	ZYM-5052	Soluble
2	*E. coli* BL21	pET30a-*sigA*	ZYM-5052	Insoluble
3	*E. coli* T7 Shuffle	pET30a-*sigA*	Terrific	Soluble
4	*E. coli* T7 Shuffle	pET30a-*sigA*	Terrific	Insoluble
5	*E. coli* BL21	pET30a-*sigA*	Terrific	Soluble
6	*E. coli* BL21	pET30a-*sigA*	Terrific	Insoluble
7	*E. coli* BL21	pET28a-*sigA*	2x YT	Soluble
8	*E. coli* BL21	pET28a-*sigA*	2x YT	Insoluble
9	*E. coli* BL21	pET28a-*sigA*	Terrific	Soluble
10	*E. coli* BL21	pET28a-*sigA*	Terrific	Insoluble
11	*E. coli* BL21	pET28a-*sigA*	ZYM-5052	Soluble
12	*E. coli* BL21	pET28a-*sigA*	ZYM-5052	Insoluble
13	*E. coli* T7 Shuffle	pET28a-*sigA*	Terrific	Soluble
14	*E. coli* T7 Shuffle	pET28a-*sigA*	Terrific	Insoluble

Figure 50. SigA expression trial. SigA 57.7 kDa. No apparent bands corresponding to SigA. The expression trial used a wide range of conditions with both manual induction and auto induction media and different *E.coli* strains. The pET30a-*sigA* plasmid was donated by Joelle Brodeur, Univerité de Sherbrooke. Due to prior protein purifications finding SigA in the insoluble fraction both insoluble and soluble fractions were examined.

3.3.11 *M. smegmatis* Purified Ribosome mCherry Assay

A crucial aspect of the protein synthesis pipeline is translation and the action of the ribosome. To identify inhibitors of the ribosome an assay was conducted to produce mCherry protein and the resulting fluorescence from the mCherry was monitored in real time. When treated with an inhibitor the activity of the ribosome decreases resulting in slower production of mCherry and a corresponding decrease in fluorescence. Ribosomes purified from *M. smegmatis* were used in conjunction with the Δ ribosome Purexpress protein synthesis kit to assay ribosome activity. RNA template of mCherry produced from a pHIT88-*mCherry* plasmid was used as a template for the ribosomes. The production of fluorescent mCherry allowed for the activity of the ribosomes to be measured directly. The fluorescence of mCherry was measured every 30 seconds for 1000 cycles. The data in Figure 51 shows the fluorescence measured across the first 500 cycles. As well as a positive control and blank, rifampicin, isoniazid, F1673-0402 (aspartyl-tRNA synthesis inhibitor)[391], and chloramphenicol were included. As expected, chloramphenicol inhibited the production of mCherry resulting in massively reduced fluorescence when compared to the positive control. The other control inhibitors showed no reduction in fluorescence. The hit compounds tested showed no inhibition of the production of mCherry and therefore do not inhibit translation by *M. smegmatis* ribosomes.

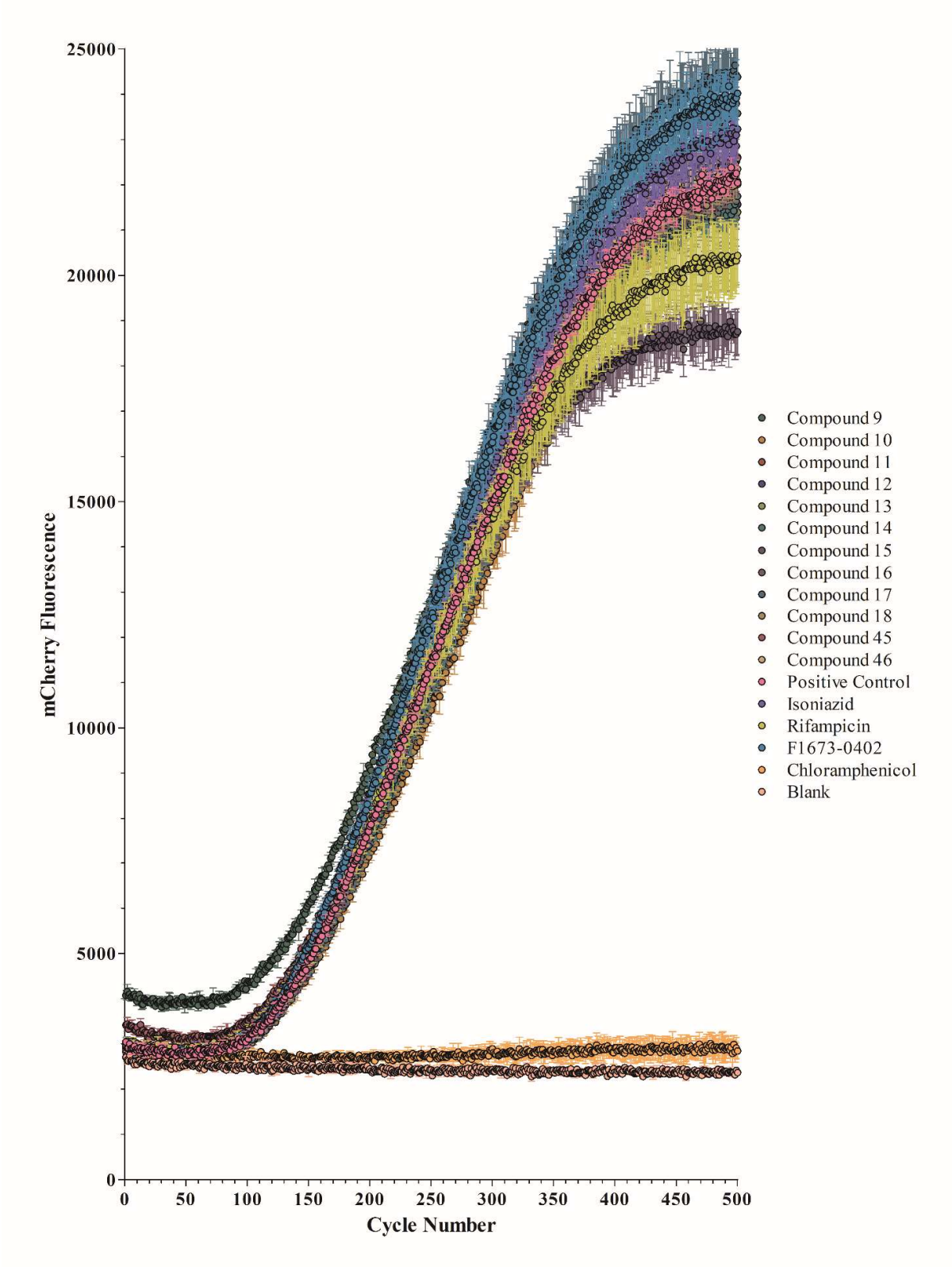


Figure 51. *M. smegmatis* ribosomal inhibition assay. Hits/compound included at 100 µM. Data shown as the mean and standard deviation of triple replicate.

3.3.12 Broken Beacon *E. coli* RNA Polymerase Holo-Enzyme Assay

The broken beacon assay uses a pair of short DNA oligos, one complimentary to a short sequence of the target RNA with an attached 5' TAMRA fluorophore, and a shorter oligo complimentary to the TAMRA oligo with an 3' attached BHQ2. When the 2 oligos are annealed together the BHQ2 quenches the TAMRA. In the presence of the target RNA, the large TAMRA oligo dissociates from the BHQ2 oligo and preferentially hybridises with the target RNA. This dissociation of the TAMRA oligo from the BHQ2 oligo causes an increase in fluorescence proportional to the amount of target RNA. This allows the measurement of RNA polymerase activity in real time. The target RNA is produced by commercial *E. coli* RNA polymerase holo-enzyme from a 493 base pair template DNA of the start of the *mmsA* gene from *M. tuberculosis* H37Rv. The *mmsA* gene was chosen as it has the ideal promotor region for SigA[398]. The data in Figure 52A shows the results for the initial assay where all hits were included at 10 μM. Hits 15, 16 and 45 caused a reduction in fluorescence compared to the positive control with 15 being the most effective. Isoniazid and F1673-0402 showed a very small effect on overall fluorescence. Rifampicin showed a large effect on fluorescence as expected. Unexpectedly, chloramphenicol showed a large reduction in fluorescence. Hits 15, 16, 45 and 46 were assayed again with higher concentrations of compound shown in Figure 52 B. Hit 46 was included on the basis of the whole genome sequencing (WGS) results. Hits 15, 16 and 45 all showed increased potency at 100 μM when compared to 10 μM. The chloramphenicol control was repeated with a fresh compound stock at 100 μM. This time chloramphenicol showed a vastly reduced level of inhibition, which indicates that the inhibition in the original assay may have been due to an incorrectly produced stock compound. These results suggest the hits 15, 16 and 45 are inhibitors of *E. coli* RNA polymerase.

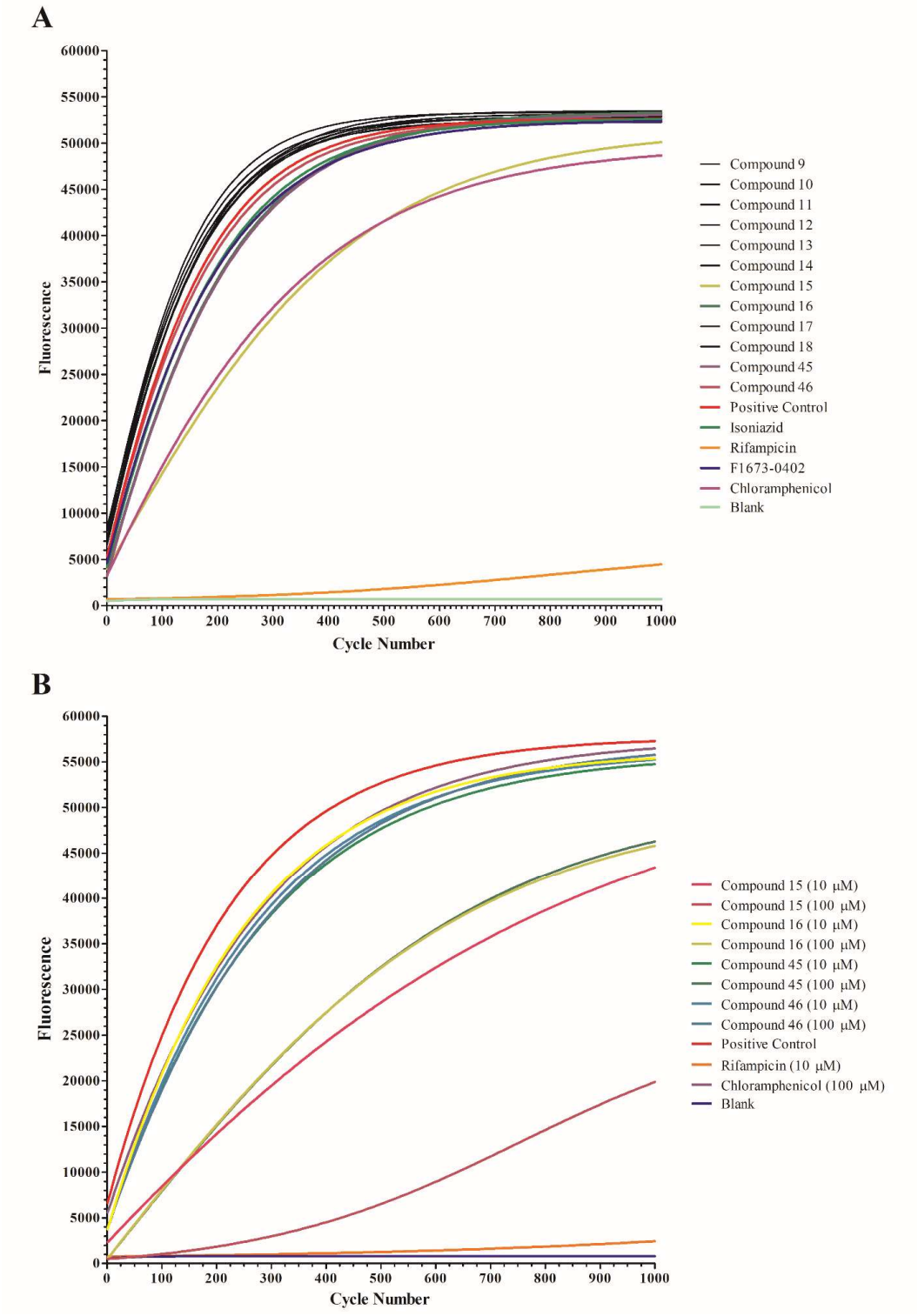


Figure 52. *E. coli* RNA polymerase holo-enzyme broken beacon inhibition assay. A. All hits/compounds including control compounds are included at 10 µM. One cycle is equal to 30 seconds. **B.** All hits/compounds included at concentrations labelled. One cycle is equal to 30 seconds. Non-linear regression is shown; there are too many data points to plot normally.

3.4 Discussion

The goals of this study were to validate and use, on a large scale, a new screening method for finding inhibitors of the protein synthesis pipeline and to verify the hits from screening with microbiological and biochemical methods. The rationale behind this screen is the detection of fluorescent mCherry produced by *M. tuberculosis* when treated with screening hits. If the hits inhibit enzymes in the protein synthesis pipeline, then a reduction in mCherry expression should be detectable by decreased fluorescence. The screening method was initially validated with a proprietary screen of 38 hits provided by Professor James Sacchettini (University of Texas A&M). These hits have been shown to inhibit protein synthesis in a cell-free ribosome assay but had not been tested with a phenotypic screening method against whole cells. When tested, twenty-one of the compounds showed an ability to pass through the cell wall and inhibit the production of mCherry fluorescent protein in addition to the blind controls. The physiology of the *M. tuberculosis* cell wall means that many compounds that may be normally effective against other bacteria are ineffective against *M. tuberculosis.* Phenotypic screening can not only provide information on the target of the compound, but also the ability of the compound to permeate into *M. tuberculosis.* Of the compounds provided and known to target protein synthesis, nearly half failed to have an effect suggesting that cell permeation was low. While assays in isolation may indicate a compound has a preferential target, phenotypic screening can provide this information too and show that the most challenging aspect of *M. tuberculosis* biology, the cell wall, can be overcome.

The large-scale screening of the GSK TB box was split into two parts. The first part, a single-shot adaptation of the screen, was designed to maximise the number of hits that could be tested. The second part was a dose response similar to the proprietary screen. Splitting the process into two parts allowed the first part to use a far more relaxed

selection criterion to account for the limited range of compound concentrations. Any false positives picked up would then be weeded out in the secondary screen. This process worked as intended, it reduced the original 2799 hits down to 91 and then reduced that again to 18. To further streamline this process the single-shot screen could be adapted to use only one compound concentration instead of two. To further increase the number of initial hits the concentration tested at could be increased to 20 μM, instead of the originally tested 10 μM and 1 μM. This would include a broader range of MICs in the initial hits.

Hits 45 and 46 are two related compounds that were not discovered as part of the mCherry screening and were merged with this study. The two hits had solid and liquid MICs measured, which indicated that hit 45 was the more potent of the pair. Whole genome sequencing (WGS) of drug resistant mutants revealed that both compounds target the RpoB subunit of *M. tuberculosis* RNA polymerase, hence why the projects were merged. The mutants were tested for rifampicin cross-resistance to see if they had a similar resistance mechanism, but the resistant mutants to 45 and 46 showed no increased resistance to rifampicin suggesting a different target site on RpoB. These compounds are structurally similar to two other compounds, D-APP1 and D-IX336, reported by Lin *et al* (2017)[396], that had a different target site to rifampicin on RpoB. Computer modelling of the 45 and 46 SNPs, the D-APP1 and D-IX336 SNP, and common rifampicin resistance SNPs onto the structure of *M. tuberculosis* RpoB indicates that these compounds target a similar area to D-APP1 and D-IX336. Liquid and solid MICs were also established for the hits identified by the mCherry screen. The solid MICs were carried out using an alternate method to hits 45 and 46 to reduce the amount of compound required and increase the number of concentrations tested. Attempts at generating drug resistant

mutants for the compounds were partially successful and whole genome sequencing (WGS) of the mutants isolated to hits 10 and 17 are ongoing.

Construction of an artificial *M. tuberculosis rpoABCZ* operon inside plasmid pMV261k was successful. It was hoped that overexpression of the *rpoABCZ* operon could be used as another screening method to specifically find inhibitors of *M. tuberculosis* RNA polymerase and, in addition, that this plasmid could be used to separate out RNA polymerase inhibitors from the mCherry screening hits. Unfortunately, overexpression of the plasmid in *M. smegmatis* mc^2155 led to no phenotypically detectable difference in cell survival when treated with inhibitors including rifampicin. It is likely that expressing 4 different genes off one constitutive *hsp60* promotor results in low protein production, or an imbalance in the subunits produced. RNA polymerase needs 2 copies of RpoA for every copy of RpoB, RpoC, and RpoZ to produce a functional RNA polymerase. The presence of only one *rpoA* copy on the plasmid may have contributed to a lack of RpoA.

Purification of *M. tuberculosis* RNA polymerase holoenzyme was carried out using two duet plasmid vectors, pACYC-*rpoA+sigA* and pCDF-*rpoB+rpoC*. This was a method used by Banerjee *et al*. (2014)[397] to produce a highly active RNA polymerase holoenzyme for assays[397]. Initial trial purification of *E. coli* expressing individual plasmids indicated the presence of all required subunits at roughly the correct kDa and a Western blot confirmed the presence of the 10x His-tag of RpoA. The majority of SigA was present in the insoluble fraction, but it was hoped that complex formation with the mostly soluble RNA polymerase subunits would pull the SigA into the soluble fraction. This proved to be the case as a large-scale protein purification did show a large increase in SigA, however it was still the least abundant of the 4 proteins. Assessments of the enzyme activity using gel electrophoresis did not show any activity. This may have been due contamination of RNase, or more likely, a lack of enzyme activity. There are a few

potential reasons that alone or combined could have contributed to a lack of activity. Firstly, while SigA levels were increased in the large-scale purification there may have still been a general deficiency, which reduced RNA polymerase activity. Additional SigA production was attempted to supplement the enzyme, but the expression trial showed no corresponding bands and the Western blot showed no specific staining. Second, as with the overexpression vector there may have been a lack of RpoA. The 100 mM imidazole fraction purified had RpoA, RpoB, and RpoC at roughly equivalent levels. Due to twice the amount of RpoA being required for complex formation, in hindsight, it would have been better to combine the 100 mM fraction and 150 mM fraction to boost the amount of RpoA. Finally, this purification method did not include the protein CarD. CarD is thought to be involved in the stabilisation of the *M. tuberculosis* RNA polymerase initiation complex[344–346]. The lack of this protein could mean that the RNA polymerase holoenzyme able to form is not stable for long enough to transcribe DNA.

The purpose of the ribosome assay was to examine the compounds for activity relating to ribosome inhibition. Purified *M. smegmatis* mc^2155 ribosomes were combined with a Δ ribosome Purexpress kit. In order to assess the activity of the ribosomes in isolation an RNA template of the mCherry gene was used. This avoided the use of the Purexpress kits RNA polymerase to convert a DNA template. To account for the effect of potential tRNA synthesis inhibitors among the unknown compounds, F1673-0402 an aspartyl-tRNA synthesis inhibitor[391] was included. Of the control compounds, rifampicin, isoniazid, F1673-0402, and chloroamphenicol, only chloramphenicol showed inhibitory activity. This shows that this assay is specific for purely the inhibition of the ribosome. The compounds tested did not display any significant reduction in ribosome activity.

Due to the inability to produce catalytic *M. tuberculosis* RNA polymerase holoenzyme the related assays were carried out using commercial *E. coli* RNA polymerase

holoenzyme. The first assay seemed to indicate that only compound 15 was causing any inhibition. Due to the WGS results for hits 45 and 46 suggesting RpoB as the target it was decided that all the compounds displaying even slight inhibition greater than 46 would be retested at a higher concentration. It must be noted that chloramphenicol appeared to show inhibition in the assay, which was not expected. It was decided that the chloramphenicol should be tested again at a higher concentration with a freshly prepared stock to rule out any mistakes with the original. The second assay showed no inhibition from chloramphenicol even at the higher concentration indicating that this assay is specific for RNA polymerase inhibition. The higher concentration of test compound also showed that hits 45, 15 and 16 are all likely to inhibit RNA polymerase.

This project has thoroughly tested twelve unknown hits, ten of which were identified using a novel screening method. Of those hits none were found to inhibit the ribosomes of *M. tuberculosis* model organism, *M. smegmatis* mc^2155. Three of the hits, 15, 16 and 45, were found to target *E. coli* RNA polymerase and are likely to have the same effect on *M. tuberculosis*. Resistance to hits 45 and 46 was caused by mutations in *M. tuberculosis* H37Rv *rpoB* and it's likely that, at higher concentrations, 46 would have inhibited *E. coli* RNA polymerase in assays. In addition, 45 and 46 appear to bind in a similar location to two other RNA polymerase inhibitors in a distinct location from rifampicin which has positive implications for co-administration of these drugs in TB treatment[396]. While the other eight hits found during screening do not target the ribosome or RNA polymerase, they perhaps target another aspect of the protein synthesis pipeline, tRNA synthesis. F1673-0402 was a compound found to inhibit aspartyl-tRNA synthesis[391] and inhibitors of other tRNA synthases are likely to be good drug targets. Future work for this project could include the development of assays to examine the activity of tRNA synthases. Whole genome sequencing of the drug resistant mutants to

hits 10 and 17 should be completed and solid MICs and drug resistant mutant generation for hits 15 and 16 should be attempted if more compound can be acquired. Additional testing and refinement of the *rpoABCZ* overexpression vector could lead to a useful plasmid to attempt other screens more specific for RNA polymerase inhibitors.

Chapter 4

The Use of Biochemical Assays and Microbiological Techniques to Assess Potential Inhibitors of *M. tuberculosis* Antigen 85

4 The Use of Biochemical Assays and Microbiological Techniques to Assess Potential Inhibitors of *M. tuberculosis* Antigen 85

4.1 Introduction

The antigen 85 family consists of four secreted proteins; antigen 85 A, B, C, and D (MPT51), that are located in the periplasm of *mycobacterial* species[399]. The genes that encode these proteins are named fibronectin binding proteins; *fbpA*, *fbpB*, *fbpC* and *fbpD* after the original finding that these proteins strongly bind with the human protein, fibronectin[51,400]. It is thought that the fibronectin binding ability of Antigen 85 is used by *M. tuberculosis* to promote adherence and resist clearance from the lungs[401]. Antigen 85A, B, and C display mycolyltransferase activity which is used for mycolation of the *M. tuberculosis* cell wall[402]. MPT51 does not display catalytic activity and it is currently thought that this protein may only be used for fibronectin binding and adherence[402,403].

The catalytic Antigen 85 enzymes perform three major roles in the construction of the mycobacterial cell wall; the attachment of mycolic acids to the terminal arabinose residues on the arabinogalactan[404], the production of trehalose mono-mycolate[402], and the production of trehalose di-mycolate[402]. These processes are crucial for the correct formation of the mycolic acid outer layer of the cell wall and essential for the survival of *M. tuberculosis*[405–408]. The essentiality of this process is further supported by the absence of a reported triple knockout of Antigen 85A, B and C. The acyl-donor substrate, usually trehalose mono-mycolate[280], is similar for each process and the acceptor molecules are similar in both the terminal arabinogalactan motif[258] and trehalose or TMM. The similarity of the substrates and active sites means that all three catalytic Antigen 85 enzymes can perform the three roles with varying levels of efficiency[409–411]. Each enzyme isoform does show a preference for a particular type of activity despite being versatile enough for the different roles[280]. Backus *et al* (2014) postulated that Antigen 85C may be

responsible for the generation of TMM and TDM going as far to suggest that Antigen 85C may also be responsible for the synthesis of TMM inside the cell before exporting. A knockout of *fbpA* showed growth impairment in macrophage infection compared to wild type but had no growth impairment in rich media[412]. Armitige *et al* (2000) claim that *fbpA* knockouts display growth impairment in nutrient limited media, however this has been later corrected by Puech *et al* (2002)[412,413]. In the same study by Armitige *et al* (2000), the *fbpB* knockout showed no such growth impairment in media or macrophages[412]. Individual *fbpA* or *fbpB* knockouts show no effect on the mycolation of arabinogalactan[413]. A *fbpC* knockout also displays a large reduction of up to 40 % of cell wall mycolation by preventing the attachment of mycolic acids[414]. The elucidation of Antigen 85 isoform roles has been hampered by a lack of double and triple knockouts. The contrasting findings of research coupled with the high versatility and flexibility of donor and acceptor substrate suggest that the preferences of Antigen 85 isoforms are only minor.

A drug that could target all three isoforms would be of significant use for the treatment of *M. tuberculosis* infection. The killing effect of the drug would have a similar effect to isoniazid but achieved in a different way. Isoniazid kills mycobacteria by preventing the synthesis of mycolic acids, which prevents the construction of the outer cell wall[405–408]. The inhibition of Antigen 85 isoforms would prevent the construction of the outer cell wall[414]. While the use of isoniazid and this hypothetical drug together would not be feasible, in isoniazid resistant infection this drug could achieve killing in the same manner but with a different mode of action. *M. tuberculosis* would potentially require two resistance conferring mutations in two of the *fbp* genes for viable resistant mutants. This is supported by the lack of double knockouts of antigen 85 isoforms, indicating that two functional copies are required for survival. Additionally, this excludes any potential cost

or benefit of effects on the fibronectin binding of Antigen 85. A reduction in binding could promote more efficient mechanical clearance of *M. tuberculosis*[415–417], however this could facilitate increased spread of the disease in the population due to a higher number of expelled bacilli. A class of inhibitors for Antigen 85B was proposed as early as 2001 and consisted of two trehalose molecules linked by an amphipathic chain to block both trehalose binding sites and mimic mycolates[410]. Several inhibitors of Antigen 85C have been discovered. These include, 6-azido-6-deoxy-α,α'-trehalose[404,418], an analogue of trehalosamine[419]; Ebselen, a synthetic organoselenium compound currently in clinical trials as a treatment for a number of human conditions, such as strokes[420,421], hearing loss[422], and bi-polar disorder[423]. Favrot *et al* (2013) has shown that ebselen inhibits Antigen 85C[424]. This inhibition occurs *via* covalent modification of the active site cysteine at position 209[424]. The authors have also shown that iodoacetamide can also react with the active site cystine *via* alkylation[424]. Additional screening methods have found a few other candidates, notably that covalently modify the active site cystine similar to ebselen[425,426]. In addition, cyclipostins and cyclophostin analogues covalently modify the active site serine at position 124[427], and an *in silico* screen has found a further seven potential inhibitors[428].

In this study multiple assays were used to examine the activity of Antigen 85A and C when treated with inhibitors. The radioactive assay was an adapation of a previously published assay[404]. This assay, as shown in Figure 53, used purified TMM and radioactive [^{14}C] trehalose. Antigen 85 transfers the mycolate from the TMM to [^{14}C] trehalose. The radioactive [^{14}C] TMM and [^{14}C] TDM is then extracted into an organic solvent and either scintillation counted or visualised *via* thin layer chromatography (TLC). The β-glucosidase assay developed by Boucau *et al*, shown in Figure 54, using 4-nitrophenyl-6-octanoly-β-D-glucopyranoside[429]. Antigen 85 removes the octanoyl chain and deposits

it onto a glucose acceptor. This leaves 4-nitrophenyl-β-D-glucopyranoside, which is then treated with a β-glucosidase to release 4-nitrophenyl. The amount of released 4-nitrophenyl is measured on a plate reader. The resorufin butyrate assay developed by Favrot *et al.* measures the release of resorufin[424]. Antigen 85 removes the butyrate from resorufin butyrate and attaches it to a trehalose acceptor as shown in Figure 55. The released resorufin butyrate can be measured *via* fluorescence in real time. The radioactive, β-glucosidase and resorufin butyrate assays all examine the production of TMM and TDM (or analogues thereof). The trehalose-C-12-Nitro-Benzoxadiazol (NBD) assay, shown in Figure 56, used purified arabinogalactan as an acceptor. The C12-NBD is removed from the trehalose donor and attached to the arabinogalactan. The remaining trehalose-C-12-NBD is washed away from the insoluble arabinogalactan. The fluorescence of the arabinogalactan with attached C12-NBD can then be measured.

In this study we use four different assay methods to examine six compounds thought to target members of the Antigen 85 complex. The compounds in question were identified *via* an overexpression screen of *fbpA* in *M. bovis* BCG, conducted by Dr Jonathan A.G. Cox at GSK. While the β-glucosidase assay did not work acceptably the other three assays showed that these compounds did not inhibit Antigen 85 in any detectable way. Lipid profiling did indicate that some of the compounds were influencing the composition of the cell wall. Due to the inability of the assays to identify Antigen 85 inhibitors among the compounds, the more traditional method of spontaneous drug resistant mutants and whole genome sequencing was used to identify the compound targets.

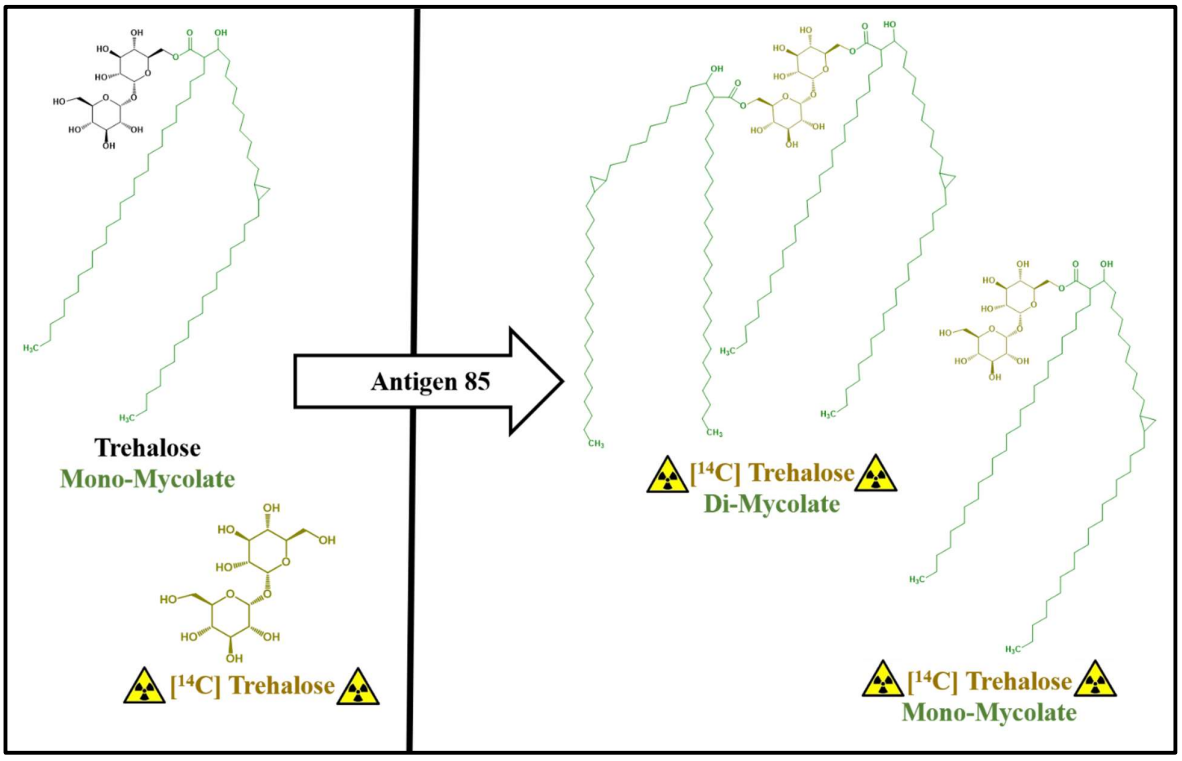


Figure 53. Antigen 85 radioactive assay.

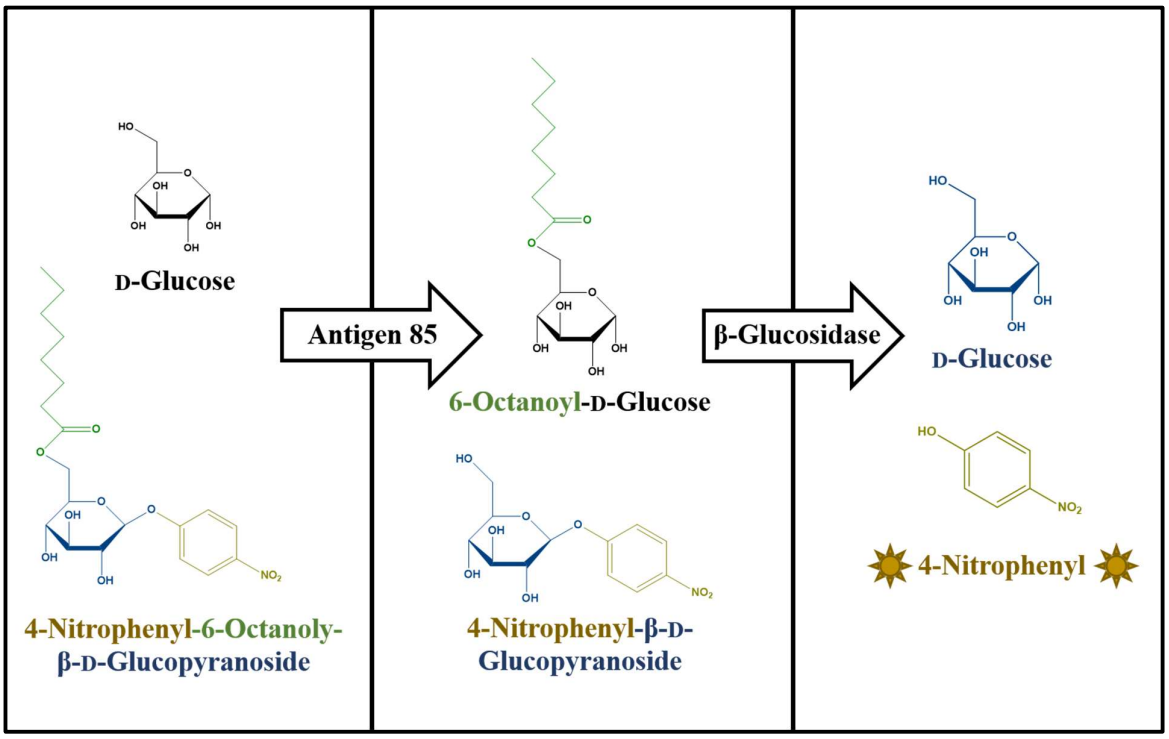


Figure 54. Antigen 85 β-glucosidase assay.

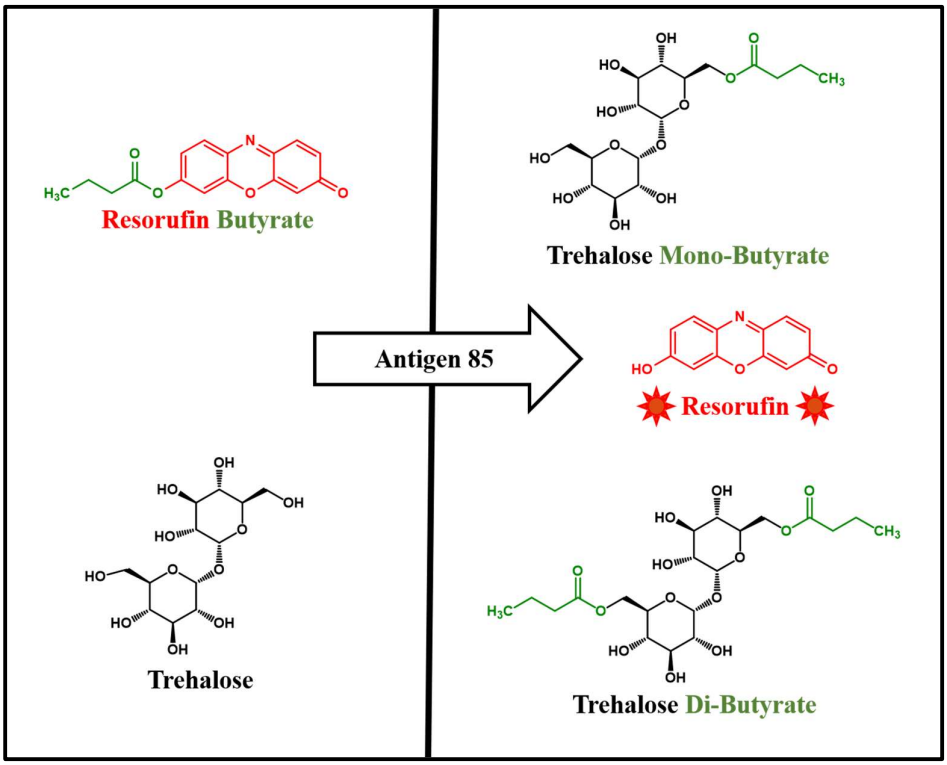


Figure 55. Antigen 85 resorufin butyrate assay.

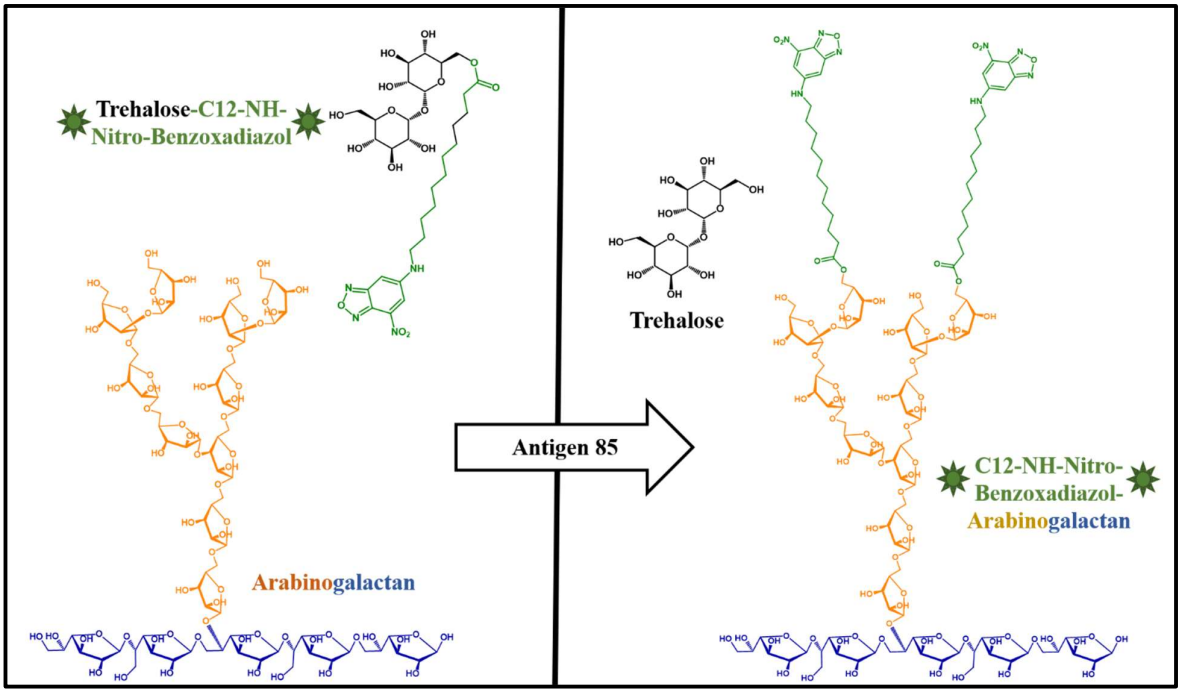


Figure 56. Antigen 85 trehalose-C-12-nitro-benzoxadiazol (NBD) assay.

4.2 Materials and Methods

4.2.1 Antigen 85A and C2 Purification

Pellets of *E. coli* BL21 containing either pMV261-*fbpA* or pMV261-*fbpC2* produced by Dr Katherine Abrahams (University of Birmingham) were used for protein purification. Antigen 85A and C2 were purified using standard the His-Trap HP method outlined in **Method 6.5.1**. A protein gel was run and the protein containing fractions were desalted using a glass desalting column packed with Bio-Gel P-6DG gel (Bio-Rad). The column was first washed with 500 mL of dH_2O and then equilibrated with 500 mL of Buffer A (50 mM tris-HCL pH 7.5, 10 % glycerol). The protein fraction was loaded onto the column and allowed to run down to the top of the gel. Without disturbing the gel 100 mL of Buffer was passed through the column and 1.5 mL fractions were collected. The fractions were assessed for protein content using the Bradford assay in a microplate. Protein containing fractions were pooled and then further purified by anion exchange chromatography (**Method 6.5.3**). The protein was analysed with a protein gel and the purest fractions were pooled and frozen in aliquots at 4 °C.

4.2.2 Production of 4-Nitrophenyl-6-Octanoyl-β-D-Glucopyranoside

The free hydroxyl groups of the glucopyranose were protected using trimethylsilyl groups. 4-Nitrophenyl-β-D-glucopyranoside (0.5 g, Sigma) was dissolved in 20 mL of pyridine and 20 mL of hexamethyldisilazane. Trimethylsilylchloride (10 mL) was added at room temperature. The mixture was then stirred at 60 °C overnight. The reaction mixture was quenched with 50 g of ice. Hexane (50 mL) was added and the reaction was stirred until the ice melted. The organic phase was separated and the aqueous phase was extracted with 50 mL of hexane. This was repeated twice. The collected organic phase

was pre-dried with a saturated brine solution and the organic phase was separated again. The organic phase was then dried further with anhydrous sodium sulphate, which was added until it was free flowing. The organic phase was dried down fully on a rotary evaporator (Buchi, Rotavapor R-215, Vacuum Pump V-710) to give per-trimethylsilyl (TMS) protected 4-nitrophenyl-β-D-glucopyranoside. The TMS group on carbon 6 was selectively removed as follows. The TMS protected 4-nitrophenyl-β-D-glucopyranoside was dissolved in 30 mL of methanol:dichloromethane (9:1, v/v) and cooled on ice. Potassium carbonate (2 mg) was added, and the mixture was stirred on ice for 15 minutes. Thin layer chromatography (TLC) of the reaction was run in hexane:ethyl acetate (9:1, v/v) to confirm selective deprotection of the carbon 6-hydroxyl group. After deprotection the reaction was quenched with 0.5 mL of acetic acid on ice. The mixture was dried down using rotary evaporation and purified by flash column chromatography. A column was packed with 100 g of soaked silica and sand laid over the top. The column was equilibrated with hexane and the selectively deprotected product was loaded onto the column. The product was eluted off the column by gradually increasing the percentage of ethyl acetate in hexane stepwise in 200 mL volumes to 10 %. The eluate was collected in fractions and TLCs were run to determine the fractions containing product. The selectively deprotected product was dried down using a rotary evaporator and 100 mg was dissolved in dry ethyl acetate. The deprotected hydroxyl group on carbon 6 of the glucopyranose was then esterified with 200 mg of octanoic acid in the presence of 200 mg of dicyclohexylcarbodiimide and 10 g of molecular sieves. This reaction was conducted under argon at room temperature for 2 days after which the molecular sieves and dicyclohexylcarbodiimide were removed by filtration. After esterification the product was fully deprotected by stirring with acidic Dowex resin. The Dowex resin was removed

by filtration to leave the finished product. The product was dried in glass tubes and weighed. It was stored in the dark at 4 °C until use.

4.2.3 4-Nitrophenyl Standard Curve

Desired concentrations 4-nitrophenyl in DMSO were pipetted into a microplate (Greiner, 96 well, PS, F-clear bottom, black, sterile. Ref – 655090). The wells were made up to 100 µL with buffer (50 mM sodium phosphate pH 7.4, 3 mM D-glucose) with DMSO at a 2 % final concentration. The microplate was read on a BMG plate reader for absorbance at 420 nm.

4.2.4 β-Glucosidase Activity on 4-Nitrophenyl-6-Octanoyl-β-D-Glucopyranoside

A 100x stock of 4-nitrophenyl-6-octanoyl-β-D-glucopyranoside desired concentrations was made up in DMSO and 1 µL was added to triplicate wells in a microplate (Greiner, 96 well, PS, F-clear bottom, black, sterile. Ref – 655090). The wells were made up to 100 µL with buffer (50 mM sodium phosphate pH 7.4, 3 mM D-glucose) with DMSO at a 1 % final concentration. To start the reaction 1.84 units of β-glucosidase (Megazyme) was added to each well. The microplate was read on a BMG plate reader for absorbance at 420 nm every 30 seconds for 10 minutes at 37 °C.

4.2.5 β-Glucosidase Activity on 4-Nitrophenyl-6-Octanoyl-β-D-Glucopyranoside including Antigen 85C2

A microplate (Greiner, 96 well, PS, F-clear bottom, black, sterile. Ref – 655090) was set up with 100 µL of 300 µM 4-nitrophenyl-6-octanoyl-β-D-glucopyranoside, 50 mM sodium phosphate pH 7.4, 3 mM D-glucose in experiment wells. 0.184 units of β-glucosidase (Megazyme) was added to each well. Half of the wells had 3 µL of 0.27

mg/mL antigen 85C2 added. The microplate was read on a BMG plate reader for absorbance at 420 nm every 30 seconds for 4 minutes at 37 °C.

4.2.6 Resorufin Standard Curve

Dilutions of resorufin in DMSO were made at 100x concentration and 1 μL was pipetted into the wells of a microplate (Greiner, 96 well, PS, F-bottom, black, sterile. Ref - 655086). The wells were made up to 100 μL with buffer (50 mM sodium phosphate pH 7.4, 4 mM trehalose). The plate was read at 37 °C with a BMG plate reader with an excitation wavelength of 544 nm and emission wavelength of 590 nm.

4.2.7 The Effect of Resorufin Butyrate on the Rate of Antigen 85C2

Dilutions of resorufin butyrate in DMSO were made at 100x concentration and 1 μL was pipetted into the wells of a microplate (Greiner, 96 well, PS, F-bottom, black, sterile. Ref - 655086), for the desired final concentration. The wells were made up to 100 μL with buffer (50 mM sodium phosphate pH 7.4, 4 mM trehalose). Antigen 85C2 (500 nM) was added to each well. The DMSO concentration was 2 %. The plate was read at 37 °C with a BMG plate reader with an excitation wavelength of 544 nm and emission wavelength of 590 nm every 40 seconds for 40 cycles.

4.2.8 The Effect of Trehalose on the Rate of Antigen 85 C2

Resorufin butyrate (1 μL) in DMSO was pipetted into the wells of a microplate (Greiner, 96 well, PS, F-bottom, black, sterile. Ref - 655086), for the desired final concentration of 100 μM. The wells were made up to 100 μL with buffer (50 mM sodium phosphate pH 7.4) with varying concentrations of trehalose. Antigen 85C2 (500 nM) was added to each

well. The DMSO concentration was 2 %. The plate was read at 37 °C with a BMG plate reader with an excitation wavelength of 544 nm and emission wavelength of 590 nm every 40 seconds for 40 cycles.

4.2.9 Resorufin Butyrate Assay for Inhibitors of Antigen 85A and C2

Dilutions of the test compounds and control compound ebselen (Sigma) were made at 1 mM in DMSO and 1 µL was pipetted into the wells of a microplate in triplicate (Greiner, 96 well, PS, F-bottom, black, sterile. Ref - 655086). Iodoacetamide was included as an additional control compound at 50 µM. Wells were made up to 99 µL with buffer (50 mM sodium phosphate pH 7.4, 4 mM trehalose). Resorufin butyrate (10 mM, 1 µL) was added for a final concentration of 100 µM and 2 % DMSO. Antigen 85A and C2 (500 nM) were added to test wells and the plate was incubated overnight at 4 °C. The plate was read at 37 °C with a BMG plate reader with an excitation wavelength of 544 nm and emission wavelength of 590 nm every 40 seconds for 40 cycles.

4.2.10 Radiometric Assay for Activity Assessment of Antigen 85 A and C2

[C^{14}] Trehalose (2.5 µL, 5,272,500 cpm, PerkinElmer) was dried down with 250 µg of TMM. This was resuspended in 125 µL of reaction buffer (100 mM sodium phosphate pH 7.4, 100 µM dithiothreitol) and sonicated to fully resuspend the TMM. To this 125 µL of reaction buffer containing 10 µg of Antigen 85A or C2 was added and mixed. The reaction was incubated at 37 °C for 1 hour. After reaction completion the volume was made up to 480 µL with reaction buffer. Chloroform and methanol were added to give a final ratio of chloroform:methanol:H_2O (4:2:1, v/v/v) and the mixture centrifuged at 3,500 rpm for 3 minutes. The aqueous phase was re-extracted using chloroform:methanol:H_2O (4 mL, 10:10:3, v/v/v). The organic phases were combined and

an additional 750 µL of dH_2O and 1.75 mL of chloroform were added, vortex mixed, and centrifuged as above. The aqueous phase was discarded. The washed organic phase was dried down and resuspended in 100 µL of chloroform. An aliquot (20 µL) was removed and dried down in scintillation vials, resuspended in 10 mL of scintillation fluid (Ecoscint A, National Diagnostics) and counted on a Tri-Carb 2700TR Liquid Scintillation Analyser. The remaining sample (80 µL) was applied to TLC plates and developed in one direction using chloroform/methanol (2:1, v/v) and exposed to X-ray films (Kodak BioMax Light Film) in light-proof cassettes. Films were exposed for 3 days and developed using an Xograph film processor.

4.2.11 Radiometric Assay for Inhibitors of Antigen 85A

[C^{14}] Trehalose (1 µL, 2,109,000 cpm, PerkinElmer) was dried down with 100 µg of TMM. This was resuspended in 50 µL of reaction buffer (100 mM sodium phosphate pH 7.4) and 50 µL of reaction buffer containing 500 nM of Antigen 85A was incubated overnight with 20 µM of the test inhibitors, 20 µM of ebselen, and 100 µM iodoacetamide. The [C^{14}] trehalose and TMM suspension was sonicated to fully resuspend the TMM and then mixed with the incubated enzyme to begin the reaction. The reaction was incubated at 37 °C for 1 hour. After reaction completion the volume was made up to 480 µL with reaction buffer. Chloroform and methanol were added to give a final chloroform:methanol:H_2O reaction mixture with a ratio of 4:2:1 (v/v/v) and the mixture centrifuged at 3,500 rpm for 3 minutes. The organic phase was re-extracted using chloroform:methanol:H_2O (4 mL, 10:10:3, v/v/v). The organic phases were combined and an additional 750 µL of dH_2O and 1.75 mL of chloroform added, vortex mixed, and centrifuged as above. The aqueous phase was discarded. The washed organic phase dried down and resuspended in 100 µL of chloroform. An aliquot (40 µL) was removed and

dried down in a scintillation vial, resuspended in 10 mL of scintillation fluid (Ecoscint A, National Diagnostics) and counted on a Tri-Carb 2700TR Liquid Scintillation Analyser. The remaining sample (60 μL) was applied to TLC plates and developed in one direction using chloroform/methanol (2:1, v/v) and exposed to X-ray films (Kodak BioMax Light Film) in light-proof cassettes. Films were exposed for 3 days and developed using Xograph film processor.

4.2.12 Arabinogalactan-Peptidoglycan Purification

A 50 ml culture of *M. smegmatis* was pelleted at 4,000 rpm for 20 minutes and the pellet was resuspended in 100 mL of cold dH_2O. The resuspended cells were refluxed in 50 mL of 4% sodium dodecyl sulfate (SDS) for 3 hours. The mixture was repeatedly washed with dH_2O (50 mL), centrifuged at 80,000 rpm for 1 hour, the pellet collected and re-washed twice to remove all the SDS. The pellet was then washed using 80% acetone (10 mL) and 100% acetone, successively. The recovered sample was then incubated at 37 °C with 0.5% potassium hydroxide (10 mL) in methanol for 4 days. The sample was centrifuged again as before and washed 3 times with methanol (10 mL) and then with diethyl ether (10 mL) to give partially purified arabinogalactan-peptidoglycan.

4.2.13 C-12 Nitro-Benzoxadiazol Fluorometric Assay

Reaction mixtures (100 μL) were set up in 1.5 mL microcentrifuge tubes with 50 mM sodium phosphate pH 7.4, 3 mg of *M. smegmatis* arabinogalactan-peptidoglycan, 500 μM of C-12 nitro-benzoxadiazol (provided by Dr. Patrick Moynihan, University of Birmingham), and 500 nM of Antigen 85A. Additionally 10 μM of the test compounds, 10 μM ebselen, or 50 μM iodoacetamide were included. The reactions were incubated overnight at 37°C with shaking at 800 rpm. The samples were dried down to leave the

pelleted arabinogalactan-peptidoglycan and unbound fluorophore. The pellet was resuspended in methanol:dH2O (1 mL, 50:50, v/v) and sonicated to break down the pelleted fluorophore. This was repeated 5 times to remove all unbound fluorophore following centrifugation. The samples were finally resuspended in 150 µL and sonicated again to homogenise the samples and 100 µL added into a microplate (Greiner, 96 well, PS, F-bottom, black, sterile. Ref - 655086) and read with a BMG plate reader on a excitation wavelength 485 nm and a emission wavelength of 520 nm.

4.2.14 Minimum Inhibitory Concentrations (MICs) of Antigen 85 Compounds

Several dilutions of the Antigen 85 compounds were made in compound plates (Greiner, 96 well, PP, V-bottom. Ref - 651201), at 100x concentration. In separate microplates (Greiner, 96 well, PS, F-bottom, black, sterile. Ref - 655086) for each compound, 1 µL of the 100x dilutions was added in triplicate to each plate as well triplicate wells of 1 µL DMSO and 100 µM rifampicin. Each well was made up to 100 µL with mid-log (OD_{600} 0.4-0.8) *M. bovis* BCG that had been normalised to a cell density of $1x10^6$ cells per mL. This gave $1x10^5$ cells per well. The plates were sealed with parafilm and tin foil and incubated at 37 °C and 5 % CO_2 for 7 days after which a resazurin survival assay was carried out (**Method 6.6.1**).

4.2.15 Overexpression of *fbpA*

Electrocompetent *M. bovis* BCG was electroporated with *fbpA*-pMV261k and empty pMV261k as *per* **Method 6.3.6**. Colonies were inoculated into 7H9 and grown until mid-log (OD_{600} 0.4-0.8). A wide range of dilutions at 100x, the desired concentration, were made up in compound plates (Greiner, 96 well, PP, V-bottom. Ref - 651201). The compound dilutions (1 µL) were pipetted into the wells of a microplate (Greiner, 96 well,

PS, F-bottom, black, sterile. Ref - 655086). Cells were adjusted to a density of $1x10^6$ cells/mL using 7H9 media and 100 µL of cell suspension pipetted into the appropriate wells. The microplates were incubated at 37 °C and 5 % CO_2 for 7 days after which a resazurin survival assay was carried out (**Method 6.6.1**).

4.2.16 Radioactive Cell Wall Labelling

M. bovis BCG, pMV261k, and *fbpA*-pMV261k were grown in 10 mL of 7H9 media to an OD_{600} 0.4 and treated with compounds at multiple concentrations for 24 hours at 37 °C. Cultures were then radiolabelled using 5 µL of [C^{14}] acetic acid (10,545,000 cpm, Perkin Elmer) and incubated at 37 °C for a further 24 hours. The cells were then harvested by centrifugation at 4,000 rpm.

4.2.17 Polar and Non-Polar Lipid Extraction

To a tube of 10 mL of media pelleted radiolabelled culture designated tube A, 2 mL of methanol:0.3% sodium chloride (100:10, v/v) and 2 mL of petroleum ether (60-80) was added. Tube A was mixed on a rotator for 30 minutes and centrifuged at 3,000 rpm for 5 minutes. The upper phase of petroleum ether was transferred to a new tube designated tube B. A further 2 mL of petroleum ether (60-80) was added to tube A and the extraction process repeated. The upper phase again was removed and added to tube B. Tube B was dried down and contained the non-polar lipids. A mixture of chloroform:methanol:0.3% sodium chloride (2.3 mL, 90:100:30, v/v/v) was added to tube A. Tube A was mixed by rotation for 30 minutes and centrifuged at 3,500 rpm for 3 minutes. The supernatant was transferred to tube C. Chloroform:methanol:0.3% sodium chloride (750 µL, 50:100:40, v/v/v) was added to tube A. The rotation and centrifugation were repeated, and the supernatant transferred to tube C. Chloroform:methanol:0.3% sodium chloride (750 µL,

50:100:40, v/v/v) was added to tube A again and the extraction repeated. Tube A contains the non-extractable lipids. Chloroform (1.3 mL) and 1.3 mL of 0.3% aqueous sodium chloride were added to tube C. Tube C was mixed by rotation for 30 minutes and centrifuged at 3,500 rpm for 3 minutes. The lower organic phase transferred into tube D. Tube C contains waste and tube D contains polar lipids. The non-polar and polar lipids were resuspended in 200 μL of chloroform and chloroform/methanol (2:1, v/v), respectively. An aliquot (40 μL) was removed and dried down in scintillation vials, resuspended in 10 mL of scintillation fluid (Ecoscint A, National Diagnostics) and counted on a Tri-Carb 2700TR Liquid Scintillation Analyser. The rest of the samples (160 μL) was dried and resuspended in 20 μL of chloroform and chloroform/methanol (2:1, v/v), for the non-polar and polar lipids, respectively. The samples were applied to silica gel plates and 2D silica TLC performed with the solvent systems described in Table 19 and exposed to X-ray films (Kodak BioMax Light Film) in light proof cassettes. Films were exposed for 3 days and developed using Xograph film processor.

Table 19. Thin layer chromatography (TLC) solvent systems for polar and non-polar lipid analysis.

	Direction 1	**Direction 2**
System A	Petroleum Ether:Ethyl Acetate x 3 98:2	Petroleum Ether:Ethyl Acetate 98:2
System B	Petroleum Ether:Acetone x 3 92:8	Toluene:Acetone 95:5
System C	Chloroform:Methanol 96:4	Toluene:Acetone 80:20
System D	Chloroform:Methanol:Water 100:14:0.8	Chloroform:Methanol:Acetone:Water 50:60:2.5:3
System E	Chloroform:Methanol:Water 60:30:6	Chloroform:Acetic Acid:Methanol:Water 40:25:3:6

4.2.18 Fatty Acid Methyl Ester (FAMEs) and Mycolic Acid Methyl Ester (MAMEs) Extraction

A 10 mL radiolabelled culture was spun down and the pellet dried. Aqueous solution of 5 % tetrabutyl ammonium hydroxide (4 mL) was added and the tube was heated to 90 °C overnight. The reaction mixture was diluted using 2 mL of dH_2O, 4 mL of dichloromethane and 300 µL iodomethane added to the tube. The tube was vortexed, mixed by rotation for 30 minutes and centrifuged for 5 minutes at 3,500 rpm. The top layer was discarded, and the lower organic layer was washed twice with 3 mL of dH_2O by repeating the rotation and centrifugation steps. The washed lower organic layer was dried and further extracted using 4 mL of diethyl ether, and the tube vortexed, mixed by rotation for 30 minutes and centrifuged for 5 minutes at 3,500 rpm. The supernatant was transferred to a fresh tube to give fatty acid methyl esters (FAMEs) and mycolic acid methyl esters (MAMEs). The lipids were resuspended in 200 µL of chloroform. An aliquot (40 µL) was removed and dried down in scintillation vials, resuspended in 10 mL of scintillation fluid (Ecoscint A, National Diagnostics) and counted on a Tri-Carb 2700TR Liquid Scintillation Analyser. The rest of the sample (160 µL) was dried and resuspended in 20 µL of chloroform. The samples were applied to silica gel plates and silica TLC performed in one direction with petroleum-ether/acetone (95:5, v/v) and exposed to X-ray films (Kodak BioMax Light Film) in light proof cassettes. Films were exposed for 3 days and developed using Xograph film processor.

4.2.19 Solid Minimum Inhibitory Concentration (MIC) of Antigen 85 Compound C4

Dilutions of compound C4 were made at 100x the desired concentration in DMSO. Compound C4 (10 μL) was pipetted into a 1.5 mL microcentrifuge tube and. 1 mL of 7H11 agar was mixed and pipetted into a 48 well microplate (Corning Costar, 48 Well Cell Culture Cluster, 3548). The agar was allowed to set. A mid-log (OD_{600} 0.4-0.8) *M. tuberculosis* H37Rv culture was adjusted to $2x10^4$ cells/μL and 5 μL were spotted into the centre of each well. The plate was incubated at 37 °C with 5 % CO_2 for 3 weeks until the control spots had grown sufficiently. The MIC was determined as the well with the lowest concentration of C4 on which there was no growth.

4.2.20 Compound C4 Drug Resistant Mutant Generation

Large 20 mL 7H11 agar plates for the growth of the *M. tuberculosis* H37Rv *ΔleuDΔpanCD* strain were set up containing compound C4 at the desired concentration with a maximum DMSO concentration of 1 %. Concentrations were 0x, 2.5x, 5x, and 10x the minimum inhibitory concentration (MIC). Plates were sent to Newcastle University where Dr Alistair Brown inoculated the plates. Mid-log (OD_{600} 0.4-0.8) *M. tuberculosis* H37Rv *ΔleuDΔpanCD* strain cultures were adjusted to $1x10^9$ cells/mL and 100 μL of cells were spread out on the agar plate for $1x10^8$ cells on each plate. The agar plates were incubated at 37 °C with 5 % CO_2 until colonies appeared (approximately 1-2 months). Mutant colonies that appeared on the 2.5x MIC plate were retested on new agar plates containing 5x MIC C4.

4.3 Results

4.3.1 Antigen 85A and C2 Protein Purification

Overexpression screens of *fbpA* conducted by Dr Jonathan A.G. Cox at GSK revealed several potential hits of Antigen 85. In order to assess these hits, it was necessary to purify proteins from the Antigen 85 family for enzymatic assays. Of the three proteins in the family it was decided to purify Antigen 85A as that was the protein originally overexpressed and Antigen 85C2 as previous studies have shown this enzyme to be easily assayed[404]. Antigen 85A and C2 were purified from *E. coli* pellets overexpressing *fbpA* and *fbpC2* produced by Dr Katherine Abrahams (University of Birmingham). Both proteins were purified using the same method. The data in Figures 57 and 58 show the protein gels run after HisTrap HP purification and HiTrap Q HP anion exchange for Antigen 85A and C2, respectively. Antigen 85A has a molecular weight of 35.686 kDa and Antigen 85C2 has a molecular weight of 36.771 kDa. All the fractions displayed in the HiTrap Q HP anion exchange of Figure 57 were pooled to give purified Antigen 85A. In Figure 58, from the HiTrap Q HP anion exchange, fractions 2, 3, and 4 (not including the protein ladder) were pooled for purified Antigen 85C2.

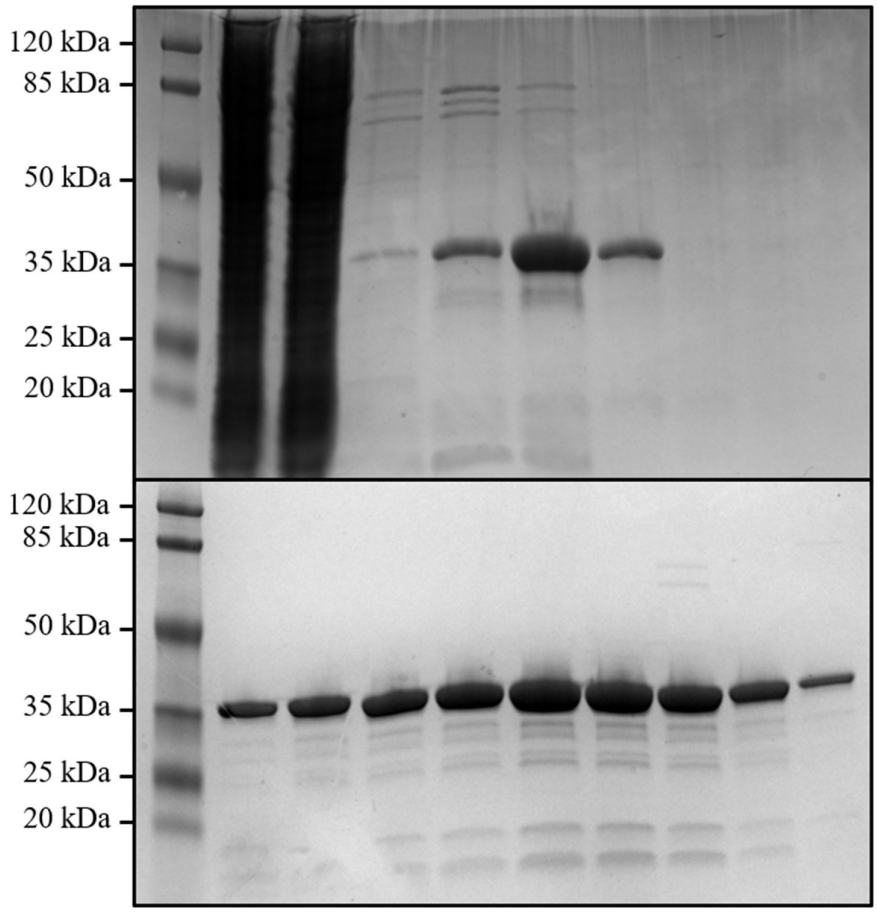


Figure 57. Protein gels of Antigen 85A purification. Molecular weight – 35.686 kDa. **Top** HisTrap HP purification. **Bottom** HiTrap Q HP anion exchange. All the fractions were used as purified Antigen 85A.

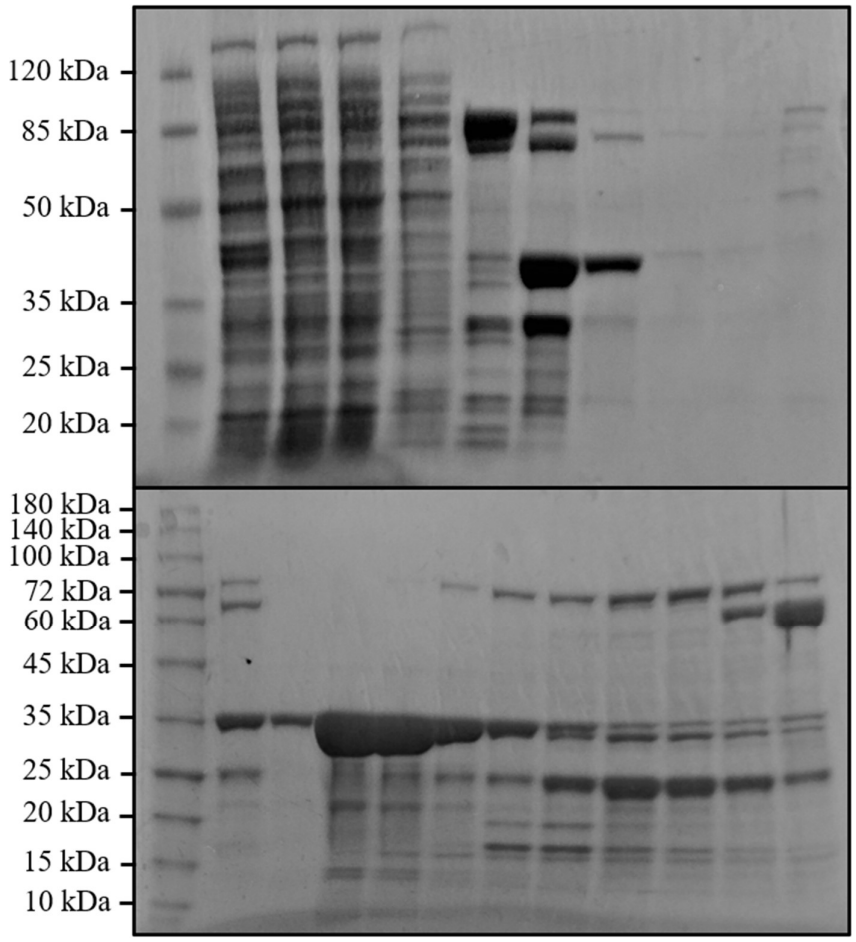


Figure 58. Protein gels of Antigen 85C2 purification. Molecular weight – 36.771 kDa. **Top** HisTrap HP purification. **Bottom** HiTrap Q HP anion exchange. Fractions 2, 3, and 4 (Not including the protein ladder) were pooled as purified Antigen 85 C2.

4.3.2 Radiometric Enzyme Activity Assessment

After purification, the activity of Antigen 85A and C2 were assessed using a radiometric assay. The assay measured the amount of [C^{14}] trehalose incorporated into the production of TMM and TDM. Both enzymes displayed measurable enzymatic activity. The data in Figure 59 shows the thin layer chromatography (TLC) of the assay reaction mixture and the scintillation counts per minute for the remaining sample. One of the preparations of Antigen 85A was purified with additional DTT to compare activity levels, which ended

up performing similar to purification without DTT. Antigen 85C2 displayed roughly 4 times the level of activity of Antigen 85A. Both enzymes produced more trehalose mono-mycolate than trehalose di-mycolate with a similar proportion of each between each enzyme.

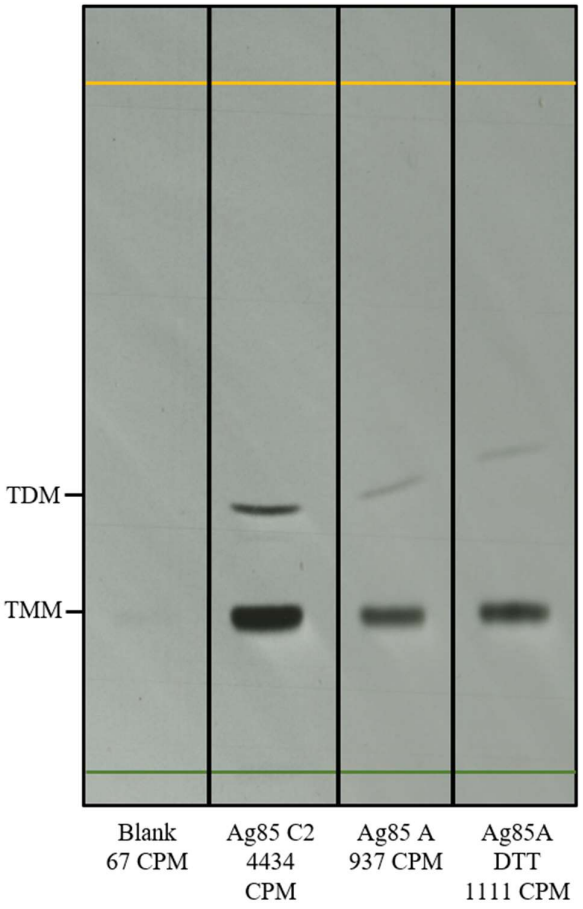


Figure 59. Thin layer chromatography (TLC) and scintillation counts of purified antigen 85 activity. The upper band is trehalose di-mycolate (TDM) and the lower band is trehalose mono-mycolate (TMM). Yellow line is the solvent front, green line is the origin.

4.3.3 Optimisation of β-Glucosiadse Antigen 85 Assay

An assay using 4-nitrophenyl-6-octanoly-β-D-glucopyranoside and β-glucosidase to assay the activity of Antigen 85 was attempted based upon a previously published

assay[429]. The assay used two enzymes to measure the activity of Antigen 85. The first step is the removal of the octanoyl chain from position 6 of the glucose of 4-nitrophenyl-6-octanoly-β-D-glucopyranoside by Antigen 85. The second step is the separation of the 4-nitrophenyl from the glucose. The amount of separated 4-nitrophenyl can be determined by measuring absorbance at 420 nm. The absorbance should be proportional to the amount of octanoyl chain removed by Antigen 85, unless β-glucosidase can also release 4-nitrophenyl from the 4-nitrophenyl-6-octanoly-β-D-glucopyranoside. A standard curve of 4-nitrophenyl was conducted measuring the absorbance at 420 nm of various concentrations of 4-nitrophenyl (Figure 60). The activity of β-glucosidase on 4-nitrophenyl-6-octanoly-β-D-glucopyranoside was tested by comparing the absorbance of reactions with and without Antigen 85C2. The data in Figure 61 shows that the absorbance of the reaction increases faster without Antigen 85C2 indicating that the β-glucosidase can release 4-nitrophenyl from 4-nitrophenyl-6-octanoly-β-D-glucopyranoside. Due to the ability of β-glucosidase to turn over the 4-nitrophenyl-6-octanoly-β-D-glucopyranoside this assay was discontinued.

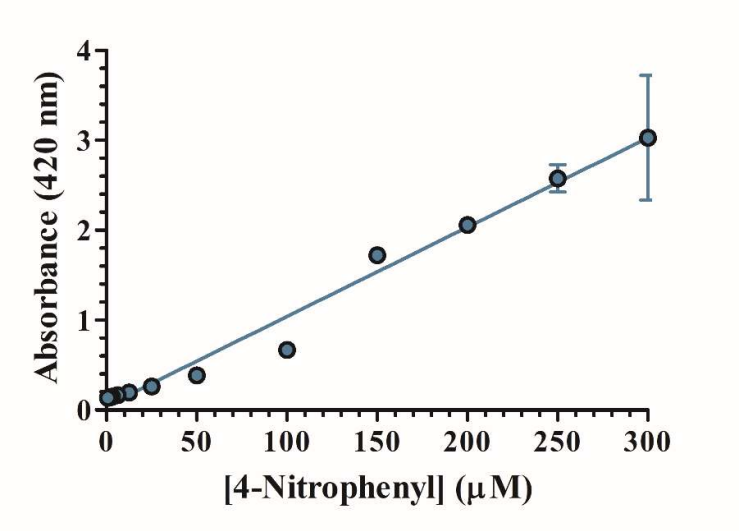


Figure 60. Standard curve of 4-nitrophenyl. Data shown as the mean and standard deviation of quadruple replicate.

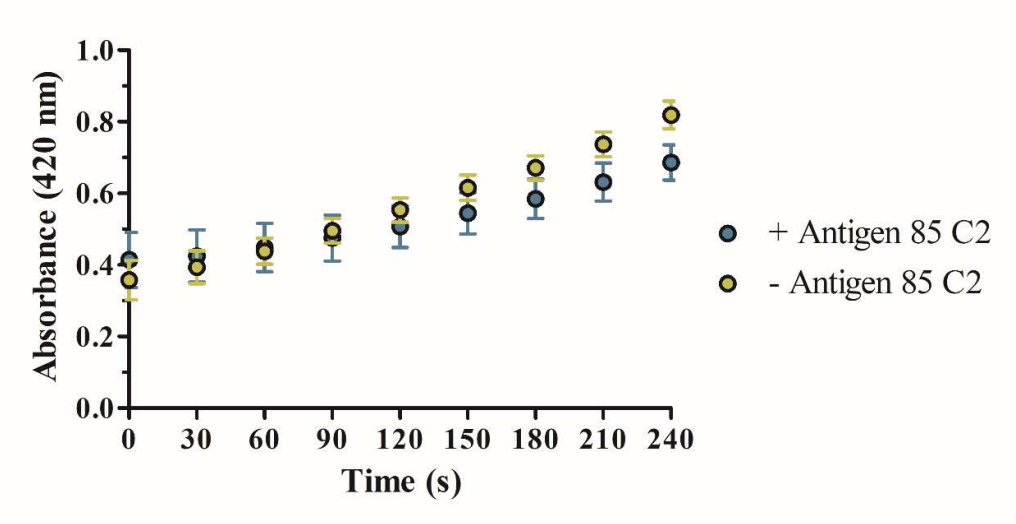


Figure 61. Rate of reaction comparison with and without Antigen 85C2. A comparison of the turnover of 4-nitrophenyl-6-octanoly-β-D-glucopyranoside by β-glucosidase alone and when accompanied by Antigen 85C2. β-glucosidase is able to release 4-nitrophenyl regardless of the state of lipidation of the substrate. Mean and standard deviation of quadruple replicate.

4.3.4 Resorufin Butyrate Assay Optimisation

The experiments described below were based upon a published Antigen 85 assay[424] using resorufin butyrate as a substrate for Antigen 85, to assesses the ability of antigen 85 to produce trehalose mono-mycolate (TMM) and trehalose di-mycolate (TDM) in real time. The butyrate is removed from the resorufin and donated to a trehalose acceptor. This releases free resorufin, which the accumulation of can be monitored *via* fluorescence over time. A standard curve for resorufin was created and used to calculate the fluorescence values for nanomoles of resorufin (Figure 62). The rate of reaction with varying concentrations of resorufin butyrate substrate and trehalose acceptor were measured (Figure 63). This was converted to Michaelis-Menten plots by plotting the mean and standard deviation of the slope for each concentration (Figure 64). The K_m of the substrates were worked out to determine the optimum concentration for the reaction. The

K_m of resorufin butyrate was determined to be approximately 25 μM and the K_m of trehalose was approximately 1 mM. All the optimisation work for the assay was done using Antigen 85C2, this was because this enzyme was shown to be more active in the radioactive assessment and the quantity purified was much greater than that of Antigen 85A.

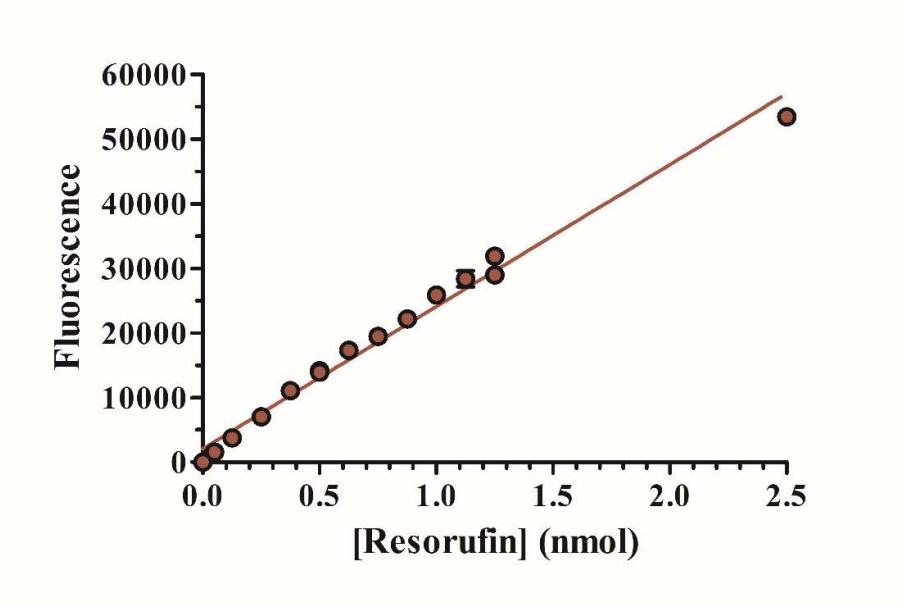


Figure 62. Resorufin standard curve. Data shown as the mean and standard deviation of triple replicate.

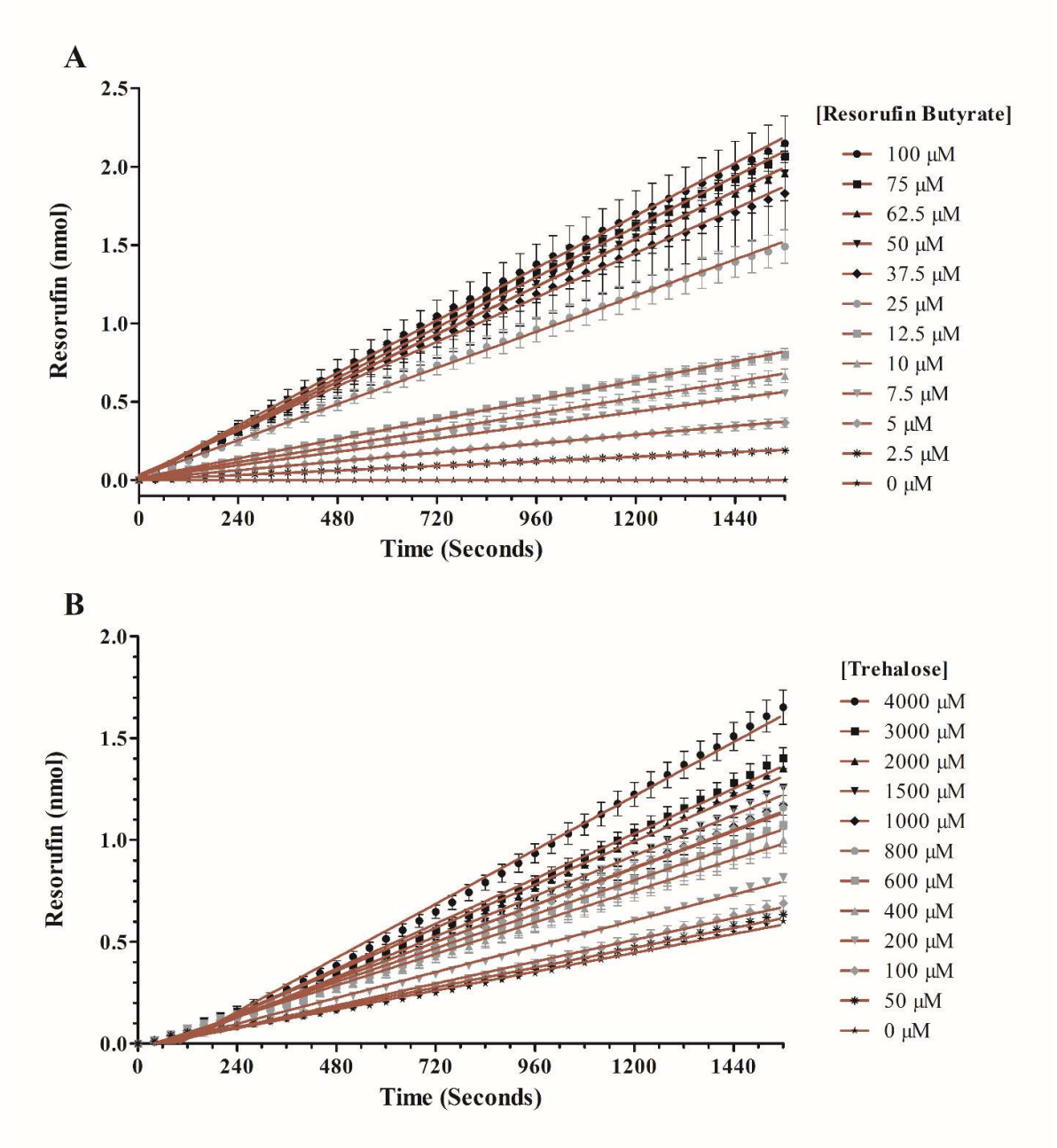


Figure 63. Rates of reaction with different substrate concentrations. A Resorufin butyrate. **B** Trehalose. Data shown as the mean and standard deviation of triple replicate.

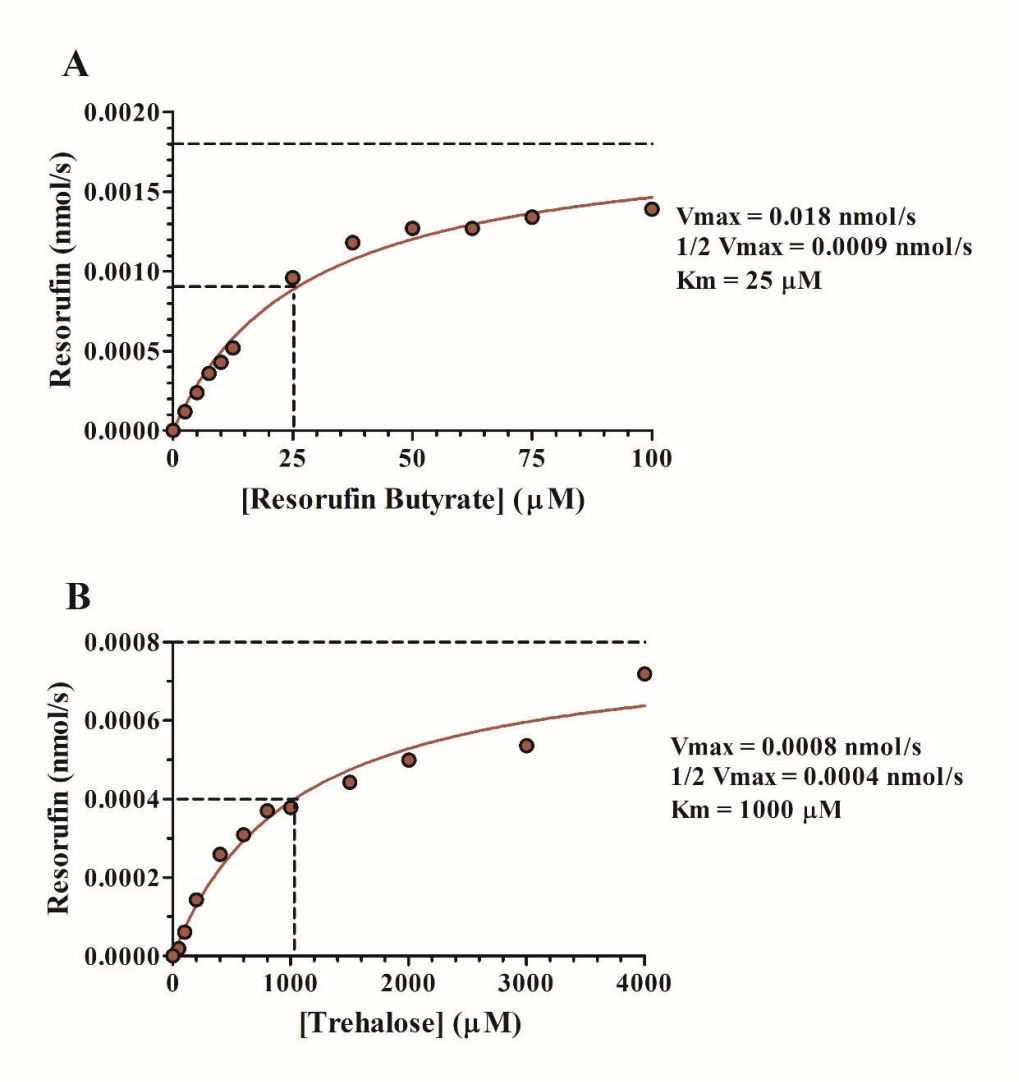


Figure 64. Michaelis-Menten curves for resorufin butyrate and trehalose. A Resorufin butyrate. **B** Trehalose. Vmax was determined as a value in excess of the maximum velocity of reaction on the curves. The K_m was determined as the concentration of substrate that resulted in a reaction velocity of half Vmax. Data plotted from the slope mean and standard deviation of the rates of reaction at the labelled substrate concentration.

4.3.5 Resorufin Butyrate Assay for Antigen 85 Hits

The full assay testing inhibitors was conducted after incubating Antigen 85C2 and Antigen 85 A with hits overnight. The amount of resorufin butyrate and trehalose used was 4 times the K_m of each to ensure that the rate of reaction was determined by the

activity of Antigen 85. The controls used were ebselen and iodoacetamide. Both are known inhibitors of Antigen 85C2 and bind covalently with the active site and prevent production of TMM and TDM. The cessation of TMM and TDM production in this assay prevents the release of free resorufin to fluoresce. Fluorescence values were converted to nanomoles. A blank was subtracted from each time point to account for the background rate of reaction. Antigen 85C2 was inhibited by ebselen and iodoacetamide strongly but there was no inhibition from the test hits. Antigen 85A was partially inhibited by iodoacetamide but not ebselen or the test hits. The error bars for Antigen 85A were large and the enzyme shows much lower activity than Antigen 85C2. Neither assay shows any indication that the test compounds inhibit Antigen 85C2 or Antigen 85A.

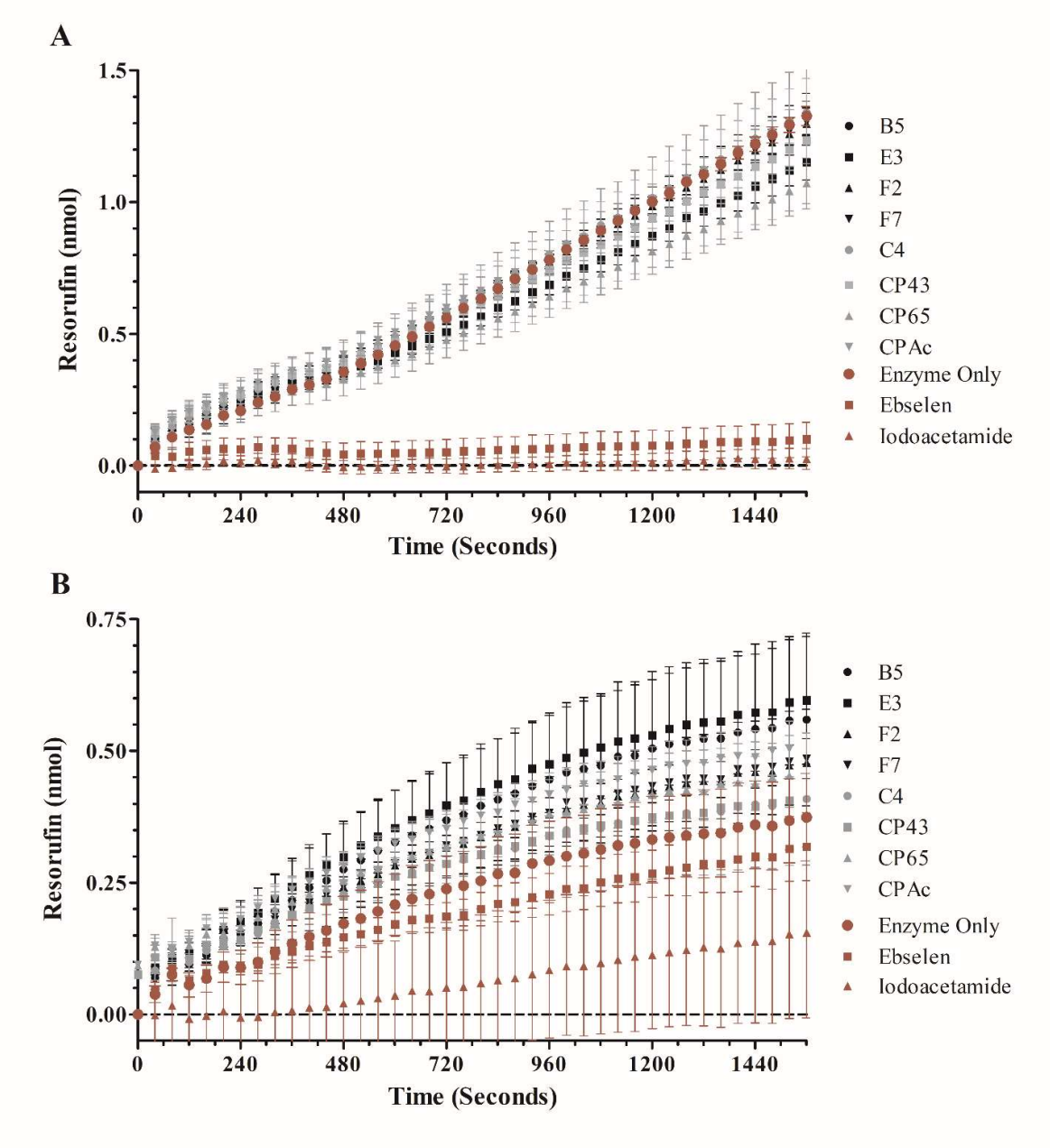


Figure 65. Resorufin butyrate assay with hits. A Antigen 85C2. **B** Antigen 85A. CPAc was included amongst the inhibitors as a blind positive control. Data shown as the mean and standard deviation of triple replicate.

4.3.6 Radiometric Assay for Antigen 85 A Inhibitors

A radiometric assay was conducted for Antigen 85A hits due to the variability seen when using the resorufin butyrate assay. This assay was the same format as the activity

assessment (**Section 4.3.2**) with the addition of incubating Antigen 85A with the test hits overnight prior. The data in Figure 66 shows the thin layer chromatography (TLC) of 60 % of the reaction mixture with the remaining counts per minute shown below. None of the test hits including ebselen and iodoacetamide showed any differences from the enzyme control samples. Additionally, all the counts of the reaction mixtures of the test hits showed greater counts than the enzyme only samples.

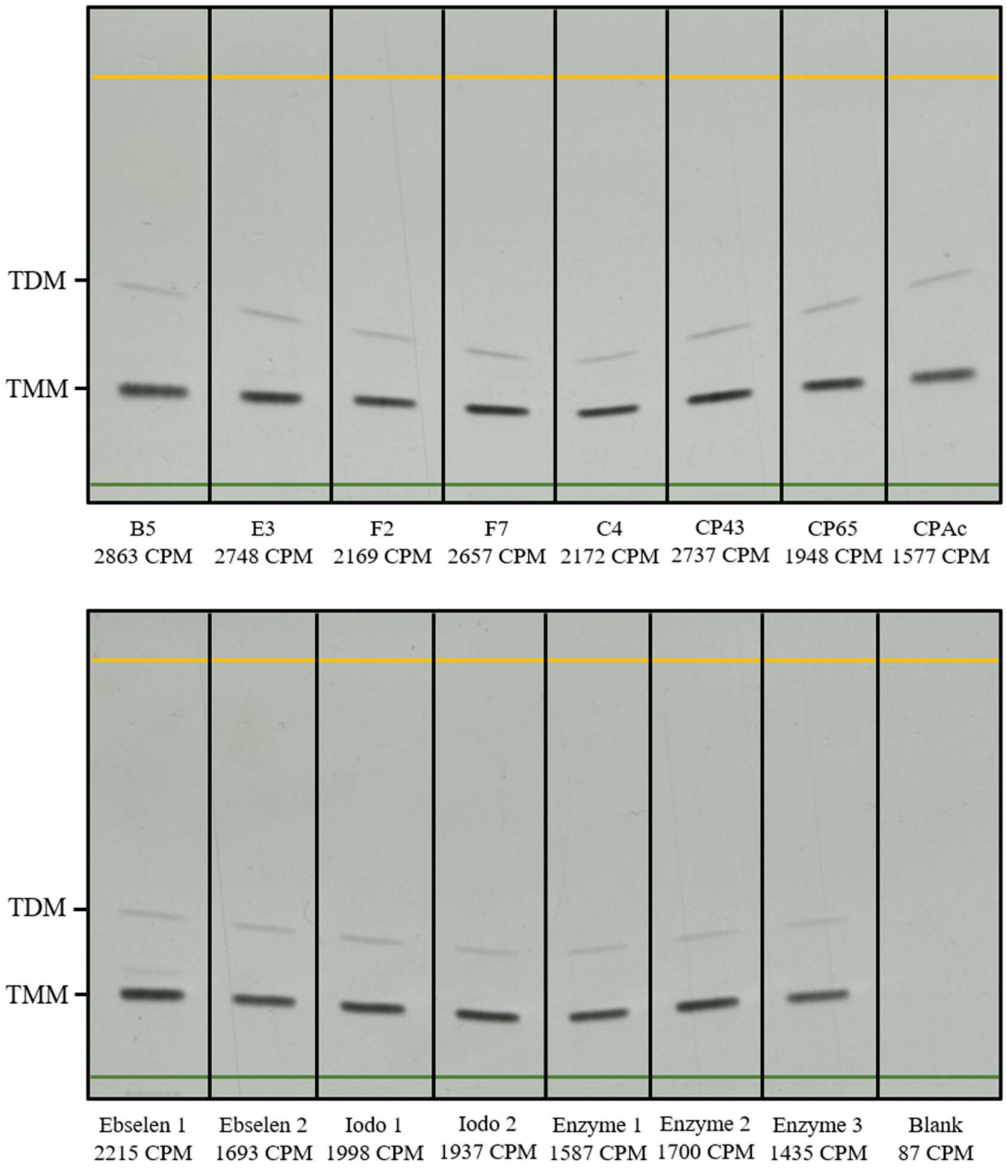


Figure 66. Thin layer chromatography (TLC) and scintillation counts of antigen 85A activity with hits. The upper band is trehalose di-mycolate (TDM) and the lower band is trehalose mono-mycolate (TMM). The yellow line is the solvent front, green line is the origin. CPAc was included amongst the inhibitors as a blind positive control.

4.3.7 Trehalose-C-12-Nitro-Benzoxadiazol Assay for Antigen 85A Hits

The ability of these hits to interfere with Antigen 85A and impact the mycolation of the cell wall was assessed. The C-12-NBD assay focuses on the ability of Antigen 85 to donate lipids to a different acceptor from trehalose, the terminal ends of arabinogalactan.

The C-12-NBD is removed from the trehalose donor and attached to arabinogalactan. The unbound trehalose-C-12-NBD is then removed through washes. The C-12-NBD attached to the arabinogalactan can be measured *via* fluorescence. The data from Figure 67 shows that none of the hits reduced the activity of Antigen 85A. The compound CPAc is used as a positive control sample. While there seems to be a decrease in some samples compared to the primary positive controls, they do not fall lower than the CPAc positive control and do not resemble the blank sample. The variability of this method is in part due to the insolubility of the arabinogalactan acceptor.

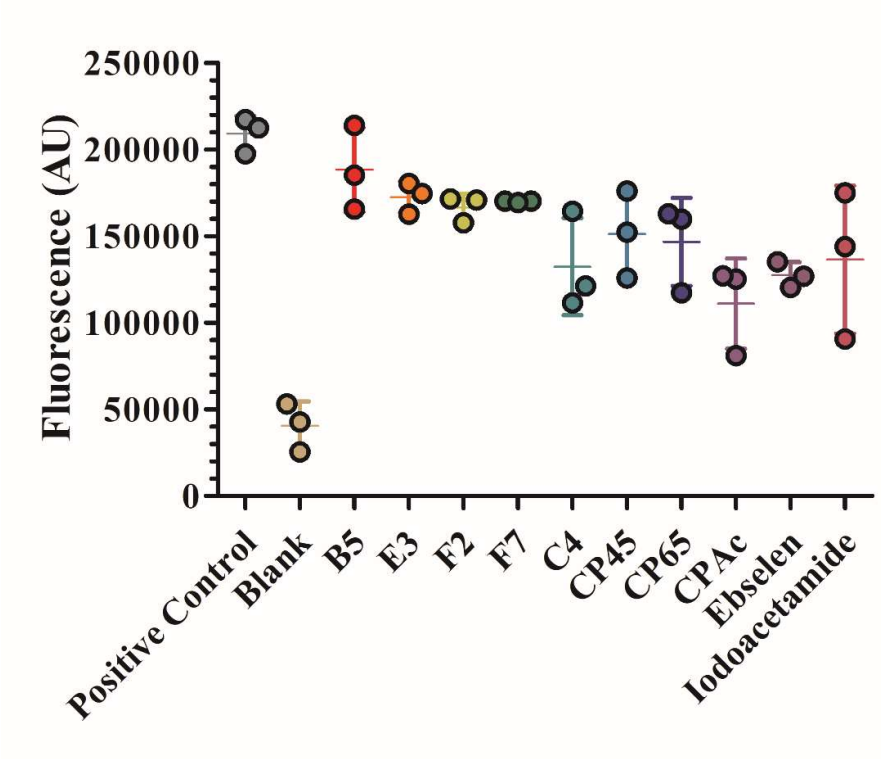


Figure 67. Trehalose-C-12-nitrobenzoxadiazol (NBD) assay results. CPAc was included amongst the hits as a blind positive control. Data shown as the mean and standard deviation of triple replicate.

4.3.8 *FbpA* Overexpression

The overexpression of *fbpA* was repeated due to the inability of the prior assays to detect any inhibition of Antigen 85A or C2. Due to limited supply, hit F7 could no longer be tested. GSK supplied a fresh supply of compound E1 for use. Two different colonies of *M. bovis* BCG overexpressing *fbpA* were compared to a *M. bovis* BCG containing an empty plasmid control to observe an increase in the MIC of the test inhibitors. The data from Figure 68 shows the results for all the hits tested. Compound B5 did not display a reasonable MIC with the control remaining unaffected. The overexpressors with compounds E3, F2, C4, and E1 all displayed an increased ability to survive against the hits.

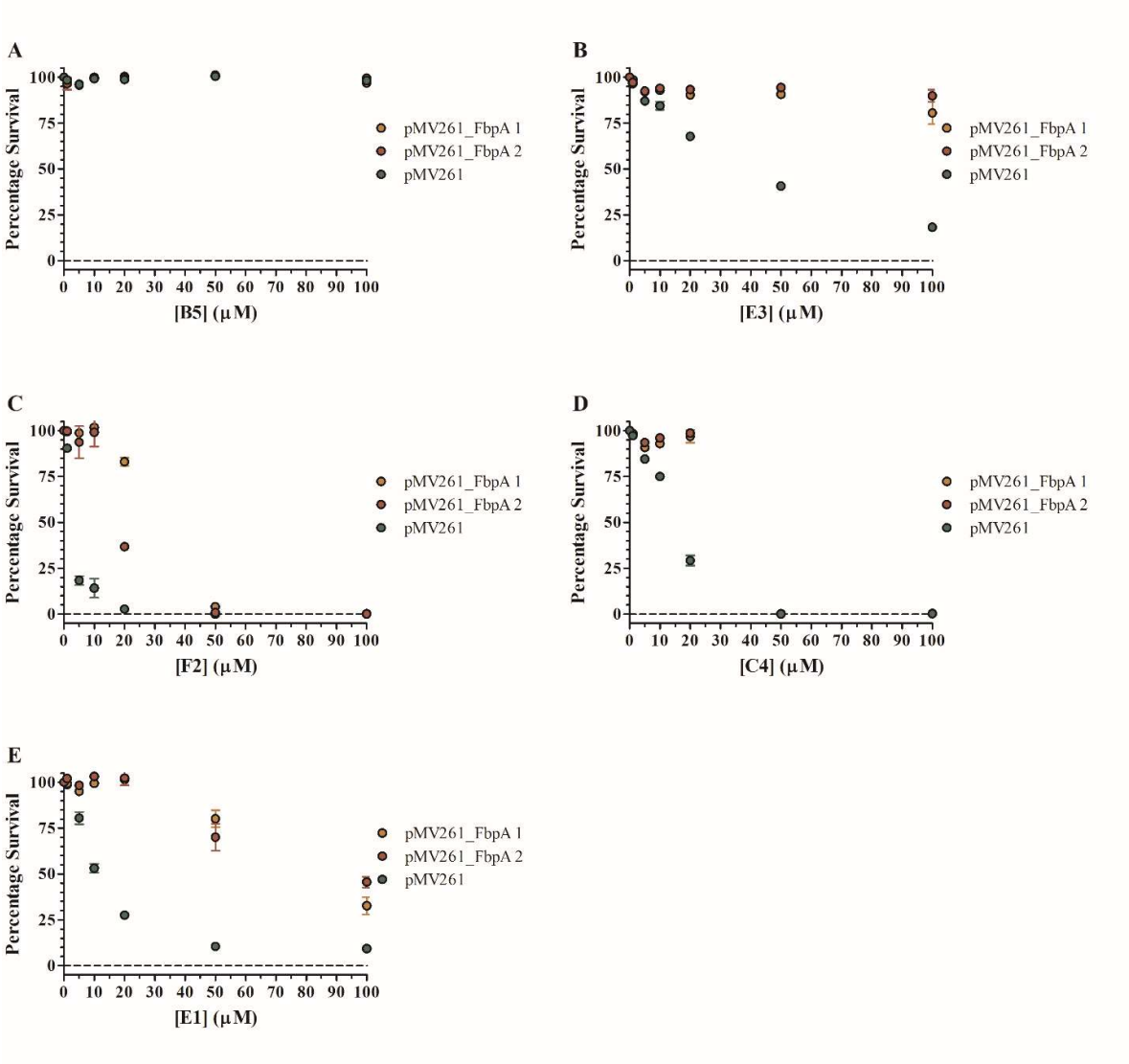


Figure 68. Antigen 85A (*FbpA*) overexpression in *M. bovis* BCG. Comparison of WT *M. bovis* BCG with *M.* bovis BCG overexpressing *fbpA* to observe changes in MIC. Data shown as the mean and standard deviation of triple replicate.

4.3.9 Liquid Minimum Inhibitory Concentrations (MICs) for *M. bovis* BCG

The liquid MICs for ebselen, isoniazid, C4, E1, and F2 were assessed and the results are displayed in Figure 51. The MIC_{99} of ebselen (Figure 69 A) was 35 µM. The MIC_{95} of isoniazid (Figure 69 B) was 0.5 µM. The MIC_{99} of compound C4 (Figure 69 C) was approximately 50 µM. The MIC of compound E1 (Figure 69 D) was found to be in excess

of 150 µM with only 85 % cell death at 150 µM, but for practicality the MIC_{85} was taken at 150 µM. The MIC_{98} of compound F2 (Figure 69 E) was approximately 55 µM.

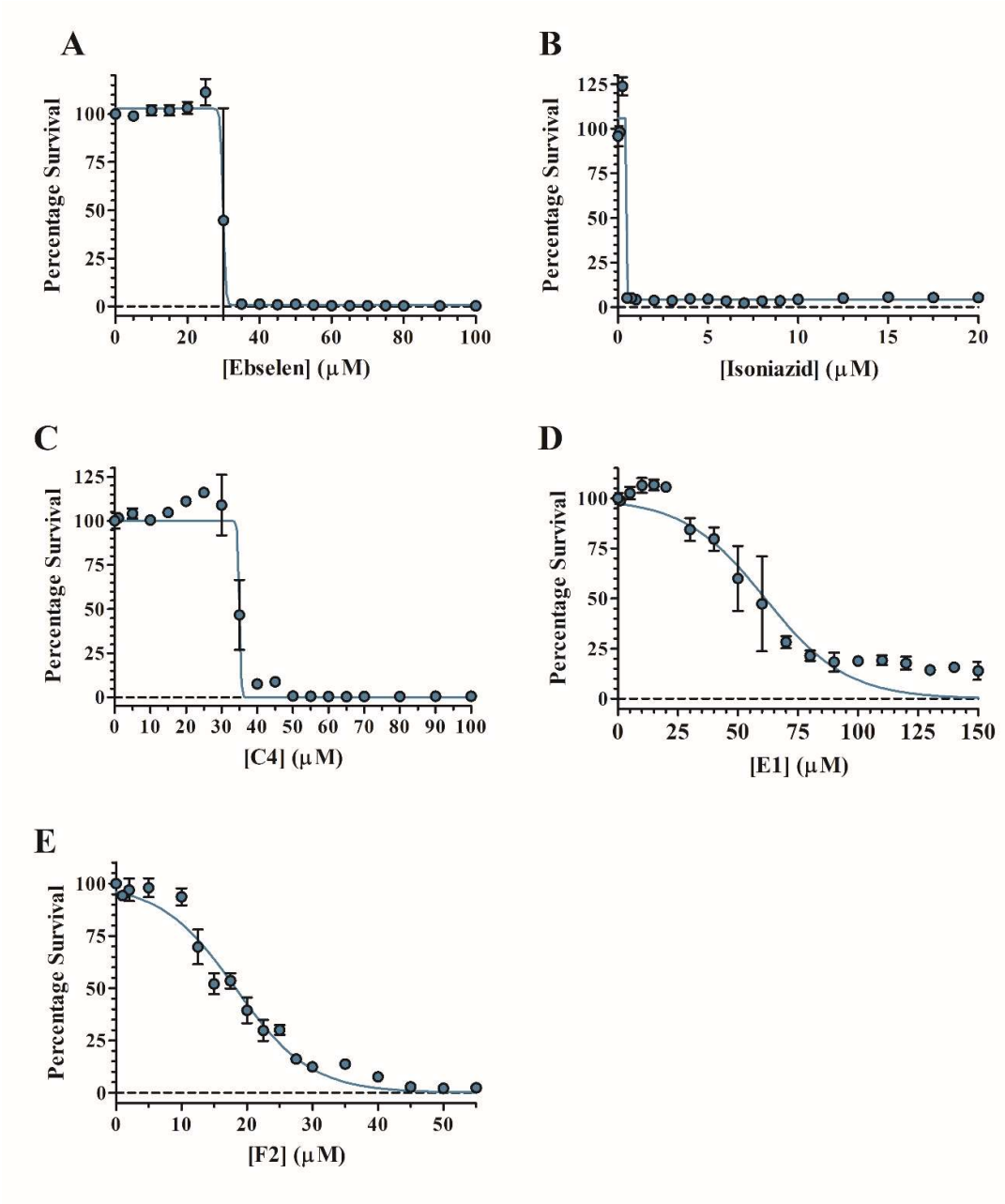


Figure 69. Minimum inhibitors concentrations (MICs) for Antigen 85 test hits. Data shown as the mean and standard deviation of triple replicate.

4.3.10 Polar and Non-Polar Lipid Profiling of *M. bovis* BCG Treated with Hits

The lipid profiles of *M. bovis* BCG were assessed using thin layer chromatography (TLC) after treatment with ebselen, isoniazid, and hits C4, E1, and F2 at multiple concentrations followed by labelling using [C^{14}] acetic acid. The extracted lipids were resolved by two-dimensional-TLCs as set out in Mycobacteria Protocols 1st and 2nd Edition. The data from Figure 70 shows the system A 2D-TLCs of the non-polar lipids. Spots A, B, and C show variant members of the phthiocerol dimycocerosate (PDIM) family and the spot labelled TAG as triacylglycerols. Both are present in the untreated as well as all the treated cells with no observable change. The data shown in Figure 71 shows system B 2D-TLCs of the non-polar lipids. Spots A and B show non-polar mycolipenates of trehalose and the spot labelled FFA is free fatty acids. For ebselen and F2 there are no observable changes on these 2D-TLCs. Isoniazid, C4, and E1 show a gradual accumulation of free fatty acids with the effect being more pronounced for isoniazid. Additionally, in isoniazid and E1 there is a slight increase in mycolipenates of trehalose. The data shown in Figure 72 shows system C 2D-TLCs of the non-polar lipids. Free fatty acids are present on this 2D-TLC as well as phenolic glycolipid (PGL). For ebselen and F2 there are no observable changes on these 2D-TLCs. Isoniazid, C4, and E1 show an increase in free fatty acids consistent with system B. In addition, isoniazid shows an increase in PGLs and C4 shows a slight decrease. The data shown in Figure 73 shows system D 2D-TLCs of the non-polar lipids. The trehalose mono-mycolate, trehalose di-mycolate and glucose mono-mycolate (GMM) of ebselen, E1, and F2 treated cells stays consistent with wild type cells. When treated with isoniazid and C4 both TMM, TDM and GMM show a decrease. The data shown in Figure 74 shows system D 2D-TLCs of the polar lipids. The TMM, TDM and GMM shows the same pattern as with the system D of the non-polar lipids for isoniazid and C4. The data shown in Figure 75 shows system E 2D-TLCs of the polar lipids. The

spots labelled Ac_1/Ac_2PIM_2 and Ac_1/Ac_2PIM_5 are variants of phosphatidylinositol mannosides (PIMs). The spot labelled PI is phosphatidylinositol. PE is phosphatidylethanolamine and DPG is diphosphatidylglycerol. The spot labelled G are glycolipids. All the TLCs remain consistent between hit treatments when compared to the untreated control.

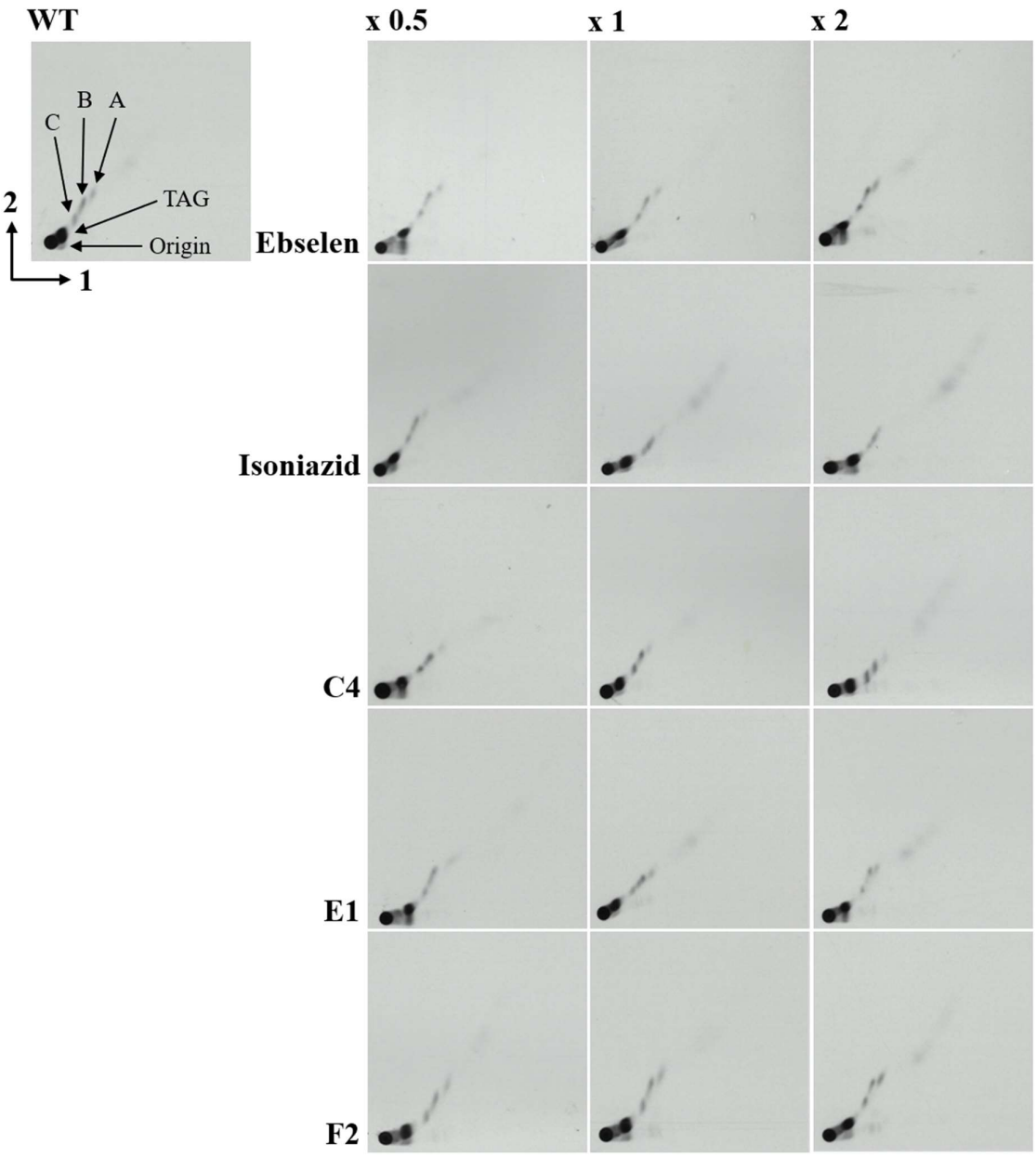


Figure 70. Thin layer chromatography (TLC) of non-polar lipids run and system A. Directions 1 and 2 shown with arrows. Test inhibitors included at concentrations relating to the liquid MICs. A-C - phthiocerol dimycocerosate (PDIM) family. TAG - triacylglycerols.

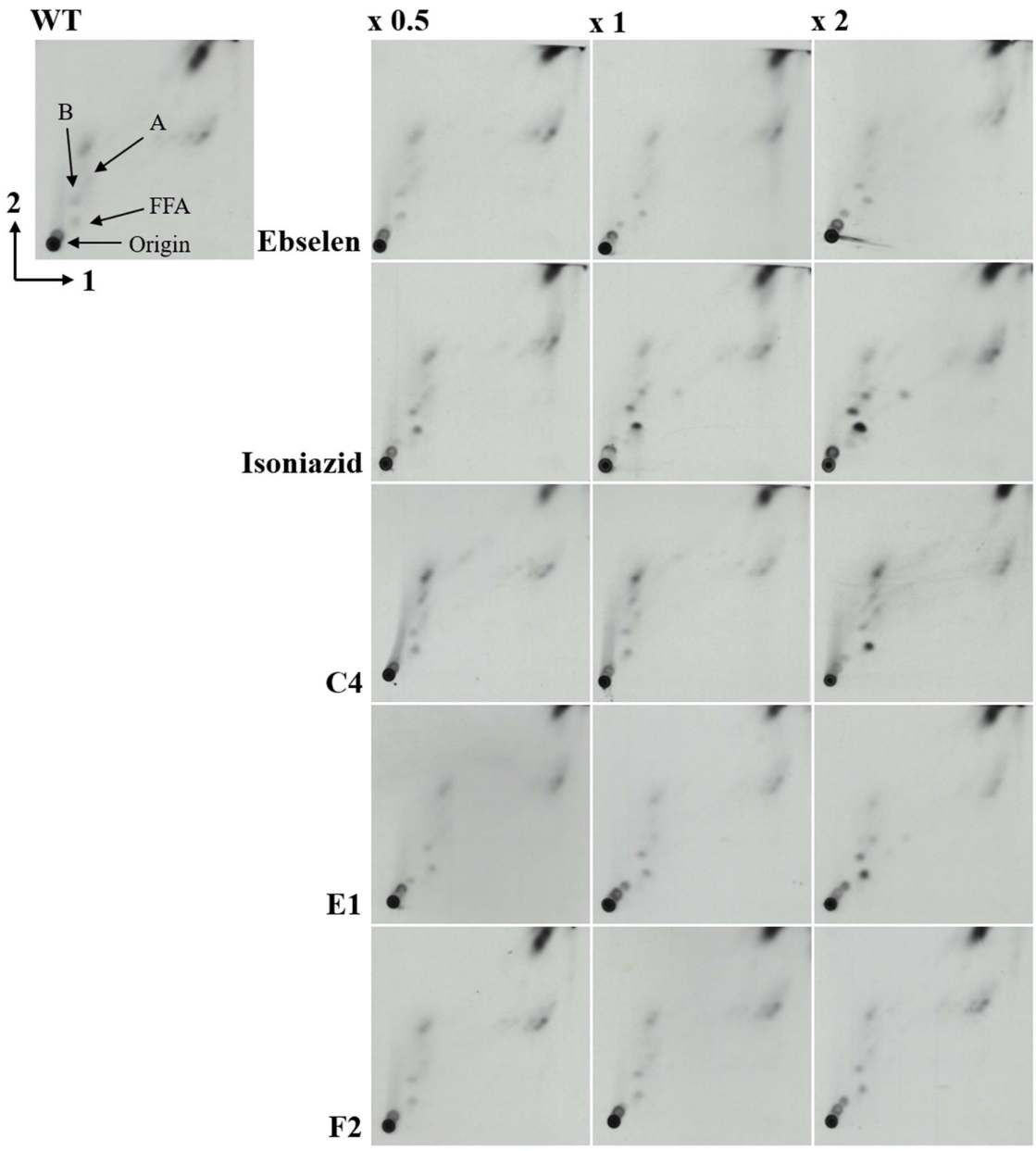


Figure 71. Thin layer chromatography (TLC) of non-polar lipids run and system B. Directions 1 and 2 shown with arrows. Test inhibitors included at concentrations relating to the liquid MICs. A, B - non-polar mycolipenates of trehalose. FFA - free fatty acids.

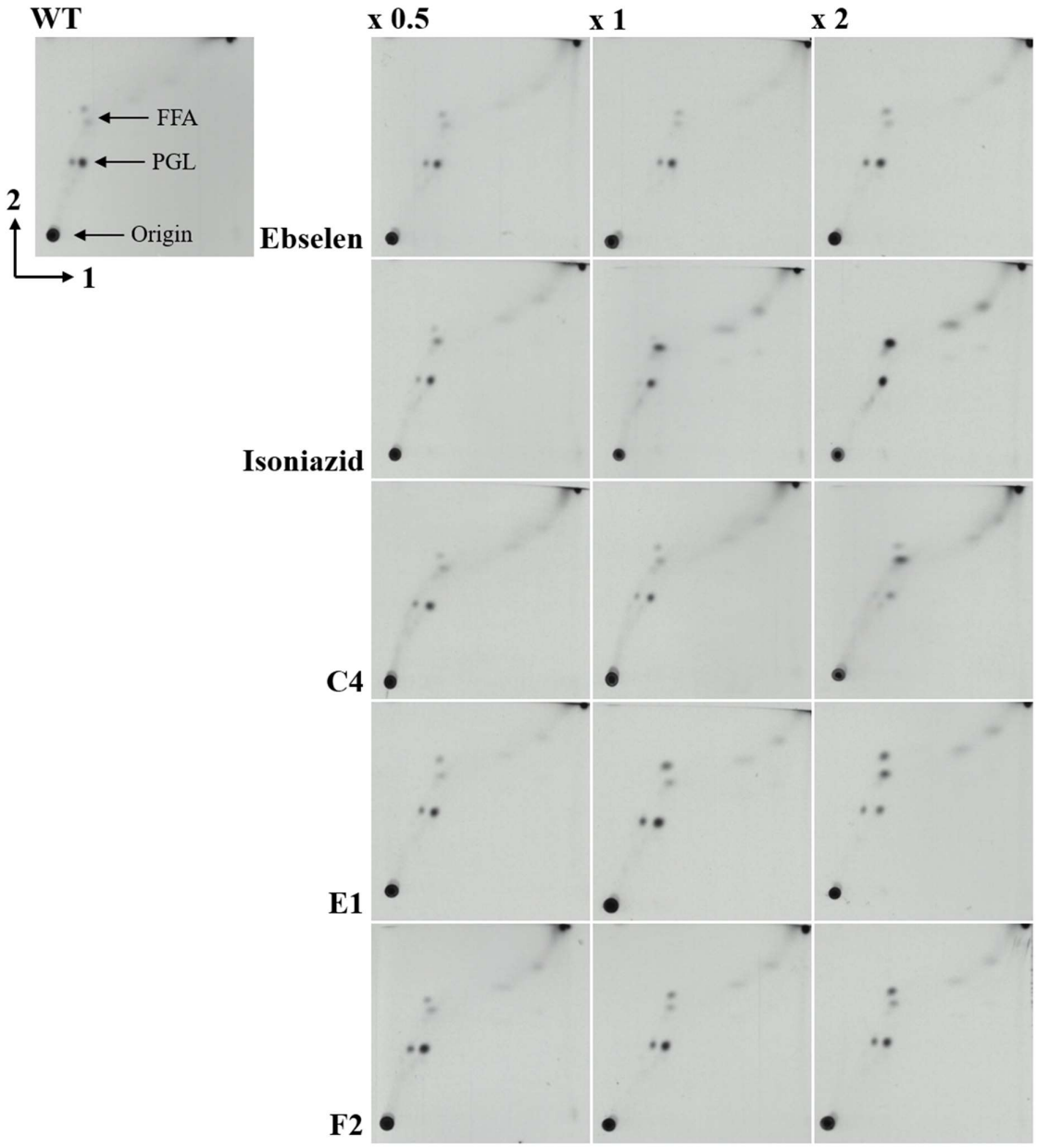


Figure 72. Thin layer chromatography (TLC) of non-polar lipids run and system C. Directions 1 and 2 shown with arrows. Test hits included at concentrations relating to the liquid MICs. FFA - free fatty acids. PGL - phenolic glycolipids.

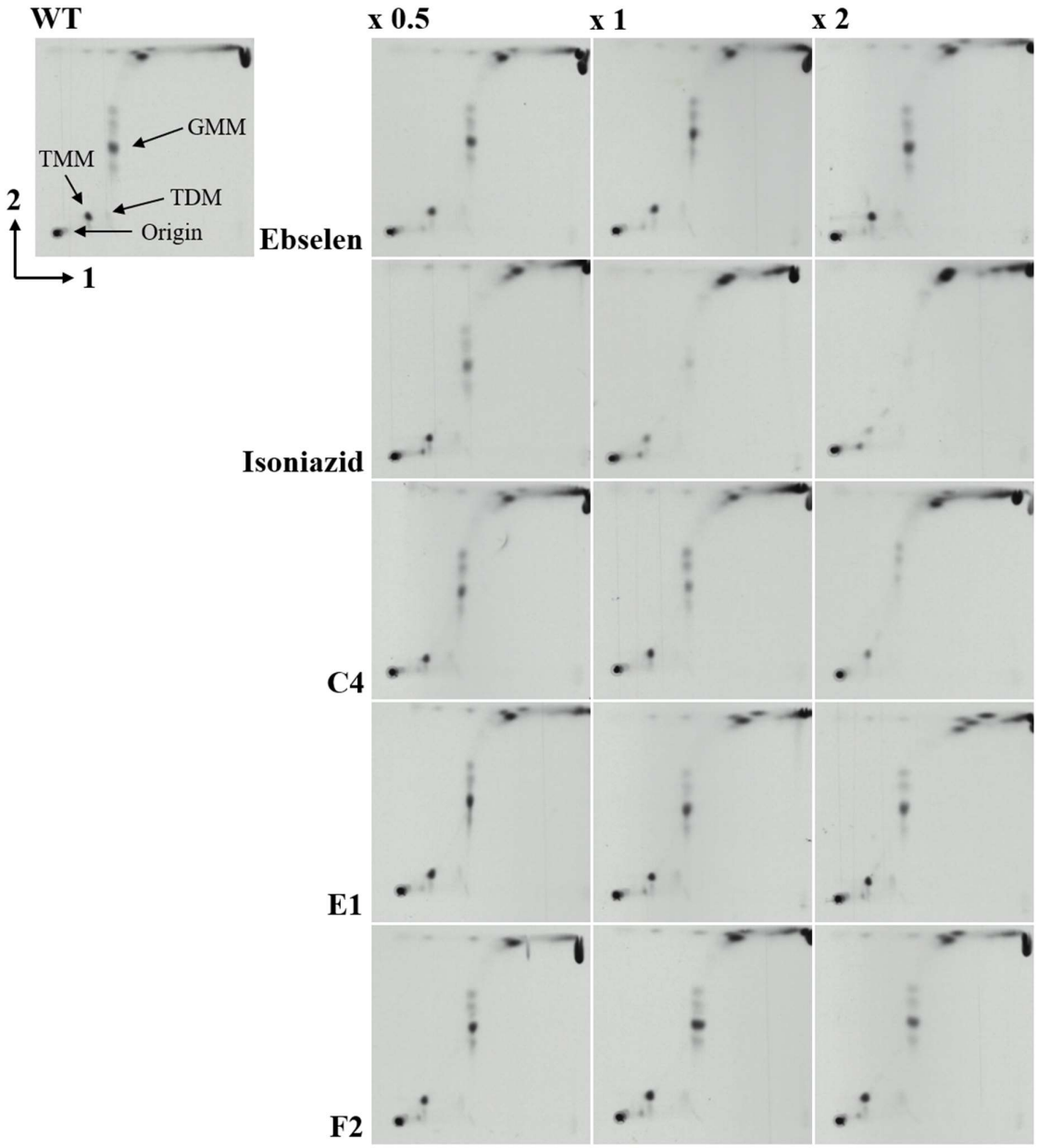


Figure 73. Thin layer chromatography (TLC) of non-polar lipids run and system D. Directions 1 and 2 shown with arrows. Test hits included at concentrations relating to the liquid MICs. TMM - trehalose mono-mycolate, TDM - trehalose di-mycolate and GMM - glucose mono-mycolate.

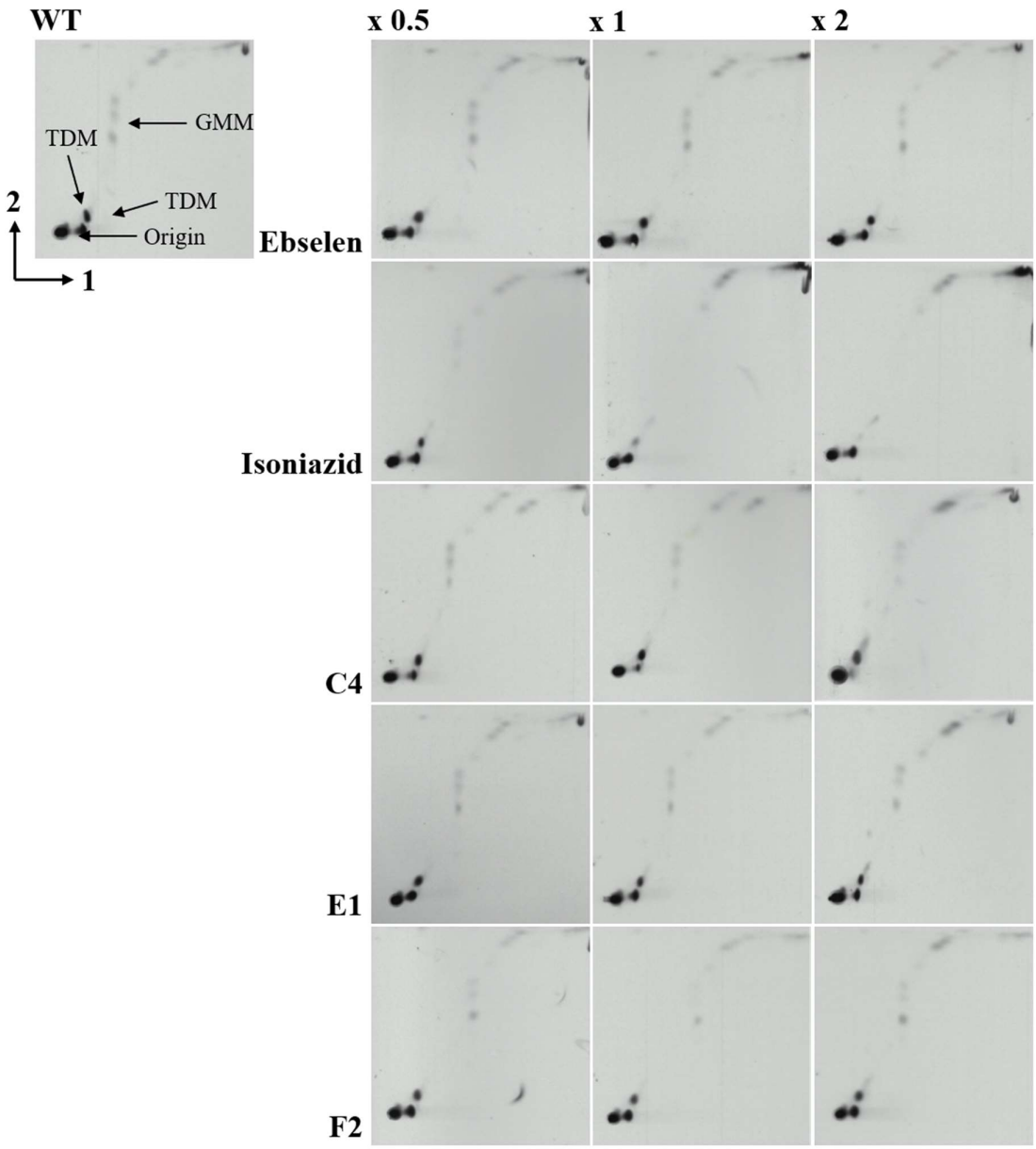


Figure 74. Thin layer chromatography (TLC) of polar lipids run and system D. Directions 1 and 2 shown with arrows. Test inhibitors included at concentrations relating to the liquid MICs. TMM - trehalose mono-mycolate, TDM - trehalose di-mycolate, GMM - glucose mono-mycolate.

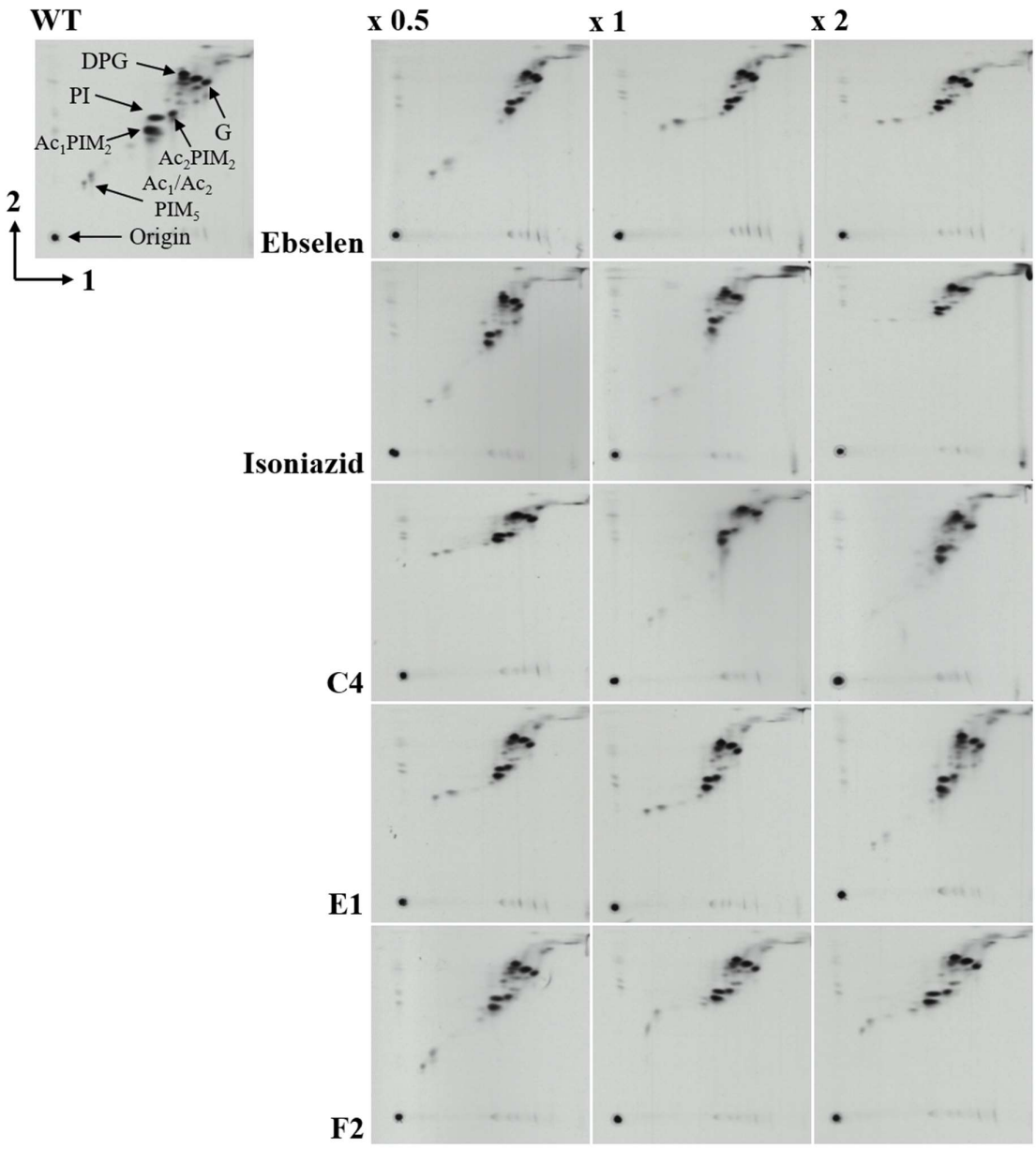


Figure 75. Thin layer chromatography (TLC) of polar lipids run and system E. Directions 1 and 2 shown with arrows. Test inhibitors included at concentrations relating to the liquid MICs. Ac_1PIM_2, Ac_2PIM_2, and $Ac1/Ac_2PIM_5$ - phosphatidylinositol mannosides. PI - phosphatidylinositol. G - glycolipid. DPG - diphosphatidylglycerol.

4.3.11 Fatty Acid Methyl Esters (MAMEs) and Mycolic Acid Methyl Esters (MAMEs) Profiling of *M. bovis* BCG Treated with Hits

The fatty acid methyl ester (FAMEs) and mycolic acid mythyl ester (MAMEs) profiles of *M. bovis* BCG were assessed using thin layer chromatography (TLC) after treatment with ebselen, isoniazid, and hits C4, E1, and F2 at multiple concentrations. The data shown in Figure 76 shows the FAMEs and MAMEs extraction of radioactively labelled *M. bovis* BCG run on a one direction TLC using petroleum ether:acetone (95:5, v/v). Ebselen, E1, and F2 show now observable difference between the x0 MIC control and the treated cells. Isoniazid and C4 both show a gradual decrease in α-MAMEs and keto-MAMEs and a gradual increase in FAMEs.

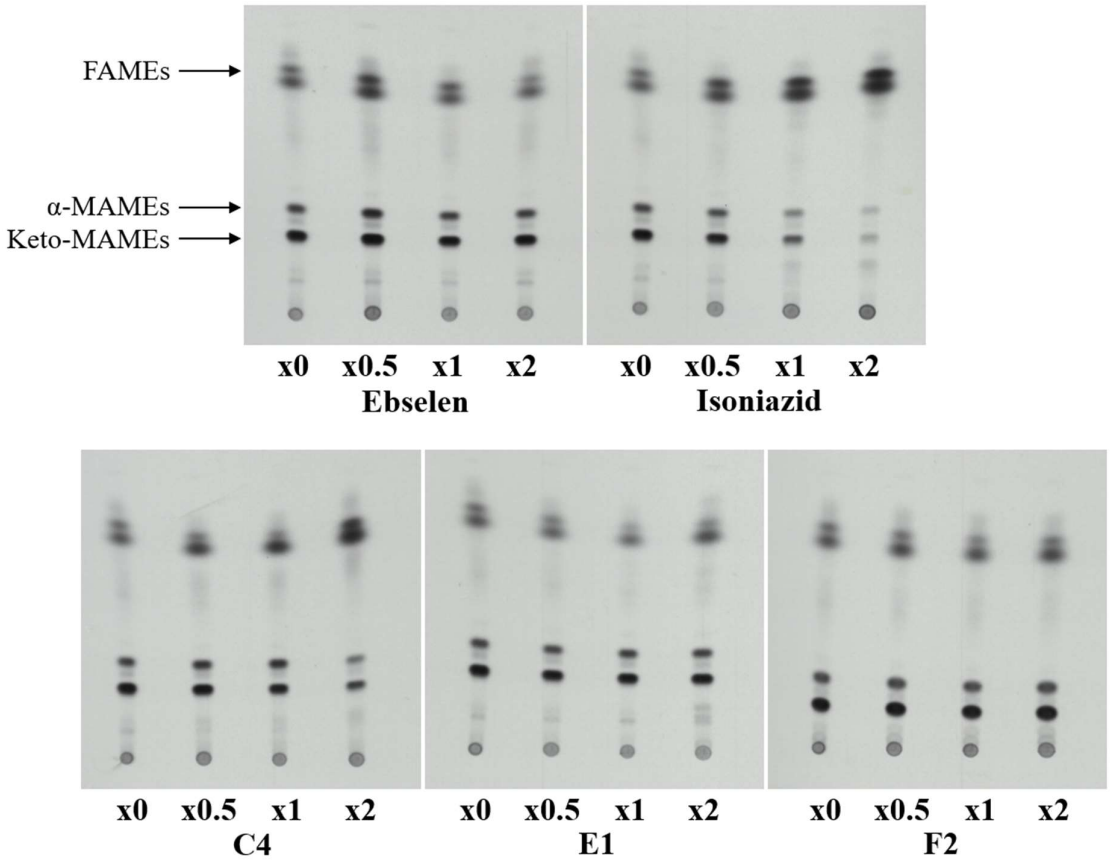


Figure 76. Thin layer chromatography (TLC) of FAMEs and MAMEs. Test hits included at concentrations relating to the liquid MICs. FAMEs –fatty acid methyl esters. α-MAMES (α-mycolic acid methyl esters), keto-MAMES (keto-mycolic acid methyl esters).

4.3.12 Polar and Non-Polar Lipid Profiling of *M. bovis* BCG Containing *fbpA* Overexpression Plasmid

The lipid profiles of *M. bovis* BCG containing empty pMV261k and *fbpA*-pMV261k were assessed and compared with wild type *M. bovis* BCG using 2D-TLC following labelling using [C^{14}] acetic acid. The 2D-TLCs were analysed as set out in Mycobacteria Protocols 1st and 2nd Edition. The data shown in Figure 77 shows 2D-TLCs of non-polar lipids run with systems A, B, C, and D, as well as polar lipids run in systems D and E. Comparing between the empty pMV261k and *fbpA*-pMV261k there seems to be no major difference in lipid profile including those of TMM, TDM and GMM.

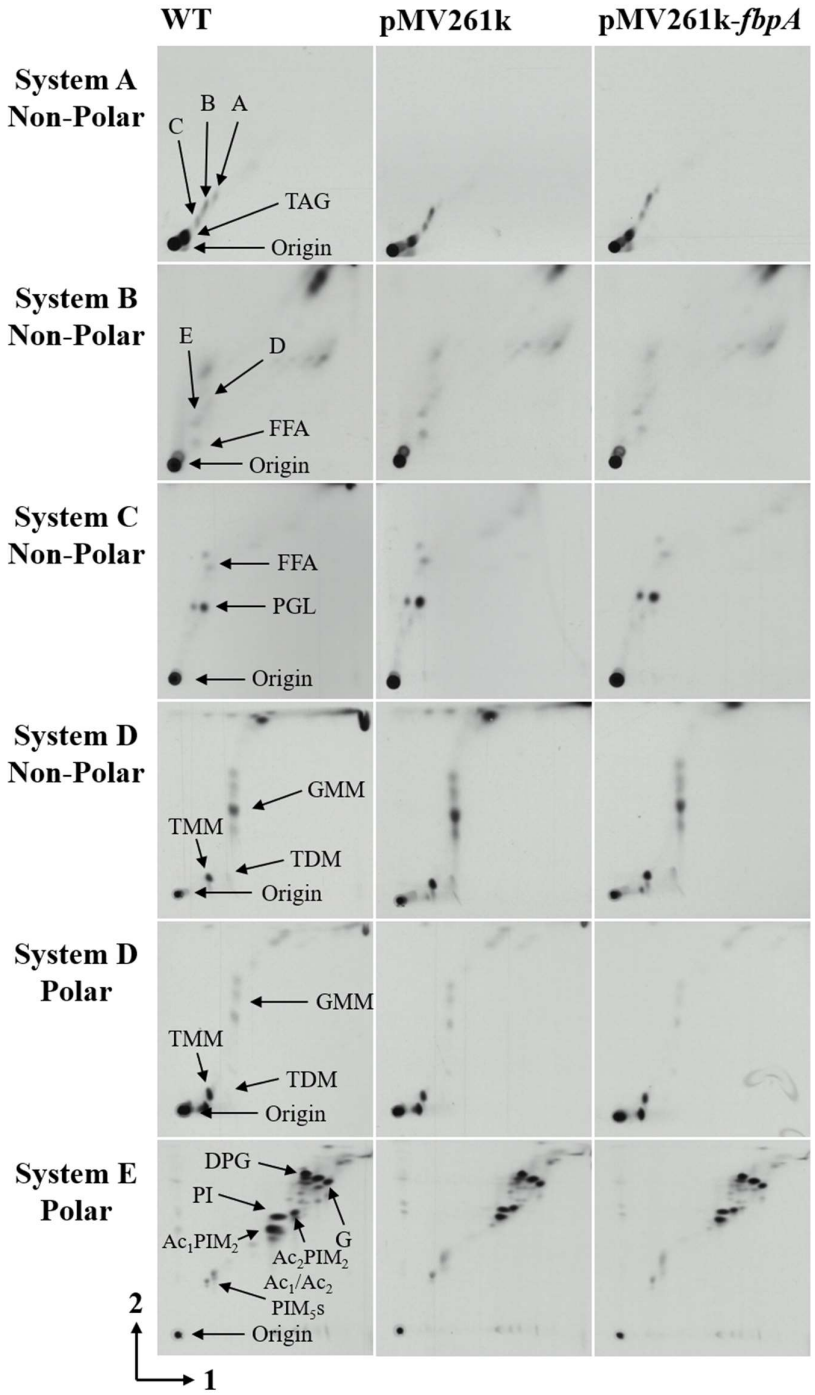


Figure 77. Thin layer chromatography (TLC) of polar and non-polar lipid analysis with systems A to E. Directions 1 and 2 shown with arrows. A-C - phthiocerol dimycocerosate (PDIM) family. TAG - triacylglycerols. D, E - non-polar mycolipenates of trehalose. FFA - free fatty acids. PGL - phenolic glycolipids. TMM - trehalose mono-mycolate. TDM - trehalose di-mycolate. GMM - glucose monomycolate. Ac_1PIM_2, Ac_2PIM_2, and Ac_1/Ac_2PIM_5 - phosphatidylinositol mannosides. PI - phosphatidylinositol. DPG - diphosphatidylglycerol.

4.3.13 Fatty Acid Methyl Esters (FAMEs) and Mycolic Acid Methyl Esters (MAMEs) Profiling of *M. bovis* BCG Containing *fbpA* Overexpression Plasmid

The FAMEs and MAMEs lipid profiles of *M. bovis* BCG containing empty pMV261k and *fbpA*-pMV261k were assessed and compared with wild type *M. bovis* BCG using thin layer chromatography (TLC). The data shown in Figure 78 shows the FAMEs and MAMEs extracted from radioactively labelled *M. bovis* BCG. Comparing between the wild type, empty pMV261k and *fbpA*-pMV261k there seems to be no major difference in FAMEs and MAMEs.

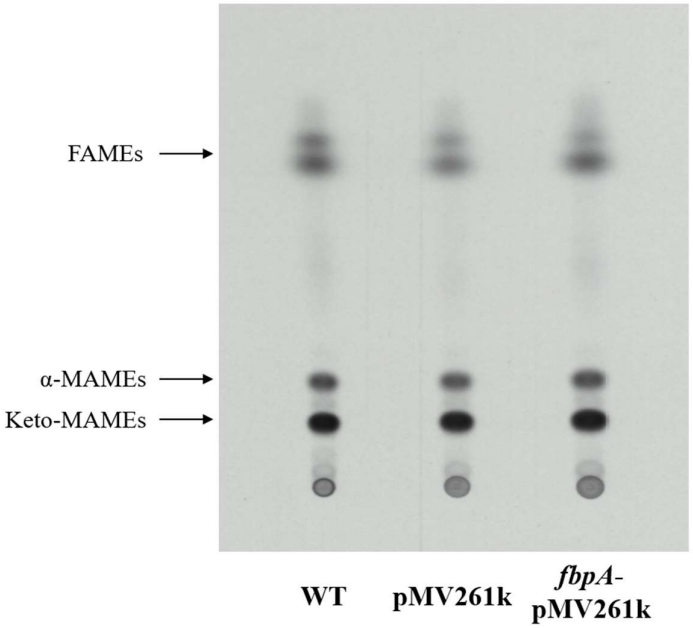


Figure 78. Thin layer chromatography (TLC) of FAMEs and MAMEs. FAMEs – fatty acid methyl esters. α-MAMES (α-mycolic acid methyl esters), keto-MAMES (keto-mycolic acid methyl esters).

4.3.14 Solid Minimum Inhibitory Concentration (MIC) of Compound C4 and Drug Resistant Mutant Generation

The solid MIC of compound C4 was determined to be 30 μM in *M. tuberculosis* H37Rv (Figure 79). Drug resistant mutants were raised on agar plates with 2.5x, 5x, and 10x the

solid MIC in *M. tuberculosis* H37Rv *ΔleuDΔpanCD* by Dr Alistair Brown (University of Newcastle). Six colonies appeared on the 2.5x MIC agar plate and were retested at 5x solid MIC. All six colony isolates grew on the 5x MIC agar plate with an abnormal raised colony morphology (Figure 80).

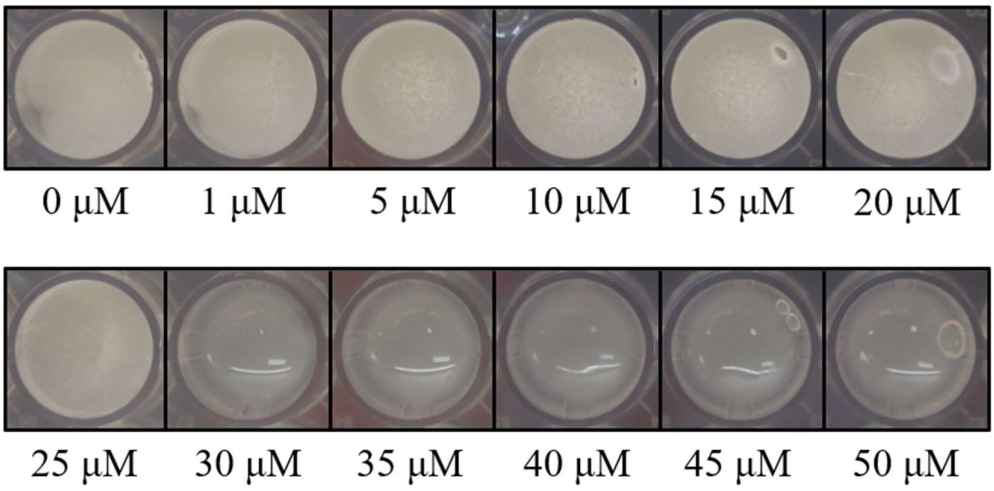


Figure 79. Solid minimum inhibitory concentration (MIC) of compound C4 in *M. tuberculosis* H37Rv *ΔleuDΔpanCD*.

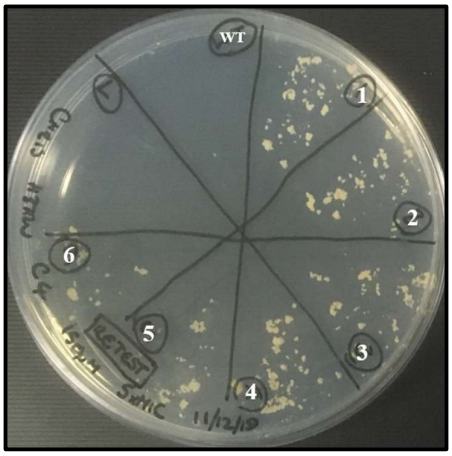


Figure 80. *M. tuberculosis* H37Rv *ΔleuDΔpanCD* drug resistant mutants to compound C4.

4.4 Discussion

This study focused on assaying the activity of six hits identified during an overexpression screen of *fbpA*, Antigen 85A, at GSK by Dr Jonathan A.G. Cox. Antigen 85A and Antigen 85C2 were purified and the activity was assessed *via* radioactive assays. Antigen 85C2 had roughly 4 times the activity of Antigen 85A (Figure 59). Originally this reduction in activity was thought to be related to damage to the active site cystine due to redox. Additional protein purification using dithiothreitol as a redox protectant showed that this was not the case. The freshly purified Antigen 85A showed virtually no improvement over the original purification (Figure 59). Despite the differences in overall enzymatic activity both enzymes showed a preference for the synthesis of TMM.

The β-glucosidase assay was the first attempted at assaying Antigen 85 activity based upon the same assay conducted by Boucau *et al*. (2009)[429]. The assay measures the ability of Antigen 85 to produce TMM and TDM. This assay used 4-nitrophenyl-6-octanoyl-β-D-glucopyranoside as a TMM substitute and D-glucose as the trehalose acceptor. The assay functioned with Antigen 85 removing the octanoyl from 4-nitrophenyl-6-octanoyl-β-D-glucopyranoside and attaching it to D-glucose. This then allows β-glucosidase to hydrolyse the bond in the 4-nitrophenyl-β-D-glucopyranoside releasing 4-nitrophenyl. The 4-nitrophenyl could then be detected and measured by a plate reader measuring absorbance at 420 nm. For this assay to work correctly the β-glucosidase should not have been able to release the 4-nitrophenyl until the octanoyl was removed. As Figure 61 shows, the absorbance of the reaction increased even without the presence of Antigen 85C2. Indeed, when compared with the full reaction with Antigen 85C2 the absorbance increased faster. This could be due to Antigen 85C2 binding some of the 4-nitrophenyl-6-octanoyl-β-D-glucopyranoside as planned reducing availability for the β-glucosidase to hydrolyse. Unfortunately, due to this the assay did not past the initial optimisation stage.

The resorufin butyrate assay measures the same aspect of Antigen 85 activity as the β-glucosidase assay but does not require an additional enzyme to do so and uses a more natural substrate in the form of a trehalose acceptor. The assay uses resorufin butyrate, the butyrate is removed and transferred to trehalose by Antigen 85. This results in the release of free resorufin, a highly fluorescent molecule that can be detected using a plate reader. The assay was optimised using Antigen 85C2 and used to assess the activity of both Antigen 85C2 and Antigen 85A. Like the β-glucosidase assay, the resorufin butyrate assay examines the ability of Antigen 85 to produce TMM and TDM. Antigen 85C2 displayed good activity in this assay, both ebselen and iodoacetamide showing inhibition of Antigen 85C2. Unfortunately, none of the hits examined showed any inhibition of Antigen 85C2. The assay did not work as well for Antigen 85A. The results were variable with large error bars. In addition, esbelen did not show any inhibition of Antigen 85A and iodoacetamide may have shown some inhibition of Antigen 85A, but the spread of the error bars makes this assay largely inconclusive. The variability of this assay could be due to substrate preferences as Antigen 85A preferentially mycolates arabinogalactan[280]. To examine the production of TDM the trehalose acceptor could be switched with a TMM analogue to better mimic the preferred substrates of Antigen 85A. In addition, dedicated assay optimisation for Antigen 85A may have made a difference in the consistency of the assay. While this assay worked well for Antigen 85C2 it was not without issues, there was a high background rate of reaction to account for that needed to be subtracted from the results.

The radioactive assaying of Antigen 85A showed similar results to the resorufin butyrate assay. Once again, this assay examines TMM and TDM production the difference being that this assay uses purified TMM as the donor substrate and attaches the donated mycolate to a radioactive [C^{14}] trehalose. It was thought that the more natural mycolate

donation substrate would improve the consistency of the results. As the scintillation counts in Figure 66 show there was still variability between samples, however the enzyme controls were consistent and lower than the experimental conditions. This assay once again demonstrated that ebselen and iodoacetamide do not inhibit Antigen 85A and that the test hits do not either.

The trehalose-C-12-NBD assay was devised to examine the other function of Antigen 85 activity, mycolation of arabinogalactan, to see if the hits affect a specific mode of Antigen 85 activity. The C-12 lipid with the attached NBD fluorophore is removed from trehalose by Antigen 85 and attached to the terminal of the arabinogalactan. Unfortunately, none of the hits including ebselen and iodoacetamide seemed to reduce Antigen 85A activity. This assay also suffers from high variability, although this is probably as a result of the substrates being highly insoluble. The arabinogalactan was never truly soluble in the reaction mix and could only be suspended. In addition, the trehalose-C-12-NBD had a tendency to form inclusion bodies. Repeated sonication and washes needed to be used to remove any unbound fluorophore from the reactions before plate reading. The result was a labour-intensive assay that displayed variable results. Despite this there was enough separation between both positive controls, the true positive control and the CPAc treated control, and the blank to use the data. The substitution of the arabinogalactan for the terminal arabinan motif similar to experiments conducted by Backus *et al.* (2014)[280] could solve some of the solubility issues to produce more reliable results.

The assays clearly show that the test hits are not having an inhibitory effect on Antigen 85. The resorufin butyrate assay shows Antigen 85C2 is unaffected by the test hits but that the activity is knocked down by the known inhibitors ebselen and iodoacetamide. Antigen 85A was harder to assay consistently, however all the assays conducted show that the inhibitors do not affect any aspect of Antigen 85A activity. The assays for Antigen

85A would have benefited heavily from a known inhibitor of antigen 85A, ebselen and iodoacetamide did not work as controls which meant that blanks had to be relied upon for activity comparison. While these assays did not find any inhibitors of Antigen 85, they could be used to examine the activity preferences of the different Antigen 85 enzymes. For example, the K_m of resorufin butyrate for Antigen 85C2 was very low, only 25 μM, given that this is a short lipid attached to resorufin rather than trehalose. In contrast the K_m of trehalose was 20 times higher at 1000 μM. This doesn't necessarily fit the current narrative of Antigen 85C2 preferentially producing TMM and TDM[280], as the K_m of trehlose would be expected to be lower indicating a higher binding affinity. Additionally, trehalose-C-12-NDB assays could look at the levels of activity between Antigen 85A and C2 to compare given Antigen 85A preference for cell wall mycolation and Antigen 85C2 for TMM production. Purification of Antigen 85B could also be performed and comparisons between all three antigen 85 isoforms made experimentally.

Due to the lack of findings from the Antigen 85 assay, the overexpression of *fbpA* was repeated to confirm the legitimacy of the original screen. When *fbpA* was overexpressed *M. bovis* BCG showed increased levels of resistance to compounds E3, F2, C4, and E1 when compared to the empty plasmid. Compound B5 did not cause a detectable reduction in survival of either the *fbpA* overexpressor or the empty plasmid even when used at concentrations up to 100 μM. For this reason, compound B5 was discontinued. Unfortunately, compound E3 stocks were also depleted and could not be replenished. Liquid MICs for the remaining compounds, ebselen and isoniazid were established in *M. bovis* BCG.

The full lipid profiling of *M. bovis* BCG treated with the ebselen, isoniazid, C4, E1, and F2 was used to determine how the test compounds affected the production and distribution of the many lipids making up the outer cell wall. When treated with ebselen the lipid

content of the cell wall did not change in any discernible way. Despite the fact that ebselen inhibits Antigen 85C2, there was no change in the amount of TMM, TDM and GMM. This is probably because from the assay experiments, we have shown that ebselen does not inhibit Antigen 85A, and in addition, potentially has no effect on Antigen 85B. This means that Antigen 85A and B can compensate for the inhibition of Antigen 85C2. This is supported by evidence from single knockouts of *fbp* genes[411], cells with only 2 functional *fbp* genes able to maintain a functional cell wall architecture. Hit F2 also showed no modification of the lipid profile when cells were treated. However, just because ebselen shows no difference does not mean that F2 is also inhibiting an Antigen 85 isoform. There is no evidence, aside from the overexpression of *fbpA* that F2 has anything to do with antigen 85 or the outer cell wall in general. Hit E1 shows some small changes in the lipid profile that may be indicative of influence in the structure of the cell wall. In systems B and C of the non-polar lipid there is a slight increase in free fatty acids as well as an increase in the non-polar mycolipenates of trehalose. While these changes are interesting, they do not seem to have much relation to the activity of Antigen 85. Isoniazid was included in this experiment as a control because of the wide range of changes it induces in cell wall structure due to the inhibition of mycolate biosynthesis. In systems B, C and the there is an increase in free fatty acids. System B also shows an increase in non-polar mycolipenates of trehalose and system C shows an increase in phenolic glycolipid (PGL). The increase in these membrane components could be due to increased availability of FAS I pathway products. Many of these products would be used to produce mycolic acids. Since the FAS II pathway is rendered non-functional by isoniazid the FAS I products can be used to synthesis other lipids, such as non-polar mycolipenates of trehalose and phenolic glycolipids. The decrease in TMM, TDM and GMM seen in system D for polar and non-polar lipids, is consistent with the mode of

action of isoniazid. The most interesting lipid profile, C4, shows a plethora of changes in some ways similar to that of isoniazid. Like isoniazid, C4 displays an increase in free fatty acids in systems B and C. In addition, the decrease in TMM, TDM and GMM remains the same between system D polar and non-polar lipids. In contrast to isoniazid, C4 shows a reduction in phenolic glycolipid (PGL) in system C and a decrease in phosphatidylinositol mannosides (PIMs). While these changes do not indicate an effect on Antigen 85, they do suggest that C4 is influencing the cell wall composition in a different way to isoniazid.

The evidence collected in this study does not clearly point to any of the inhibitors found in the *fbpA* overexpression screen directly targeting two of the three Antigen 85 isoforms, A and C2. The overexpression of *fbpA* may have led to more efficient mycolation of the cell wall, which decreased the permeability of the cells. This combined with the poor physiochemical properties of some of the compounds may explain why there has been an apparent MIC shift and increase in resistance with the *fbpA* overexpressor. To test this hypothesis cell permeability experiments with dyes could be used to examine if overexpression of *fbpA* can influence permeability.

Some aspects of this study could be improved. Many of the radioactive experiments are only single replicates due to limitations with the amount of hit compound provided. Given the chance, these experiments would be repeated fully with triple replicates. Additionally, of the six hits found during screening only five were initially available for use meaning one of the compounds was not assayed at all. Only one compound, C4 has been progressed to the point of drug resistant mutant generation. Six mutants were generated and retested at a higher compound concentration. The genomes of these six isolates are to be purified and the whole genomes sequenced. Future work could include the generation of resistant mutants for all the experimental hits and the purification and

assaying of Antigen 85B. Cell wall permeability experiments would be interesting to determine the value of overexpressing *fbpA/B/C2* or other genes that potentially influence the cell wall structure for screening to avoid false positive results.

5 Conclusion

Increasing numbers of drug resistant infections has resulted in rising interest in identifying novel inhibitors for the treatment of *M. tuberculosis*. Improving standard TB drug therapy to make the treatment regime more tolerable and faster could greatly cut down on the non-compliance of patients. This in turn would decrease the amount of recurrent and relapsed infections that are more likely to display drug resistance. New drugs will also be useful in the treatment of drug resistant infections. The drug discovery process is a long and arduous process taking many years from initial discovery, through target validation, and clinical trials. Promising candidates can spend years in development only to be mothballed during the process due to unfavourable characteristics. This process is also incredibly expensive and unlikely to be funded unless the candidate in question can be funded by a pharmaceutical company. Focusing on known effective drug targets instead of novel drug targets can alleviate some of these issues. This thesis has focused on using methods that streamline the resource intensive drug discovery process to identify inhibitors of known drug targets.

The amino acid biosynthetic pathways of *M. tuberculosis* are well developed and essential for survival and proliferation inside the host. The essentiality of amino acids to protein synthesis makes amino acid biosynthesis a network of potential drug targets. In the first project we used a method of media supplementation to selectively identify inhibitors of amino acid biosynthesis. Supplementing the media with amino acids allowed us to treat the 'symptoms' of amino acid biosynthesis inhibition and rescue cells from death in a detectable manner. The drop-out screening used this method in an attempt to determine the particular biosynthetic pathway targeted by the hit compounds. While both these strategies worked well for the validation compounds, inhibitors of BCAA biosynthesis, in testing the GSK TB box set they were not as successful. In addition, the drop out can

identify a specific pathway, but there may be several genes in that pathway which cannot be distinguished by this method. Future work for this project could expand to involve construction of an overexpression vector library containing the genes of all amino acid biosynthetic pathways. These could be used after hit compounds have been identified to determine the drug target without the use of drug resistant mutants and whole genome sequencing. These screening methods could then be rolled out to larger compound libraries to identify new inhibitors.

RNA polymerase and the ribosome are both drug targets of high importance. A great number of TB treatments target these complexes. While RNA polymerase and the ribosome perform different functions, they both fall into the protein synthesis pipeline. Protein synthesis is a function essential to all cellular life and as such drugs that target the enzymes within the protein synthesis pipeline are highly effective. The second aspect of this thesis used phenotypic screening to identify inhibitors of the protein synthesis pipeline from compound libraries. The hits from these screens could include a wide range of inhibitors including RNA polymerase, the ribosome, and tRNA synthetases. From screening 2799 compounds, multiple hit compounds were found. Upon additional testing of these compounds it was found that two of them inhibit *E. coli* RNA polymerase *in vitro*. Coupled with results from a merged project a total of four inhibitors of RNA polymerase were discovered, two of which compounds 45 and 46 had related structures. Compounds 45 and 46 are likely to have a similar binding site to previously described inhibitors[396] on RNA polymerase based upon the location of resistance mutations. While the assays of this project were successful, it would have been better if the RNA polymerase assays could have used *M. tuberculosis* RNA polymerase. Future work could prioritise the purification of *M. tuberculosis* RNA polymerase including transcription initiation factor CarD. One aspect of this project that was not explored was that of tRNA

synthesis. Due to the amount of tRNA synthetases it was out of the scope of this project to include assays for them, however future work could include the construction of a tRNA synthetase overexpression vector library for further screening of hit compounds.

The Antigen 85 complex is widely regarded as an excellent drug target due to the essentiality of the mycobacterial outer membrane. While the effectiveness of Antigen 85 specific inhibitors have not been validated as effective treatment in humans, treatment with an Antigen 85 inhibitor is likely to have a similar effect on *M. tuberculosis* as isoniazid or ethambutol. The third aspect of this thesis focused on confirming the Antigen 85 complex as a target for inhibitors identified in an overexpression screen of *fbpA*. A range of biochemical assays, were used examining different aspects of Antigen 85 activity to test the influence of the hit compounds on the enzymes. The inhibitors tested did not target Antigen 85A or C2, however Antigen 85B was not purified and tested. Future work could include testing Antigen 85B with the inhibitors and testing Antigen 85C2 with the C12-NBD assay. Additionally, optimisation of the resorufin butyrate assay specifically for Antigen 85A could improve results. One factor that should be tested is the influence of overexpressing *fbpA* on the permeability of the cell wall. While lipid profiling showed no discernible differences, the permeability could be measured with a dye, such as congo red. A decrease in permeability would explain why the overexpressor was better protected from the hit compounds. Once these questions have been resolved then the screening can be repeated with other compound libraries.

6 General Materials and Methods

6.1 Chemicals and Reagents

All chemicals, reagents and solvents were purchased from Sigma-Aldrich (UK) or Thermo Fischer Scientific (USA) and enzymes were purchased from New-England Bio Labs (USA) unless noted otherwise.

6.2 Culture Media

6.2.1 Luria-Bertani broth

7.5 g of Luria-Bertani (LB) pellets were dissolved in 300 mL of dH_2O and sterilised by autoclaving at 121 °C for 25 minutes.

6.2.2 Luria-Bertani Agar

11.1 g of LB agar pellets were dissolved in 300 mL of dH_2O and sterilised by autoclaving at 121 °C for 25 minutes.

6.2.3 Middlebrook 7H9 Media

2.35 g of Middlebrook 7H9 broth base powder was dissolved in 450 mL of dH_2O. 2 mL of 50 % glycerol (0.2 % final) and 1.25 mL of 20 % Tween 80 (0.05 % Final) was added. 50 mL (10 % final) of either OADC (Oleic acid, Albumin, Dextrose, Catalase) or ADC (Albumin, Dextrose, Catalase) was added depending on the cultured organism. The final mixture was filter sterilised. 2x 7H9 was made as above but with 200 mL of dH_2O instead of 450 mL.

6.2.4 Middlebrook 7H11 Agar

7 g of Middlebrook 7H11 Agar Base was dissolved in 270 mL of dH_2O. 3 mL of 50 % glycerol (0.5 % final) was added. The mixture was autoclaved at 121 °C for 25 minutes. After autoclaving 30 mL of OADC was added.

6.2.5 2xYT Media

4.8 g of tryptone powder, 3 g of yeast extract and 1.5 g of sodium chloride were added to 300 mL of dH_2O. The mixture was autoclaved at 121 °C for 25 minutes.

6.2.6 Terrific Broth

14.3 g of terrific broth powder was added to 300 mL of dH_2O. 4.8 mL of 50 % glycerol was added, and the mixture was autoclaved at 121 °C for 25 minutes.

6.2.7 Brain Heart Infusion Broth

11.1 g of Brain Heart Infusion (BHI) broth powder was added to 300 mL of dH_2O. Optionally for certain *C. glutamicum* gene deletions 27.3 g of sorbitol was added. The mixture was then autoclaved at 121 °C for 25 minutes.

6.2.8 ZYM-5052 Autoinduction Media

ZYM-5052 autoinduction media was prepared by mixing 50 mL of 0.5 pH 7.2 M Na_2HPO_4, 50 mL of 0.5 M pH 7.2 K_2HPO_4, 50 mL of 1 M NH_4Cl, 5 mL of 1 M Na_2SO_4 and 2 mL of 1 M $MgSO_4$. 10 g of tryptone, 5 g of yeast extract, 10 mL of 50 % glycerol, 0.5 g of glucose, 2 g of lactose, 1 mL of 1000x trace metal solution was added to the

mixture and made up to 1 L with dH_2O. The mixture was then autoclaved at 121 °C for 25 minutes.

6.2.9 1000x Trace Metal Solution

Table 20 shows the composition of the 1000x trace metal solution. After the components were combined the mixture was sterilized via filtration with a 0.2 µm filter unit.

Table 20. 1000x trace metal solution mixture.

Stock Solution	Amount for 100 mL
Sterile dH_2O	36 mL
0.1 M $FeCl_3$	50 mL
1 M $CaCl_2$	2 mL
1 M $MnCl_2$	1 mL
1 M $ZnSO_4$	1 mL
0.2 M $CoCl_2$	1 mL
0.1 M $CuCl_2$	2 mL
0.2 M $NiCl_2$	1 mL
0.1 M Na_2MoO_4	2 mL
0.1 M Na_2SeO_3	2 mL
0.1 M H_3BO_3	2 mL

6.2.10 Tryptic Soy Broth

30 g of Tryptic Soy Broth (TSB) powder was dissolved in 1 L of dH_2O. The mixture was then autoclaved at 121 °C for 25 minutes.

6.3 Bacterial Culture and Transformation

6.3.1 Culture of Bacterial Strains

E. coli strains used for DNA extraction (Top10) and protein production (BL21, T7 Shuffle) were grown in culture tubes or conical flasks in LB media at 37 °C with shaking at 180 rpm. BL21 and T7 shuffle were also grown on a large scale in 2xYT media, terrific broth and ZYM-5052 autoinduction media depending on the protein desired. *M. smegmatis* mc^2155 was grown on a small scale in 7H9 media without OADC/ADC at 37 °C with shaking at 180 rpm. Large scale cultures were grown in LB or TSB under the same conditions. *M. bovis* BCG was grown in 7H9 with OADC in culture flasks at 37 °C and 5 % CO_2. *M. tuberculosis* H37Rv was grown in 7H9 with OADC in culture flasks at 37 °C and 5 % CO_2. *M. tuberculosis* H37Rv *ΔleuDΔpanCD* deletion mutants required additional supplementation of 24 μg/mL calcium pantothenate, 0.02% w/v casamino acids, 10 μg/mL cycloheximide, and 10 μg/mL carbenicillin disodium salt. *C. glutamicum* ATCC 13032 was grown in BHI broth at 30 °C. The *C. glutamicumΔUbiA* deletion mutant requires additional supplementation of 0.5 M sorbitol and 25 μg/mL kanamycin.

6.3.2 Cell Number Estimation

Some protocols required an estimated number of cells to be added which was calculated from OD_{600}. An OD_{600} of 1.0 equals approximately $2.5x10^8$ cells/mL. The volume of initial cell culture from a starting culture to be added to a volume of media for a set cells/mL was calculated using the equations below -

$$Culture\ cells\ per\ mL = OD_{600} \times 2.5 \times 10^8$$

$$Culture\ required\ (mL) = \frac{Cells\ per\ mL\ desired \times Volume\ of\ media\ (mL)}{Culture\ cells\ per\ mL}$$

6.3.3 Chemically Competent *E. coli*

A 5 mL overnight culture of *E. coli* (Top10, BL21, T7 Shuffle) in LB was used to inoculate 100 mL of LB in a conical flask. The culture was incubated at 37 °C with 180 rpm shaking until it reached a mid-log (OD_{600} of 0.6-0.8). The culture was aliquoted into 50 mL falcon tubes and centrifuged at 4,000 rpm and 4 °C for 20 minutes. The supernatant was discarded, and the pelleted cells were resuspended in 10 mL of ice cold sterile 100 mM $CaCl_2$ and incubated on ice for 10 minutes. The cells were centrifuged again, and the supernatant removed as before. The pelleted cells were then resuspended in 2.5 mL of ice cold sterile 100 mM $CaCl_2$ with 15 % glycerol. The cells were separated into 100 µL aliquots and flash frozen in liquid nitrogen. Cells were stored at -80 °C until use.

6.3.4 Electrocompetent Mycobacteria

A 50 ml culture of mycobacteria (*M. smegmatis* mc^2155, *M. bovis* BCG, *M. tuberculosis* H37Rv) was grown until it reached a mid-log (OD_{600} of 0.4-0.8). The cells were put into a 50 mL falcon tube and harvested with centrifugation at 4,000 rpm and 4 °C for 20 minutes. The supernatant was discarded, and the cells were resuspended in 10 mL of ice-cold 10 % glycerol in dH_2O. The centrifugation was repeated, and the cells were then resuspended in 2 mL of ice-cold 10 % glycerol in dH_2O. Cells were split into 400 µL aliquots and flash frozen with liquid nitrogen. Cells were stored at -80 °C until use.

6.3.5 Transformation of Competent *E. coli*

Plasmid DNA (1 µL) was added to 50 µL of *E. coli* competent cells and chilled on ice for 5 minutes. The mixture was heat shocked at 42 °C for 30 seconds. The mixture was then cooled on ice again for 2 minutes before 250 µL of LB broth was added. The cells were

rescued at 37 °C with shaking for 1 hour. Cells (100 µL) were plated out onto LB agar plates with selective antibiotic relevant to the plasmid being transformed. The plates were then incubated at 37 °C overnight.

6.3.6 Electroporation of Electrocompetent Mycobacteria

Plasmid DNA (1 µg) was mixed with 400 µL of electrocompetent mycobacterial cells in an electroporation cuvette at room temperature. The electroporation cuvette was inserted into an Eppendorf 2510 Electroporator and pulsed at 1800 V. Media 7H9 (1 mL) for *M. bovis BCG* and *M. tuberculosis* H37Rv, LB for *M. smegmatis*) was added to the cells and incubated (24 hours for *M. bovis BCG* and *M. tuberculosis* H37Rv, 4 hours for *M. smegmatis*) under standard conditions for the organism. The cells were pelleted at 4,000 rpm for 20 minutes and the supernatant was discarded. The cells were resuspended in 100 µL of media and spread onto agar plates (7H11 agar for *M. bovis BCG* and *M. tuberculosis* H37Rv, LB agar for *M. smegmatis*) with selective antibiotic relevant to the plasmid being transformed. The plates were then incubated under standard conditions for the organism until colonies appeared.

6.4 Molecular Biology Methods

6.4.1 Mycobacterial Genomic Extraction

Mid-log cultures at an OD_{600} 0.6-0.8 (25 mL) of mycobacterial culture was harvested by centrifugation at 4,000 rpm for 30 minutes. The supernatant was discarded, and the pellet was resuspended in 450 µL of GTE-RNase buffer (25 mM Tris-HCl pH 8, 10 mM EDTA, 50 mM glucose, 0.1 mg/mL RNase A). Lysozyme (50 µL of 10 mg/mL) was added and the extraction was incubated overnight at 37 °C. An additional 10 µL of 10 mg/mL RNase A was added and the extraction was incubated for 30 minutes at 37 °C. SDS (10%, 100

µL) and 20 µL of 15 mg/mL Proteinase K was added and incubated at 55 °C for 3 hours. 200 µL of 5 M sodium chloride (200 µL) was added and the proteins were removed by 1 mL of chloroform:isoamylalcohol extraction (24:1, v/v) and centrifuged at 13,000 rpm for 10 minutes. The aqueous top layer was removed, and the extraction was repeated on the aqueous layer in a fresh tube. After extraction the aqueous layer was removed, and 700 µL of isopropanol was added and gently mixed. This was then centrifuged at 4 °C at 13,000 rpm for 30 minutes to form a DNA pellet. The supernatant was removed, and the pellet was washed with 700 µL of 70 % ethanol. The centrifugation was repeated, the supernatant was removed, and the pellet allowed to dry. The DNA pellet was then resuspended in 20 µL of EB Buffer (10 mM Tris-HCl pH 8.5).

6.4.2 Polymerase Chain Reaction

Polymerase Chain Reaction (PCR) was carried out using Q5 High-Fidelity DNA Polymerase (NEB, M0491S). Primers were supplied by Eurofins Genomics at a concentration of 100 µM. For a 100 µL PCR, 20 µL of 5x Q5 Reaction Buffer, 20 µL of 5x Q5 High GC Enhancer, 2 µL of 10 mM dNTPs (NEB, N0447S), 2 µL of template genomic DNA (1 ng-1 µg), 1 µL of each undiluted primer, 1 µL of Q5 DNA Polymerase and 53 µL of dH_2O were mixed and kept ice cold. The reaction is conducted in a thermocycler under the conditions listed in Table 21. This method was also used for colony PCR by substituting the template genomic DNA with a *E. coli* colony scraping.

Table 21. Thermocycling Conditions for Routine PCR.

Step	Temperature	Time	Cycles
Initial Denaturation	98 °C	120 Seconds	1
Denaturation	98 °C	30 Seconds	35
Annealing	50-72 °C	30 Seconds	35
Elongation	72 °C	30 Seconds/kb	35
Final Extension	72 °C	300 Seconds	1

6.4.3 Agarose Gel Electrophoresis

A 1 % w/v agarose gel is produced by adding 1 g of agarose powder to 100 mL of 1 x TAE Buffer (40 mM Tris-acetate, 2 mM Na_2EDTA). The agarose was dissolved by heating in a microwave. The heated agarose is poured into a mould and 2.5 µL/100 mL of Midori Green Advance (Nippon Genetics) is mixed in. A gel comb is inserted into the mould and the gel is allowed to set. Once set the gel is removed from the mould and put into a gel tank filled with 1 x TAE Buffer. The comb is removed from the gel. DNA samples are mixed with 6x Gel Loading Dye Purple (NEB, B7024S). The samples are loaded into the gel wells along with a well of Quick-Load Purple 1 kb DNA Ladder (NEB, N0552S). The gel is run at 140 V, 400 mA for 40 minutes. The gel can be visualised using a Bio-Rad Gel Dock XR+ UV imager or a blue light box. Bands can be cut out from the gel using a scalpel for DNA extraction.

6.4.4 DNA Extraction from Agarose Gel

DNA extraction from agarose gel used a Qiagen QIAquick Gel Extraction Kit. DNA bands excised from a gel were weighed in a tube. 3 volumes of QG Buffer (5.5 M guanidine thiocyanate, 20 mM Tris-HCl pH 6.6) was added to 1 volume (100 mg gel =

100 µL QG Buffer) of gel. The tube was agitated until the gel dissolved and 10 µL of 3 M sodium acetate pH 5 was added. 1 volume of isopropanol was added, and the mixture was applied to a QIAguick column or a Monarch DNA Clean Up column (NEB, T1034L). The column was centrifuged in a microcentrifuge at 13,000 rpm for 1 minute. The flow-through was discarded and 500 µL of QG Buffer was applied to the column and centrifuged again. The flow-through was discarded again and 750 µL of PE Buffer (10 mM Tris-HCl pH 7.5, 80 % Ethanol) was applied to the column and centrifuged again. The flow-through was discarded again and the residual buffer was removed by centrifuging again. The column is placed into a 1.5 mL microcentrifuge tube and 30 µL of EB Buffer (10 mM Tris-HCl pH 8.5). The column is allowed to stand for 1 minute and then centrifuged again to elute the DNA.

6.4.5 PCR Clean Up

DNA produced by PCR was cleaned by using a Qiagen QIAquick PCR Purification Kit. 5 volumes of PB Buffer (5 M guanidinium chloride, 30 % isopropanol) was added to 1 volume of PCR mix. Sodium acetate pH5 (10 µL) was added and the mixture was applied to a QIAguick column or a Monarch DNA Clean Up column (NEB, T1034L). The column was centrifuged in a microcentrifuge at 13,000 rpm for 1 minute. PE Buffer 10 mM Tris-HCl pH 7.5 containing 80 % ethanol (750 µL) was applied to the column and centrifuged again. The flow-through was discarded again and the residual buffer was removed by centrifuging again. The column is placed into a 1.5 mL microcentrifuge tube and 30 µL of EB Buffer (10 mM Tris-HCl pH 8.5). The column is allowed to stand for 1 minute and then centrifuged again to elute the DNA.

6.4.6 Restriction Digest of PCR Products and Plasmids

PCR product or plasmid DNA (1 µg) were made up to a volume of 20.5 µL with dH_2O. CutSmart Buffer (2.5 µL, NEB, B7204S) was added and mixed. A list of commonly used restriction enzymes and the cut sites is displayed in Table 22. The reaction is mixed and incubated at 37 °C for at least 1 hour and up to overnight.

Table 22. Cut sites of NEB restriction enzymes.

Restriction Enzyme	Cut Site
BamHI-HF (NEB, R3136S)	G|GATCC CCTAG|G
SacI-HF (NEB, R3156S)	GAGCT|C C|TCGAG
EcoRI-HF (NEB, R3101S)	G|AATTC CTTAA|G
NdeI-HF (NEB, R0111S)	CA|TATG GTAT|AC
MscI (NEB, R0534S)	TGG|CCA ACC|GGT
DpnI (NEB, R0176S)	GA|TC CT|AG
NotI (NEB, R0189S)	GC|GGCCGC CGCCGG|CG
NcoI-HF (NEB, R3193S)	C|CATGG GGTAC|C
HindIII-HF (NEB, R3104S)	A|AGCTT TTCGA|A
EcoRV-HF (NEB, R3195S)	GAT|ATC CTA|TAG
PacI (NEB, R0547S)	TTAAT|TAA AAT|TAATT

6.4.7 DNA Ligation Reaction

Restriction digested PCR product and plasmid were ligated using T4 DNA Ligase (NEB, M0202S) in a 20 µL reaction. T4 DNA Ligase Reaction Buffer (10x, 2 µL), 50 ng of plasmid DNA, and PCR product (see equation below) were made up to 19 µL with dH_2O. T4 DNA Ligase (1 µL) was added and the reaction was mixed. The reaction tube was placed in an ice bath and allowed to warm up gradually overnight.

$$\frac{Plasmid\ DNA\ (50\ ng)\ \times\ Size\ of\ Insert\ (kb)}{Plasmid\ Size\ (kb)}\ \times\ 3 = PCR\ Product\ Required\ (ng)$$

6.4.8 Extraction of Plasmid DNA from *E. coli*

Plasmid was extracted from *E. coli* using a Qiagen QIAprep Spin Miniprep Kit. A 5 mL overnight culture of *E. coli* was pelleted by centrifugation at 4,000 rpm for 20 minutes. The supernatant was discarded, and the pellet was resuspended in 250 µL of P1 Buffer (50 mM Tris-HCl pH 8, 10 mM EDTA, 100 µg/mL RNase A) and transferred to a microcentrifuge tube. P2 Buffer (250 µL; 200 mM NaOH, 1 % SDS) was added and the tube was mixed by inversion. N3 Buffer (350 µL; 4.2 M guanidinium chloride, 0.9 M potassium acetate, pH 4.8) was added and the tube was mixed by inversion again. The tube was centrifuged in a microcentrifuge for 10 minutes at 13,000 rpm and the supernatant was removed into a QIAprep 2.0 column or Monarch Plasmid Miniprep column (NEB, T1017L). The column was centrifuged in a microcentrifuge for 1 minute at 13,000 rpm and the flow-through was removed. PE Buffer (750 µL; 10 mM Tris-HCl pH 7.5, 80 % ethanol) and centrifuged again for 1 minute and the flow-through was discarded. The residual buffer was removed by centrifuging again. The column is placed

into a 1.5 mL microcentrifuge tube and 30 µL of EB Buffer (10 mM Tris-HCl pH 8.5). The column is allowed to stand for 1 minute and then centrifuged again to elute the DNA.

6.5 Protein Biochemistry

6.5.1 Protein Expression and Purification

Transformed *E. coli* BL21 or T7 Shuffle were grown to mid-log (OD_{600} 0.4-0.8) at 37 °C and 180 rpm shaking in 50 mL of LB, terrific or 2xYT media containing the appropriate selection antibiotics. Large 1 L cultures of the respective media or ZYM-5052 autoinduction media containing selection antibiotics were inoculated with 10 mL of starter culture and were incubated as before until mid-log (OD_{600} 0.4). At this point the cultures were cooled in an ice bath and isopropyl β-D-1-thiogalactopyranoside (IPTG) was added to cultures in LB, terrific or 2xYT media to a final concentration of 1 mM. The cultures were incubated at 16 °C for 12 hours at which point they were harvested by centrifugation at 4,000 rpm and frozen until use. Cell pellets were resuspended in binding buffer (50 mM sodium phosphate pH 7.5, 500 mM sodium chloride, 25 mM imidazole) and an EDTA free protease inhibitor cocktail tablet (Roche) was added. The resuspended cells were probe sonicated (MSE Soniprep 150) for 12 cycles of 30 seconds sonication, 30 seconds rest while being kept on ice. The cell lysate was centrifuged at 18,000 rpm at 4 °C for 45 minutes to produce clarified lysate. The clarified lysate was run over a 1 mL HisTrap HP column (GE Healthcare) equilibrated with binding buffer at a rate of 1 mL/minute using a peristaltic pump. The protein was eluted off the column using a step wise gradient of binding buffer with increasing imidazole (25 mM, 50 mM, 100 mM, 150 mM, 200 mM, 300 mM, 1000 mM). Fractions (10 mL) were collected separately and analysed for protein purity using sodium dodecyl sulfate-polyacrylamide gel electrophoresis (SDS-PAGE).

6.5.2 Buffer Exchange/Salt Removal using Dialysis

The protein of interest was loaded into dialysis tubing (Medicell Membranes Ltd MWCO-12-14,000 daltons) and tied off and clamped both ends. The tubing was placed into 2 L of chilled desired buffer and left in the fridge for 4 hours with gentle mixing. The buffer was then replaced with 2 L of fresh chilled buffer and left overnight. The protein was then removed from the dialysis tubing and poured into a falcon tube.

6.5.3 Hi-Trap Q HP Anion Exchange

A Hi-Trap Q HP anion exchange chromatography column (GE Healthcare) was equilibrated with Buffer A (50 mM tris-HCl pH 7.5, 10 % glycerol) on a BioLogic LP system (Bio-Rad). The desalted protein was run over the column and a gradient of Buffer A to Buffer B (50 mM Tris-HCl pH 7.5, 10 % glycerol, 1 m sodium chloride) was started progressively increasing the concentration of sodium chloride. Eluate was monitored for ultra-violet absorbance at 280 nm and collected in 1 mL fractions. Fractions with high absorbance were examined with SDS-PAGE.

6.5.4 Sodium Dodecyl Sulfate-Polyacrylamide Gel Electrophoresis

Protein sample (15 μL) was mixed with 5 μL of protein loading dye (10 % SDS, 500 mM dithiothreitol, 50 % glycerol, 250 mM Tris-HCl pH 6.8, 0.5 % bromophenol blue). The sample was boiled for 10 minutes. A Mini-Protean TGX Any kD precast gel (Bio-Rad) was loaded into a Bio-Rad protein gel tank. The tank was filled with 1x Tris/Glycine/SDS Buffer (25 mM Tris-HCl, 192 mM glycine, 0.1 % SDS) and the sample was loaded into the gel. Blue Prestained Protein Standard Broad Range (5 μL, NEB, P7718S) was also loaded. The gel was run at 200 V and 50 mA for 35 minutes. After running the gel was

removed from the plastic outer case and stained overnight in Instant Blue (Expedeon) and then excess stain was removed by soaking in water.

6.5.5 Western Blot

Western blots were run using unstained SDS-PAGE gels. A blotting cassette was set up using a protein gel and Amersham Protean Premium Nitrocellulose Blotting Membrane (GE Healthcare) and run in Transfer Buffer (25 mM Tris-HCl, 192 mM glycine, 10 % methanol) at 20 V and 300 mA for 1 hour. After running, the nitrocellulose was removed and washed in 5 % (w/v) skimmed milk powder in Tris-buffered saline (20 mM Tris-HCl pH 7.5, 150 mM sodium chloride) with 0.05 % Tween 20 (TBST) overnight. The nitrocellulose was then treated with 5 μL of Penta-His Mouse IgG primary antibody (Qiagen) in 50 mL of 0.1 % (w/v) skimmed milk powder TBST for 30 minutes. The nitrocellulose was then washed 3 times with TBST for 5 minutes each. Anti-Mouse IgG-Alkaline Phosphatase secondary antibody (2 μL, Sigma) in 50 mL of TBST was applied for 30 minutes and then the nitrocellulose was washed 2 more times with TBST. The nitrocellulose was then washed in Tris buffered saline (20 mM Tris-HCl pH 7.5, 150 mM sodium chloride) to remove residual Tween 20. BCIP solution was made by dissolving a SIGMAFAST BCIP/NBT tablets (Sigma) in 10 mL of dH_2O. The nitrocellulose was then incubated with the BCIP solution and monitored for the appearance of bands.

6.6 Microplate Techniques

6.6.1 Resazurin Survival Assays

Resazurin sodium salt (30 mL, 0.2 mg/mL, Sigma) solution was mixed with 12.25 mL of 20 % Tween 80 (Sigma) and filter sterilised. 42.25 μL of the resulting mixture was pipetted into the wells of microplate for every 100 μL of culture in the wells. The plates

were then incubated further under standard conditions for 24 hours for *M. tuberculosis* and *M. bovis* BCG or 4 hours for *M. smegmatis*. The plates were read with a BMG plate reader with an excitation wavelength of 544 nm and emission wavelength of 590 nm.

6.6.2 Z' Calculation

Some microplate-based assays and screens had Z' calculated. Z' is a measure of the separation of positive and negative controls on the plate. Z' used the following equation:

$$Z' = 1 - \frac{3(\sigma_p + \sigma_n)}{(\mu_p - \mu_n)}$$

The standard deviation of the positive and negative controls was represented by σ_p and σ_n, and the mean of the positive and negative controls was represented by μ_p and μ_n. Any result value of less than 0.5 was a poor assay. Any result above 0.5 was a good assay and above 0.75 was an excellent assay.

6.6.3 Percentage Normalisation

Percentage normalisation was applied to quantitative data with clearly defined positive (100 %) and negative (0 %) controls. The test values were then displayed as a percentage score of the positive control. This was applied to cell survival data (resazurin survival assay) and protein expression data (mCherry expression) in the context of a phenotypic measurement. Percentage normalization used the following equation:

$$Percentage\ Normalization = \left(\frac{x - \hat{n}}{\hat{p} - \hat{n}}\right) \times 100$$

The experimental value was represented by x, and the mean of the positive and negative controls was represented by $\hat{p}$ and $\hat{n}$ respectively.

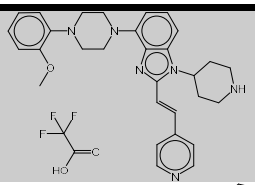
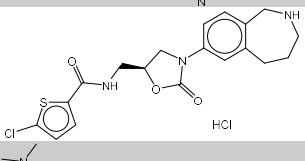
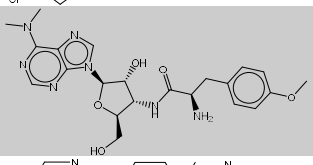
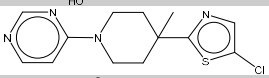
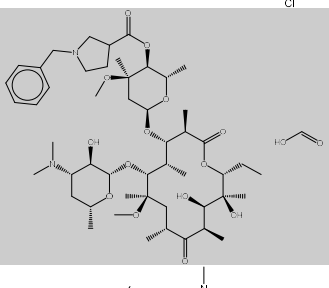
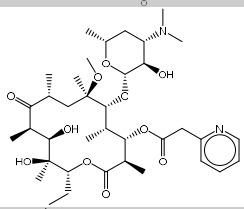
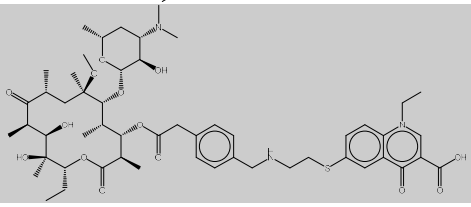
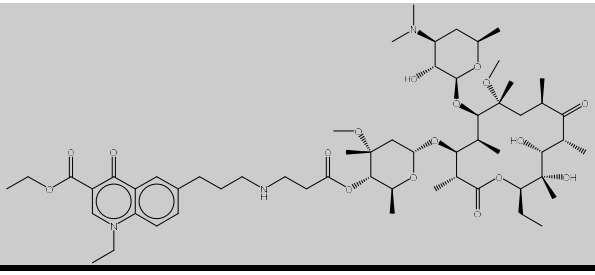
6.7 Other Methods

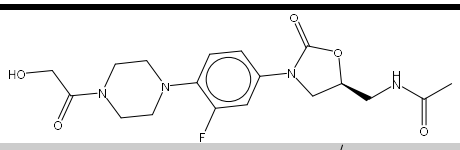
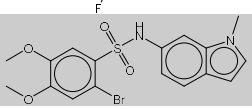
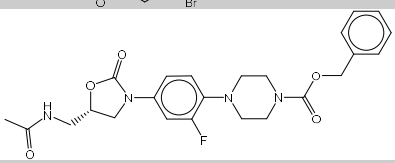
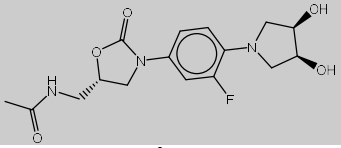
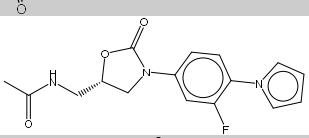
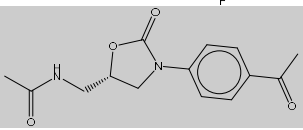
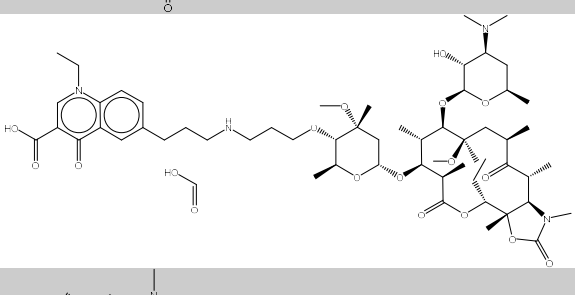
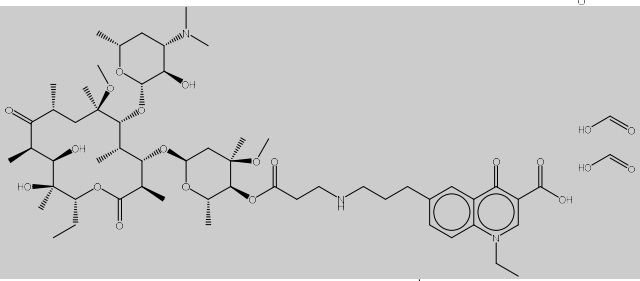
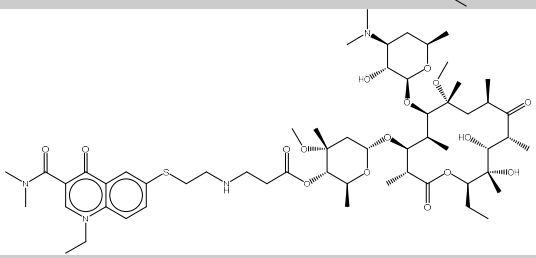
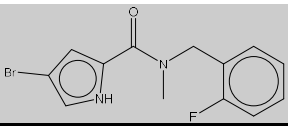
6.7.1 Thin Layer Chromatography (TLC)

TLC was performed using silica gel bonded to aluminium sheets (Merck, TLC Silica Gel 60 F_{254}). Sheets were cut to size and samples were spotted onto the TLC plates 1 cm above the base. The plates are inserted into a TLC solvent tank (solvent systems specified in methods) and run until the solvent front reaches the top. The TLC is allowed to dry and visualised. Visualization can be with sugar stain or phosphate stain. Radioactive TLCs are exposed to X-ray film.

7 Appendix

Table 23. Letter designation and structures of hit compounds from Section 3.3.1.

Letter	Structure
A	
B	
C	
D	
E	
F	
G	
H	**Structure Not Released**
I	

J	
K	
L	
M	
N	
O	
P	
Q	
R	
S	

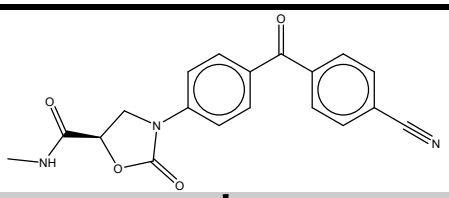
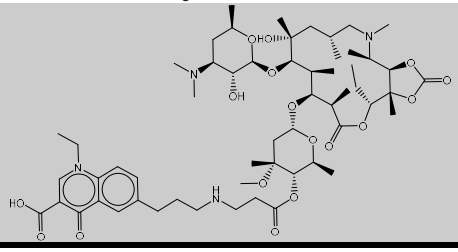
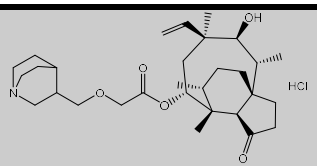
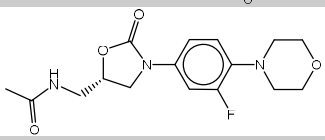
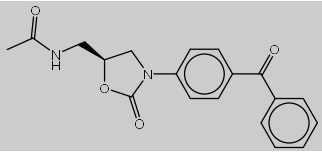
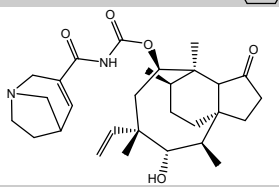
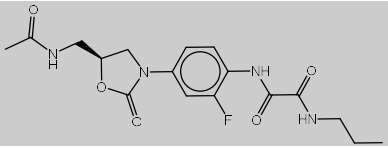
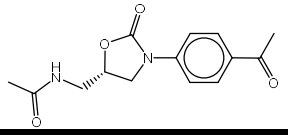
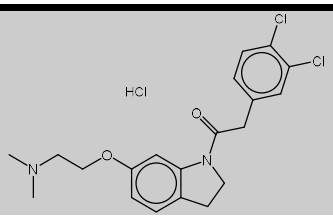
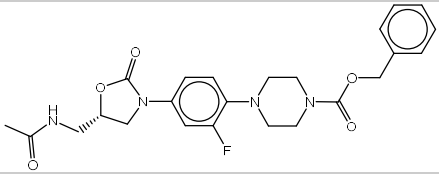
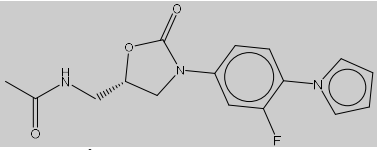
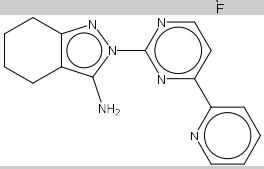
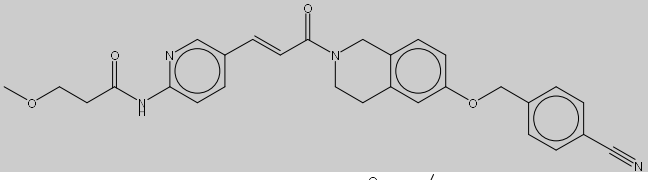
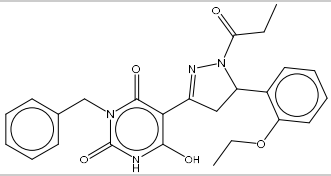
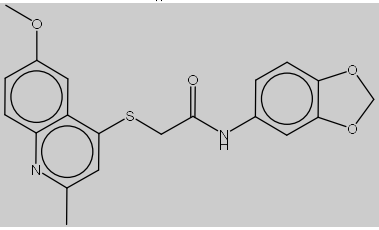
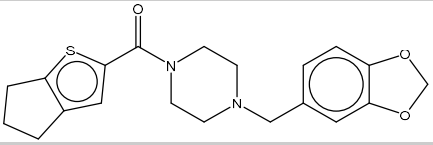
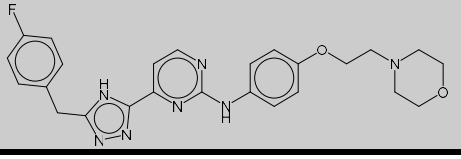
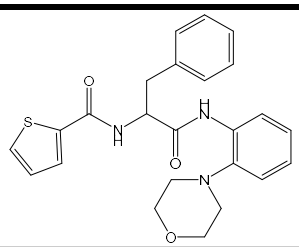
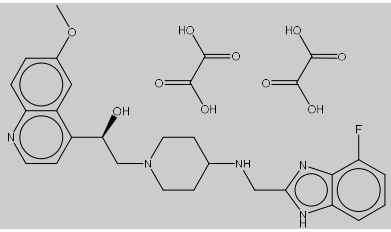
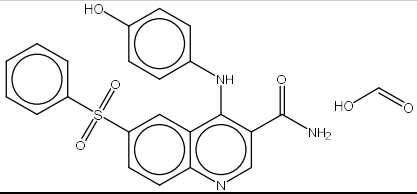
T	
U	

Table 24. Number designation and structures of hit compounds from **Section 3.3.3**.

Number	Structure
1	
2 Linezolid Blind Control	
3	
4	
5	
6	

7	
8	
9	
10	
11	
12	
13	
14	
15	

16 (45) 16 was discovered to be the same structure as 45 during writing. While they are the same, they were treated separately throughout all the experiments.	
17	
18	

8 References

1. Barka, E. A., Vatsa, P., Sanchez, L., Gaveau-Vaillant, N., Jacquard, C., Klenk, H.-P., Clément, C., Ouhdouch, Y. & van Wezel, G. P. Taxonomy, Physiology, and Natural Products of Actinobacteria. *Microbiology and Molecular Biology Reviews* **80**, 1–43 (2016).
2. Buchanan, R. E. Studies in the nomenclature and classification of the bacteria II. The primary subdivisions of the Schizomycetes. *The Journal of Bacteriology* **2**, 155–164 (1917).
3. Forbes, B. A. Mycobacterial taxonomy. *Journal of Clinical Microbiology* **55**, 380–383 (2017).
4. de Lima Procópio, R. E., da Silva, I. R., Martins, M. K., de Azevedo, J. L. & de Araújo, J. M. Antibiotics produced by Streptomyces. *Brazilian Journal of Infectious Diseases* vol. 16 466–471 (2012).
5. Bernard, K. The genus Corynebacterium and other medically relevant coryneform-like bacteria. *Journal of Clinical Microbiology* vol. 50 3152–3158 (2012).
6. Euzéby, J. P. List of bacterial names with standing in nomenclature: A folder available on the internet. *International Journal of Systematic Bacteriology* vol. 47 590–592 (1997).
7. Parte, A. C. LPSN - List of prokaryotic names with standing in nomenclature. *Nucleic Acids Research* **42**, D613–D616 (2014).
8. Parte, A. C. LPSN - List of prokaryotic names with standing in nomenclature (Bacterio.net), 20 years on. *International Journal of Systematic and Evolutionary Microbiology* **68**, 1825–1829 (2018).
9. Grange, J. M. The biology of the genus Mycobacterium. *Journal of Applied Bacteriology Symposium Suppliment* **81**, 1S-9S (1996).
10. Kim, C. J., Kim, N. H., Song, K. H., Choe, P. G., Kim, E. S., Park, S. W., Kim, H. Bin, Kim, N. J., Kim, E. C., Park, W. B. & Oh, M. don. Differentiating rapid- and slow-growing mycobacteria by difference in time to growth detection in liquid media. *Diagnostic Microbiology and Infectious Disease* **75**, 73–76 (2013).
11. Brown-Elliott, B. A. & Philley, J. V. Rapidly Growing Mycobacteria. *Microbiology Spectrum* **5**, (2017).
12. Sinha, P., Gupta, A., Prakash, P., Anupurba, S., Tripathi, R. & Srivastava, G. N. Differentiation of Mycobacterium tuberculosis complex from non-tubercular mycobacteria by nested multiplex PCR targeting IS6110, MTP40 and 32kD alpha antigen encoding gene fragments. *BMC Infectious Diseases* **16**, (2016).
13. Johansen, M. D., Herrmann, J.-L. & Kremer, L. Non-tuberculous mycobacteria and the rise of Mycobacterium abscessus. *Nature Reviews Microbiology* **18**, 392–407 (2020).
14. Inderlied, C. B., Kemper, C. A. & Bermudez, L. E. M. The Mycobacterium avium complex. *Clinical Microbiology Reviews* vol. 6 266–310 (1993).

15. Frothingham, R., Hills, H. G. & Wilson, K. H. Extensive DNA sequence conservation throughout the Mycobacterium tuberculosis complex. *Journal of Clinical Microbiology* **32**, 1639–1643 (1994).

16. Alexander, K. A., Laver, P. N., Williams, M. C., Sanderson, C. E., Kanipe, C. & Palmer, M. V. Pathology of the Emerging Mycobacterium tuberculosis Complex Pathogen, Mycobacterium mungi , in the Banded Mongoose (Mungos mungo). *Veterinary Pathology* **55**, 303–309 (2018).

17. van Ingen, J., Rahim, Z., Mulder, A., Boeree, M. J., Simeone, R., Brosch, R. & van Soolingen, D. Characterization of Mycobacterium orygis as M. tuberculosis Complex Subspecies. *Emerging Infectious Diseases* **18**, 653–655 (2012).

18. Roe, W. D., Lenting, B., Kokosinska, A., Hunter, S., Duignan, P. J., Gartrell, B., Rogers, L., Collins, D. M., De Lisle, G. W., Gedye, K. & Price-Carter, M. Pathology and molecular epidemiology of Mycobacterium pinnipedii tuberculosis in native New Zealand marine mammals. *PLoS ONE* **14**, 1–14 (2019).

19. Thompson, P. J., Cousins, D. V., Gow, B. L., Collins, D. M., Williamson, B. H. & Dagnia, H. T. Seals, Seal Trainers, and Mycobacterial Infection. *American Review of Respiratory Disease* **147**, 164–167 (1993).

20. Nebreda, T., Álvarez-Prida, E., Blanco, B., Remacha, M. A., Samper, S. & Jiménez, M. S. Peritoneal tuberculosis due to Mycobacterium caprae. *IDCases* **4**, 50–52 (2016).

21. Pfyffer, G. E., Auckenthaler, R., Van Embden, J. D. A. & Van Soolingen, D. Mycobacterium canettii, the smooth variant of M. tuberculosis, isolated from a Swiss patient exposed in Africa. *Emerging Infectious Diseases* **4**, 631–634 (1998).

22. Koch Robert. The etiology of tuberculosis. *Reviews of Infectious Diseases* **4**, 1270–1274 (1982).

23. Ehrlich, P. A method for staining the tubercle bacillus. *Deutsche Mediznische Wochenschrift* **8**, 269–270 (1882).

24. Brennan, P. J. & Nikaido, H. The Envelope of Mycobacteria. *Annual Review of Biochemistry* **64**, 29–63 (1995).

25. M. Cistina, G., Brisse, S., Brosch, R., Fabre, M., Omaïs, B., Marmiesse, M., Supply, P. & Vincent, V. Ancient origin and gene mosaicism of the progenitor of Mycobacterium tuberculosis. *PLoS Pathogens* **1**, 0055–0061 (2005).

26. Hayman, J. Mycobacterium Ulcerans: an Infection From Jurassic Time? *The Lancet* **324**, 1015–1016 (1984).

27. Kappelman, J., Alçiçek, M. C., Kazanci, N., Schultz, M., Özkul, M. & Şen, Ş. Brief Communication: First Homo erectus from Turkey and Implications for Migrations into Temperate Eurasia. *American Journal of Physical Anthropology* **135**, 110–116 (2008).

28. Kapur, V., Whittam, T. S. & Musser, J. M. Is mycobacterium tuberculosis 15, 000 years old? *Journal of Infectious Diseases* **170**, 1348–1349 (1994).

29. Brosch, R., Gordon, S. V., Marmiesse, M., Brodin, P., Buchrieser, C., Eiglmeier, K., Garnier, T., Gutierrez, C., Hewinson, G., Kremer, K., Parsons, L. M., Pym, A. S., Samper, S., van Soolingen, D. & Cole, S. T. A new evolutionary scenario for the Mycobacterium tuberculosis complex. *Proceeding of the National Academy of Sciences* **99**, 3684–3689 (2002).

30. Hershkovitz, I., Donoghue, H. D., Minnikin, D. E., Besra, G. S., Lee, O. Y. C., Gernaey, A. M., Galili, E., Eshed, V., Greenblatt, C. L., Lemma, E., Bar-Gal, G. K. & Spigelman, M. Detection and molecular characterization of 9000-year-old Mycobacterium tuberculosis from a neolithic settlement in the Eastern mediterranean. *PLoS ONE* **3**, (2008).

31. Zink, A., Haas, C. J., Reischl, U., Szeimies, U. & Nerlich, A. G. Molecular analysis of skeletal tuberculosis in an ancient egyptian population. *Journal of Medical Microbiology* **50**, 355–366 (2001).

32. Hippocrates. *Book 1 - Of the Epidemics (460-370 BCE)*. *The Genuine Works of Hippocrates* vol. 1 (1849).

33. Barberis, I., Bragazzi, N. L., Galluzzo, L. & Martini, M. The history of tuberculosis: From the first historical records to the isolation of Koch's bacillus. *Journal of Preventive Medicine and Hygiene* vol. 58 E9–E12 (2017).

34. Herzog, H. History of Tuberculosis. *Respiration* **65**, 5–15 (1998).

35. Doetsch, R. N. Benjamin Marten and his New Theory of Consumptions'. *Microbiological Reviews* **42**, 521–528 (1978).

36. Dobson, J. Percivall Pott. *Annals of the Royal College of Surgeons of England* **50**, 54–65 (1972).

37. Moore, T. *The Works of Lord Byron: With His Letters and Journals, and His Life*. (John Murray, Albemarle Street, 1835).

38. Riedel, S. Edward Jenner and the History of Smallpox and Vaccination. *Baylor University Medical Center Proceedings* **18**, 21–25 (2005).

39. Calmette, A. *L'infection bacillaire et la tuberculose, chez l'homme et chez les animaux*. *British Journal of Tuberculosis* vol. 31 (1937).

40. Luca, S. & Mihaescu, T. *History of BCG Vaccine*. *Maedica A Journal of Clinical Medicine* vol. 8 (2013).

41. Dockrell, H. M. & Smith, S. G. What have we learnt about BCG vaccination in the last 20 years? *Frontiers in Immunology* vol. 8 1134 (2017).

42. Cohn, D. L. The effect of BCG vaccination on tuberculin skin testing: Does it matter? *American Journal of Respiratory and Critical Care Medicine* **164**, 915–916 (2001).

43. Schatz, A., Bugle, E. & Waksman, S. A. Streptomycin, a Substance Exhibiting Antibiotic Activity Against Gram-Positive and Gram-Negative Bacteria. *Experimental Biology and Medicine* **55**, 66–69 (1944).

44. Lehmann, J. Determination of Pathogenicity of Tubercle Bacilli By Their Intermediate Metabolism. *The Lancet* **247**, 14–15 (1946).

45. Lehmann, J. Para-Aminosalicylic Acid in the Treatment of Tuberculosis. *Postgraduate Medical Journal* **24**, 455–462 (1946).

46. Robitzek, E. H., Selikoff, I. J. & Ornstein, G. G. Chemotherapy of human tuberculosis with hydrazine derivatives of isonicotinic acid; preliminary report of representative cases. *Quarterly bulletin of Sea View Hospital* **13**, 27–51 (1952).

47. Malone, L., Schurr, A., Lindh, H., McKenzie, D., Kiser, J. S. & Williams, J. H. The Effect of Pyrazinamide (Aldinamide) on Experimental Tuberculosis in Mice. *Ameircan Review of Tuberculosis and Pulmonary Diseases* **65**, 511–518 (1952).

48. Karlson, A. G. The in Vitro Activity of Ethambutol (Dextro-2,2′-[Ethylenediimino]-Di-l-Butanol) Against Tubercle Bacilli and Other Microorganisms. *American Review of Respiratory Disease* 905–906 (1961) doi:10.1164/ARRD.1961.84.6.905.

49. Maggi, N., Pallanza, R. & Sensi, P. New Derivatives of Rifamycin SV. *Antimicrobial Agents and Chemotherapy* 765–769 (1966).

50. Maggi, N., Pasqualucci, C. R., Ballotta, R. & Sensi, P. Rifampicin: A New Orally Active Rifamycin. *Chemotherapia* **11**, 285–292 (1966).

51. Cole, S. T., Brosch, R., Parkhill, J., Garnier, T., Churcher, C., Harris, D., Gordon, S. V., Eiglmeier, K., Gas, S., Barry, C. E., Tekaia, F., Badcock, K., Basham, D., Brown, D., Chillingworth, T., Connor, R., Davies, R., Devlin, K., Feltwell, T., *et al.* Deciphering the biology of mycobacterium tuberculosis from the complete genome sequence. *Nature* **393**, 537–544 (1998).

52. World Health Organisation. *Global Tuberculosis Report 2019*. (2019).

53. World Health Organisation. *Global Tuberculosis Report 2016*. http://apps.who.int/iris/bitstream/handle/10665/250441/9789241565394-eng.pdf?sequence=1 (2016) doi:10.1183/09031936.00188313.

54. World Health Organisation. *Global Tuberculosis Report 2017*. http://apps.who.int/iris/bitstream/handle/10665/259366/9789241565516-eng.pdf?sequence=1 (2017) doi:WHO/HTM/TB/2017.23.

55. Migliori, G. B., De Iaco, G., Besozzi, G., Centis, R. & Cirillo, D. M. First tuberculosis cases in Italy resistant to all tested drugs. *Euro surveillance* **12**, (2007).

56. Velayati, A. A., Masjedi, M. R., Farnia, P., Tabarsi, P., Ghanavi, J., ZiaZarifi, A. H. & Hoffner, S. E. Emergence of New Forms of Totally Drug-Resistant Tuberculosis Bacilli. *Chest* **136**, 420–425 (2009).

57. Udwadia, Z. F., Amale, R. A., Ajbani, K. K. & Rodrigues, C. Totally drug-resistant tuberculosis in India. *Clinical Infectious Diseases* vol. 54 579–581 (2012).

58. Udwadia, Z. & Vendoti, D. Totally drug-resistant tuberculosis (TDR-TB) in India: Every dark cloud has a silver lining. *Journal of Epidemiology and Community Health* **67**, 471–472 (2013).

59. Klopper, M., Warren, R. M., Hayes, C., van Pittius, N. C. G., Streicher, E. M., Müller, B., Sirgel, F. A., Chabula-Nxiweni, M., Hoosain, E., Coetzee, G., van

Helden, P. D., Victor, T. C. & Trollip, A. P. Emergence and spread of extensively and totally drug-resistant tuberculosis, South Africa. *Emerging Infectious Diseases* **19**, 449–455 (2013).

60. World Health Organisation. WHO | Drug-resistant TB: Totally drug-resistant TB FAQ. https://www.who.int/tb/areas-of-work/drug-resistant-tb/totally-drug-resistant-tb-faq/en/ (2018).

61. Zumla, A., Raviglione, M., Hafner, R. & Fordham von Reyn, C. Tuberculosis. *New England Journal of Medicine* **368**, 745–755 (2013).

62. Campbell, I. A. & Bah-Sow, O. Pulmonary tuberculosis: diagnosis and treatment. *BMJ* **332**, 1194–1197 (2006).

63. Miller, L. G., Asch, S. M., Yu, E. I., Knowles, L., Gelberg, L. & Davidson, P. A Population-Based Survey of Tuberculosis Symptoms: How Atypical Are Atypical Presentations? *Clinical Infectious Diseases* **30**, 293–299 (2000).

64. Golden, M. P. & Vikram, H. R. Extrapulmonary tuberculosis: An overview. *American Family Physician* **72**, 1761–1768 (2005).

65. Moulis, G. & Martin-Blondel, G. Scrofula, the king's evil. *Canadian Medical Association Journal* **184**, 1061 (2012).

66. Zhai, K., Lu, Y. & Shi, H.-Z. Tuberculous pleural effusion. *Journal of Thoracic Disease* **8**, E486–E494 (2016).

67. Sharma, S. K., Mohan, A. & Sharma, A. Challenges in the diagnosis & treatment of miliary tuberculosis. *The Indian journal of medical research* **135**, 703–30 (2012).

68. Mani, M. & Jayanthi, N. V. G. A case of miliary tuberculosis with tuberculous meningitis in intensive care. *Anaesthesia* **64**, 802–803 (2009).

69. del Giudice, P., Bernard, E., Perrin, C., Bernardin, G., Fouche, R., Boissy, C., Durant, J. & Dellamonica, P. Unusual Cutaneous Manifestations of Miliary Tuberculosis. *Clinical Infectious Diseases* **30**, 201–204 (2000).

70. Annamalai, R. & Biswas, J. Bilateral choroidal tuberculoma in miliary tuberculosis - report of a case. *Journal of Ophthalmic Inflammation and Infection* **5**, 4 (2015).

71. Pigrau-Serrallach, C. & Rodríguez-Pardo, D. Bone and joint tuberculosis. *European Spine Journal* **22**, 556–566 (2013).

72. Hunter, R. L. Pathology of post primary tuberculosis of the lung: An illustrated critical review. *Tuberculosis* **91**, 497–509 (2011).

73. Smith, I. Mycobacterium tuberculosis pathogenesis and molecular determinants of virulence. *Clinical Microbiology Reviews* vol. 16 463–496 (2003).

74. Modlin, R. L. & Bloom, B. R. TB or not TB: That is no longer the question. *Science Translational Medicine* **5**, 1–16 (2013).

75. Getahun, H., Matteelli, A., Chaisson, R. E. & Raviglione, M. Latent Mycobacterium tuberculosis Infection. *New England Journal of Medicine* **372**, 2127–2135 (2015).

76. Lipscomb, M. F. & Masten, B. J. Dendritic Cells: Immune Regulators in Health and Disease. *Physiological Reviews* **82**, 97–130 (2002).

77. Pagán, A. J. & Ramakrishnan, L. Immunity and Immunopathology in the Tuberculous Granuloma. *Cold Spring Harbor Perspectives in Medicine* **5**, a018499 (2015).

78. Dimitrakopoulos, I., Zouloumis, L., Lazaridis, N., Karakasis, D., Trigonidis, G. & Sichletidis, L. Primary tuberculosis of the oral cavity. *Oral Surgery, Oral Medicine, Oral Pathology and Oral Radiology* **72**, 712–715 (1991).

79. Jain, P. & Puwar, P. Primary tuberculosis of tongue. *Journal of Association of Physicians of India* **64**, 78–79 (2016).

80. Sasikumar, S., Ayub, I. I., Kannan, S. & Swaminathan, R. Primary tonsillar tuberculosis. *BMJ Case Reports* **2018**, bcr-2017-223634 (2018).

81. Marten, R. H. Primary Tuberculosis of the Skin. *Proceedings of the Royal Society of Medicine* **49**, 424–425 (1956).

82. Altaf Mir, M., Ahmad, I. & Yaseen, M. Primary Tuberculosis of Hand Soft Tissue. *World journal of plastic surgery* **5**, 313–318 (2016).

83. Saleh, M., Saeedi, A. A. & Pooran, A. A. Brain tuberculomas: A case report. *Jundishapur Journal of Microbiology* **7**, 11252 (2014).

84. Kumar, R., Kshetrimayum, S., Kumar, S. & Garg, R. Primary Tuberculosis of Breast: a Rare Presentation. *Journal of Case Reports* **7**, 127–129 (2017).

85. Syed, T. A., Salem, G., Rubin, E. & Guild, R. Not everything that glitters in the terminal ileum is Crohn's: Primary Tuberculosis of the Appendix. *Journal of Gastroenterology and Hepatobiliary Disorders* **3**, 1–3 (2017).

86. Niyogi, D., Goel, M., Shinde, R. S. & Patkar, S. Primary hepatic tuberculosis: A rare occurrence. *Annals of Hepato-Biliary-Pancreatic Surgery* **23**, 80 (2019).

87. Calabrò, E. & Pastorino, U. Primary sternal tuberculosis mimicking a lytic bone tumor lesion. *Monaldi Archives for Chest Disease* **88**, 87–89 (2018).

88. Phyu, S., Mustafa, T., Hofstad, T., Nilsen, R., Fosse, R. & Bjune, G. A mouse model for latent tuberculosis. *Scandinavian Journal of Infectious Diseases* **30**, 59–68 (1998).

89. Kassaza, K., Orikiriza, P., Llosa, A., Bazira, J., Nyehangane, D., Page, A. L. & Boum, Y. Lowenstein-Jensen selective medium for reducing contamination in Mycobacterium tuberculosis culture. *Journal of Clinical Microbiology* **52**, 2671–2673 (2014).

90. WHO. *Implementing tuberculosis diagnostics*. http://www.who.int/tb/publications/implementing_TB_diagnostics/en/ (2015) doi:WHO/HTM/TB/2015.11.

91. Yang, H., Kruh-Garcia, N. A. & Dobos, K. M. Purified Protein Derivatives of Tuberculin - Past, Present, and Future. *FEMS Immunology and Medical Microbiology* **66**, 273–280 (2012).

92. Nayak, S. & Acharjya, B. Mantoux test and its interpretation. *Indian*

Dermatology Online Journal **3**, 2 (2012).

93. World Health Organisation. *Chest Radiography in Tuberculosis*. *WHO Press* http://www.who.int/about/licensing/copyright_form%0Ahttp://www.who.int/about/licensing/copyright_form) (2016) doi:ISBN 978 92 4 151150 6.

94. World Health Organisation. *The use of molecular line probe assays for the detection of resistance to second-line anti-tuberculosis drugs*. (2016).

95. Stop TB Department. *Rapid Implementation of the Xpert MTB / RIF diagnostic test*. *World Health* (2011). doi:WHO/HTM/TB/2011.2.

96. Pai, M., Denkinger, C. M., Kik, S. V., Rangaka, M. X., Zwerling, A., Oxlade, O., Metcalfe, J. Z., Cattamanchi, A., Dowdy, D. W., Dheda, K. & Banaei, N. Gamma interferon release assays for detection of Mycobacterium tuberculosis infection. *Clinical Microbiology Reviews* **27**, 3–20 (2014).

97. Lalvani, A. & Pareek, M. Interferon gamma release assays: principles and practice. *Enfermedades Infecciosas y Microbiología Clínica* **28**, 245–252 (2010).

98. Pai, M., Zwerling, A. & Menzies, D. Systematic review: T-cell-based assays for the diagnosis of latent tuberculosis infection: An update. *Annals of Internal Medicine* **149**, 177–184 (2008).

99. WHO. *Use of tuberculosis release assays (IGRAs) in low and middle-income countries*. *World Health Organization Policy Statement* (2011).

100. Broger, T., Sossen, B., du Toit, E., Kerkhoff, A. D., Schutz, C., Ivanova Reipold, E., Ward, A., Barr, D. A., Macé, A., Trollip, A., Burton, R., Ongarello, S., Pinter, A., Lowary, T. L., Boehme, C., Nicol, M. P., Meintjes, G. & Denkinger, C. M. Novel lipoarabinomannan point-of-care tuberculosis test for people with HIV: a diagnostic accuracy study. *The Lancet Infectious Diseases* **19**, 852–861 (2019).

101. World Health Organisation. *The use of lateral flow urine lipoarabinomannan assay (LF-LAM) for the diagnosis and screening of active tuberculosis in people living with HIV*. www.who.int (2015).

102. World Health Organisation. *Treatment of Tuberculosis Guidelines*. (World Health Organisation Press, 2010). doi:10.1164/rccm.201012-1949OC.

103. World Health Organization. *Consolidated Guidelines on Tuberculosis Treatment*. (World Health Organisation Press, 2019).

104. Streptomycin treatment of pulmonary tuberculosis. *British medical journal* **2**, 769–82 (1948).

105. Cox, E. C., White, J. R. & Flaks, J. G. Streptomycin action and the ribosome. *Proceeding of the National Academy of Sciences* **51**, 703–709 (1964).

106. Davies, J., Gilbert, W. & Gorini, L. Streptomycin, Suppression, and the Code. *Proceedings of the National Academy of Sciences of the United States of* **51**, 883–890 (1964).

107. Abad, J. P. & Amils, R. Location of the streptomycin ribosomal binding site explains its pleiotropic effects on protein biosynthesis. *Journal of Molecular Biology* vol. 235 1251–1260 (1994).

108. Ruusala, T. & Kurland, C. G. Streptomycin preferentially perturbs ribosomal proofreading. *MGG Molecular & General Genetics* **198**, 100–104 (1984).

109. Smailov, S. K. & Gavrilova, L. P. Effect of streptomycin on the stoichiometry of GTP hydrolysis in a poly(U)-dependent cell-free translation systerm. *FEBS* **192**, 165–169 (1985).

110. Demirci, H., Murphy, F., Murphy, E., Gregory, S. T., Dahlberg, A. E. & Jogl, G. A structural basis for streptomycin-induced misreading of the genetic code. *Nature Communications* **4**, 1355–1358 (2013).

111. Villellas, C., Aristimuño, L., Vitoria, M. A., Prat, C., Blanco, S., De Viedma, D. G., Domínguez, J., Samper, S. & Aínsa, J. A. Analysis of mutations in streptomycin-resistant strains reveals a simple and reliable genetic marker for identification of the Mycobacterium tuberculosis Beijing genotype. *Journal of Clinical Microbiology* **51**, 2124–2130 (2013).

112. Wong, S. Y., Lee, J. S., Kwak, H. K., Via, L. E., Boshoff, H. I. M. & Barry, C. E. Mutations in gidB confer low-level streptomycin resistance in Mycobacterium tuberculosis. *Antimicrobial Agents and Chemotherapy* **55**, 2515–2522 (2011).

113. Ramón-García, S., Mick, V., Dainese, E., Martín, C., Thompson, C. J., De Rossi, E., Manganelli, R. & Aínsa, J. A. Functional and genetic characterization of the tap efflux pump in Mycobacterium bovis BCG. *Antimicrobial Agents and Chemotherapy* **56**, 2074–2083 (2012).

114. FOX, H. H. Synthetic Tuberculostats. III. Isonicotinaldehyde Thiosemicarbazone and some Related Compounds. *The Journal of Organic Chemistry* **17**, 555–562 (1952).

115. Selikoff, I. J. & Robitzek, E. H. Tuberculosis chemotherapy with hydrazine derivatives of isonicotinic acid. *Diseases of the chest* **21**, 385–438 (1952).

116. Zhang, Y., Heym, B., Allen, B., Young, D. & Cole, S. The catalase-peroxidase gene and isoniazid resistance of Mycobacterium tuberculosis. *Nature* **358**, 591–593 (1992).

117. Banerjee, A., Dubnau, E., Quemard, A., Balasubramanian, V., Um, K. S., Wilson, T., Collins, D., De Lisle, G. & Jacobs, W. R. inhA, a gene encoding a target for isoniazid and ethionamide in Mycobacterium tuberculosis. *Science* **263**, 227–230 (1994).

118. Quémard, A., Sacchettini, J. C., Dessen, A., Vilcheze, C., Bittman, R., Jacobs, W. R. & Blanchard, J. S. Enzymatic Characterization of the Target for Isoniazid in Mycobacterium tuberculosis. *Biochemistry* **34**, 8235–8241 (1995).

119. Rozwarski, D. A., Grant, G. A., Barton, D. H. R., Jacobs, W. R. & Sacchettini, J. C. Modificafion of the NADH of the lsoniazid Target (InhA) from Mycobacterium tuberculosis. *Science* **279**, 19–23 (1998).

120. Zhang, Y. & Yew, W. Mechanisms of drug resistance in Mycobacterium tuberculosis. *International Journal of Tuberculosis and Lung Disease* **13**, 1320–1330 (2009).

121. Chorine, V. Action de l'amide nicotinique sur les bacilles du genre Mycobacterium. *Comptes rendus de l'Académie des Sciences* **220**, 150–151

(1945).

122. Zhang, Y. & Mitchison, D. The curious characteristics of pyrazinamide: A review. *International Journal of Tuberculosis and Lung Disease* **7**, 6–21 (2003).

123. Scorpio, A. & Zhang, Y. Mutations in pncA, a gene encoding pyrazinamidase/nicotinamidase, cause resistance to the antituberculous drug pyrazinamide in tubercle bacillus. *Nature Medicine* **2**, 662–667 (1996).

124. Zhang, Y., Scorpio, A., Nikaido, H. & Sun, Z. Role of Acid pH and Deficient Efflux of Pyrazinoic Acid in Unique Susceptibility of Mycobacterium tuberculosis to Pyrazinamide. *Microbiology* **181**, 2044–2049 (1999).

125. Zhang, Y., Wade, M. M., Scorpio, A., Zhang, H. & Sun, Z. Mode of action of pyrazinamide: Disruption of Mycobacterium tuberculosis membrane transport and energetics by pyrazinoic acid. *Journal of Antimicrobial Chemotherapy* **52**, 790–795 (2003).

126. Zhang, Y., Shi, W., Zhang, W. & Mitchison, D. Mechanisms of Pyrazinamide Action and Resistance. *Microbiology Spectrum* **2**, 1–12 (2014).

127. Shi, W., Zhang, X., Jiang, X., Ruan, H., Barry, C. E., Wang, H., Zhang, W. & Zhang, Y. Pyrazinamide inhibits trans-translation in Mycobacterium tuberculosis. *Science* **333**, 1630–1632 (2011).

128. Yang, J., Liu, Y., Bi, J., Cai, Q., Liao, X., Li, W., Guo, C., Zhang, Q., Lin, T., Zhao, Y., Wang, H., Liu, J., Zhang, X. & Lin, D. Structural basis for targeting the ribosomal protein S1 of Mycobacterium tuberculosis by pyrazinamide. *Molecular Microbiology* **95**, 791–803 (2015).

129. Keiler, K. C. Biology of trans -Translation . *Annual Review of Microbiology* **62**, 133–151 (2008).

130. Dillon, N. A., Peterson, N. D., Feaga, H. A., Keiler, K. C. & Baughn, A. D. Anti-tubercular Activity of Pyrazinamide is Independent of trans-Translation and RpsA. *Scientific Reports* **7**, 1–8 (2017).

131. Raynaud, C., Lanéelle, M. A., Senaratne, R. H., Draper, P., Lanéelle, G. & Daffé, M. Mechanisms of pyrazinamide resistance in mycobacteria: Importance of lack of uptake in addition to lack of pyrazinamidase activity. *Microbiology* **145**, 1359–1367 (1999).

132. Konno, K., Feldmann, F. M. & McDermott, W. Pyrazinamide susceptibility and amidase activity of tubercle bacilli. *American Review of Respiratory Disease* **95**, 461–469 (1967).

133. Hirano, K., Takahashi, M., Kazumi, Y., Fukasawa, Y. & Abe, C. Mutation in pncA is a major mechanism of pyrazinamide resistance in Mycobacterium tuberculosis. *Tubercle and Lung Disease* **78**, 117–122 (1998).

134. Juréen, P., Werngren, J., Toro, J. C. & Hoffner, S. Pyrazinamide resistance and pncA gene mutations in Mycobacterium tuberculosis. *Antimicrobial Agents and Chemotherapy* **52**, 1852–1854 (2008).

135. Takayama, K. & Kilburn, J. O. Inhibition of synthesis of arabinogalactan by ethambutol in Mycobacterium smegmatis. *Antimicrobial Agents and*

Chemotherapy **33**, 1493–1499 (1989).

136. Mikusová, K., Slayden, R. A., Besra, G. S. & Brennan, P. J. Biogenesis of the mycobacterial cell wall and the site of action of ethambutol . Biogenesis of the Mycobacterial Cell Wall and the Site of Action of Ethambutol. *Antimicrobial Agents and Chemotherapy* **39**, 2484–2489 (1995).

137. Zhang, N., Torrelles, J. B., McNeil, M. R., Escuyer, V. E., Khoo, K. H., Brennan, P. J. & Chatterjee, D. The Emb proteins of mycobacteria direct arabinosylation of lipoarabinomannan and arabinogalactan via an N-terminal recognition region and a C-terminal synthetic region. *Molecular Microbiology* **50**, 69–76 (2003).

138. Sassetti, C. M. & Rubin, E. J. Genetic requirements for mycobacterial survival during infection. *Proceedings of the National Academy of Sciences* **100**, 12989–12994 (2003).

139. Amin, A. G., Goude, R., Shi, L., Zhang, J., Chatterjee, D. & Parish, T. EmbA is an essential arabinosyltransferase in Mycobacterium tuberculosis. *Microbiology* **154**, 240–248 (2008).

140. Griffin, J. E., Gawronski, J. D., DeJesus, M. A., Ioerger, T. R., Akerley, B. J. & Sassetti, C. M. High-resolution phenotypic profiling defines genes essential for mycobacterial growth and cholesterol catabolism. *PLoS Pathogens* **7**, 1–9 (2011).

141. Shi, L., Berg, S., Lee, A., Spencer, J. S., Zhang, J., Vissa, V., McNeil, M. R., Khoo, K. H. & Chatterjee, D. The carboxy terminus of EmbC from Mycobacterium smegmatis mediates chain length extension of the arabinan in lipoarabinomannan. *Journal of Biological Chemistry* **281**, 19512–19526 (2006).

142. Alderwick, L. J., Lloyd, G. S., Ghadbane, H., May, J. W., Bhatt, A., Eggeling, L., Fütterer, K. & Besra, G. S. The C-terminal domain of the arabinosyltransferase mycobacterium tuberculosis EmbC is a lectin-like carbohydrate binding module. *PLoS Pathogens* **7**, (2011).

143. Alderwick, L. J., Radmacher, E., Seidel, M., Gande, R., Hitchen, P. G., Morris, H. R., Dell, A., Sahm, H., Eggeling, L. & Besra, G. S. Deletion of Cg-emb in corynebacterianeae leads to a novel truncated cell wall arabinogalactan, whereas inactivation of Cg-ubiA results in an Arabinan-deficient mutant with a cell wall galactan core. *Journal of Biological Chemistry* **280**, 32362–32371 (2005).

144. Alderwick, L. J., Seidel, M., Sahm, H., Besra, G. S. & Eggeling, L. Identification of a novel arabinofuranosyltransferase (AftA) involved in cell wall arabinan biosynthesis in Mycobacterium tuberculosis. *Journal of Biological Chemistry* **281**, 15653–15661 (2006).

145. Sreevatsan, S., Stockbauer, K. E., Pan, X., Kreiswirth, B. N., Moghazeh, S. L., Jacobs, W. R., Telenti, A. & Musser, J. M. Ethambutol resistance in Mycobacterium tuberculosis: Critical role of embB mutations. *Antimicrobial Agents and Chemotherapy* **41**, 1677–1681 (1997).

146. Zhao, L. L., Sun, Q., Liu, H. C., Wu, X. C., Xiao, T. Y., Zhao, X. Q., Li, G. L., Jiang, Y., Zeng, C. Y. & Wan, K. L. Analysis of embCAB mutations associated with ethambutol resistance in multidrug-resistant mycobacterium tuberculosis isolates from China. *Antimicrobial Agents and Chemotherapy* **59**, 2045–2050 (2015).

147. Sensi, P., Greco, A. M. & Ballotta, R. Rifomycins. I. Isolation and Properties of Rifomycin B and Rifomycin Complex. *Antibiotic Annual 1959-1960* 262–270 (1960).

148. Lechevalier, M. P., Prauser, H., Labeda, D. P. & Ruan, J. S. Two new genera of nocardioform actinomycetes: Amycolata gen. nov. and Amycolatopsis gen. nov. *International Journal of Systematic Bacteriology* **36**, 29–37 (1986).

149. Wehrli, W. & Staehelin, M. Actions of the rifamycins. *Bacteriological reviews* **35**, 290–309 (1971).

150. Sensi, P., Maggi, N., Fürész, S. & Maffi, G. Chemical Modifications and Biological Properties of Rifamycins. *Antimicrobial Agents and Chemotherapy* 699–714 (1966).

151. Sensi, P. History of the Development of Rifampin. *Reviews of Infectious Disease* **5**, (1983).

152. Hartmann, G., Honikel, K. O., Knüsel, F. & Nüesch, J. The specific inhibition of the DNA-directed RNA synthesis by rifamycin. *BBA Section Nucleic Acids And Protein Synthesis* **145**, 843–844 (1967).

153. Umezawa, H., Mizuno, S., Yamazaki, H. & Nitta, K. Inhibition of DNA-Dependent RNA Synthesis by Rifamycins. *The Journal of Antibiotics* **21**, 234–236 (1968).

154. Telenti, A., Imboden, P., Marchesi, F., Matter, L., Schopfer, K., Bodmer, T., Lowrie, D., Colston, M. J. & Cole, S. Detection of rifampicin-resistance mutations in Mycobacterium tuberculosis. *The Lancet* **341**, 647–651 (1993).

155. McClure, W. R. & Cech, C. L. On the mechanism of rifampicin inhibition of RNA synthesis. *Journal of Biological Chemistry* **253**, 8949–8956 (1978).

156. Campbell, E. A., Korzheva, N., Mustaev, A., Murakami, K., Nair, S., Goldfarb, A. & Darst, S. A. Structural mechanism for rifampicin inhibition of bacterial RNA polymerase. *Cell* **104**, 901–912 (2001).

157. Taniguchi, H., Aramaki, H., Nikaido, Y., Mizuguchi, yasuo, Nakamura, M., Koga, T. & Yoshida, S. Rifampicin resistance and mutation of the *rpoB* gene in *Mycobacterium tuberculosis*. *FEMS Microbiology Letters* **144**, 103–108 (1996).

158. Molodtsov, V., Scharf, N. T., Stefan, M. A., Garcia, G. A. & Murakami, K. S. Structural basis for rifamycin resistance of bacterial RNA polymerase by the three most clinically important RpoB mutations found in Mycobacterium tuberculosis. *Molecular Microbiology* **103**, 1034–1045 (2017).

159. Lesher, G. Y., Froelich, E. J., Gruett, M. D., Bailey, J. H. & Brundage, R. P. 1,8-Naphthyridine Derivatives. A New Class of Chemotherapeutic Agents. *Journal of Medicinal Chemistry* **5**, 1063–1065 (1962).

160. Goss, W. A., Deitz, W. H. & Cook, T. M. Mechanism of Action of Nalidixic Acid on Escherichia coli. II. Inhibition of Deoxyribonucleic Acid Synthesis. *Journal of bacteriology* **89**, 1068–74 (1965).

161. Crumplin, G. C. & Smith, J. T. Nalidixic acid and bacterial chromosome replication. *Nature* **260**, 643–645 (1976).

162. Kampranis, S. C., Bates, A. D. & Maxwell, A. A model for the mechanism of strand passage by DNA gyrase. *Proceeding of the National Academy of Sciences* **96**, 8414–8419 (1999).

163. Laponogov, I., Sohi, M. K., Veselkov, D. A., Pan, X. S., Sawhney, R., Thompson, A. W., McAuley, K. E., Fisher, L. M. & Sanderson, M. R. Structural insight into the quinolone-DNA cleavage complex of type IIA topoisomerases. *Nature Structural and Molecular Biology* **16**, 667–669 (2009).

164. Blower, T. R., Williamson, B. H., Kerns, R. J. & Berger, J. M. Crystal structure and stability of gyrase-fluoroquinolone cleaved complexes from Mycobacterium tuberculosis. *Proceedings of the National Academy of Sciences* **113**, 1706–1713 (2016).

165. Maruri, F., Sterling, T. R., Kaiga, A. W., Blackman, A., van der heijden, Y. F., Mayer, C., Cambau, E. & Aubry, A. A systematic review of gyrase mutations associated with fluoroquinolone-resistant Mycobacterium tuberculosis and a proposed gyrase numbering system. *Journal of Antimicrobial Chemotherapy* **67**, 819–831 (2012).

166. ModolfllL, J. & Vazquez, D. The Inhibition of Ribosomal Translocation by Viomycin. *European Journal of Biochemistry* **81**, 491–497 (1977).

167. Holm, M., Borg, A., Ehrenberg, M. & Sanyal, S. Molecular mechanism of viomycin inhibition of peptide elongation in bacteria. *Proceedings of the National Academy of Sciences* **113**, 978–983 (2016).

168. Lin, Y., Li, Y., Zhu, N., Han, Y., Jiang, W., Wang, Y., Si, S. & Jiang, J. The antituberculosis antibiotic capreomycin inhibits protein synthesis by disrupting interaction between ribosomal proteins L12 and L10. *Antimicrobial Agents and Chemotherapy* **58**, 2038–2044 (2014).

169. Donald, P. R. & Diacon, A. H. Para-aminosalicylic acid: The return of an old friend. *The Lancet Infectious Diseases* **15**, 1091–1099 (2015).

170. Zheng, J., Rubin, E. J., Bifani, P., Mathys, V., Lim, V., Au, M., Jang, J., Nam, J., Dick, T., Walker, J. R., Pethe, K. & Camacho, L. R. Para-aminosalicylic acid is a prodrug targeting dihydrofolate reductase in mycobacterium tuberculosis. *Journal of Biological Chemistry* **288**, 23447–23456 (2013).

171. Blanco, J., Coque, J. J. R. & Martin, J. F. The folate branch of the methionine biosynthesis pathway in Streptomyces lividans: Disruption of the 5,10-methylenetetrahydrofolate reductase gene leads to methionine auxotrophy. *Journal of Bacteriology* **180**, 1586–1591 (1998).

172. Wang, F., Langley, R., Gulten, G., Dover, L. G., Besra, G. S., Jacobs, W. R. & Sacchettini, J. C. Mechanism of thioamide drug action against tuberculosis and leprosy. *Journal of Experimental Medicine* **204**, 73–78 (2007).

173. Quemard, A., Laneelle, G. & Lacave, C. Mycolic acid synthesis: A target for ethionamide in mycobacteria? *Antimicrobial Agents and Chemotherapy* **36**, 1316–1321 (1992).

174. Heath, R. J., Rubin, J. R., Holland, D. R., Zhang, E., Snow, M. E. & Rock, C. O. Mechanism of Triclosan Inhibition of Bacterial Fatty Acid Synthesis. *Journal of*

Biological Chemistry **274**, 11110–11114 (1999).

175. Halouska, S., Chacon, O., Fenton, R. J., Zinniel, D. K., Barletta, R. G. & Powers, R. Use of NMR metabolomics to analyze the targets of D-cycloserine in mycobacteria: Role of D-alanine racemase. *Journal of Proteome Research* **6**, 4608–4614 (2007).

176. Lambert, M. P. & Neuhaus, F. C. Mechanism of D-cycloserine action: alanine racemase from Escherichia coli W. *Journal of Bacteriology* **110**, 978–987 (1972).

177. David, H. L., Takayama, K. & Goldman, D. S. Susceptibility of mycobacterial D-alanyl-D-alanine synthetase to D-cycloserine. *American Review of Respiratory Disease* **100**, 579–581 (1969).

178. Bruning, J. B., Murillo, A. C., Chacon, O., Barletta, R. G. & Sacchettini, J. C. Structure of the Mycobacterium tuberculosis D-alanine:D-alanine ligase, a target of the antituberculosis drug D-cycloserine. *Antimicrobial Agents and Chemotherapy* **55**, 291–301 (2011).

179. Halouska, S., Fenton, R. J., Zinniel, D. K., Marshall, D. D., Barletta, R. G. & Powers, R. Metabolomics analysis identifies D-alanine-D-alanine ligase as the primary lethal target of D-cycloserine in mycobacteria. *Journal of Proteome Research* **13**, 1065–1076 (2014).

180. Mulubwa, M. & Mugabo, P. Amount of Cycloserine Emanating from Terizidone Metabolism and Relationship with Hepatic Function in Patients with Drug-Resistant Tuberculosis. *Drugs in R and D* **19**, 289–296 (2019).

181. Kurz, S. G. & Bonomo, R. A. Reappraising the use of β-lactams to treat tuberculosis. *Expert Review of Anti-Infective Therapy* vol. 10 999–1006 (2012).

182. Pandey, S. D., Pal, S., N, G. K., Bansal, A., Mallick, S. & Ghosh, A. S. Two DD-carboxypeptidases from Mycobacterium smegmatis affect cell surface properties through regulation of peptidoglycan cross-linking and glycopeptidolipids. *Journal of Bacteriology* **200**, (2018).

183. Wang, F., Cassidy, C. & Sacchettini, J. C. Crystal structure and activity studies of the Mycobacterium tuberculosis β-lactamase reveal its critical role in resistance to β-lactam antibiotics. *Antimicrobial Agents and Chemotherapy* **50**, 2762–2771 (2006).

184. Sanders, C. C., Sanders, W. E., Thomson, K. S. & Iaconis, J. P. Meropenem: Activity against resistant gram-negative bacteria and interactions with β-lactamases. *Journal of Antimicrobial Chemotherapy* **24**, 187–196 (1989).

185. Labia, R., Morand, A. & Guionie, M. ß-Lactamase stability of imipenem. *Journal of Antimicrobial Chemotherapy* **18**, 1–8 (1986).

186. Norrby, S. R. Imipenem/cilastatin: rationale for a fixed combination. *Reviews of Infectious Diseases* **7**, 447–451 (1985).

187. Lechartier, B. & Cole, S. T. Mode of action of clofazimine and combination therapy with benzothiazinones against Mycobacterium tuberculosis. *Antimicrobial Agents and Chemotherapy* **59**, 4457–4463 (2015).

188. Mazzei, T., Mini, E., Novelli, A. & Periti, P. Chemistry and mode of action of

macrolides. *Journal of Antimicrobial Chemotherapy* **31**, 1–9 (1993).

189. Garza-Ramos, G., Xiong, L., Zhong, P. & Mankin, A. Binding site of macrolide antibiotics on the ribosome: New resistance mutation identifies a specific interaction of ketolides with rRNA. *Journal of Bacteriology* **183**, 6898–6907 (2001).

190. Leclercq, R. Mechanisms of Resistance to Macrolides and Lincosamides: Nature of the Resistance Elements and Their Clinical Implications. *Antimicrobial Resistance* **34**, 482–492 (2002).

191. Conradie, F., Diacon, A. H., Ngubane, N., Howell, P., Everitt, D., Crook, A. M., Mendel, C. M., Egizi, E., Moreira, J., Timm, J., McHugh, T. D., Wills, G. H., Bateson, A., Hunt, R., Van Niekerk, C., Li, M., Olugbosi, M. & Spigelman, M. Treatment of Highly Drug-Resistant Pulmonary Tuberculosis. *New England Journal of Medicine* **382**, 893–902 (2020).

192. Koul, A., Vranckx, L., Dendouga, N., Balemans, W., Van den Wyngaert, I., Vergauwen, K., Göhlmann, H. W. H., Willebrords, R., Poncelet, A., Guillemont, J., Bald, D. & Andries, K. Diarylquinolines Are Bactericidal for Dormant Mycobacteria as a Result of Disturbed ATP Homeostasis. *Journal of Biological Chemistry* **283**, 25273–25280 (2008).

193. Haagsma, A. C., Podasca, I., Koul, A., Andries, K., Guillemont, J., Lill, H. & Bald, D. Probing the Interaction of the Diarylquinoline TMC207 with Its Target Mycobacterial ATP Synthase. *PLoS ONE* **6**, e23575 (2011).

194. Worley, M. V. & Estrada, S. J. Bedaquiline: A novel antitubercular agent for the treatment of multidrug-resistant tuberculosis. *Pharmacotherapy* **34**, 1187–1197 (2014).

195. Manjunatha, U., Boshoff, H. I. & Barry, C. E. The mechanism of action of PA-824. *Communicative & Integrative Biology* **2**, 215–218 (2009).

196. Lewis, J. M. & Sloan, D. J. The role of delamanid in the treatment of drug-resistant tuberculosis. *Therapeutics and Clinical Risk Management* **11**, 779–791 (2015).

197. Shinabarger, D. L., Marotti, K. R., Murray, R. W., Lin, A. H., Melchior, E. P., Swaney, S. M., Dunyak, D. S., Demyan, W. F. & Buysse, J. M. Mechanism of action of oxazolidinones: effects of linezolid and eperezolid on translation reactions. *Antimicrobial Agents and Chemotherapy* **41**, 2132–2136 (1997).

198. Hashemian, S. M., Farhadi, T. & Ganjparvar, M. Linezolid: a review of its properties, function, and use in critical care. *Drug Design, Development and Therapy* **12**, 1759–1767 (2018).

199. Lechevalier, M. P. & Lechevalier, H. Chemical composition as a criterion in the classification of aerobic actinomycetes. *International Journal of Systematic Bacteriology* **20**, 435–443 (1970).

200. Schlesinger, L. S., Hull, S. R. & Kaufman, T. M. Binding of the terminal mannosyl units of lipoarabinomannan from a virulent strain of Mycobacterium tuberculosis to human macrophages. *Journal of immunology* **152**, 4070–9 (1994).

201. Nigou, J., Gilleron, M., Rojas, M., García, L. F., Thurnher, M. & Puzo, G.

Mycobacterial lipoarabinomannans: Modulators of dendritic cell function and the apoptotic response. *Microbes and Infection* **4**, 945–953 (2002).

202. Maeda, N., Nigou, J., Herrmann, J.-L., Jackson, M., Amara, A., Lagrange, P. H., Puzo, G., Gicquel, B. & Neyrolles, O. The Cell Surface Receptor DC-SIGN Discriminates between Mycobacterium Species through Selective Recognition of the Mannose Caps on Lipoarabinomannan. *Journal of Biological Chemistry* **278**, 5513–5516 (2003).

203. Vollmer, W., Blanot, D. & De Pedro, M. A. Peptidoglycan structure and architecture. *FEMS Microbiology Reviews* vol. 32 149–167 (2008).

204. Mahapatra, S., Scherman, H., Brennan, P. J. & Crick, D. C. N glycolylation of the nucleotide precursors of peptidoglycan biosynthesis of Mycobacterium spp. is altered by drug treatment. *Journal of Bacteriology* **187**, 2341–2347 (2005).

205. Schleifer, K. H. & Kandler, O. Peptidoglycan types of bacterial cell walls and their taxonomic implications. *Bacteriological reviews* **36**, 407–477 (1972).

206. Lavollay, M., Arthur, M., Fourgeaud, M., Dubost, L., Marie, A., Veziris, N., Blanot, D., Gutmann, L. & Mainardi, J. L. The peptidoglycan of stationary-phase Mycobacterium tuberculosis predominantly contains cross-links generated by L,D-transpeptidation. *Journal of Bacteriology* **190**, 4360–4366 (2008).

207. Kumar, P., Arora, K., Lloyd, J. R., Lee, I. Y., Nair, V., Fischer, E., Boshoff, H. I. M. & Barry, C. E. Meropenem inhibits D,D-carboxypeptidase activity in Mycobacterium tuberculosis. *Molecular Microbiology* **86**, 367–381 (2012).

208. Mahapatra, S., Yagi, T., Belisle, J. T., Espinosa, B. J., Hill, P. J., McNeil, M. R., Brennan, P. J. & Crick, D. C. Mycobacterial lipid II is composed of a complex mixture of modified muramyl and peptide moieties linked to decaprenyl phosphate. *Journal of Bacteriology* **187**, 2747–2757 (2005).

209. Zhang, Z., Bulloch, E. M. M., Bunker, R. D., Baker, E. N. & Squire, C. J. Structure and function of GlmU from Mycobacterium tuberculosis. *Acta Crystallographica Section D: Biological Crystallography* **65**, 275–283 (2009).

210. De Smet, K. A. L., Kempsell, K. E., Gallagher, A., Duncan, K. & Young, D. B. Alteration of a single amino acid residue reverses fosfomycin resistance of recombinant MurA from Mycobacterium tuberculosis. *Microbiology* **145**, 3177–3184 (1999).

211. Eniyan, K., Dharavath, S., Vijayan, R., Bajpai, U. & Gourinath, S. Crystal structure of UDP-N-acetylglucosamine-enolpyruvate reductase (MurB) from Mycobacterium tuberculosis. *Biochimica et Biophysica Acta - Proteins and Proteomics* **1866**, 397–406 (2018).

212. Raymond, J. B., Mahapatra, S., Crick, D. C. & Pavelka, M. S. Identification of the namH gene, encoding the hydroxylase responsible for the N-glycolylation of the mycobacterial peptidoglycan. *Journal of Biological Chemistry* **280**, 326–333 (2005).

213. Kurosu, M., Mahapatra, S., Narayanasamy, P. & Crick, D. C. Chemoenzymatic synthesis of Park's nucleotide: toward the development of high-throughput screening for MraY inhibitors. *Tetrahedron Letters* **48**, 799–803 (2007).

214. Munshi, T., Gupta, A., Evangelopoulos, D., Guzman, J. D., Gibbons, S., Keep, N. H. & Bhakta, S. Characterisation of ATP-Dependent Mur Ligases Involved in the Biogenesis of Cell Wall Peptidoglycan in Mycobacterium tuberculosis. *PLoS ONE* **8**, 60143 (2013).

215. Chen, K. T., Chen, P. T., Lin, C. K., Huang, L. Y., Hu, C. M., Chang, Y. F., Hsu, H. T., Cheng, T. J. R., Wu, Y. T. & Cheng, W. C. Structural Investigation of Park's Nucleotide on Bacterial Translocase MraY: Discovery of Unexpected MraY Inhibitors. *Scientific Reports* **6**, (2016).

216. Mengin-Lecreulx, D., Texier, L., Rousseau, M. & Van Heijenoort, J. The murG gene of Escherichia coli codes for the UDP-N-acetylglucosamine:N-acetylmuramyl-(pentapeptide) pyrophosphoryl-undecaprenol N-acetylglucosamine transferase involved in the membrane steps of peptidoglycan synthesis. *Journal of Bacteriology* **173**, 4625–4636 (1991).

217. Ruiz, N. Bioinformatics identification of MurJ (MviN) as the peptidoglycan lipid II flippase in Escherichia coli. *Proceedings of the National Academy of Sciences* **105**, 15553–15557 (2008).

218. Ruiz, N. Lipid flippases for bacterial peptidoglycan biosynthesis. *Lipid Insights* **8**, 21–31 (2015).

219. Mohammadi, T., Van Dam, V., Sijbrandi, R., Vernet, T., Zapun, A., Bouhss, A., Diepeveen-De Bruin, M., Nguyen-Distéche, M., De Kruijff, B. & Breukink, E. Identification of FtsW as a transporter of lipid-linked cell wall precursors across the membrane. *EMBO Journal* **30**, 1425–1432 (2011).

220. Sham, L. T., Butler, E. K., Lebar, M. D., Kahne, D., Bernhardt, T. G. & Ruiz, N. MurJ is the flippase of lipid-linked precursors for peptidoglycan biogenesis. *Science* **345**, 220–222 (2014).

221. Leclercq, S., Derouaux, A., Olatunji, S., Fraipont, C., Egan, A. J. F., Vollmer, W., Breukink, E. & Terrak, M. Interplay between Penicillin-binding proteins and SEDS proteins promotes bacterial cell wall synthesis. *Scientific Reports* **7**, 1–13 (2017).

222. Zheng, S., Sham, L.-T., Rubino, F. A., Brock, K. P., Robins, W. P., Mekalanos, J. J., Marks, D. S., Bernhardt, T. G. & Kruse, A. C. Structure and mutagenic analysis of the lipid II flippase MurJ from Escherichia coli. *Proceedings of the National Academy of Sciences* **115**, 6709–6714 (2018).

223. Meeske, A. J., Riley, E. P., Robins, W. P., Uehara, T., Mekalanos, J. J., Kahne, D., Walker, S., Kruse, A. C., Bernhardt, T. G. & Rudner, D. Z. SEDS proteins are a widespread family of bacterial cell wall polymerases. *Nature* **537**, 634–638 (2016).

224. Emami, K., Guyet, A., Kawai, Y., Devi, J., Wu, L. J., Allenby, N., Daniel, R. A. & Errington, J. RodA as the missing glycosyltransferase in Bacillus subtilis and antibiotic discovery for the peptidoglycan polymerase pathway. *Nature microbiology* **2**, 1–8 (2017).

225. Taguchi, A., Welsh, M. A., Marmont, L. S., Lee, W., Sjodt, M., Kruse, A. C., Kahne, D., Bernhardt, T. G. & Walker, S. FtsW is a peptidoglycan polymerase that is functional only in complex with its cognate penicillin-binding protein.

Nature Microbiology vol. 4 587–594 (2019).

226. Kuk, A. C. Y., Hao, A., Guan, Z. & Lee, S. Y. Visualizing conformation transitions of the Lipid II flippase MurJ. *Nature Communications* **10**, 1–12 (2019).

227. Kumar, S., Rubino, F. A., Mendoza, A. G. & Ruiz, N. The bacterial lipid II flippase MurJ functions by an alternating-access mechanism. *Journal of Biological Chemistry* **294**, 981–990 (2019).

228. Patru, M. M. & Pavelka, M. S. A role for the class a penicillin-binding protein PonA2 in the survival of Mycobacterium smegmatis under conditions of nonreplication. *Journal of Bacteriology* **192**, 3043–3054 (2010).

229. Kieser, K. J., Boutte, C. C., Kester, J. C., Baer, C. E., Barczak, A. K., Meniche, X., Chao, M. C., Rego, E. H., Sassetti, C. M., Fortune, S. M. & Rubin, E. J. Phosphorylation of the Peptidoglycan Synthase PonA1 Governs the Rate of Polar Elongation in Mycobacteria. *PLoS Pathogens* **11**, 1–28 (2015).

230. Böth, D., Steiner, E. M., Stadler, D., Lindqvist, Y., Schnell, R. & Schneider, G. Structure of Ldt Mt2 , an L , D -transpeptidase from Mycobacterium tuberculosis. *Acta Crystallographica Section D Biological Crystallography* **69**, 432–441 (2013).

231. McNeil, M., Wallner, S. J., Hunter, S. W. & Brennan, P. J. Demonstration that the galactosyl and arabinosyl residues in the cell-wall arabinogalactan of Mycobacterium leprae and Myobacterium tuberculosis are furanoid. *Carbohydrate Research* **166**, 299–308 (1987).

232. Daffé, M., Brennan, P. J. & McNeil, M. Predominant Structural features of The Cell wall arabinogalactan of Mycobacterium fragments by gas chromatography / mass Predominant Structural Features of the Cell Wall Arabinogalactan Mycobacterium tuberculosis as Revealed through Characterization Oligo. *The Journal of antimicrobial chemotherapy* **265**, 6734–6743 (1990).

233. Harrison, J., Lloyd, G., Joe, M., Lowary, T. L., Reynolds, E., Walters-Morgan, H., Bhatt, A., Lovering, A., Besra, G. S. & Alderwick, L. J. Lcp1 is a phosphotransferase responsible for ligating arabinogalactan to peptidoglycan in Mycobacterium tuberculosis. *mBio* **7**, 1–12 (2016).

234. Besra, G. S., Khoo, K.-H., McNeil, M. R., Dell, A., Morris, H. R. & Brennan, P. J. A New Interpretation of the Structure of the Mycolyl—Arabinogalactan Complex of Mycobacterium Tuberculosis as Revealed Through Characterization of Oligoglycosylalditol Fragments by Fast-Atom Bombardment Mass Spectrometry and 1H Nuclear Magnetic Resonance . *Biochemistry* **34**, 4257–4266 (1995).

235. McNeil, M., Daffe, M. & Brennan, P. J. Location of the mycolyl ester substituents in the cell walls of mycobacteria. *Journal of Biological Chemistry* **266**, 13217–13223 (1991).

236. Draper, P., Khoo, K. H., Chatterjee, D., Dell, A. & Morris, H. R. Galactosamine in walls of slow-growing mycobacteria. *Biochemical Journal* **327**, 519–525 (1997).

237. Lee, A., Wu, S. W., Scherman, M. S., Torrelles, J. B., Chatterjee, D., McNeil, M. R. & Khoo, K. H. Sequencing of oligoarabinosyl units released from mycobacterial arabinogalactan by endogenous arabinanase: Identification of distinctive and novel structural motifs. *Biochemistry* **45**, 15817–15828 (2006).

238. Škovierová, H., Larrouy-Maumus, G., Pham, H., Belanová, M., Barilone, N., DasGupta, A., Mikušová, K., Gicquel, B., Gilleron, M., Brennan, P. J., Puzo, G., Nigou, J. & Jackson, M. Biosynthetic origin of the galactosamine substituent of arabinogalactan in Mycobacterium tuberculosis. *Journal of Biological Chemistry* **285**, 41348–41355 (2010).

239. Peng, W., Zou, L., Bhamidi, S., McNeil, M. R. & Lowary, T. L. The galactosamine residue in mycobacterial arabinogalactan is α-linked. *Journal of Organic Chemistry* **77**, 9826–9832 (2012).

240. Bhamidi, S., Scherman, M. S., Rithner, C. D., Prenni, J. E., Chatterjee, D., Khoo, K. H. & McNeil, M. R. The identification and location of succinyl residues and the characterization of the interior arabinan region allow for a model of the complete primary structure of Mycobacterium tuberculosis mycolyl arabinogalactan. *Journal of Biological Chemistry* **283**, 12992–13000 (2008).

241. Jin, Y., Xin, Y., Zhang, W. & Ma, Y. Mycobacterium tuberculosis Rv1302 and Mycobacterium smegmatis MSMEG-4947 have WecA function and MSMEG-4947 is required for the growth of M. smegmatis. *FEMS Microbiology Letters* **310**, 54–61 (2010).

242. Mills, J. A., Motichka, K., Jucker, M., Wu, H. P., Uhlik, B. C., Stern, R. J., Scherman, M. S., Vissa, V. D., Pan, F., Kundu, M., Yu, F. M. & McNeil, M. Inactivation of the mycobacterial rhamnosyltransferase, which is needed for the formation of the arabinogalactan-peptidoglycan linker, leads to irreversible loss of viability. *Journal of Biological Chemistry* **279**, 43540–43546 (2004).

243. Ma, Y., Pan, F. & McNeil, M. Formation of dTDP-rhamnose is essential for growth of mycobacteria. *Journal of Bacteriology* **184**, 3392–3395 (2002).

244. Mikušová, K., Beláňová, M., Korduláková, J., Honda, K., McNeil, M. R., Mahapatra, S., Crick, D. C. & Brennan, P. J. Identification of a novel galactosyl transferase involved in biosynthesis of the mycobacterial cell wall. *Journal of Bacteriology* **188**, 6592–6598 (2006).

245. Alderwick, L. J., Dover, L. G., Veerapen, N., Gurcha, S. S., Kremer, L., Roper, D. L., Pathak, A. K., Reynolds, R. C. & Besra, G. S. Expression, purification and characterisation of soluble GlfT and the identification of a novel galactofuranosyltransferase Rv3782 involved in priming GlfT-mediated galactan polymerisation in Mycobacterium tuberculosis. *Protein Expression and Purification* **58**, 332–341 (2008).

246. Belánová, M., Dianišková, P., Brennan, P. J., Completo, G. C., Rose, N. L., Lowary, T. L. & Mikušova, K. Galactosyl transferases in mycobacterial cell wall synthesis. *Journal of Bacteriology* **190**, 1141–1145 (2008).

247. Kremer, L., Dover, L. G., Morehouse, C., Hitchin, P., Everett, M., Morris, H. R., Dell, A., Brennan, P. J., McNeil, M. R., Flaherty, C., Duncan, K. & Besra, G. S. Galactan biosynthesis in Mycobacterium tuberculosis: Identification of a

bifunctional UDP-galactofuranosyltransferase. *Journal of Biological Chemistry* **276**, 26430–26440 (2001).

248. Rose, N. L., Completo, G. C., Lin, S. J., McNeil, M., Palcic, M. M. & Lowary, T. L. Expression, purification, and characterization of a galactofuranosyltransferase involved in Mycobacterium tuberculosis arabinogalactan biosynthesis. *Journal of the American Chemical Society* **128**, 6721–6729 (2006).

249. Dianišková, P., Korduláḱová, J., Sǩovierová, H., Kaur, D., Jackson, M., Brennan, P. J. & Mikusŏvá, K. Investigation of ABC transporter from mycobacterial arabinogalactan biosynthetic cluster. *General Physiology and Biophysics* **30**, 239–250 (2011).

250. Alderwick, L. J., Lloyd, G. S., Lloyd, A. J., Lovering, A. L., Eggeling, L. & Besra, G. S. Biochemical characterization of the Mycobacterium tuberculosis phosphoribosyl-1-pyrophosphate synthetase. *Glycobiology* **21**, 410–425 (2011).

251. Huang, H., Scherman, M. S., D'Haeze, W., Vereecke, D., Holsters, M., Crick, D. C. & McNeil, M. R. Identification and active expression of the Mycobacterium tuberculosis gene encoding 5-phospho-α-D-ribose-1-diphosphate: Decaprenyl-phosphate 5-phosphoribosyltransferase, the first enzyme committed to decaprenylphosphoryl- D-arabinose synthesis. *Journal of Biological Chemistry* **280**, 24539–24543 (2005).

252. Huang, H., Berg, S., Spencer, J. S., Vereecke, D., D'Haeze, W., Holsters, M. & McNeil, M. R. Identification of amino acids and domains required for catalytic activity of DPPR synthase, a cell wall biosynthetic enzyme of Mycobacterium tuberculosis. *Microbiology* **154**, 736–743 (2008).

253. Jiang, T., He, L., Zhan, Y., Zang, S., Ma, Y., Zhao, X., Zhang, C. & Xin, Y. The effect of MSMEG_6402 gene disruption on the cell wall structure of Mycobacterium smegmatis. *Microbial Pathogenesis* **51**, 156–160 (2011).

254. Mikušová, K., Huang, H., Yagi, T., Holsters, M., Vereecke, D., D'Haeze, W., Scherman, M. S., Brennan, P. J., McNeil, M. R. & Crick, D. C. Decaprenylphosphoryl arabinofuranose, the donor of the D-arabinofuranosyl residues of mycobacterial arabinan, is formed via a two-step epimerization of decaprenylphosphoryl ribose. *Journal of Bacteriology* **187**, 8020–8025 (2005).

255. Alderwick, L. J., Seidel, M., Sahm, H., Besra, G. S. & Eggeling, L. Identification of a novel arabinofuranosyltransferase (AftA) involved in cell wall arabinan biosynthesis in Mycobacterium tuberculosis. *Journal of Biological Chemistry* **281**, 15653–15661 (2006).

256. Birch, H. L., Alderwick, L. J., Bhatt, A., Rittmann, D., Krumbach, K., Singh, A., Bai, Y., Lowary, T. L., Eggeling, L. & Besra, G. S. Biosynthesis of mycobacterial arabinogalactan: Identification of a novel α(1→3) arabinofuranosyltransferase. *Molecular Microbiology* **69**, 1191–1206 (2008).

257. Škovierová, H., Larrouy-Maumus, G., Zhang, J., Kaur, D., Barilone, N., Korduláková, J., Gilleron, M., Guadagnini, S., Belanová, M., Prevost, M. C., Gicquel, B., Puzo, G., Chatterjee, D., Brennan, P. J., Nigou, J. & Jackson, M. AftD, a novel essential arabinofuranosyltransferase from mycobacteria. *Glycobiology* **19**, 1235–1247 (2009).

258. Seidel, M., Alderwick, L. J., Birch, H. L., Sahm, H., Eggeling, L. & Besra, G. S. Identification of a novel arabinofuranosyltransferase AftB involved in a terminal step of cell wall arabinan biosynthesis in Corynebacterianeae, such as Corynebacterium glutamicum and Mycobacterium tuberculosis. *Journal of Biological Chemistry* **282**, 14729–14740 (2007).

259. Scherman, H., Kaur, D., Pham, H., Škovierová, H., Jackson, M. & Brennan, P. J. Identification of a polyprenylphosphomannosyl synthase involved in the synthesis of mycobacterial mannosides. *Journal of Bacteriology* **191**, 6769–6772 (2009).

260. Rana, A. K., Singh, A., Gurcha, S. S., Cox, L. R., Bhatt, A. & Besra, G. S. Ppm1-Encoded Polyprenyl Monophosphomannose Synthase Activity Is Essential for Lipoglycan Synthesis and Survival in Mycobacteria. *PLoS ONE* **7**, 48211 (2012).

261. Liu, J., Barry, C. E., Besra, G. S. & Nikaido, H. Mycolic Acid Structure Determines the Fluidity of the Mycobacterial Cell Wall. *Journal of Biological Chemistry* **271**, 29545–29551 (1996).

262. Watanabe, M., Aoyagi, Y., Ridell, M. & Minnikin, D. E. Separation and characterization of individual mycolic acids in representative mycobacteria. *Microbiology* **147**, 1825–1837 (2001).

263. Watanabe, M., Aoyagi, Y., Mitome, H., Fujita, T., Naoki, H., Ridell, M. & Minnikin, D. E. Location of functional groups in mycobacterial meromycolate chains; the recognition of new structural principles in mycolic acids. *Microbiology* **148**, 1881–1902 (2002).

264. Kremer, L., Nampoothiri, K. M., Lesjean, S., Dover, L. G., Graham, S., Betts, J., Brennan, P. J., Minnikin, D. E., Locht, C. & Besra, G. S. Biochemical Characterization of Acyl Carrier Protein (AcpM) and Malonyl-CoA:AcpM Transacylase (mtFabD), Two Major Components of Mycobacterium tuberculosis Fatty Acid Synthase II. *Journal of Biological Chemistry* **276**, 27967–27974 (2001).

265. Choi, K. H., Kremer, L., Besra, G. S. & Rock, C. O. Identification and substrate specificity of β-Ketoacyl [Acyl carrier protein] synthase III (mtFabH) from mycobacterium tuberculosis. *Journal of Biological Chemistry* **275**, 28201–28207 (2000).

266. Marrakchi, H., Ducasse, S., Labesse, G., Montrozier, H., Margeat, E., Emorine, L., Charpentier, X., Daffé, M. & Quémard, A. MabA (FabG1), a Mycobacterium tuberculosis protein involved in the long-chain fatty acid elongation system FAS-II. *Microbiology* **148**, 951–960 (2002).

267. Sacco, E., Covarrubias, A. S., O'Hare, H. M., Carroll, P., Eynard, N., Jones, T. A., Parish, T., Daffé, M., Bäckbro, K. & Quémard, A. The missing piece of the type II fatty acid synthase system from Mycobacterium tuberculosis. *Proceedings of the National Academy of Sciences* **104**, 14628–14633 (2007).

268. Schaeffer, M. L., Agnihotri, G., Volker, C., Kallender, H., Brennan, P. J. & Lonsdale, J. T. Purification and Biochemical Characterization of the Mycobacterium tuberculosis β-Ketoacyl-acyl Carrier Protein Synthases KasA and KasB. *Journal of Biological Chemistry* **276**, 47029–47037 (2001).

269. Kremer, L., Dover, L. G., Carrère, S., Nampoothiri, K. M., Lesjean, S., Brown, A. K., Brennan, P. J., Minnikin, D. E., Locht, C. & Besra, G. S. Mycolic acid biosynthesis and enzymic characterization of the β-ketoacyl-ACP synthase A-condensing enzyme from Mycobacterium tuberculosis. *Biochemical Journal* **364**, 423–430 (2002).

270. Dubnau, E., Chan, J., Raynaud, C., Mohan, V. P., Lanéelle, M.-A., Yu, K., Quémard, A., Smith, I. & Daffé, M. Oxygenated mycolic acids are necessary for virulence of Mycobacterium tuberculosis in mice. *Molecular Microbiology* **36**, 630–637 (2000).

271. Glickman, M. S., Cox, J. S. & Jacobs, W. R. A Novel Mycolic Acid Cyclopropane Synthetase Is Required for Cording, Persistence, and Virulence of Mycobacterium tuberculosis. *Molecular Cell* **5**, 717–727 (2000).

272. Glickman, M. S. The mmaA2 Gene of Mycobacterium tuberculosis Encodes the Distal Cyclopropane Synthase of the α-Mycolic Acid. *Journal of Biological Chemistry* **278**, 7844–7849 (2003).

273. Barkan, D., Rao, V., Sukenick, G. D. & Glickman, M. S. Redundant Function of cmaA2 and mmaA2 in Mycobacterium tuberculosis cis Cyclopropanation of Oxygenated Mycolates. *Journal of Bacteriology* **192**, 3661–3668 (2010).

274. Trivedi, O. A., Arora, P., Sridharan, V., Tickoo, R., Mohanty, D. & Gokhale, R. S. Enzymic activation and transfer of fatty acids as acyl-adenylates in mycobacteria. *Nature* **428**, 441–445 (2004).

275. Gande, R., Gibson, K. J. C., Brown, A. K., Krumbach, K., Dover, L. G., Sahm, H., Shioyama, S., Oikawa, T., Besra, G. S. & Eggeling, L. Acyl-CoA Carboxylases (accD2 and accD3), Together with a Unique Polyketide Synthase (Cg-pks), Are Key to Mycolic Acid Biosynthesis in Corynebacterianeae Such as Corynebacterium glutamicum and Mycobacterium tuberculosis. *Journal of Biological Chemistry* **279**, 44847–44857 (2004).

276. Portevin, D., de Sousa-D'Auria, C., Houssin, C., Grimaldi, C., Chami, M., Daffe, M. & Guilhot, C. A polyketide synthase catalyzes the last condensation step of mycolic acid biosynthesis in mycobacteria and related organisms. *Proceedings of the National Academy of Sciences* **101**, 314–319 (2004).

277. Bhatt, A., Brown, A. K., Singh, A., Minnikin, D. E. & Besra, G. S. Loss of a Mycobacterial Gene Encoding a Reductase Leads to an Altered Cell Wall Containing β-oxo- Mycolic Acid Analogs and Accumulation of Ketones. *Chemistry & Biology* **15**, 930–939 (2008).

278. Xu, Z., Meshcheryakov, V. A., Poce, G. & Chng, S.-S. MmpL3 is the flippase for mycolic acids in mycobacteria. *Proceedings of the National Academy of Sciences* **114**, 7993–7998 (2017).

279. Takayama, K., Wang, C. & Besra, G. S. Pathway to Synthesis and Processing of Mycolic Acids in Mycobacterium tuberculosis. *Clinical Microbiology Reviews* **18**, 81–101 (2005).

280. Backus, K. M., Dolan, M. A., Barry, C. S., Joe, M., McPhie, P., Boshoff, H. I. M., Lowary, T. L., Davis, B. G. & Barry, C. E. The three Mycobacterium tuberculosis antigen 85 isoforms have unique substrates and activities determined

by non-active site regions. *Journal of Biological Chemistry* **289**, 25041–25053 (2014).

281. Abrahams, K. A. & Besra, G. S. Mycobacterial cell wall biosynthesis: a multifaceted antibiotic target. *Parasitology* **145**, 1–18 (2016).

282. Ortalo-Magné, A., Lemassu, A., Lanéelle, M. A., Bardou, F., Silve, G., Gounon, P., Marchal, G. & Daffé, M. Identification of the surface-exposed lipids on the cell envelopes of Mycobacterium tuberculosis and other mycobacterial species. *Journal of Bacteriology* **178**, 456–461 (1996).

283. Grāve, K., Bennett, M. D. & Högbom, M. Structure of Mycobacterium tuberculosis phosphatidylinositol phosphate synthase reveals mechanism of substrate binding and metal catalysis. *Communications Biology* **2**, 1–11 (2019).

284. Ballou, C. E., Vilkas, E. & Lederer, E. Structural studies on the myo-inositol phospholipids of Mycobacterium tuberculosis (var. bovis, strain BCG). *The Journal of biological chemistry* **238**, 69–76 (1963).

285. Lee, Y. C. & Ballou, C. E. Structural Studies on the Myo-inositol Mannosides from the Glycolipids of Mycobacterium tuberculosis and Mycobacterium phlei. *Journal of Biological Chemistry* **239**, 1316–1327 (1964).

286. Nigou, J., Gilleron, M., Brando, T. & Puzo, G. Structural Analysis of Mycobacterial Lipoglycans. *Applied Biochemistry and Biotechnology* **118**, 253–268 (2004).

287. Korduláková, J., Gilleron, M., Mikušová, K., Puzo, G., Brennan, P. J., Gicquel, B. & Jackson, M. Definition of the First Mannosylation Step in Phosphatidylinositol Mannoside Synthesis. *Journal of Biological Chemistry* **277**, 31335–31344 (2002).

288. Guerin, M. E., Kordulakova, J., Schaeffer, F., Svetlikova, Z., Buschiazzo, A., Giganti, D., Gicquel, B., Mikusova, K., Jackson, M. & Alzari, P. M. Molecular recognition and interfacial catalysis by the essential phosphatidylinositol mannosyltransferase PimA from mycobacteria. *Journal of Biological Chemistry* **282**, 20705–20714 (2007).

289. Guerin, M. E., Kaur, D., Somashekar, B. S., Gibbs, S., Gest, P., Chatterjee, D., Brennan, P. J. & Jackson, M. New insights into the early steps of phosphatidylinositol mannoside biosynthesis in mycobacteria: PimB′ is an essential enzyme of Mycobacterium smegmatis. *Journal of Biological Chemistry* **284**, 25687–25696 (2009).

290. Korduláková, J., Gilleron, M., Puzo, G., Brennan, P. J., Gicquel, B., Mikušová, K. & Jackson, M. Identification of the Required Acyltransferase Step in the Biosynthesis of the Phosphatidylinositol Mannosides of Mycobacterium Species. *Journal of Biological Chemistry* **278**, 36285–36295 (2003).

291. Kremer, L., Gurcha, S. S., Bifani, P., Hitchen, P. G., Baulard, A., Morris, H. R., Dell, A., Brennan, P. J. & Besra, G. S. Characterization of a putative α-mannosyltransferase involved in phosphatidylinositol trimannoside biosynthesis in Mycobacterium tuberculosis. *Biochemical Journal* **363**, 437–447 (2002).

292. Gurcha, S. S., Baulard, A. R., Kremer, L., Locht, C., Moody, D. B., Muhlecker,

W., Costello, C. E., Crick, D. C., Brennan, P. J. & Besra, G. S. Ppm1, a novel polyprenol monophosphomannose synthase from Mycobacterium tuberculosis. *Biochemical Journal* **365**, 441–450 (2002).

293. Berg, S., Kaur, D., Jackson, M. & Brennan, P. J. The glycosyltransferases of Mycobacterium tuberculosis - Roles in the synthesis of arabinogalactan, lipoarabinomannan, and other glycoconjugates. *Glycobiology* **17**, 35–56 (2007).

294. Morita, Y. S., Sena, C. B. C., Waller, R. F., Kurokawa, K., Sernee, M. F., Nakatani, F., Haites, R. E., Billman-Jacobe, H., McConville, M. J., Maeda, Y. & Kinoshita, T. PimE is a polyprenol-phosphate-mannose-dependent mannosyltransferase that transfers the fifth mannose of phosphatidylinositol mannoside in mycobacteria. *Journal of Biological Chemistry* **281**, 25143–25155 (2006).

295. Mishra, A. K., Alderwick, L. J., Rittmann, D., Tatituri, R. V. V., Nigou, J., Gilleron, M., Eggeling, L. & Besra, G. S. Identification of an α(1→6) mannopyranosyltransferase (MptA), involved in Corynebacterium glutamicum lipomanann biosynthesis, and identification of its orthologue in Mycobacterium tuberculosis. *Molecular Microbiology* **65**, 1503–1517 (2007).

296. Mishra, A. K., Alderwick, L. J., Rittmann, D., Wang, C., Bhatt, A., Jacobs, W. R., Takayama, K., Eggeling, L. & Besra, G. S. Identification of a novel α(1→6) mannopyranosyltransferase MptB from Corynebacterium glutamicum by deletion of a conserved gene, NCgl1505, affords a lipomannan- and lipoarabinomannan-deficient mutant. *Molecular Microbiology* **68**, 1595–1613 (2008).

297. Kaur, D., Obregón-Henao, A., Pham, H., Chatterjee, D., Brennan, P. J. & Jackson, M. Lipoarabinomannan of Mycobacterium: Mannose capping by a multifunctional terminal mannosyltransferase. *Proceedings of the National Academy of Sciences* **105**, 17973–17977 (2008).

298. Mishra, A. K., Krumbach, K., Rittmann, D., Appelmelk, B., Pathak, V., Pathak, A. K., Nigou, J., Geurtsen, J., Eggeling, L. & Besra, G. S. Lipoarabinomannan biosynthesis in Corynebacterineae: The interplay of two α(1→2)-mannopyranosyltransferases MptC and MptD in mannan branching. *Molecular Microbiology* **80**, 1241–1259 (2011).

299. Birch, H. L., Alderwick, L. J., Bhatt, A., Rittmann, D., Krumbach, K., Singh, A., Bai, Y., Lowary, T. L., Eggeling, L. & Besra, G. S. Biosynthesis of mycobacterial arabinogalactan: Identification of a novel α(1→3) arabinofuranosyltransferase. *Molecular Microbiology* **69**, 1191–1206 (2008).

300. Dinadayala, P., Kaur, D., Berg, S., Amin, A. G., Vissa, V. D., Chatterjee, D., Brennan, P. J. & Crick, D. C. Genetic basis for the synthesis of the immunomodulatory mannose caps of lipoarabinomannan in Mycobacterium tuberculosis. *Journal of Biological Chemistry* **281**, 20027–20035 (2006).

301. Ludwiczak, P., Gilleron, M., Bordat, Y., Martin, C., Gicquel, B. & Puzo, G. Mycobacterium tuberculosis phoP mutant: lipoarabinomannan molecular structure. *Microbiology* **148**, 3029–3037 (2002).

302. Turnbull, W. B., Shimizu, K. H., Chatterjee, D., Homans, S. W. & Treumann, A. Identification of the 5-methylthiopentosyl substituent in Mycobacterium

tuberculosis lipoarabinomannan. *Angewandte Chemie - International Edition* **43**, 3918–3922 (2004).

303. Garnier, T., Eiglmeier, K., Camus, J. C., Medina, N., Mansoor, H., Pryor, M., Duthoy, S., Grondin, S., Lacroix, C., Monsempe, C., Simon, S., Harris, B., Atkin, R., Doggett, J., Mayes, R., Keating, L., Wheeler, P. R., Parkhill, J., Barrell, B. G., *et al.* The complete genome sequence of Mycobacterium bovis. *Proceedings of the National Academy of Sciences* **100**, 7877–7882 (2003).

304. Altaf, M., Miller, C. H., Bellows, D. S. & O'Toole, R. Evaluation of the Mycobacterium smegmatis and BCG models for the discovery of Mycobacterium tuberculosis inhibitors. *Tuberculosis* **90**, 333–337 (2010).

305. Tattoli, I., Sorbara, M. T., Vuckovic, D., Ling, A., Soares, F., Carneiro, L. A. M., Yang, C., Emili, A., Philpott, D. J. & Girardin, S. E. Amino acid starvation induced by invasive bacterial pathogens triggers an innate host defense program. *Cell Host and Microbe* **11**, 563–575 (2012).

306. Rottenberg, M. E., Gigliotti Rothfuchs, A., Gigliotti, D., Ceausu, M., Une, C., Levitsky, V. & Wigzell, H. Regulation and Role of IFN-γ in the Innate Resistance to Infection with Chlamydia pneumoniae . *The Journal of Immunology* **164**, 4812–4818 (2000).

307. Fujigaki, S., Saito, K., Takemura, M., Maekawa, N., Yamada, Y., Wada, H. & Seishima, M. L-tryptophan-L-kynurenine pathway metabolism accelerated by Toxoplasma gondii infection is abolished in gamma interferon-gene-deficient mice: Cross-regulation between inducible nitric oxide synthase and indoleamine-2,3-dioxygenase. *Infection and Immunity* **70**, 779–786 (2002).

308. Silva, N. M., Rodrigues, C. V, Santoro, M. M., Reis, L. F. L., Alvarez-Leite, J. I. & Gazzinelli, R. T. Expression of indoleamine 2,3-dioxygenase, tryptophan degradation, and kynurenine formation during in vivo infection with Toxoplasma gondii: Induction by endogenous gamma interferon and requirement of interferon regulatory factor 1. *Infection and Immunity* **70**, 859–868 (2002).

309. Zhang, Y. J., Reddy, M. C., Ioerger, T. R., Rothchild, A. C., Dartois, V., Schuster, B. M., Trauner, A., Wallis, D., Galaviz, S., Huttenhower, C., Sacchettini, J. C., Behar, S. M. & Rubin, E. J. Tryptophan biosynthesis protects mycobacteria from CD4 T-Cell-mediated Killing. *Cell* **155**, 1296–1308 (2013).

310. McAdam, R. A., Weisbrod, T. R., Martin, J., Scuderi, J. D., Brown, A. M., Cirillo, J. D., Bloom, B. R. & Jacobs, W. R. In vivo growth characteristics of leucine and methionine auxotrophic mutants of Mycobacterium bovis BCG generated by transposon mutagenesis. *Infection and Immunity* **63**, 1004–1012 (1995).

311. Awasthy, D., Gaonkar, S., Shandil, R. K., Yadav, R., Bharath, S., Marcel, N., Subbulakshmi, V. & Sharma, U. Inactivation of the ilvB1 gene in mycobacterium tuberculosis leads to branched-chain amino acid auxotrophy and attenuation of virulence in mice. *Microbiology* **155**, 2978–2987 (2009).

312. Grandoni, J. A., Marta, P. T. & Schloss, J. V. Inhibitors of branched-chain amino acid biosynthesis as potential antituberculosis agents. *Journal of Antimicrobial Chemotherapy* **42**, 475–482 (1998).

313. Hondalus, M. K., Bardarov, S., Russell, R., Chan, J., Jacobs, W. R. & Bloom, B. R. Attenuation of and Protection Induced by a Leucine Auxotroph of Mycobacterium tuberculosis Attenuation of and Protection Induced by a Leucine Auxotroph of Mycobacterium tuberculosis. *Infection and Immunity* **68**, 2888–2898 (2000).

314. Pavelka, M. S., Chen, B., Kelley, C. L., Collins, F. M. & Jacobs, W. R. Vaccine Efficacy of a Lysine Auxotroph of Mycobacterium tuberculosis. *Infection and Immunity* **71**, 4190–4192 (2003).

315. Gordhan, B. G., Smith, D. A., Alderton, H., Mcadam, R. A., Bancroft, G. J. & Mizrahi, V. Construction and Phenotypic Characterization of an Auxotrophic Mutant of Mycobacterium tuberculosis Defective in L-Arginine Biosynthesis. *Infection and Immunity* **70**, 3080–3084 (2002).

316. Berney, M., Berney-Meyer, L., Wong, K.-W., Chen, B., Chen, M., Kim, J., Wang, J., Harris, D., Parkhill, J., Chan, J., Wang, F. & Jacobs, W. R. Essential roles of methionine and S-adenosylmethionine in the autarkic lifestyle of Mycobacterium tuberculosis. *Proceeding of the National Academy of Sciences* **112**, 10008–10013 (2015).

317. Senaratne, R. H., De Silva, A. D., Williams, S. J., Mougous, J. D., Reader, J. R., Zhang, T., Chan, S., Sidders, B., Lee, D. H., Chan, J., Bertozzi, C. R. & Riley, L. W. 5′-Adenosinephosphosulphate reductase (CysH) protects Mycobacterium tuberculosis against free radicals during chronic infection phase in mice. *Molecular Microbiology* **59**, 1744–1753 (2006).

318. Smith, D., Parish, T., Stoker, N. & Bancroft, G. Characterization of Auxotrophic Mutants of Mycobacterium tuberculosis and their Potential as Vaccine Candidates. *Infection and Immunity* **69**, 1142–1150 (2001).

319. Sharma, R., Keshari, D., Singh, K. S., Yadav, S. & Singh, S. K. MRA-1571 is required for isoleucine biosynthesis and improves Mycobacterium tuberculosis H37Ra survival under stress. *Nature Scientific Reports* **6**, 1–12 (2016).

320. Parish, T. & Stoker, N. G. The common aromatic amino acid biosynthesis pathway is essential in Mycobacterium tuberculosis. *Microbiology (Reading, England)* **148**, 3069–77 (2002).

321. Parish, T. Starvation survival response of Mycobacterium tuberculosis. *Journal of Bacteriology* **185**, 6702–6706 (2003).

322. Kanehisa, M. & Goto, S. KEGG: Kyoto encyclopedia of genes and genomes. *Nucleic Acids Research* vol. 28 27–30 (1999).

323. Kanehisa, M. Toward understanding the origin and evolution of cellular organisms. *Protein Science* vol. 28 1947–1951 (2019).

324. Kanehisa, M., Sato, Y., Furumichi, M., Morishima, K. & Tanabe, M. New approach for understanding genome variations in KEGG. *Nucleic Acids Research* **47**, D590–D595 (2019).

325. Khanapur, M., Alvala, M., Prabhakar, M., Shiva Kumar, K., Edwin, R. K., Sri Saranya, P. S. V. K., Patel, R. K., Bulusu, G., Misra, P. & Pal, M. Mycobacterium tuberculosis chorismate mutase: A potential target for TB.

Bioorganic and Medicinal Chemistry **25**, 1725–1736 (2017).

326. Gordon, S., Simithy, J., Goodwin, D. C. & Calderón, A. I. Selective mycobacterium tuberculosis shikimate kinase inhibitors as potential antibacterials. *Perspectives in Medicinal Chemistry* **7**, 9–20 (2015).

327. Reichau, S., Jiao, W., Walker, S. R., Hutton, R. D., Baker, E. N. & Parker, E. J. Potent inhibitors of a shikimate pathway enzyme from Mycobacterium tuberculosis: Combining mechanism- and modeling-based design. *Journal of Biological Chemistry* **286**, 16197–16207 (2011).

328. Segura-Cabrera, A. & Rodríguez-Pérez, M. A. Structure-based prediction of Mycobacterium tuberculosis shikimate kinase inhibitors by high-throughput virtual screening. *Bioorganic and Medicinal Chemistry Letters* **18**, 3152–3157 (2008).

329. Burke, C., Abrahams, K. A., Richardson, E. J., Loman, N. J., Alemparte, C., Lelievre, J. & Besra, G. S. Development of a whole-cell high-throughput phenotypic screen to identify inhibitors of mycobacterial amino acid biosynthesis. *FASEB BioAdvances* **1**, 1–9 (2019).

330. Due, A. V, Kuper, J., Geerlof, A., Von Kries, J. P. & Wilmanns, M. Bisubstrate specificity in histidine/tryptophan biosynthesis isomerase from Mycobacterium tuberculosis by active site metamorphosis. *Proceedings of the National Academy of Sciences of the United States of America* **108**, 3554–3559 (2011).

331. Abrahams, K. A., Cox, J. A. G., Fütterer, K., Rullas, J., Ortega-Muro, F., Loman, N. J., Moynihan, P. J., Pérez-Herrán, E., Jiménez, E., Esquivias, J., Barros, D., Ballell, L., Alemparte, C. & Besra, G. S. Inhibiting mycobacterial tryptophan synthase by targeting the inter-subunit interface. *Scientific Reports* **7**, 1–15 (2017).

332. Wellington, S., Nag, P. P., Michalska, K., Johnston, S. E., Jedrzejczak, R. P., Kaushik, V. K., Clatworthy, A. E., Siddiqi, N., McCarren, P., Bajrami, B., Maltseva, N. I., Combs, S., Fisher, S. L., Joachimiak, A., Schreiber, S. L. & Hung, D. T. A small-molecule allosteric inhibitor of Mycobacterium tuberculosis tryptophan synthase. *Nature Chemical Biology* **13**, 943–950 (2017).

333. Haufroid, M. & Wouters, J. Targeting the serine pathway: A promising approach against tuberculosis? *Pharmaceuticals* **12**, 1–20 (2019).

334. Arora, G., Tiwari, P., Mandal, R. S., Gupta, A., Sharma, D., Saha, S. & Singh, R. High throughput screen identifies small molecule inhibitors specific for Mycobacterium tuberculosis phosphoserine phosphatase. *Journal of Biological Chemistry* **289**, 25149–25165 (2014).

335. Pierson, E., Haufroid, M., Gosain, T. P., Chopra, P., Singh, R. & Wouters, J. Identification and Repurposing of Trisubstituted Harmine Derivatives as Novel Inhibitors of Mycobacterium tuberculosis Phosphoserine Phosphatase. *Molecules* **25**, 1–17 (2020).

336. McCourt, J. A., Pang, S. S., Guddat, L. W. & Duggleby, R. G. Elucidating the specificity of binding of sulfonylurea herbicides to acetohydroxyacid synthase. *Biochemistry* **44**, 2330–2338 (2005).

337. Epelbaum, S., LaRossa, R. A., VanDyk, T. K., Elkayam, T., Chipman, D. M. & Barak, Z. Branched-chain amino acid biosynthesis in Salmonella typhimurium: a quantitative analysis. *Journal of Bacteriology* **180**, 4056–4067 (1998).

338. Amorim Franco, T. M. & Blanchard, J. S. Bacterial Branched-Chain Amino Acid Biosynthesis: Structures, Mechanisms, and Drugability. *Biochemistry* **56**, 5849–5865 (2017).

339. Vyazmensky, M., Sella, C., Barak, Z. & Chipman, D. M. Isolation of subunits of acetohydroxy acid synthase isozyme III and reconstitution of holoenzyme. in *Biochemistry* vol. 35 10339–10346 (1996).

340. Choi, K.-J., Yu, Y. G., Hahn, H. G., Choi, J.-D. & Yoon, M.-Y. Characterization of acetohydroxyacid synthase from Mycobacterium tuberculosis and the identification of its new inhibitor from the screening of a chemical library. *FEBS Letters* **579**, 4903–4910 (2005).

341. Singh, V., Chandra, D., Srivastava, B. S. & Srivastava, R. Biochemical and transcription analysis of acetohydroxyacid synthase isoforms in Mycobacterium tuberculosis identifies these enzymes as potential targets for drug development. *Microbiology* **157**, 29–37 (2011).

342. Murakami, K. S., Masuda, S., Campbell, E. A., Muzzin, O. & Darst, S. A. Structural basis of transcription initiation: An RNA polymerase holoenzyme-DNA complex. *Science* **296**, 1285–1290 (2002).

343. Vassylyev, D. G., Sekine, S., Laptenko, O., Lee, J., Vassylyeva, M. N., Borukhov, S. & Yokoyama, S. Crystal structure of a bacterial RNA polymerase holoenzyme at 2.6 A resolution. *Nature* **417**, 712–719 (2002).

344. Stallings, C. L., Stephanou, N. C., Chu, L., Hochschild, A., Nickels, B. E. & Glickman, M. S. CarD Is an Essential Regulator of rRNA Transcription Required for Mycobacterium tuberculosis Persistence. *Cell* **138**, 146–159 (2009).

345. Srivastava, D. B., Leon, K., Osmundson, J., Garner, A. L., Weiss, L. A., Westblade, L. F., Glickman, M. S., Landick, R., Darst, S. A., Stallings, C. L. & Campbell, E. A. Structure and function of CarD, an essential mycobacterial transcription factor. *Proceedings of the National Academy of Sciences* **110**, 12619–12624 (2013).

346. Hubin, E. A., Fay, A., Xu, C., Bean, J. M., Saecker, R. M., Glickman, M. S., Darst, S. A. & Campbell, E. A. Structure and function of the mycobacterial transcription initiation complex with the essential regulator RbpA. *eLife* **6**, 1–40 (2017).

347. Boyaci, H., Saecker, R. M. & Campbell, E. A. Transcription initiation in mycobacteria: a biophysical perspective. *Transcription* 1–13 (2019) doi:10.1080/21541264.2019.1707612.

348. Bae, B., Chen, J., Davis, E., Leon, K., Darst, S. A. & Campbell, E. A. CarD uses a minor groove wedge mechanism to stabilize the RNA polymerase open promoter complex. *eLife* **4**, 1–19 (2015).

349. Davis, E., Chen, J., Leon, K., Darst, S. A. & Campbell, E. A. Mycobacterial RNA polymerase forms unstable open promoter complexes that are stabilized by

CarD. *Nucleic Acids Research* **43**, 433–445 (2015).

350. Boyaci, H., Chen, J., Jansen, R., Darst, S. A. & Campbell, E. A. Structures of an RNA polymerase promoter melting intermediate elucidate DNA unwinding. *Nature* **565**, 382–385 (2019).

351. Sachdeva, P., Misra, R., Tyagi, A. K. & Singh, Y. The sigma factors of Mycobacterium tuberculosis: Regulation of the regulators. *FEBS Journal* **277**, 605–626 (2010).

352. Bashyam, M. D., Kaushal, D., Dasgupta, S. K. & Tyagi, A. K. A study of the mycobacterial transcriptional apparatus: Identification of novel features in promoter elements. *Journal of Bacteriology* **178**, 4847–4853 (1996).

353. Kapanidis, A. N., Margeat, E., Ho, S. O., Kortkhonjia, E., Weiss, S. & Ebright, R. H. Initial Transcription by RNA Polymerase Proceeds Through a DNA-Scrunching Mechanism. *Science* **314**, 1144–1147 (2006).

354. Revyakin, A., Liu, C., Ebright, R. H. & Strick, T. R. Abortive initiation and productive initiation by RNA polymerase involve DNA scrunching. *Science* **314**, 1139–1143 (2006).

355. Vassylyev, D. G., Vassylyeva, M. N., Perederina, A., Tahirov, T. H. & Artsimovitch, I. Structural basis for transcription elongation by bacterial RNA polymerase. *Nature* **448**, 157–162 (2007).

356. Farnham, P. J. & Platt, T. Rho-independent termination: Dyad symmetry in DNA causes RNA polymerase to pause during transcription in vitro. *Nucleic Acids Research* **9**, 563–577 (1981).

357. Epshtein, V., Dutta, D., Wade, J. & Nudler, E. An allosteric mechanism of Rho-dependent transcription termination. *Nature* **463**, 245–249 (2010).

358. Hollands, K., Sevostiyanova, A. & Groisman, E. A. Unusually long-lived pause required for regulation of a Rho-dependent transcription terminator. *Proceedings of the National Academy of Sciences* **111**, E1999–E2007 (2014).

359. Kriner, M. A. & Groisman, E. A. RNA secondary structures regulate three steps of Rho-dependent transcription termination within a bacterial mRNA leader. *Nucleic Acids Research* **45**, 631–642 (2017).

360. Hentschel, J., Burnside, C., Mignot, I., Leibundgut, M., Boehringer, D. & Ban, N. The Complete Structure of the Mycobacterium smegmatis 70S Ribosome. *Cell Reports* **20**, 149–160 (2017).

361. Yang, K., Chang, J. Y., Cui, Z., Li, X., Meng, R., Duan, L., Thongchol, J., Jakana, J., Huwe, C. M., Sacchettini, J. C. & Zhang, J. Structural insights into species-specific features of the ribosome from the human pathogen Mycobacterium tuberculosis. *Nucleic Acids Research* **45**, 10884–10894 (2017).

362. Schuwirth, B. S., Borovinskaya, M. A., Hau, C. W., Zhang, W., Vila-Sanjurjo, A., Holton, J. M. & Cate, J. H. D. Structures of the Bacterial Ribosome at 3.5 Å Resolution. *Science* **310**, 827–834 (2005).

363. Hatzopoulos, G. N. & Mueller-Dieckmann, J. Structure of translation initiation factor 1 from Mycobacterium tuberculosis and inferred binding to the 30S

ribosomal subunit. *FEBS Letters* **584**, 1011–1015 (2010).

364. Brandi, L., Marzi, S., Fabbretti, A., Fleischer, C., Hill, W. E., Gualerzi, C. O. & Lodmell, J. S. The Translation Initiation Functions of IF2: Targets for Thiostrepton Inhibition. *Journal of Molecular Biology* **335**, 881–894 (2004).

365. Petrelli, D., LaTeana, A., Garofalo, C., Spurio, R., Pon, C. L. & Gualerzi, C. O. Translation initiation factor IF3: two domains, five functions, one mechanism? *EMBO Journal* **20**, 4560–4569 (2001).

366. Sawyer, E. B., Grabowska, A. D. & Cortes, T. Survey and summary: Translational regulation in mycobacteria and its implications for pathogenicity. *Nucleic Acids Research* **46**, 6950–6961 (2018).

367. Shell, S. S., Wang, J., Lapierre, P., Mir, M., Chase, M. R., Pyle, M. M., Gawande, R., Ahmad, R., Sarracino, D. A., Ioerger, T. R., Fortune, S. M., Derbyshire, K. M., Wade, J. T. & Gray, T. A. Leaderless Transcripts and Small Proteins Are Common Features of the Mycobacterial Translational Landscape. *PLoS Genetics* **11**, 1005641 (2015).

368. Giliberti, J., O'Donnell, S., Van Etten, W. J. & Janssen, G. R. A 5′-terminal phosphate is required for stable ternary complex formation and translation of leaderless mRNA in Escherichia coli. *RNA* **18**, 508–518 (2012).

369. Moll, I., Hirokawa, G., Kiel, M. C., Kaji, A. & Bläsi, U. Translation initiation with 70S ribosomes: An alternative pathway for leaderless mRNAs. *Nucleic Acids Research* **32**, 3354–3363 (2004).

370. Sajid, A., Arora, G., Gupta, M., Singhal, A., Chakraborty, K., Nandicoori, V. K. & Singh, Y. Interaction of Mycobacterium tuberculosis elongation factor Tu with GTP is regulated by phosphorylation. *Journal of Bacteriology* **193**, 5347–5358 (2011).

371. Shoji, S., Walker, S. E. & Fredrick, K. Ribosomal translocation: One step closer to the molecular mechanism. *ACS Chemical Biology* vol. 4 93–107 (2009).

372. Kawashima, T., Berthet-Colominas, C., Wulff, M., Cusack, S. & Leberman, R. The structure of the Escherichia coli EF-Tu·EF-Ts complex at 2.5 Å resolution. *Nature* **379**, 511–518 (1996).

373. Mora, L., Zavialov, A., Ehrenberg, M. & Buckingham, R. H. Stop codon recognition and interactions with peptide release factor RF3 of truncated and chimeric RF1 and RF2 from Escherichia coli. *Molecular Microbiology* **50**, 1467–1476 (2003).

374. Andersson, S. G. E. & Sharp, P. M. Codon usage in the Mycobacterium tuberculosis complex. *Microbiology* **142**, 915–925 (1996).

375. Scolnick, E., Tompkins, R., Caskey, T. & Nirenberg, M. Release factors differing in specificity for terminator codons. *Proceedings of the National Academy of Sciences* **61**, 768–774 (1968).

376. Freistroffer, D. V, Kwiatkowski, M., Buckingham, R. H. & Ehrenberg, M. The accuracy of codon recognition by polypeptide release factors. *Proceedings of the National Academy of Sciences* **97**, 2046–2051 (2000).

377. Freistroffer, D. V., Pavlov, M. Y., MacDougall, J., Buckingham, R. H. & Ehrenberg, M. Release factor RF3 in E. coli accelerates the dissociation of release factors RF1 and RF2 from the ribosome in a GTP-dependent manner. *EMBO Journal* **16**, 4126–4133 (1997).

378. Zavialov, A. V., Buckingham, R. H. & Ehrenberg, M. A Posttermination Ribosomal Complex Is the Guanine Nucleotide Exchange Factor for Peptide Release Factor RF3. *Cell* **107**, 115–124 (2001).

379. Zavialov, A. V., Mora, L., Buckingham, R. H. & Ehrenberg, M. Release of peptide promoted by the GGQ motif of class 1 release factors regulates the GTPase activity of RF3. *Molecular Cell* **10**, 789–798 (2002).

380. Hirashima, A. & Kaji, A. Factor dependent breakdown of polysomes. *Biochemical and Biophysical Research Communications* **41**, 877–883 (1970).

381. Hirashima, A. & Kaji, A. Factor-dependent release of ribosomes from messenger RNA. Requirement for two heat-stable factors. *Journal of Molecular Biology* **65**, 43–58 (1972).

382. Hirashima, A. & Kaji, A. Purification and Properties of Ribosome-Releasing Factor. *Biochemistry* **11**, 4037–4044 (1972).

383. Hirashima, A. & Kaji, A. Role of elongation factor G and a protein factor on the release of ribosomes from messenger ribonucleic acid. *Journal of Biological Chemistry* **248**, 7580–7587 (1973).

384. Chen, Y., Kaji, A., Kaji, H. & Cooperman, B. S. The kinetic mechanism of bacterial ribosome recycling. *Nucleic Acids Research* **45**, 10168–10177 (2017).

385. Shepherd, J. & Ibba, M. Bacterial transfer RNAs. *FEMS Microbiology Reviews* vol. 39 280–300 (2015).

386. Sun, F. J. & Caetano-Anollés, G. The ancient history of the structure of ribonuclease P and the early origins of Archaea. *BMC Bioinformatics* **11**, 1–21 (2010).

387. Singh, A. & Batra, J. K. Insight into the functional role of unique determinants in RNA component of RNase P of Mycobacterium tuberculosis. *International Journal of Biological Macromolecules* **119**, 937–944 (2018).

388. Kapopoulou, A., Lew, J. M. & Cole, S. T. The MycoBrowser portal: A comprehensive and manually annotated resource for mycobacterial genomes. *Tuberculosis* **91**, 8–13 (2011).

389. Ibba, M. & Söll, D. Aminoacyl-tRNA Synthesis. *Annual Review of Biochemistry* **69**, 617–650 (2000).

390. Reynolds, N. M., Lazazzera, B. A. & Ibba, M. Cellular mechanisms that control mistranslation. *Nature Reviews Microbiology* vol. 8 849–856 (2010).

391. Gurcha, S. S., Usha, V., Cox, J. A. G., Fütterer, K., Abrahams, K. A., Bhatt, A., Alderwick, L. J., Reynolds, R. C., Loman, N. J., Nataraj, V., Alemparte, C., Barros, D., Lloyd, A. J., Ballell, L., Hobrath, J. V. & Besra, G. S. Biochemical and structural characterization of mycobacterial aspartyl-tRNA synthetase AspS, a promising TB drug target. *PLoS ONE* **9**, 1–14 (2014).

392. Palencia, A., Li, X., Bu, W., Choi, W., Ding, C. Z., Easom, E. E., Feng, L., Hernandez, V., Houston, P., Liu, L., Meewan, M., Mohan, M., Rock, F. L., Sexton, H., Zhang, S., Zhou, Y., Wan, B., Wang, Y., Franzblau, S. G., *et al.* Discovery of novel oral protein synthesis inhibitors of mycobacterium tuberculosis that target leucyl-tRNA synthetase. *Antimicrobial Agents and Chemotherapy* **60**, 6271–6280 (2016).

393. Li, X., Hernandez, V., Rock, F. L., Choi, W., Mak, Y. S. L., Mohan, M., Mao, W., Zhou, Y., Easom, E. E., Plattner, J. J., Zou, W., Pérez-Herrán, E., Giordano, I., Mendoza-Losana, A., Alemparte, C., Rullas, J., Angulo-Barturen, I., Crouch, S., Ortega, F., *et al.* Discovery of a Potent and Specific M. tuberculosis Leucyl-tRNA Synthetase Inhibitor: (S)-3-(Aminomethyl)-4-chloro-7-(2-hydroxyethoxy)benzo[c][1,2]oxaborol-1(3H)-ol (GSK656). *Journal of Medicinal Chemistry* **60**, 8011–8026 (2017).

394. Soto, R., Perez-Herran, E., Rodriguez, B., Duma, B. M., Cacho-Izquierdo, M., Mendoza-Losana, A., Lelievre, J., Aguirre, D. B., Ballell, L., Cox, L. R., Alderwick, L. J. & Besra, G. S. Identification and characterization of aspartyl-tRNA synthetase inhibitors against Mycobacterium tuberculosis by an integrated whole-cell target-based approach. *Scientific Reports* **8**, 12664 (2018).

395. Blair, R. H., Dawson, E. D., Kuck, L. R., Rowlen, K. L., Rosenblum, E. S. & Kuchta, R. D. Real-time quantification of RNA polymerase activity using a 'broken beacon'. *Analytical Biochemistry* **362**, 213–220 (2007).

396. Lin, W., Mandal, S., Degen, D., Liu, Y., Ebright, Y. W., Li, S., Feng, Y., Zhang, Y., Mandal, S., Jiang, Y., Liu, S., Gigliotti, M., Talaue, M., Connell, N., Das, K., Arnold, E. & Ebright, R. H. Structural Basis of Mycobacterium tuberculosis Transcription and Transcription Inhibition. *Molecular Cell* **66**, 169-179.e8 (2017).

397. Banerjee, R., Rudra, P., Prajapati, R. K., Sengupta, S. & Mukhopadhyay, J. Optimization of recombinant Mycobacterium tuberculosis RNA polymerase expression and purification. *Tuberculosis* **94**, 397–404 (2014).

398. Agarwal, N. & Tyagi, A. K. Mycobacterial transcriptional signals: Requirements for recognition by RNA polymerase and optimal transcriptional activity. *Nucleic Acids Research* **34**, 4245–4257 (2006).

399. Wiker, H. G. & Harboe, M. The antigen 85 complex: A major secretion product of Mycobacterium tuberculosis. *Microbiological Reviews* vol. 56 648–661 (1992).

400. Abou-Zeid, C., Ratliff, T. L., Wiker, H. G., Harboe, M., Bennedsen, J. & Rook, G. A. W. Characterization of fibronectin-binding antigens released by Mycobacterium tuberculosis and Mycobacterium bovis BCG. *Infection and Immunity* **56**, 3046–3051 (1988).

401. Viljoen, A., Alsteens, D. & Dufrêne, Y. Mechanical Forces between Mycobacterial Antigen 85 Complex and Fibronectin. *Cells* **9**, 1–14 (2020).

402. Kremer, L., Maughan, W. N., Wilson, R. A., Dover, L. G. & Besra, G. S. The M. tuberculosis antigen 85 complex and mycolyltransferase activity. *Letters in Applied Microbiology* **34**, 233–237 (2002).

403. Wilson, R. A., Maughan, W. N., Kremer, L., Besra, G. S. & Fütterer, K. The Structure of Mycobacterium tuberculosis MPT51 (FbpC1) Defines a New Family of Non-catalytic α/β Hydrolases. *Journal of Molecular Biology* **335**, 519–530 (2004).

404. Belisle, J. T., Vissa, V. D., Sievert, T., Takayama, K., Brennan, P. J. & Besra, G. S. Role of the Major Antigen of Mycobacterium tuberculosis in Cell Wall Biogenesis. *Science* **276**, 1420–1422 (1997).

405. Winder, F. G. & Collins, P. B. Inhibition by isoniazid of synthesis of mycolic acids in Mycobacterium tuberculosis. *Journal of general microbiology* **63**, 41–48 (1970).

406. Takayama, K., Wang, L. & David, H. L. Effect of isoniazid on the in vivo mycolic acid synthesis, cell growth, and viability of Mycobacterium tuberculosis. *Antimicrobial agents and chemotherapy* **2**, 29–35 (1972).

407. Takayama, K., Schnoes, H. K., Armstrong, E. L. & Boyle, R. W. Site of inhibitory action of isoniazid in the synthesis of mycolic acids in Mycobacterium tuberculosis. *Journal of Lipid Research* **16**, 308–317 (1975).

408. Larsen, M. H., Vilchèze, C., Kremer, L., Besra, G. S., Parsons, L., Salfinger, M., Heifets, L., Hazbon, M. H., Alland, D., Sacchettini, J. C. & Jacobs, W. R. Overexpression of inhA, but not kasA, confers resistance to isoniazid and ethionamide in mycobacterium smegmatis, M. bovis BCG and M. tuberculosis. *Molecular Microbiology* **2**, 453–466 (2002).

409. Ronning, D. R., Klabunde, T., Besra, G. S., Vissa, V. D., Belisle, J. I. & Sacchettini, J. C. Crystal structure of the secreted form of antigen 85C reveals potential targets for mycobacterial drugs and vaccines. *Nature Structural Biology* **7**, 141–146 (2000).

410. Anderson, D. H., Harth, G., Horwitz, M. A. & Eisenberg, D. An interfacial mechanism and a class of inhibitors inferred from two crystal structures of the Mycobacterium tuberculosis 30 kDa major secretory protein (antigen 85B), a mycolyl transferase. *Journal of Molecular Biology* **307**, 671–681 (2001).

411. Ronning, D. M., Vissa, V., Besra, G. S., Belisle, J. T. & Sacchettini, J. C. Mycobacterium tuberculosis antigen 85A and 85C structures confirm binding orientation and conserved substrate specificity. *Journal of Biological Chemistry* **279**, 36771–36777 (2004).

412. Armitige, L. Y., Jagannath, C., Wanger, A. R. & Norris, S. J. Disruption of the genes encoding antigen 85A and antigen 85B of Mycobacterium tuberculosis H37Rv: Effect on growth in culture and in macrophages. *Infection and Immunity* **68**, 767–778 (2000).

413. Puech, V., Guilhot, C., Perez, E., Tropis, M., Armitige, L. Y., Gicquel, B. & Daffé, M. Evidence for a partial redundancy of the fibronectin-binding proteins for the transfer of mycoloyl residues onto the cell wall arabinogalactan termini of Mycobacterium tuberculosis. *Molecular Microbiology* **44**, 1109–1122 (2002).

414. Jackson, M., Raynaud, C., Lanéelle, M. A., Guilhot, C., Laurent-Winter, C., Ensergueix, D., Gicquel, B. & Daffé, M. Inactivation of the antigen 85C gene profoundly affects the mycolate content and alters the permeability of the

Mycobacterium tuberculosis cell envelope. *Molecular Microbiology* **31**, 1573–1587 (1999).

415. Krachler, A. M. & Orth, K. Targeting the bacteria-host interface strategies in anti-adhesion therapy. *Virulence* vol. 4 284–294 (2013).

416. Ramsugit, S. & Pillay, M. Identification of mycobacterium tuberculosis adherence-mediating components: A review of key methods to confirm adhesin function. *Iranian Journal of Basic Medical Sciences* vol. 19 579–584 (2016).

417. Govender, V. S., Ramsugit, S. & Pillay, M. Mycobacterium tuberculosis adhesins: Potential biomarkers as anti-tuberculosis therapeutic and diagnostic targets. *Microbiology* vol. 160 1821–1831 (2014).

418. Warrier, T., Tropis, M., Werngren, J., Diehl, A., Gengenbacher, M., Schlegel, B., Schade, M., Oschkinat, H., Daffe, M., Hoffner, S., Eddine, A. N. & Kaufmann, S. H. E. Antigen 85C inhibition restricts Mycobacterium tuberculosis growth through disruption of cord factor biosynthesis. *Antimicrobial Agents and Chemotherapy* **56**, 1735–1743 (2012).

419. Hanessian, S. & Lavallee, P. Synthesis of 6-amino-6-deoxy-α-α-trehalose : A Positional Isomer of Trehalosamine. *Journal of Antibiotics* **25**, 683–684 (1972).

420. Yamaguchi, T., Sano, K., Takakura, K., Saito, I., Shinohara, Y., Asano, T. & Yasuhara, H. Ebselen in Acute Ischemic Stroke. *Stroke* **29**, 12–17 (1998).

421. Parnham, M. & Sies, H. Ebselen: Prospective therapy for cerebral ischaemia. *Expert Opinion on Investigational Drugs* vol. 9 607–619 (2000).

422. Kil, J., Pierce, C., Tran, H., Gu, R. & Lynch, E. D. Ebselen treatment reduces noise induced hearing loss via the mimicry and induction of glutathione peroxidase. *Hearing Research* **226**, 44–51 (2007).

423. Singh, N., Halliday, A. C., Thomas, J. M., Kuznetsova, O., Baldwin, R., Woon, E. C. Y., Aley, P. K., Antoniadou, I., Sharp, T., Vasudevan, S. R. & Churchill, G. C. A safe lithium mimetic for bipolar disorder. *Nature Communications* **4**, 1–7 (2013).

424. Favrot, L., Grzegorzewicz, A. E., Lajiness, D. H., Marvin, R. K., Boucau, J., Isailovic, D., Jackson, M. & Ronning, D. R. Mechanism of inhibition of Mycobacterium tuberculosis antigen 85 by ebselen. *Nature Communications* **4**, 1–10 (2013).

425. Favrot, L., Lajiness, D. H. & Ronning, D. R. Inactivation of the Mycobacterium tuberculosis antigen 85 complex by covalent, allosteric inhibitors. *Journal of Biological Chemistry* **289**, 25031–25040 (2014).

426. Goins, C. M., Dajnowicz, S., Thanna, S., Sucheck, S. J., Parks, J. M. & Ronning, D. R. Exploring Covalent Allosteric Inhibition of Antigen 85C from Mycobacterium tuberculosis by Ebselen Derivatives. *ACS Infectious Diseases* **3**, 378–387 (2017).

427. Viljoen, A., Richard, M., Nguyen, P. C., Fourquet, P., Camoin, L., Paudal, R. R., Gnawali, G. R., Spilling, C. D., Cavalier, J. F., Canaan, S., Blaise, M. & Kremer, L. Cyclipostins and cyclophostin analogs inhibit the antigen 85C from Mycobacterium tuberculosis both in vitro and in vivo. *Journal of Biological*

Chemistry **293**, 2755–2769 (2018).

428. Gahoi, S., Mandal, R. S., Ivanisenko, N., Shrivastava, P., Jain, S., Singh, A. K., Raghunandanan, M. V., Kanchan, S., Taneja, B., Mandal, C., Ivanisenko, V. A., Kumar, A., Kumar, R., Open Source Drug Discovery Consortium & Ramachandran, S. Computational screening for new inhibitors of M. tuberculosis mycolyltransferases antigen 85 group of proteins as potential drug targets. *Journal of Biomolecular Structure and Dynamics* **31**, 30–43 (2012).

429. Boucau, J., Sanki, A. K., Voss, B. J., Sucheck, S. J. & Ronning, D. R. A coupled assay measuring Mycobacterium tuberculosis antigen 85C enzymatic activity. *Analytical Biochemistry* **385**, 120–127 (2009).